Silk biomaterial based islet encapsulation platform conferring immunoisolation and immunomodulation toward bio-artificial pancreas development

A Thesis

Submitted in Partial Fulfillment of the Requirements for the Degree of

DOCTOR OF PHILOSOPHY

by

MANISHEKHAR KUMAR

Department of Biosciences and Bioengineering
Indian Institute of Technology Guwahati
Guwahati-781039, Assam, India

May 2018

Silk biomaterial based islet encapsulation platform conferring immunoisolation and immunomodulation toward bio-artificial pancreas development

A Thesis

Submitted in Partial Fulfillment of the Requirements for the Degree of

DOCTOR OF PHILOSOPHY

by

MANISHEKHAR KUMAR

Department of Biosciences and Bioengineering
Indian Institute of Technology Guwahati
Guwahati-781039, Assam, India

May 2018

Dedicated to my Family and Friends

INDIAN INSTITUTE OF TECHNOLOGY GUWAHATI

DEPARTMENT OF BIOSCIENCES AND BIOENGINEERING

STATEMENT

I do hereby declare that the research findings of this thesis is the result of research work carried out by me in the Department of Biosciences and Bioengineering, Indian Institute of Technology Guwahati, Guwahati, India, under the supervision of Dr. Biman B. Mandal.

As per the general norms of reporting research findings, due acknowledgements have been made, wherever the research findings of other researchers have been cited in this thesis.

Date: **Manishekhar Kumar**

INDIAN INSTITUTE OF TECHNOLOGY GUWAHATI

DEPARTMENT OF BIOSCIENCES AND BIOENGINEERING

CERTIFICATE

It is certified that the work described in this thesis entitled " **Silk biomaterial based islet encapsulation platform conferring immunoisolation and immunomodulation toward bio-artificial pancreas development**" by Mr. Manishekhar Kumar for the award of degree of Doctor of Philosophy is an authentic record of the results obtained from the research work carried out under my supervision in the Department of Biosciences and Bioengineering, Indian Institute of Technology Guwahati, India, and this work has not been submitted elsewhere for the award of any other degree.

CERTIFIED

Manishekhar Kumar

(Candidate)

Roll No: 126106017

Biman B. Mandal, Ph.D.

(Thesis Supervisor)

Date:

ACKNOWLEDGEMENT

First and foremost, I would like to express my sincere gratitude to my Ph.D. advisor Dr. Biman B. Mandal for the continuous support and encouragement. His guidance helped me in all the time of research and writing of this thesis. I could not have imagined having a better advisor and mentor for my Ph.D. study.

Besides my advisor, I would like to thank my committee members Professor Siddhartha Sankar Ghosh (Chairman), Dr. Manish Kumar and Dr. A. S. Achalkumar for serving on my committee and taking the time to evaluate this thesis work. Also, they are acknowledged for their insightful comments, encouragement and insightful questions which incented me to widen my research from various perspectives. I would also like to acknowledge Dr. Piruthivi Sukumar, former Chairman of my doctoral committee for his support and encouragement.

My sincere gratitude goes to my Fulbright advisor Professor David L. Kaplan (Tufts University, USA), who provided me an opportunity to join his team as a visiting researcher and gave access to Tufts research facilities. I extend my gratitude to everyone at Professor Kaplan's lab, in particular, Dr. Jeannine M. Coburn for assisting me in my research and stay at Tufts.

I would also like to thank Dr. Samit Kumar Nandi, West Bengal University of Animal and Fishery Sciences (WBUAFS) for providing us animal house facility. I would like to thank Piyali, Bipasha and Vinod for assisting me in animal studies.

I would like to acknowledge Professor K. Pakshirajan, Head of the Department of Biosciences and Bioengineering (BSBE), IIT Guwahati and Professor V.V. Dasu and Professor Arun Goyal, former Heads of the Department for providing me the necessary facilities that helped me to pursue my research at IIT Guwahati.

I am also grateful to all faculty members and staff of Department of Biosciences and Bioengineering for supporting me throughout my Ph.D. tenure. I would like to thank Department of Biosciences and Bioengineering for providing infrastructural facility for my research work. I would also like to thank Central Instruments Facility (CIF), IIT Guwahati for providing high-end equipments to execute my experiments.

I am grateful to Department of Biotechnology (DBT), Department of Science and Technology (DST) and Department of Atomic Energy (DAE) Government of India (GoI) for supporting my research and fellowship through research grants. I am also grateful to Ministry of Human Resource Development (MHRD) and IIT Guwahati for providing research fellowship and International Travel Support - Science and Engineering Research Board (ITS-SERB) DST for funding my international conference visit. I have much gratitude for the financial support provided by the Institute of International Education (IIE), New York and Fulbright fellowship. I would like to acknowledge Student Travel Assistance Fund (STAF) IITG for partially funding my international conference visit.

It is my pleasure to thank my current lab members Praveen, Dimple, Ankit, Bibhas, Shreya, Prerak, Yogendra, Janani, Joseph, Sohenii, Ashutosh, Namit, Suvro, Tarishi, Triya, Souradeep, Shoumasree, Jennie, Monisha, Rajiv, Smriti, Dr. Aparajita and Dr. Vimal for their feedback, cooperation and stimulating discussions. I am also thankful to my former lab members Salma, Dr. Rocktotpal, Dr. Biswajeet, Dr. Deepika, Prerna, Garima, Ranjana, Deepak, Surodeep, Sween, Korah and Sonu for their support during my PhD tenure.

I would like to extend my sincere gratitude to Professor A. Srinivasan, Department of Physics IIT Guwahati, Professor G. Krisnamoorthy, Department of Chemistry IIT Guwahati, and Professor Niranjan Karak, Department of Chemical Sciences, Tezpur University for the scientific collaborations.

I wish to thank my friends, Sandipan, Nilanjan, Mahesh, Ziauddin, Doordarshi, and Rana, for having enriched me as a person. I would like to acknowledge all the individuals who supported me throughout and contributed significantly to the outcome of this dissertation, their time and effort is greatly appreciated.

Last but not the least; I would like to thank my family: my grandparents, parents and my brothers and sisters for supporting me spiritually throughout this journey and my life in general. Thanks to God, the Almighty, for showers of blessings to complete the research work successfully.

Manishekhar Kumar

CONTENTS

Contents i

Abbreviations viii

List of Tables xiii

List of Figures xiv

CHAPTER 1: Introduction and Literature Review 1

1.1. Introduction 3

1.2. Literature Review 7

1.2.1. Current therapeutic strategies for Type 1 diabetes treatment 7

1.2.1.1. Exogenous insulin therapy 7

1.2.1.2. Whole pancreas transplantation 8

1.2.1.3. Islet transplantation 9

1.2.1.4. Artificial pancreas 9

1.2.2. Biomaterials used in islet culture and encapsulation 12

1.2.2.1. Alginate 12

1.2.2.2. Agarose 14

1.2.2.3. Polycations and anions 15

1.2.2.4. Chitosan 15

1.2.2.5. Collagen 16

1.2.2.6. Silica 16

1.2.3. Macrodevices/macrocapsules 16

1.2.4. Islet encapsulation and immunoisolation 18

1.2.5. Islet encapsulation and immunomodulation 19

1.2.6. Exploring silk as a potential biomaterial for islet encapsulation, immunoisolation and immunomodulation 21

1.2.6.1. Properties of silk: chemistry and structure 23

1.2.7. Silk as a biomaterial 23

1.2.7.1. Biocompatibility 24

1.2.7.2. Biodegradation 24

1.2.7.3. Mechanical properties 25

1.2.8. Silk matrices used for islet culture and encapsulation 25

1.2.8.1. Hydrogels 25

1.2.8.2. Scaffolds 26

1.2.8.2.1. Silkworm silk scaffolds 26

1.2.8.2.2. Spider silk scaffolds 27

Motivation and Objectives of the Present Research Work 31

CHAPTER 2: Development of Localized Immunomodulatory Silk-Alginate/ Agarose-based Scaffolds for Islet-like Spheroid Formation and Immunoisolation 35

Abstract 37

2.1. Introduction 38

2.2. Materials and Methods 41

2.2.1. Isolation of silk fibroin protein 41

2.2.2. Silk scaffold fabrication 41

2.2.3. Morphological analysis of scaffolds 42

2.2.4. Density and porosity measurements 42

2.2.5. Swelling 42

2.2.6. Maintenance of RIN-5 cell line 42

2.2.7. Isolation and culture of primary rat islets 43

2.2.8. Preparation of cell macroencapsulating scaffolds 43

2.2.9. Cell proliferation 44

2.2.10. Evaluation of spheroid formation and cell distribution in the scaffolds 45

2.2.11. *In vitro* cell function assessment in scaffolds 45

2.2.11.1. Insulin release study and enzyme-linked immunosorbent assay (ELISA) 45

2.2.11.2. Immunofluorescence for insulin and glucagon 46

2.2.11.3. RNA extraction and gene expression analysis by real-time RT-qPCR 46

2.2.12. Material biocompatibility assay 47

2.2.12.1. Macrophage stimulation and determination of *in vitro* inflammatory response 47

2.2.12.2. *In vivo* immune response to scaffolds 48

2.2.13. Dexamethasone (Dex) and IL-4 release from scaffolds 49

2.2.14. Islet cytotoxicity study 49

2.2.15. Immunomodulation study 50

2.2.16. Statistical analysis 50

2.3. Results 51

2.3.1. Scaffold morphology 51

2.3.2. Porosity and density of scaffolds 51

2.3.3. Swelling ratio and water uptake 51

2.3.4. Cell proliferation studies in 3D scaffolds 53

2.3.5. Evaluation of spheroid formation and cell distribution in the scaffolds 54

2.3.6. Functional assessment of the encapsulated cells *in vitro* 55

2.3.6.1. Insulin release 55

2.3.6.2. Insulin and glucagon immunofluorescence study 56

2.3.6.3. Gene expression analysis 56

2.3.7. Macrophage stimulation and determination of *in vitro* inflammatory response 56

2.3.8. *In vivo* immune response to scaffolds 57

2.3.9. Dexamethasone and IL-4 release 59

2.3.10. Cytotoxicity study on islets 59

2.3.11. Immunomodulation analysis 60

2.4. Discussion 61

2.5. Significant Findings 66

CHAPTER 3: Macrophage Polarization for Immunomodulation and Tailoring Local Biological Response 69

Abstract 71

3.1. Introduction 72

3.2. Materials and Methods 74

3.2.1. Silk processing and fibroin isolation 74

3.2.2. Silk hydrogel preparations 75

3.2.2.1. Silk-PEG (SP) hydrogel preparation 75

3.2.2.2. Silk-HRP (SH) hydrogel preparation 76

3.2.2.3. Silk-sonicated (SS) hydrogel preparation 76

3.2.3. Cytokine loading on hydrogels and *in vitro* release 76

3.2.4. *In vitro* cytotoxicity of hydrogels with human mesenchymal stem cell (hMSCs) 76

3.2.5. THP-1 cell culture and polarization in 2D 78

3.2.6. Polarization in hydrogel-encapsulated M0 macrophages 80

3.2.7. Polarization in hydrogel co-encapsulated macrophages and cytokines 80

3.2.8. RNA extraction and gene expression by RT-qPCR 81

3.2.9. Statistical analysis 82

3.3.	Results		82
	3.3.1.	*In vitro* cytokine release profile	82
	3.3.2.	*In vitro* cytocompatibility of hydrogels with human mesenchymal stem cells (hMSCs)	83
	3.3.3.	THP-1 cell culture and polarization in 2D	84
	3.3.4.	Polarization of hydrogel-encapsulated M0 macrophages	86
	3.3.5.	Macrophage plasticity in hydrogel co-encapsulated macrophages and cytokines	88
3.4.	Discussion		90
3.5.	Significant Findings		96
CHAPTER 4: Development of Minimally Invasive Injectable Silk Hydrogel as Potential Islet Encapsulation and Delivery Matrix			99
Abstract			101
4.1.	Introduction		102
4.2.	Materials and Methods		105
	4.2.1.	Silk fibroin isolation from *B. mori* cocoon	105
	4.2.2.	Silk fibroin isolation from *A. Assama* silkworm glands	106
	4.2.3.	Silk blended hydrogel fabrication	106
	4.2.4.	Gelation pattern and time analysis	106
	4.2.5.	Rheological characterization (gelation time and complex viscosity study)	106
	4.2.6.	Morphological analysis of hydrogels	107
	4.2.7.	*In vitro* enzymatic degradation	107
	4.2.8.	Fourier Transform Infrared spectroscopy (FTIR)	107
	4.2.9.	Isolation of primary rat islets and maintenance of islets and RIN-5 cell line	108
	4.2.10.	Cell viability and proliferation studies with hydrogels	108

4.2.10.1. RIN-5 cell proliferation on hydrogel surface 108

4.2.10.2. RIN-5 and islet cell viability in 3D encapsulated hydrogels 109

4.2.11. Functional assessment of islet cells encapsulated in hydrogels 109

4.2.11.1. RNA extraction and gene expression analysis 109

4.2.11.2. Glucose challenge assay 110

4.2.11.3. Immunohistochemistry and Hematoxylin and Eosin (H & E) staining 110

4.2.12. Interleukin-4 (IL-4) and Dexamethasone (Dex) release from hydrogels 111

4.2.13. Immunomodulation study 111

4.2.14. Cytotoxicity study with islets 112

4.2.15. Endothelial cell culture and functional studies 112

4.2.15.1. Isolation, culture and maintenance of primary endothelial cells 112

4.2.15.2. Endothelial cell viability and proliferation on silk hydrogel 112

4.2.15.3. Functional assessment of endothelial cells 113

4.2.16. *In vitro* inflammatory response towards hydrogels 113

4.2.17. *In vivo* immunomodulation study 114

4.2.18. Statistical analysis 114

4.3. Results 115

4.3.1. Hydrogel fabrication and gelation time estimation 115

4.3.2. Rheology (Gelation kinetics and complex viscosity) 116

4.3.3. Morphological analysis of hydrogels (FESEM) 116

4.3.4. Enzymatic degradation 117

4.3.5. FTIR 117

4.3.6. Cell proliferation studies with hydrogels 118

4.3.7. Functional assessment of islets encapsulated in hydrogels 122

4.3.7.1. RNA extraction and gene expression analysis 122

4.3.7.2. Glucose challenge assay 122

4.3.7.3. Immunohistochemistry for insulin and glucagon 123

4.3.8. Interleukin-4 and Dexamethasone release profile 124

4.3.9. Immunomodulation study 125

4.3.10. Cytotoxicity and immunomodulation study on islets 127

4.3.11. Endothelial cell culture and functional studies 127

4.3.11.1. Viability and proliferation of endothelial cells 127

4.3.11.2. Functionality of endothelial cells 127

4.3.12. *In vitro* inflammatory response towards hydrogels 129

4.3.13. *In vivo* immunomodulation study 129

4.4. Discussion 131

4.5. Significant Findings 137

Summary and Future Perspective 139

Bibliography 145

Appendix 171

List of Publications 177

ABBREVIATIONS

µg	Microgram
µL	Microliter
µM	Micromolar
A. assama	*Antheraea assama*
ANOVA	Analysis of variance
AU	Arbitrary unit
BAP	Bio-artificial Pancreas
$BaCl_2$	Barium chloride
B. mori	*Bombyx mori*
BSA	Bovine serum albumin
$CaCl_2$	Calcium chloride
CCR7	C-C chemokine receptor 7
CD4	Cluster of differentiation 4
CD68	Cluster of differentiation 68
CD206	Cluster of differentiation 206
CD209	Cluster of differentiation 209
Da	Dalton
DCCT	Diabetes Control and Complications Trial
DMEM	Dulbecco's modified eagles medium
DMSO	Dimethyl sulfoxide
DNA	Deoxyribonucleic Acid
dNTP	Deoxynucleoside triphosphate
ECGS	Endothelial cell growth supplement
ECM	Extracellular matrix
EDTA	Ethylenediaminetetraacetic acid
Ex	Excitation
Em	Emission
ELISA	Enzyme-linked immunosorbent assay
EWC	Equilibrium water content
FBS	Fetal bovine serum

FCM	Flow cytometry
FDA	Food and Drug Administration
FESEM	Field emission scanning electron microscope
FITC	Fluorescein isothiocyanate
FN	Fibronectin
FTIR	Fourier Transform Infrared spectroscopy
G'	Storage modulus
G"	Loss modulus
GAPDH	Glyceraldehyde-3-phosphate-dehydrogenase
h	Hour
H & E	Hematoxylin and Eosin
HBSS	Hanks' balanced salt solution
H-chain	Heavy chain
HEK	Human endoderm kidney
HEPES	4-(2-hydroxyethyl)-1-piperazineethanesulfonic acid
hMSCs	Human mesenchymal stem cells
H_2O_2	Hydrogen peroxide
HRP	Horseradish peroxidase
H-SF	Heparin-releasing silk fibroin scaffold
ICMR	Indian Council of Medical Research
IL-1β	Interleukin-1 beta
IL-4	Interleukin-4
IL-10	Interleukin-10
IL-13	Interleukin-13
IFN-γ	Interferon-γ
IPGTT	Intraperitoneal glucose tolerance test
KBr	Potassium bromide
kDa	Kilo Dalton
L-chain	Light chain
LiBr	Lithium bromide
LiSCN	Lithium thiocyanate
LPS	Lipopolysaccharide
mg	Milligram
min	Minute
mL	Milliliter

mM	Millimolar
MSCs	Mesenchymal stromal cells
MTT	3-(4,5-Dimethylthiazol-2-yl)-2,5-Diphenyltetrazolium Bromide
MWCO	Molecular weight cut-off
Na_2CO_3	Sodium carbonate
NBF	Neutral buffered formalin
NCCS	National Centre for Cell Science
nm	Nanometer
NO	Nitric oxide
NOD	Non-obese diabetic
ns	Not significant
PBMCs	Peripheral blood mononuclear cells
PBS	Phosphate buffered saline
PDGF	Platelete-derived growth factor
PDMS	Polydimethylsiloxane
PDX-1	Pancreatic and duodenal homeobox 1
PEG	Poly ethylene glycol
PLA	Poly (lactic acid)
PLGA	Poly (lactic-co-glycolic acid)
PLL	Poly -L-lysine
PLO	Poly-L-ornithine
PMA	Phorbol 12-myristate 13-acetate
PVA	Poly vinyl alcohol
RGD	Arg-Gly-Asp or Arginine-Glycine-Aspartic acid
RGE	Arg-Gly-Glu or Arginine-Glycine-Glutamic acid
rpm	Revolutions per minute
RPMI	Roswell Park Memorial Institute medium
RT-qPCR	Quantitative reverse transcription polymerase chain reaction
s	Second
sCR1	Soluble domain of human complement receptor 1
SD	Standard deviation
SDS	Sodium dodecyl sulfate
SEM	Scanning electron microscope
SF	Silk fibroin

SI	Stimulation index
SH	Silk-horseradish peroxidase
SP	Silk-poly (ethylene glycol)
SS	Silk-sonicated
STZ	Streptozotocin
TAMs	Tumour-associated macrophages
TCP	Tissue culture plate
T_{effs}	Effector T cells
TGF-β1	Transforming growth factor-beta 1
Th1	Type 1 T helper
TNF-α	Tumor necrosis factor α
T_{regs}	Regulatory T cells
UV	Ultraviolet
VEGF	Vascular endothelial growth factor
VEGFR2	Vascular endothelial growth factor receptor2
VN	Vimentin
vWF	von Willebrand factor
ω	Angular frequency

भारतीय प्रौद्योगिकी संस्थान गुवाहाटी
Indian Institute of Technology Guwahati

LIST OF TABLES

CHAPTER 1 **Page No.**

Table 1.1.	Therapeutic strategies for diabetes therapy, advantages and limitations	8
Table 1.2.	Biomaterial formats used for islet encapsulation	11
Table 1.3.	Biomaterials used for islet encapsulation, advantages and limitations	13
Table 1.4.	Islet donor and recipient animal models used for encapsulated islet transplantation	17
Table 1.5.	Biomaterial-based immunomodulation approach for islet encapsulation	20

CHAPTER 2

Table 2.1.	Primers for RT-qPCR	47
Table 2.2.	Density and percentage of water uptake for the different scaffold compositions	53

CHAPTER 3

Table 3.1.	Primers for RT-qPCR	82

CHAPTER 4

Table 4.1.	Primers for RT-qPCR	110

LIST OF FIGURES

CHAPTER 1 **Page No.**

Figure 1.1. Schematic illustration of the overall approach for islet protection using silk-based macroencapsulation which confers immunoisolation and immunomodulation. In macroencapsulation approach, silk-scaffold was utilized as islet culture platform and alginate/agarose was incorporated as barrier to provide protection i.e. immunoisolation. The barrier prevents the infiltration of host immune cells, simultaneously allowing the exchange of glucose, oxygen, and insulin. Immunomodulation approach involves localized and controlled release of dexamethasone and interleukin-4 from functionalized silk matrices creating a favourable local immunomodulatory microenvironment by promoting local anti-inflammatory macrophages (M2). 28

CHAPTER 2

Figure 2.1. Principle of silk-based bio-artificial pancreas (BAP) with three different attributes of spheroid formation, local immunomodulation and immunoisolation. 40

Figure 2.2. Scheme representing fabrication of cell encapsulating silk scaffolds. 51

Figure 2.3. Physical characterization. (A) FESEM images representing cross sectional morphology and interconnectivity within 3D scaffolds: (i) silk-control, (ii) silk-alginate, (iii) silk-agarose, (iv) alginate coating layer, and (v) agarose coating layer (white arrows). Scale bar 100 μm. (B) Porosity of different scaffolds. (C) Swelling ratio of scaffolds in PBS at 37 ºC (pH 7.4) against time. (*$p \leq 0.05$, **$p \leq 0.01$). 52

Figure 2.4. Cell proliferation and islet culture. (A) Cell proliferation for 35 days in macroencapsulated 3D scaffolds prepared with different compositions using RIN-5 cell line spheroids (**$p \leq 0.01$). (B) Primary rat islets clusters growing in 2D culture plate after isolation. (C) Small primary islet aggregates (D) Calcein AM stained live primary islets. Scale bar: 50 μm. 53

Figure 2.5. Comparative morphology of RIN-5 cells and islets in 2D and 3D culture. (A) Fluorescent images of RIN-5 cells showing live islet-like spheroid on 3D scaffolds (35 days culture) and compared with TCP (7 days culture). Green color shows calcein-stained live cells. (B) Islet-like 3D spheroids after fixation and 54

staining compared with TCP (7 days). Red shows cellular actin filaments, and blue shows nucleus. Scale bar: 200 µm. (C) Fluorescent microscopic images of primary islets after 14 days culture. Red shows adipo red-stained silk matrices, and blue shows nucleus. Scale bar: 100 µm.

Figure 2.6. Glucose challenge assay showing insulin secretion from (A) RIN-5 spheroids and (B) primary islets encapsulated in different scaffolds. Stimulation index (SI) was calculated as the ratio of insulin secreted in high glucose to low glucose. Immunofluorescence images showing insulin in (C) RIN-5 seeded scaffolds (35 days), (D) primary islets (14 days) and (E) glucagon in primary islets (14 days), cultured on scaffolds. Blue color shows nucleus. Scale bar: 50 µm. (*p < 0.05). "ns" indicates not significant (p > 0.05). 55

Figure 2.7. Relative expression of functional islet genes in different scaffolds after 14 days culture of rat islets. Gene expression was relative to GAPDH gene and normalized to non-encapsulated islets in 2D. (A) insulin I, (B) insulin II, (C) glucagon, (D) somatostatin, and (E) PDX-1 (*$p \leq 0.05$). 57

Figure 2.8. *In vitro* and *in vivo* immune response. (A) TNF alpha production by RAW 264.7 macrophages (*in vitro* study; *p < 0.05, **p < 0.01). (B) H & E staining and (C) immunofluorescence of retrieved acellular scaffolds after 4 weeks of subcutaneous implantation in mice. Symbols S, AL, AR, and H stand for silk scaffold, alginate, agarose, and host tissue, respectively. Arrows indicate infiltrating monocytes/macrophage (green), and dashed lines indicate scaffold-host tissue interface. Scale bar: 400 µm. 58

Figure 2.9. Immunomodulation analysis. (A) Cumulative Dex (i) and IL-4 (ii) release from different scaffold compositions. (B) Gene expression analysis for M1 and M2 macrophage surface markers (relative to untreated M0 monocytes) when incubated with IL-4-loaded silk-alginate scaffolds for 72 h. (C) MTT assay showing islet viability post-incubation with Dex and IL-4 eluting silk-alginate scaffolds compared with control (islets without treatment). (D) Glucose stimulated insulin release by islet incubated with Dex and IL-4-eluting silk-alginate scaffolds. The results are representative from three independent experiments and performed as n=3 (*p < 0.05, **p < 0.01, ***p < 0.001). "ns" indicates not significant (p > 0.05). 60

CHAPTER 3

Figure 3.1. Schematic representation of silk hydrogel preparation. Covalent cross-linking of tyrosine residues on silk protein chains in enzymatically formed SH hydrogels (A). Sonication-induced 75

assembly of silk solution into hydrogels (B). Silk-PEG gel formation with β-sheet structure (C).

Figure 3.2. Study design for *in vitro* macrophage polarization and plasticity using three different approaches. General scheme showing monocyte (THP-1) to macrophage (M0) conversion using PMA. Further, macrophage polarization and plasticity studies were conducted using pro-inflammatory IFN-γ and anti-inflammatory IL-4 cytokines (A). In the first approach, M0 cells were cultured in TCP wells and cytokine-loaded hydrogels were placed in transwell inserts. H-IFN-γ and H-IL-4 represent IFN-γ and IL-4 encapsulated in hydrogels, respectively (B). In the second approach, M0 cells were encapsulated in hydrogels (placed in transwell inserts); polarizing cytokines were provided through cell culture media. H-M0, H-M1 and H-M2 represent hydrogel-encapsulated M0, polarized M1 and polarized M2, respectively at different stages of polarization (C). In the third approach, M0 cells and individual cytokines were co-encapsulated in silk hydrogels. H-IFN-γ-M0, H-IFN-γ-M1, H-IL-4-M0 and H-IL-4-M2 represent M0 encapsulated with IFN-γ, polarized M1 encapsulated with IFN-γ, M0 encapsulated with IL-4, and polarized M2 encapsulated with IL-4, respectively (D). 79

Figure 3.3. Cumulative IFN-γ and IL-4 release (Picogram (pg)) from the silk-based hydrogels. Each hydrogel (20 µL) was loaded with 1 µg cytokine (A and C). Cumulative IFN-γ and IL-4 release (%) from all the six hydrogels (B and D) was monitored via ELISAs. Data represents mean ± standard deviation (n=3). Statistical differences were determined with one-way ANOVA. (* $p \leq 0.05$, ** $p \leq 0.01$). 83

Figure 3.4. Human mesenchymal stem cell interaction with hydrogel surfaces. Viable cells were stained in green using Calcein AM (A). Cell attachment on TCP (i), 5% SP (ii), 5% SH (iii), and 5% SS gels (iv). Scale bar represents 200 µm. Cell proliferation after hMSCs encapsulation in silk hydrogels (5% w/v) over 7 days period as determined by AlamarBlue assay and presented as fold change compared to day 1 (B). (*$p \leq 0.05$, **$p \leq 0.01$). 84

Figure 3.5. Morphology of macrophage when polarized with cytokine-releasing silk hydrogels. Morphology of THP-1 cells (M0) after overnight PMA (162 nM) treatment and incubation with control SH hydrogel (A). Morphology of M0 cells after treatment for 60 h with 20 ng/mL IFN-γ directly added to culture media (i), with SP (ii), SH (iii) and SS hydrogel (iv) loaded with 1µg IFN-γ (B). Morphology of M0 cells after treatment for 60 h with 20 ng/mL IL-4 directly added to culture media (i), with SP (ii), SH (iii) and SS hydrogel (iv) loaded with 1µg IL-4 (C). Scale bar represents 100 µm. 85

Figure 3.6. Monolayer macrophage plasticity upon cytokine release from silk hydrogels. Macrophages were initially differentiated with H-IFN-γ for 60 h then media was switched to H-IL-4 for the following 60 h (A). Macrophages were initially differentiated with H-IL-4 for 60 h then media was switched to H-IFN-γ for the following 60 h (B). Expression of CCR7 and CD206 was quantified by qPCR at 60 h after initial polarization and 120 h after hydrogel switching. $*p \leq 0.01$ vs. control, $^{\#}p \leq 0.05$ vs. SH. H-IFN-γ represents. IFN-γ encapsulated in hydrogels and H-IL-4 represents IL-4 encapsulated in hydrogels. 86

Figure 3.7. Images of monolayer and silk hydrogel-encapsulated M0 macrophage. Cultured on TCP (A), encapsulated in 5% SP (B), 5% SH (C), and 5% SS hydrogels (D). Viable cells were stained in green using Calcein AM on culture day 5. Scale bar represents 50 μm. 87

Figure 3.8. Encapsulated macrophage plasticity upon exposure to free-cytokines in the media. H-M0 was initially differentiated with IFN-γ in media for 60 h then hydrogels were switched to IL-4 containing media for the following 60 h (A). H-M0 was initially differentiated with IL-4 in media for 60 h then hydrogels were switched to IFN-γ containing media for the following 60 h (B). Expression of CCR7 and CD206 was quantified by qPCR at 60 h after initial polarization and 120 h after media switching. $*p \leq 0.01$ vs. control and $^{\#}p \leq 0.05$ vs. SP. H-M0, H-M1 and H-M2 represent hydrogel-encapsulated M0, polarized M1 and polarized M2, respectively. 88

Figure 3.9. Representative images of M0 macrophages encapsulated in hydrogels with IL-4 cytokine after 120 h. Encapsulated in 5% SP (A), 5% SH (B), 5% SS (C), and 5% SH hydrogels (D). Red shows silk matrices stained with Adipo red, blue shows nucleus and green for cytoskeleton. Scale bars represent 50 μm. 89

Figure 3.10. M0 macrophage polarization when encapsulated in silk hydrogels containing cytokines. M0 macrophages encapsulated in 5% SP, 5% SH, and 5% SS hydrogels with IFN-γ (A) and IL-4 (B) cytokine for five day (120 h). Expression of CCR7, IL1B, CD206 and CD209 was quantified by qPCR at 60 h after initial polarization and 120 h after media switching. $*p \leq 0.01$ vs. control, $^{\#}p \leq 0.05$ vs. SP. H-IFN-γ-M0, H-IFN-γ-M1, H-IL-4-M0 and H-IL-4-M2 H-M2 means M0 encapsulated with IFN-γ, polarized M1 encapsulated with IFN-γ, M0 encapsulated with IL-4, and polarized M2 encapsulated with IL-4, respectively. 90

CHAPTER 4

Figure 4.1. Silk blend hydrogel fabrication and hydrogelation study. (A) Scheme representing fabrication of silk hydrogel blend (BA1, BA2 and BA3). (B) Change in absorbance observed after mixing *B. mori* (8, 6, 4 and 2% w/v) with *A. assama* (2% w/v) silk solutions in equal volume (i). Change in absorbance observed after mixing *B. mori* (2% w/v) with *A. assama* (2% w/v) in different ratio (2:1, 1:1 and 1:2) (ii). Absorbance was recorded at 550 nm. Table showing gelation time for different hydrogel blend ratio (iii). 116

Figure 4.2. Physico-chemical characterization. (A) FESEM images showing hydrogel morphology and interconnectivity; BA1 (i), BA2 (ii) and BA3 (iii). (B) Enzymatic degradation profile of hydrogels in protease XIV and PBS control (pH 7.4). Mass remaining was determined by comparing the wet weight at each time point with original wet weight. (C) FTIR spectra of BA3 blend hydrogel and individual silk proteins. Scale bar 20 μm. (n = 3,***$p \leq 0.001$, **$p \leq 0.01$). 117

Figure 4.3. RIN-5 cell and primary islets viability, proliferation and functional tests.(A) Alamar blue cell proliferation assay with RIN-5 cells seeded on silk hydrogel blend (BA1, BA2 and BA3) film (2D) (i). RIN-5 cell proliferation study by DNA quantification (PicoGreen assay) with encapsulation in 3D hydrogel (ii). (B) Primary rat islets viability quantified by PicoGreen assay. (C) Expression of functional islet genes after 14 days of encapsulation (normalized to 2D islet culture). (D) Glucose challenge assay showing insulin secretion from primary rat islets encapsulated in silk hydrogels (BA1, BA2 and BA3) and TCP (control) on day 7 (i) and day 14 (ii). (n = 3, ***$p \leq 0.001$, **$p \leq 0.01$, *$p \leq 0.05$). 119

Figure 4.4. Representative images for RIN-5 cell viability, distribution and insulin expression in 2D and 3D silk hydrogel (BA3). (A) Calcein AM stained live RIN-5 cells (green) on silk blend hydrogel 2D coating. (B) Immunofluorescence images showing insulin (green) and nucleus (blue) in 2D. (C) Calcein AM stained live RIN-5 cells (green) encapsulated in silk blend hydrogel. (D) Immunofluorescence images showing insulin (green) and nucleus (blue) in 3D. (E) Distribution of encapsulated RIN-5 in 3D silk hydrogel. Cells are stained with hematoxylin (nucleus) and eosin (cytoplasm). Scale bar 50 μm. 121

Figure 4.5. Representative images for primary rat islet viability, insulin/ glucagon expression and islet distribution post-encapsulation in 3D silk hydrogel (BA3) on day 3, 7 and 14. (A) Viable islets encapsulated in silk blend hydrogel (green) inset images show individual islet. (B) Immunofluorescence images showing the 124

expression of insulin (green) and nucleus (blue). (C) Images showing the expression of glucagon (red). (D) Distribution of encapsulated islets in 3D silk hydrogel. Islets are stained with hematoxylin (nucleus) and eosin (cytoplasm). Scale bar 50 µm.

Figure 4.6. Interleukin-4 (IL-4)/ Dexamethasone (Dex) release and immunomodulation study with silk hydrogels. (A) Cumulative IL-4 (i) and Dex (ii) release from different hydrogel compositions (BA1, BA2 and BA3). (B) Gene expression analysis for M1 (CCR7) and M2 (CD206 & CD209) macrophage surface markers when incubated with IL-4-loaded silk hydrogel blend (BA3) for 72 h. (C) Islet physiology assessment after incubation with Dex and IL-4-silk hydrogels for 72 h. PicoGreen assay showing islet viability post-incubation with islet co-encapsulated Dex and IL-4 in silk hydrogel blend (BA3) compared with control (islets without IL-4/Dex) (i). Glucose stimulated insulin release by the encapsulated islets (ii). "ns" indicates not significant ($p > 0.05$). (D) Representative images for macrophage polarization. Induced M0 macrophages from THP-1 monocytes after overnight PMA (162 nM) treatment (i) M0 to M2 polarized macrophage when incubated with IL-4-eluting silk hydrogel blend (BA3) (ii) and M2 surface marker CD206 (green) expression counterstained with Hoechst33342 (nucleus, blue) (iii). Scale bar 200 µm. (n = 3, *$p \leq 0.05$, **$p \leq 0.01$). 126

Figure 4.7. Cytocompatibility, cell adhesion, proliferation and functional study with porcine aortic endothelial cells after 7 days of culture. (A) Phase contrast and (B) fluorescence images of the cells cultured on TCP and silk hydrogel blend (BA3). Green colour shows live cells. Scale bar: 500 µm. (C) Immunostaining for endothelial cell marker, Von Willebrand factor (vWF) on TCP and silk hydrogel (BA3). Green, red and blue colours represent positive staining for vWF, cellular cytoskeleton and the nucleus, respectively. Scale bar: 100 µm. (D) Alamar blue dye reduction assay and (E) production of NO from the cultured endothelial cells. n = 3, *$p \leq 0.05$, "ns" indicates not significant ($p > 0.05$). 128

Figure 4.8. Representative images showing immunohistochemistry of retrieved BA3 control, BA3 + IL-4 and BA3 + Dex hydrogels after 3 days of implantation. Blue, green and red colours represent nucleus, CD68 expression and CD206 expression, respectively. Scale bar represents 100 µm. 3D surface plot of IHC stained images showing distribution of CD206 positive cells using the ImageJ (NIH, USA) software. Symbols H and T stand for silk hydrogel and host tissue, respectively. 130

Figure 4.9. Representative images showing immunohistochemistry of retrieved BA3 control, BA3 + IL-4 and BA3 + Dex hydrogels after 10 days of implantation. Blue, green and red colours 131

represent nucleus, CD68 expression and CD206 expression, respectively. Scale bar represents 100 μm. 3D surface plot of IHC stained images showing distribution of CD206 positive cells using the ImageJ (NIH, USA) software. Symbols H and T stand for silk hydrogel and host tissue, respectively.

Chapter 1

Introduction and Literature Review

भारतीय प्रौद्योगिकी संस्थान गुवाहाटी
Indian Institute of Technology Guwahati

Introduction and Literature Review

1.1. Introduction

Diabetes is a metabolic disorder affecting millions of people globally and a leading cause of morbidity and mortality (Daneman, 2006; Muthyala et al., 2011). The global incidence of diabetes is exemplified by recent statistical data mined from two geographically different locations where >30.3 million Americans (National Diabetes Statistics Reports, 2017) and ~66.8 million Indians (Indian Council of Medical Research (ICMR) Report, 2016) were diabetic. Within this cohort, type 1 diabetes represents around 10% of all diabetic patients worldwide (Shalaly et al., 2016). Clinically, this form of diabetes is associated with hyperglycemia due to defects in insulin secretion, insulin production or both. Type 1 diabetes is an autoimmune disease characterized by destruction of insulin-producing β-cells by the body's own immune system, resulting in hyperglycemia and accumulation of toxic acids in blood and urine (Foster and García, 2017b; Go et al., 2014; Mathis et al., 2001). The resultant symptomatic hyperglycemia is associated with eventual failure of several vital organs (Association, 2006) and the patients suffer from higher rates of morbidity and mortality (Go et al., 2014). The diabetic patients are at a risk of severe secondary complications like, neuropathy, retinopathy, chronic kidney disease, cardiovascular complications and infections (Foster and García, 2017b; Kort et al., 2011; Miller et al., 2016; Opara et al., 2010).

Till date insulin therapy has remained the ideal choice for treating type 1 diabetes and pancreatic transplantation is performed in severe hyperglycaemic conditions (Shapiro et al., 2000). However, fluctuations in blood glucose level and complications associated with surgical procedure have posed limitations in these traditional approaches so far. In order to address these challenges, islet transplantation might be a promising approach for therapeutic intervention in type 1 diabetes as it is minimally invasive and restores normoglycemia in the patients. Moreover, islets can function as a glucose sensor as well as a source of new insulin thereby making it more preferable than insulin injections (Niknamasl et al., 2014; Shapiro et al., 2000). However, the application of this technique has been limited due to shortage of donors, high rate of implant rejection, long term immunosuppression and islet dysfunction in post-transplantation period (Hirshberg et al., 2003). Furthermore, the considerable loss

of islets (~60%) during islet infusion to portal vein demands multiple donors (2-4) for one diabetic patient (Del Toro-Arreola et al., 2016; Vlahos et al., 2017) which needs to be reviewed.

To rein in the "Type 1 diabetes epidemic", tissue engineering and regenerative medicine present a novel and effective solution for the replacement of diseased pancreas with bioengineered implants (Vacanti and Langer, 1999). Biomaterial-based islet encapsulation approach provides an attractive alternative proposition for islet delivery *in vivo* by providing protective three-dimensional (3D) support for islet function (Liao et al., 2013). In the native pancreas, islets are surrounded by a capsule of extracellular matrix (ECM) comprising of different matrix components which bind to integrins on the islet surface to mediate islet adhesion, proliferation, and insulin secretion (Daoud et al., 2010). During islet isolation, due to enzymatic digestion, majority of islet microvasculature and islet-matrix connections are disrupted resulting in islet fragmentation, and glucose irresponsiveness (Brendel et al., 1994; Ilieva et al., 1999). Upon encapsulation in 3D biomimetic microenvironment with ECM-like biochemical cues, the islet functions are preserved as the 3D matrix compensates for the native ECM (Daoud et al., 2011; Davis et al., 2012; Shalaly et al., 2016).

In this reference, earlier several natural and synthetic biomaterials have been utilized with success to a certain extent (Borg and Bonifacio, 2011). Natural biopolymers (collagen, heparin, gelatin) often suffer from drawbacks like batch-to-batch variation, pathogen contamination, lack of tunability, and immunogenicity (Liao et al., 2013). On the other hand, synthetic polymers (poly (lactic acid) (PLA) and poly (lactic-co-glycolic acid) (PLGA)) demand pre-fabricated scaffolds with additional ECM components. Also, the biodegradation of these synthetic polymers release acidic by-products leading to pro-inflammatory responses *in vivo* (Blomeier et al., 2006; Liao et al., 2013; Salvay et al., 2008). Furthermore, the application of poly (vinyl alcohol) (PVA) for islet encapsulation necessitates sub-zero temperature to form hydrogels resulting in islet dysfunction and glucose irresponsiveness (Liao et al., 2013; Saudek et al., 1999). Polyethylene glycol (PEG) has been explored extensively for islet encapsulation, however, despite numerous favorable features; PEG has many restrictions including poor islet viability, non-degradable backbone and lack of functionality (Liao et al., 2013; Lin and Anseth, 2009). To overcome these limitations, herein, we explored silk protein polymer as a potential biomaterial for islet encapsulation and bio-artificial pancreas development.

Silk, a structural protein, is biocompatible, non-immunogenic, mechanically robust biomaterial with tunable degradation rates (Kundu et al., 2013). Silk protein is easy to process (under physiological-like conditions), and its degradation products are amino acids which can easily be metabolized *in vivo* (Davis et al., 2012; Vepari and Kaplan, 2007b). Silk resources are available in abundance and have demonstrated exceptional advantages over conventional synthetic and natural biomaterials (Thurber et al., 2015; Vepari and Kaplan, 2007a). The Food and Drug Administration (FDA) approved Mulberry *Bombyx mori* silk-based scaffolding matrices have been widely explored for the regeneration of a plethora of tissues including bone, cartilage, tendon, kidney, skin, liver, trachea, nerve, cornea, meniscus, eardrum, and urinary bladder (Kundu et al., 2013; Rockwood et al., 2011). The exciting prospect of exploring silk-based matrices as new biomaterial for islet encapsulation has received impetus with emerging reports that demonstrate their potential in *in vitro* islet culture maintenance and diabetes reversal in murine model (Davis et al., 2012; Hamilton et al., 2017; Mao et al., 2017). To harness the true potential of silk-based matrices for islet encapsulation, it is imperative to develop judicious system that would be islet-supporting, immunoisolatory and immunomodulatory. Recently, it has been reported that a non mulberry silk, *Antheraea assama* is enriched with intrinsic cell binding Arg-Gly-Asp (RGD) sequences (Gupta et al., 2015). Due to the presence of cell-binding RGD motif, this variety of silk supports better proliferation of cells from different tissues viz; bone, cartilage, blood vessels, skin, liver and cardiac tissues compared to its mulberry counterpart, *B. mori* (Gupta et al., 2016a; Gupta et al., 2016b; Konwarh et al., 2017). In this context, exploring non-mulberry silk-based matrix as a new biomaterial could provide a promising platform for successful islet encapsulation.

Despite the biological cues provided by 3D matrices, the islet transplantation process is associated with many challenges (Liu et al., 2016). Being an autoimmune disease, pancreatic beta cells are selectively destroyed by the patient's own immune system. Also, surgery-associated tissue damages evoke inflammation and alter the immune environment of the implants (Piemonti et al., 2002; Weaver et al., 2015). Under such adverse conditions, encapsulated islets undergo tremendous stress and secrete their own pro-inflammatory molecules amplifying the local inflammation and culminating in considerable islet loss and dysfunction (McDaniel et al., 1996; Weaver et al., 2015; Wilson and Chaikof, 2008). To prevent such drawbacks, the recipients require life-long administration of systemic immunosuppressive drugs which pose

systemic side-effects. In this circumstance, localized delivery of immunosuppressant at the implantation site has shown promising outcomes as an effective therapy to prevent immune targeting of islets and thereby eliminating the need for systemic immunosuppression (Weaver et al., 2015).

Herein, this thesis presents two possible strategies of silk biomaterial-based islet encapsulation for the local mitigation of inflammation in the islet microenvironment: 1) Encapsulation of islets to prevent infiltration of immune cells and, 2) local release of immunomodulatory molecules (dexamethasone and interleukin-4) from silk-based biomaterial systems that suppress local immunity. The aim of this work was to develop biomaterials with the capacity to reduce local inflammation, thereby improving long-term viability and functionality of the transplanted cells.

Based on this rationale, the initial attempt was to develop silk-based matrix that might display native islet-like niche and support islet culture and glucose responsive insulin secretion. Furthermore, the major emphases were on the development of matrices with immunoisolation and immunomodulation attributes and test their potential towards bio-artificial pancreas development. Moreover, with increasing number of type 1 diabetic patients and challenges encountered with several therapeutic approaches, this study strives to generate potent silk-based matrices addressing a serious health issue that demands attention. The following section provides a detailed literature review pertinent to the research area under investigation.

1.2. Literature Review

1.2.1. Current therapeutic strategies for Type 1 diabetes treatment

The current treatment approach for type 1 diabetes includes exogenous insulin therapy, pancreas transplantation and islet transplantation. The techniques of insulin therapy and pancreas transplantation are associated with many limitations. A frequent glucose fluctuations and poor glucose control in insulin therapy and major surgery, donor shortage and life-long immunosuppression in case of pancreas transplantation are the major limitations. Therefore, there is an urgent clinical need for alternative new approach like bio-artificial pancreas based on islet encapsulation (Opara et al., 2010; Pareta et al., 2013). The advantages and the associated limitations of these approaches are enlisted in **Table 1.1** and elaborated in the following sections.

1.2.1.1. Exogenous insulin therapy

Blood glucose control by exogenous insulin administration has been a routine therapy (Pareta et al., 2013). In this procedure, the amount of carbohydrates consumed is estimated by measuring food which is used to estimate the required insulin amount. Further, the calculated adequate amount of insulin is injected per the measured blood glucose. A high blood glucose level requires increased insulin amount and vice versa. Then, the requisite amount of insulin is injected subcutaneously which enters the blood in approximately 15 min. Further, the blood glucose is adjusted by either injecting additional insulin or consuming additional carbohydrates till the balance is achieved (Pareta et al., 2013). This strategy has associated limitations like, rapid fluctuations in blood glucose and patient inconvenience. The rapid glucose fluctuations lead to many severe secondary complications like, nephropathy, retinopathy, neuropathy and cardiovascular diseases (Kort et al., 2011; Opara et al., 2010). Per the Diabetes Control and Complications Trial (DCCT), non-fluctuating blood glucose levels may have positive impacts on prevention of diabetes-related secondary complications (Pareta et al., 2013).

Table 1.1. *Therapeutic strategies for diabetes therapy, advantages and limitations*

Serial No.	Therapeutic Strategies	Advantages	Limitations	References
1.	Exogenous Insulin Therapy	Standard therapy since the discovery of insulin, Popular technique	Rapid glucose fluctuations & poor glucose control, Secondary complications (nephropathy, neuropathy, retinopathy)	(Control and Group, 1993; Kort et al., 2011; Opara et al., 2010; Pareta et al., 2013)
2.	Pancreas Transplantation	Reproducibly achieves normoglycemia	Shortage of donor, Major surgery, Life-long immunosuppression required, Limited survival rate	(Kelly et al., 1967; O'sullivan et al., 2011; Pareta et al., 2013; Sutherland et al., 2012)
3.	Islet Transplantation	As effective as pancreas transplantation, Less invasive, Shorter hospital stay, Lower-associated morbidity	Low islet isolation efficiency (< 50%), Two or more donors required for one patient, Expensive, Autoimmunity & immune attack, Graft failure	(Blondet et al., 2007; Frank et al., 2004; Hatziavramidis et al., 2013; O'sullivan et al., 2011; Pareta et al., 2013; Shapiro et al., 2000)
4.	Bio-artificial Pancreas	Substitute the native pancreas, Good alternative to pancreas/ islet transplantation	To be explored more	(Calafiore et al., 2006a; Elliott et al., 2007; Pareta et al., 2012; Pareta et al., 2013)

1.2.1.2. Whole pancreas transplantation

As a better treatment option, Kelly et al. performed the first clinical pancreas transplant at the University of Minnesota in 1966 (Kelly et al., 1967). Pancreas transplantation is the only strategy available that reproducibly achieves normoglycemia by re-establishing glucose responsiveness. However, most of the transplanted pancreatic grafts are from cadaveric donors and the transplantation process necessitates major

traumatic surgery and dependence on life-long immunosuppression to prevent graft rejection (Robertson, 2000; Sutherland et al., 2001; Sutherland et al., 2012). Due to the limited availability of human pancreases and the need for immunosuppression, relatively fewer pancreas transplants are performed in relation to the entire diabetic population and it hinders the progress in treatment of a large section of diabetic patients globally (Pareta et al., 2013).

1.2.1.3. Islet transplantation

Islet transplantation is considered a promising treatment to restore normoglycemia in type 1 diabetic patients; more successful than exogenous insulin injections and as effective as pancreas transplantation because the islets can function both as sensors of glucose and source of new insulin (Hatziavramidis et al., 2013; Niknamasl et al., 2014; O'sullivan et al., 2011; Pareta et al., 2013; Shapiro et al., 2000). In islet transplantation, blood glucose level matches much closer to physiological level which results in a reduction in the frequent blood glucose fluctuations (Pareta et al., 2013). This approach is much less invasive compared to whole pancreas transplantation, with lower-associated morbidity and patients have shorter hospital stay. However, it is associated with the burden of immunosuppression but the drugs are not as strong as administered in whole pancreas transplantation (Faradji et al., 2008; Shapiro et al., 2000). The immunosuppression strategy has many associated side-effects and the complications of undesired over-immunosuppression. The other limitation are lower islet isolation/ harvesting efficiency (< 50%), considerable loss of islets (~60%) during islet infusion through portal vein therefore necessitates multiple donors (2-4) for one diabetic patient (Del Toro-Arreola et al., 2016; Vlahos et al., 2017). Autoimmunity/ immune attack, severe shortage of donors and graft failures are other concerns associated with islet transplantation (Hatziavramidis et al., 2013; Pareta et al., 2013).

1.2.1.4. Artificial pancreas

To circumvent the aforementioned problems, a new concept of artificial pancreas came into picture. The artificial pancreas is a device which enables Type 1 diabetes patients to automatically control their blood glucose by releasing requisite amount of insulin like a healthy pancreas (Pareta et al., 2013). There are various approaches to artificial pancreas development as listed below:

(a) Medical equipment approach – An insulin pump under closed-loop control which utilizes real-time data from a continuous blood glucose sensor (Pareta et al., 2013).

(b) Gene therapy approach – This approach involves therapeutic infection of a few intestinal cells in diabetic patient by genetically engineered virus. The infection causes DNA transformation turning intestinal cells to insulin-producing cells. Although, it is a novel and efficient approach for diabetes treatment, still it is in infancy with many unanswered questions associated with it. This approach has been advocated as procedure to tackle autoimmunity and destruction of β cell (Pareta et al., 2013; Rothman et al., 2005).

(c) Bioengineering approach – This approach utilizes the principle to develop bio-artificial pancreas by islet encapsulation in semi-permeable membrane to protect islets from host's immune system. The bio-artificial pancreas is a device which encapsulates and maintains islets of Langerhans and works as a replacement of the destroyed β cells in Type 1 diabetes patients. It may be developed as microcapsules, macrocapsules, conformal coatings, scaffold, hydrogel, microsphere, membrane, layer-by-layer coating and 3D foam as listed in **Table 1.2** (Hamilton et al., 2017; Inoo et al., 2018; Jiang et al., 2017; Liu et al., 2016; Luan et al., 2010; O'sullivan et al., 2011; Qi et al., 2010; Shalaly et al., 2016; Vaithilingam et al., 2017; Weber et al., 2008). The macrocapsules are usually in the range of 3-800 μm while the macrocapsules are generally larger than 1 mm in diameter (Rabanel et al., 2009). When implanted *in vivo*, these devices substitute the defective native pancreas and respond to blood glucose levels by secreting adequate amount of insulin (Calafiore et al., 2006a; Elliott et al., 2007; Pareta et al., 2013). A bio-artificial pancreas is consists of living and non-living parts. The living part, islets acts as a glucose sensor and secretes adequate amount of insulin in the blood stream. The non-living part provides native-like micromilieu to the islets and protects from host's destructive immune mechanisms (Borg and Bonifacio, 2011; Pareta et al., 2013)

Table 1.2. *Biomaterial formats used for islet encapsulation*

Serial No.	Biomaterial	Encapsulation device	References
1.	Alginate - Calcium/ Barium Chloride	Microcapsule	(Duvivier-Kali et al., 2001; O'sullivan et al., 2011; Safley et al., 2008; Vaithilingam et al., 2017)
2.	Poly ethylene glycol (PEG)	Conformal coating, Microcapsule, Macrocapsule	(Lee et al., 2004; Weber et al., 2008)
3.	Agarose	Macrocapsule, Microcapsule	(Iwata et al., 1994; Luan et al., 2010; Wong and Chang, 1991)
4.	Collagen, Gelatin	Scaffold, Hydrogel, Microsphere	(Hiscox et al., 2008; Inoo et al., 2018; Riopel and Wang, 2014)
5.	Poly vinyl alcohol (PVA)	Macrocapsule, Sheet, Conformal coating	(Nafea et al., 2011; Qi et al., 2004; Qi et al., 2010)
6.	Poly (lactic-co-glycolic acid) (PLGA)	Scaffold	(Daoud et al., 2011; Kheradmand et al., 2011; Liao et al., 2013; Liu et al., 2016)
7.	Chitosan	Hydrogel capsule, Conformal coating	(O'sullivan et al., 2011; Zhi et al., 2010)
8.	Poly -L-lysine (PLL)	Microcapsule	(de Vos et al., 2007; O'sullivan et al., 2011)
9.	Poly-L-ornithine (PLO)	Membrane	(Calafiore et al., 2006b; O'sullivan et al., 2011)
10.	Silica	Membrane, Gaseous deposition	(Boninsegna et al., 2003; O'sullivan et al., 2011)
11.	PVA-PEG blend	Conformal coating	(Nafea et al., 2011; Teramura et al., 2007)
12.	PLL-PEG blend	Conformal coating	(O'sullivan et al., 2011; Wilson et al., 2008)
13.	Poly (diallyldimethyl ammonium chloride)	Layer-by-layer coating	(O'sullivan et al., 2011)
14.	Polydimethylsiloxane (PDMS)	Scaffold	(Jiang et al., 2017; Weaver et al., 2015)

15.	Recombinant spider silk	3D Foam	(Johansson et al., 2015; Shalaly et al., 2016)
16.	Silkworm silk fibroin	Hydrogel, Scaffold	(Davis et al., 2012; Hamilton et al., 2017; Mao et al., 2017)

1.2.2. Biomaterials used in islet culture and encapsulation

The key aspects of islet encapsulation are: 1) Biocompatible matrix which closely mimics the pancreatic extracellular matrix (ECM) niche, 2) Matrix with immunoisolatory properties, 3) Matrix which supports drug/biomolecules loading for sustained and localized release, and 4) Vascularisation for exchange of nutrients and wastes (Pareta et al., 2013). The biomaterial which would be clinically more feasible for islet encapsulation should have the desirable properties viz., injectability, mechanical robustness , porosity to allow for tissue in-growth, vascularization for mass transport, ease of manufacturing, tuneability and lower cost.

Over the last three decades, there has been increase in developing novel scaffolds from various materials in different formats. The following section deals with various biomaterials used in fabricating islet encapsulation devices and their advantages and limitations are listed in **Table 1.3**.

1.2.2.1. Alginate

Alginate, an anionic polysaccharide, is biocompatible and its excellent gelling behaviour projects it for islet encapsulation applications (Fotino et al., 2015; Martinsen et al., 1989). Improper alginate purification leads to increased alginate immunogenicity and decreased islet viability as the impure alginate induces islet necrosis and inflammation (De Vos et al., 1997). The purified alginate polymers when added to water form a hydrogel when cross-linked with divalent cations (O'sullivan et al., 2011). To form microcapsules, an alginate-cell suspension is extruded as droplets from a syringe pump device into a cross-linking solution. Alginate, a biocompatible and easy to cross-link polymer has been extensively explored for islet encapsulation (Duvivier-Kali et al., 2001; O'sullivan et al., 2011; Safley et al., 2008; Vaithilingam et al., 2017). Alginate-calcium/barium chloride-based microcapsules have been utilized in mouse, dog and rat for successful diabetes reversal (**Table 1.4**). Alginate-based capsules have also been explored in human subjects with diabetes (O'sullivan et al., 2011; Soon-Shiong et al., 1993; Soon-Shiong et al., 1994; Vaithilingam et al., 2017; Vegas et al.,

2016). In our study, we would explore this gelling and encapsulating property of alginate in combination with silk matrices to develop islet encapsulating macrocapsules.

Table 1.3. *Biomaterials used for islet encapsulation, advantages and limitations*

Serial No.	Biomaterial	Advantages	Limitations	References
1.	Alginate - Calcium/ Barium Chloride	Biocompatible, Easy cross-linking	Inferior mechanical strength, Endotoxins	(Duvivier-Kali et al., 2001; O'sullivan et al., 2011; Safley et al., 2008; Vaithilingam et al., 2017)
2.	Poly ethylene glycol (PEG)	Injectable	ECM components required	(Lee et al., 2004; Weber et al., 2008)
3.	Agarose	Biocompatible, Immunobarrier	Thermogelation, Thermosensitivity	(Iwata et al., 1994; Luan et al., 2010; Wong and Chang, 1991)
4.	Collagen, Gelatin	Biocompatible, Biodegradable, Pre-vascularization	Immunogenicity, Improper immunoisolation	(Hiscox et al., 2008; Inoo et al., 2018; Riopel and Wang, 2014)
5.	Poly vinyl alcohol (PVA)	Injectable	Sub-zero temp. required for gelation	(Nafea et al., 2011; Qi et al., 2004; Qi et al., 2010)
6.	Poly (lactic-co-glycolic acid) (PLGA)	Enhanced mechanical strength	ECM peptide coating required, Pro-inflammatory, Acidic degradation product	(Daoud et al., 2011; Kheradmand et al., 2011; Liao et al., 2013; Liu et al., 2016)
7.	Chitosan	Biocompatible, Tunable	Thermosensitivity	(O'sullivan et al., 2011; Zhi et al., 2010)
8.	Poly -L-lysine	Perm-selectivity, Superior mechanical strength	Pro-inflammatory, Bioreactive	(de Vos et al., 2007; O'sullivan et al., 2011)

9.	Poly-L-ornithine	Perm-selectivity, Superior mechanical strength	Pro-inflammatory, Bioreactive	(Calafiore et al., 2006b; O'sullivan et al., 2011)
10.	Silica	Bio-inert, Immunoisolatory, Glucose responsive	Toxicity of by-products	(Boninsegna et al., 2003; O'sullivan et al., 2011)
11.	PVA-PLO blend	Perm-selective	Pro-inflammatory	(O'sullivan et al., 2011; Pareta et al., 2013)
12.	PVA-PEG blend	Enhanced islet viability	Lack of tuneability	(Nafea et al., 2011; Teramura et al., 2007)
13.	PLL-PEG blend	Enhanced islet viability, Better diffusion	Glucose irresponsive, Transient diabetes reversal	(O'sullivan et al., 2011; Wilson et al., 2008)
14.	Poly (diallyldimethlammonium chloride)	Provides layer-by-layer coating	Poor islet viability	(O'sullivan et al., 2011)
15.	Polydimethyl siloxane (PDMS)	Biostability, Fabricated into many geometries	Scaffold modifications required	(Jiang et al., 2017; Weaver et al., 2015)
16.	Recombinant spider silk	Easy functionalization	Lesser amount produced, High production cost	(Johansson et al., 2015; Nilebäck et al., 2017; Shalaly et al., 2016)
17.	Silkworm silk fibroin	Mimic native islet niche, easy to process, injectable, neo-vascularization, inherent RGD	Not much explored for islet encapsulation	(Davis et al., 2012; Hamilton et al., 2017; Kundu et al., 2013; Mao et al., 2017; Wang et al., 2008a)

1.2.2.2. Agarose

Agarose is another biocompatible and naturally occurring thermo-sensitive polymer found in the cell walls of seaweed that has been used for islet microencapsulation (O'sullivan et al., 2011). Agarose hydrogel with a gelling temperature of 15–30 ºC has been used for cell encapsulation and the gelling temperature is dependent on the

concentration of agarose used. Generally, formulations that remain gelled up to 60 ºC are used such that the capsules once formed will not melt in the range of mammalian body temperature. For agarose based cell encapsulation, either droplet extrusion (like alginate) or immersion in oil technique is used for cell encapsulation. Agarose-based islet encapsulation has been employed for islet encapsulation and transplantation in mouse and dog models with successful diabetes reversal (**Table 1.4**) (Gazda et al., 2007; Kin et al., 2002; Luan et al., 2010; O'sullivan et al., 2011). An agarose layer has been shown to be sufficient for islet immobilization, and an additional agarose coating prevents extrusion of cells and appears to be biocompatible, at least in the short term study (O'sullivan et al., 2011; Wong and Chang, 1991).

1.2.2.3. Polycations and anions

Poly-L-lysine (PLL) has been used as a positively charged coating on alginate to confer greater perm-selectivity and mechanical strength. However, the resulting capsules have the disadvantage of greater bioreactivity because PLL has been shown to initiate a pro-inflammatory response in the transplant setting (O'sullivan et al., 2011; Strand et al., 2001). To counteract this, an additional thin coating layer of alginate is usually added to serve as a barrier between the polycation and the host tissues. An alternative polycation, poly-L-ornithine (PLO) has also been explored in place of PLL owing to its perm-selectivity and better mechanical strength (Calafiore et al., 2006b; O'sullivan et al., 2011). Alginate microcapsules have been used with anionic polymer cellulose sulphate with some success (Fotino et al., 2015; O'sullivan et al., 2011).

1.2.2.4. Chitosan

Chitosan is derived from naturally occurring chitin found in the shells of crustaceans and insects. Its biocompatibility and good handling properties make it useful in a range of applications such as a vehicle for the delivery of pharmaceuticals, filler in orthopaedic surgery and wound dressings to promote healing (Khor and Lim, 2003). When cross-linked with glutaraldehyde, it forms a hydrogel which is tuneable and biocompatible. Chitosan microcapsules have been reported to protect rat islets transplanted to diabetic mice for up to 4 weeks (O'sullivan et al., 2011; Yang et al., 2010). It has also shown promising results for diabetes reversal in canine model (**Table 1.4**) (Yang et al., 2016; Yang et al., 2010).

1.2.2.5. Collagen

Collagen has also been used for islet transplantation as it is a key component of extracellular matrix having biocompatibility and biodegradability attributes (Dufour et al., 2005). It has not proved useful as an immunoisolation material in itself but may provide benefits when pre-vascularized to promote survival of transplanted islets (Hiscox et al., 2008; O'sullivan et al., 2011). Collagen/gelatin has been explored in scaffold, hydrogel or microsphere formats for islet transplantation (Hiscox et al., 2008; Inoo et al., 2018; Riopel and Wang, 2014) and has shown promising results in mice and rat models (**Table 1.4)** (Lee et al., 2012; O'sullivan et al., 2011).

1.2.2.6. Silica

Silica encapsulation of islets has also proven to be an effective immune-barrier (Boninsegna et al., 2003). Deposition of gaseous silicon alkoxides occurs under inert conditions to form a porous siliceous matrix around the islets, with greater exposure time leading to greater thickness. This siliceous membrane is a fairly bio-inert surface that displays good transport properties and could serve as a reasonable alginate substitute. Most islet cells appear to be viable after silica deposition process and show glucose-dependent insulin secretion, but there is still concern over the toxicity of alcohol by-products associated with the process. Transplantation of silica-encapsulated rat islets showed normoglycemia in diabetic rat models for up to 12 week (**Table 1.4**). Despite evaluation of an extensive range of candidate materials for islet immunoisolation, there is yet no convincing evidence that the newer materials are superior to the more established alginate, agarose and PEG (O'sullivan et al., 2011).

1.2.3. Macrodevices/macrocapsules

In microencapsulation, islets have been encapsulated within selectively permeable polymeric membranes that permit the diffusion of glucose, nutrients, oxygen and insulin while restricting the influx of immune cells and their molecular components (Lim and Sun, 1980; Narang and Mahato, 2006). This strategy circumvented/reduced the use of immunosuppressive drugs and their multiple side-effects that encompass systemic immune suppression and secondary complications (O'sullivan et al., 2011). The general immunoisolation techniques include both micro and macroencapsulation. Much of the work for bio-artificial pancreas (BAP) development has focused on microencapsulation of single or small groups of islets. This technique has inherent

Table 1.4. *Islet donor and recipient animal models used for encapsulated islet transplantation*

Serial No.	Biomaterials	Islet source	Diabetic animal model used	References
1.	Alginate - Calcium/ Barium Chloride	Mouse, Rat, Dog, Pig, Human	Mouse, Dog, Rat Human	(O'sullivan et al., 2011; Soon-Shiong et al., 1993; Soon-Shiong et al., 1994; Vaithilingam et al., 2017; Vegas et al., 2016)
2.	Poly ethylene glycol (PEG)	Mouse, Rat, Pig	Mouse	(Hill et al., 1997; Lin and Anseth, 2009; Wilson et al., 2008)
3.	Agarose	Mouse, Hamster, Pig	Mouse, Dog	(Gazda et al., 2007; Kin et al., 2002; Luan et al., 2010; O'sullivan et al., 2011)
4.	Collagen, Gelatin	Mouse	Mouse, Rat	(Lee et al., 2012; O'sullivan et al., 2011)
5.	Poly vinyl alcohol (PVA)	Hamster, Rat, Mouse	Mouse	(Nafea et al., 2011; Qi et al., 2004; Qi et al., 2010; Teramura et al., 2007)
6.	Poly (lactic-co-glycolic acid) (PLGA)	Human, Mouse	Mouse	(Daoud et al., 2011; Kheradmand et al., 2011; Liu et al., 2016)
7.	Chitosan	Mouse, Pig, Dog	Mouse, Dog	(Yang et al., 2016; Yang et al., 2010)
8.	Silica	Mouse, Rat	Mouse	(Boninsegna et al., 2003; O'sullivan et al., 2011)
9.	PVA-PEG blend	Hamster	Mouse	(Nafea et al., 2011; Teramura et al., 2007)
10.	PLL-PEG blend	Human, Mouse	Mouse	(O'sullivan et al., 2011; Wilson et al., 2008)
11.	Polydimethyl siloxane (PDMS)	Mouse	Mouse	(Jiang et al., 2017; Weaver et al., 2015)
12.	Recombinant spider silk	Mouse, Human	Mouse	(Johansson et al., 2015; Shalaly et al., 2016)

13.	Silkworm silk fibroin	Mouse	Mouse	(Davis et al., 2012; Hamilton et al., 2017; Mao et al., 2017)

detrimental limitations like low mechanical strength of the capsules, poor retrieval if necessary and short lifespan *in vivo* (O'sullivan et al., 2011). These limitations establish the portal for exploiting 'macroencapsulation', endowed with multiple advantages including concepts such as reloadable scaffolds with cells (O'sullivan et al., 2011; Qi et al., 2004).

Macrocapsules are a larger device designed to contain a greater amount of islets. An attractive aspect of macrodevices is that they may be retrieved and/or reloaded. Various designs and materials consisting of polymer membranes have been used including planar devices that could be discs or sheets, between which tissue resides as a thin layer (Suzuki et al., 1998). Similarly, hollow fibers have also been used as macrodevice (Lacy et al., 1991). The issues about biocompatibility and porosity are similar to those considered for microencapsulation, but macrodevices typically have greater mechanical strength. Considering the size of the macrodevices the packing density must be maximized so as to minimize the size of the device. Through bioengineering and the use of pro-angiogenic factors, there may be ways to promote development of a vascular network or indeed pre-vascularize macrodevices before insertion of the islets/cells to be transplanted (Lee et al., 2009; Trivedi et al., 2000). Although countless materials in various configurations have been tested, it remains to be seen whether any of these will be suitable for islet transplantation in humans. The available materials are not perfectly biocompatible; some degree of tissue reaction in the host is always evident, especially in larger animals. The geometry and diffusion properties of encapsulation devices are also critical for optimizing encapsulated tissue oxygenation (O'sullivan et al., 2011).

1.2.4. Islet encapsulation and immunoisolation

One approach to improve the outcomes of islet transplantation is immunoisolation, where islets are encapsulated in a selectively permeable polymeric membrane that allows the exchange of glucose, oxygen, nutrients, and insulin while restricting the entry of immune cells and protects the islets against the host immune response (Hatziavramidis et al., 2013; Lim and Sun, 1980). If a sufficiently effective and safe immune-isolation device for use in islet transplantation in humans can be found, it will

lead to an escape from harmful immunosuppressive drugs (O'sullivan et al., 2011). Semi-permeable microcapsules for immune-isolation were first described by Chang in the 1960s (Chang, 1964). He proposed the use of polymer membranes to contain and deliver enzymes and cells to the bloodstream to treat a deficiency (Chang, 1964). The concept of immune-barrier protection for islets was first described in 1977 by Chick et al (Chick et al., 1977). A device was implanted in diabetic rats in which islets were placed on the outside of hollow tubes made of a semi-permeable acrylic copolymer, which carried blood as an arteriovenous shunt. The idea behind this vascularized bio-artificial pancreas was that the membrane should be permeable to small molecules like glucose, oxygen, insulin, and nutrients but impermeable enough to prevent immune destruction (Colton, 1995; Lacy et al., 1991; Lim and Sun, 1980; O'sullivan et al., 2011). The devices restored normoglycemia for a period of hours before their removal (Chick et al., 1977).

Macrodevices, which rely on diffusion, have also been used to provide immune-protection to transplanted islets (O'sullivan et al., 2011). In 1991, Lacy et al. reported reversal of diabetes in rats transplanted subcutaneously and intraperitonially with acrylic hollow fibers containing islets immobilized in alginate for up to 60 days (Lacy et al., 1991). With both micro- and macroencapsulation, inadequate oxygenation has been a significant obstacle in the way of long-term graft success (Colton, 1995). Central necrosis is commonly observed in islets recovered after transplantation. In preclinical studies, the biocompatibility of the materials and device design issues remain ongoing problems. If these issues can be addressed, immunoisolation provides an attractive means of protecting transplanted islets from rejection (O'sullivan et al., 2011).

1.2.5. Islet encapsulation and immunomodulation

Although, the necessary biological cues for the islets are provided by the 3D biomaterial matrices as mentioned in **Table 1.2 & 1.3**, the autoimmunity in case of type 1 diabetes and tissue damage due to surgery evokes inflammation and alters the immune environment of the implants (Kumar et al., 2017; Liu et al., 2016). This process poses additional hurdles as the transplanted islets under such stress secrete pro-inflammatory factors thus amplifying local inflammation (Kumar et al., 2017; Piemonti et al., 2002; Weaver et al., 2015). In order to improve the long-term function of transplanted islets, an islet encapsulating matrix primed with anti-inflammatory and

immunomodulatory factors is a better option as it facilitates implant vascularization and islet engraftment simultaneously preventing islet destruction by immune cells (**Table 1.5**) (Davis et al., 2012; Foster and García, 2017a; Hamilton et al., 2017; Jiang et al., 2017; Kumar et al., 2017; Liu et al., 2016). Localized delivery of such factors at implantation site has shown promising outcomes as an effective therapy to prevent immune targeting of islets and eliminate the need for lifelong systemic immunosuppression (Foster and García, 2017a). Macrophages, the key players in immunoregulation, are actively involved in tissue remodelling and vascularization. Mature macrophages (M0) when exposed to appropriate stimuli (cytokines, pathogens etc.) are polarized towards pro-inflammatory (M1) or anti-inflammatory (M2) phenotype (Arango Duque and Descoteaux, 2014; Italiani and Boraschi, 2014).

Table 1.5. *Biomaterial-based immunomodulation approach for islet encapsulation*

Serial No.	Biomaterials	Immunomodulatory factors used	References
1.	Alginate	Mesenchymal stem cells, Nitric oxide-synthase inhibitor with erythrocytes; Sertoli enriched testicular cell fractions	(Vaithilingam et al., 2017; Wiegand et al., 1993; Yang and Wright Jr, 1999)
2.	Poly ethylene glycol (PEG)	Interleukin -1 receptor; Tumor necrosis factor α (TNFα)-antagonizing peptide; Human endoderm kidney (HEK293) cells	(Lin et al., 2009; Su et al., 2010)
3.	Agarose	Soluble domain of human complement receptor 1 (sCR1)	(Luan et al., 2010)
4.	Poly (lactic-co-glycolic acid) (PLGA)	Transforming growth factor-beta 1 (TGF-β1); Splenocytes	(Kheradmand et al., 2011; Liu et al., 2016)
5.	Polydimethylsiloxane (PDMS)	Dexamethasone	(Jiang et al., 2017; Weaver et al., 2015)
6.	Silkworm silk fibroin	Mesenchymal stromal cells (MSCs)	(Davis et al., 2012; Hamilton et al., 2017)

Recent advances in tissue engineering and regenerative medicine illustrate the importance of 'immuno-informed' biomaterials to regulate the microenvironment of

biomedical implants (Kumar et al., 2016a; Reeves et al., 2015). Macrophages are also the prevalent infiltrating immune cells attacking islets post-transplantation which play crucial role in implant rejection (Kumar et al., 2017; Wu et al., 2000). In this regard, biomaterials loaded with bioactive molecules is an ideal ferry for sustained release at transplantation site (Jiang et al., 2017; Kumar et al., 2016a; Kumar et al., 2017; Zhang et al., 2011). When primed with anti-inflammatory and immunomodulatory factors, islet encapsulating matrices help in islet protection by inhibiting the immune cell infiltration and polarizing them to anti-inflammatory and immunosuppressive phenotypes (Kumar et al., 2016a; Kumar et al., 2017; Reeves et al., 2015; Weaver et al., 2015). The initial release of these molecules post-transplantation prevents the production of pro-inflammatory cytokines within/near implant thus avoiding rejection (Liu et al., 2016).

Anti-inflammatory molecules/drugs polarize the M0 macrophages to M2 phenotype thus making the implant environment favourable (Kumar et al., 2016a; Kumar et al., 2017; Reeves et al., 2015). Out of several cytokines (Interleukins; IL-4, IL-10 and IL-13) known to influence an anti-inflammatory phenotype, IL-4 is known as immunosuppressive (Kumar et al., 2015). It encourages pro-inflammatory M1 macrophages to re-enter the cell cycle towards M2 by decreasing M1 activation and inducing M2 cell proliferation (Kumar et al., 2015). Furthermore, IL-4-induced secretion of IL-4, IL-10, transforming growth factor-β (TGF-β) and platelete-derived growth factor (PDGF) results in an amplification of M2 response (Kumar et al., 2015). These M2 macrophages help in decreasing inflammation through macrophage polarization or immunomodulation (from M0/M1 to M2) (Kumar et al., 2016a; Kumar et al., 2017; Kumar et al., 2015; Reeves et al., 2015). The secreted TGF-β promotes the differentiation of naïve $CD4^+$ T cells into regulatory T cells (T_{regs}) and deletion of effector T cells (T_{effs}) (Liu et al., 2016). Also, IL-4 prevents insulin dependent type 1 diabetes mellitus in nonobese diabetic mice by potentiating regulatory T helper-2 cells (Cameron et al., 1997). Similarly, M1 to M2 polarization has been reported by localized delivery of glucocorticoids, like Dexamethasone (Jiang et al., 2017).

1.2.6. Exploring silk as a potential biomaterial for islet encapsulation, immunoisolation and immunomodulation

The journey of silk from the domain of oriental medicine to the field of biomaterials is fascinating. Silk fibroin (SF) is obtained from varied sources like silkworms, spiders,

scorpions, honey bees, mites and flies (Kumar et al., 2016b; Vepari and Kaplan, 2007a). Mulberry (domesticated) and non-mulberry (wild) silkworm fibroins with distinct amino acid abundance (Wang et al., 2006); (Mandal and Kundu, 2009) have a long history of application as suture material in human body (Shao and Vollrath, 2002). Assured supply of domesticated silkworms, ease in processing and translation into different formats, complemented by superior mechanical properties and tuneable degradability make SF a suitable material for tissue engineering applications (Shao and Vollrath, 2002). High permeability to water and oxygen, low inflammatory response, low thrombogenicity, and adequate support for cell adhesion and growth are other desirable facets of SF as biomaterial (Gupta et al., 2011; Thurber et al., 2015). Silkworms can be classified into mulberry and non-mulberry. *Bombyx mori*, belonging to the family of Bombycidae produces mulberry silk and forms the centre of textile industry, whereas non-mulberry silk is produced by the members of Saturniidae and Lasiocampidae (Konwarh et al., 2017; Kundu et al., 2012). Processing of native silk obtained from the cocoons of silkworms is a prerequisite for the fabrication of silk based biomaterials. Degumming removes the water soluble sericin from fibroin (Vepari and Kaplan, 2007a). This is followed by regeneration of SF by dissolution in various solvents like chaotropic agents, ionic liquids or strong acids. The regenerated silk solution may be fabricated into a wide array of biocompatible formats (Rockwood et al., 2011).

In contrast to the mulberry, hydrogen bonds and hydrophobic regions lead to difficulty in dissolution of non-mulberry silk fibroin. Although there are few reports on dissolution of non-mulberry silk using chaotropic agents like LiSCN and ionic liquids, the low yield of protein through these methods has led to the utilization of glandular protein from non-mulberry silkworms (Kundu et al., 2012). Dissection of silk gland from mature larva of non-mulberry silk worms, followed by squeezing out of the gel-like silk and final dissolution in sodium dodecyl sulfate (SDS) offer an alternative harvesting strategy from the wild varieties (Mandal and Kundu, 2008). The presence of RGD (Arginine-Glycine-Aspartic acid or Arg-Gly-Asp) sequence in the wild type silks, and its absence in the domesticated silks, play a vital role in the differential cell-material interactions (Mandal et al., 2010). This is borne out by the integrin-binding RGD peptide sequence which improves cell adhesion and proliferation (Mandal et al., 2010). Various SF-based processed formats including films, nets, 3D porous sponges,

hydrogels, capsules, nonwoven mats and microspheres have been investigated for tissue engineering applications (Vepari and Kaplan, 2007a).

1.2.6.1. Properties of silk: chemistry and structure

Silk protein in its natural form is comprised of two types of components: silk fibroin - the filamentous core protein and; sericin - the glue-like protein which holds fibroin together. *B. mori* silk fibroin from cocoons consists of two proteins, one heavy chain (H-chain) of ~390 kDa and another light chain (L-chain) of ~26 kDa which are present in a 1:1 ratio. Both the chains are linked by a single disulfide bond (Vepari and Kaplan, 2007a). Silk fibroin has high molecular weight in the range of 200-350 kDa or more. They are comprised of bulky repetitive hydrophobic domains interrupted by small hydrophilic domains (Konwarh et al., 2017; Kundu et al., 2013). The hydrophobic domains consist of short side chain amino acids in their primary sequence which assist in tight packing of the hydrogen bonded anti-parallel chains (β-sheets) of the protein (Vepari and Kaplan, 2007b). Another glycoprotein, P25 (25 kDa) is also non-covalently linked to the chains. H-chain, L-chain and P25 are held in the ratio of 6:6:1. The H-chain consists of hydrophobic domains which is comprised of Gly-X (X being Ala, Ser, Thr, Val) repeats that forms the beta-sheets. L-chain is hydrophilic in nature (Konwarh et al., 2017; Kundu et al., 2013). However, non-mulberry silk lacks L-chain and P25, and contains homodimer of H-chain. Higher Alanine:Glycine ratio and poly-alanine blocks in non-mulberry silk forms beta-sheets. It also possess higher ratios of basic/acidic, polar/non-polar, hydrophilllic/hydrophobic, bulky/non-bulky amino acids. As a result, non-mulberry silk differ from mulberry silk in various aspects such as mechanical properties, biodegradation etc. (Kundu et al., 2013; Vepari and Kaplan, 2007b). Non-mulberry silk is also characterized by the presence of tri-peptide motif RGD which is a recognition site for integrin mediated cell adhesion (Konwarh et al., 2017).

1.2.7. Silk as a biomaterial

Many polymeric materials, synthetic and natural, have been widely explored for islet encapsulation applications. Each material has its own advantages and limitations (**Table 1.3**). Protein being a component of extracellular matrix seems to be a rational choice as biomaterial. Silk protein has various advantages as compared to other biopolymers because of its enhanced mechanical properties, good biocompatibility,

bulk production, easy water-based processing, biodegradability and functional modifications (Konwarh et al., 2017; Kundu et al., 2013).

1.2.7.1. Biocompatibility

Silk has been most extensively used as sutures and surpassed even collagen-based sutures; like Catgut™ (Kurosaki et al., 1999). Silk induced lower inflammatory response compared to collagen and poly-lactic acid (PLA) (Meinel et al., 2005). In this regard, silk fiber-based non-woven mats when subcutaneously implanted into rats showed very mild inflammation, without invasion of lymphocytes (Dal Pra et al., 2005). Further, 3D silk scaffolds when implanted in Lewis rats, led to mild immune response at the end of one year (Kundu et al., 2013; Wang et al., 2008b). The studies thus indicated that silk-based biomaterials have good biocompatibility and can be used for biomedical applications. Food and Drug Administration (FDA) has approved silk-based surgical mesh, SeriScaffold™, SericaTechnologies Inc, for clinical applications (Horan et al., 2009; Kundu et al., 2013). Also, silk based scaffolds have been successfully tested for various tissue engineering applications such as bone, cartilage, skin, liver, blood vessel, inter vertebral tissue, meniscus, cornea, pancreas etc (Konwarh et al., 2017; Kundu et al., 2013).

1.2.7.2. Biodegradation

Silk is an enzymatically degradable biopolymer (Arai et al., 2004; Nair and Laurencin, 2007). The *in vitro* biodegradation of silk is estimated by evaluating loss in matrix mass, alteration in morphology and analysis of degraded products. On the other hand, *in vivo* degradation is quantified by analysing mechanical properties and structural integrity of the retrieved matrices using histology or fluorescent imaging (Kundu et al., 2013). Silk sponges, when implanted in rats, were completely degraded within one year and the degradation process was mediated by macrophages indicating that the silk is bioresorbable (Wang et al., 2008b). Rate of degradation of silk matrices can be tuned by varying the processing parameters. Sponges of higher protein concentration degrade slower than that of lower concentration likewise, the aqueous-based scaffolds degrade faster than solvent-based scaffolds (Kim et al., 2005; Kundu et al., 2013).

1.2.7.3. Mechanical properties

Silk from silkworm has excellent mechanical properties owing to the presence of ordered crystalline regions of beta sheets (Altman et al., 2003; Vollrath and Knight, 2001). It has an attractive elongation, breaking strength and modulus which provides strength and toughness. The strength-to-density ratio of silk is up to ten times higher than that of steel and silk fibers are even tougher than Kevlar (Giesa et al., 2011; Kundu et al., 2013).

1.2.8. Silk matrices used for islet culture and encapsulation

1.2.8.1. Hydrogels

There are few recent reports wherein the utility of *B. mori* silk hydrogel for islet encapsulation has been reported for *in vitro* (Davis et al., 2012) and *in vivo* (Hamilton et al., 2017) studies. In the *in vitro* study, mice islets in silk hydrogel were co-encapsulated with ECM proteins (collagen IV and laminin) and mesenchymal stromal cells (MSCs) for providing native-like microenvironment to enhance the islet viability and functions (Davis et al., 2012). The MSCs are known to have immunomodulatory attributes which help in maintenance of islet graft. In a 7 day *in vitro* encapsulation study, islets maintained viability and retained glucose responsiveness and insulin secretion. Islets with collagen IV and laminin proteins showed enhanced insulin secretion at day 2 and day 7, respectively. Also, when co-encapsulated with MSCs, a synergistic increment in insulin secretion was noted (Davis et al., 2012). Similarly, for co-encapsulated islets, upregulated expressions of functional islet genes (insulin I, insulin II, glucagon, somatostatin, PDX-1) and lower expressions of de-differentiation genes cytokeratin 19 and vimentin were reported. In the follow up animal study of 42 days, encapsulated islets were transplanted into the epididymal fat pads of streptozotocin (STZ)-induced diabetic mice (Hamilton et al., 2017). For these experiments three combinations were tested- (i) islets co-encapsulated in silk with 1×10^6 MSCs, (ii) islets encapsulated in silk alone; and (iii) islets pelleted in medium alone (no silk and MSCs) (Hamilton et al., 2017). Blood glucose levels of the transplanted mice were monitored and intraperitoneal glucose tolerance test (IPGTT) was performed upon return to euglycaemia. As per the result, mice with islets encapsulated in silk (only silk and silk with MSCs groups) showed a prompt euglycaemia. Recepient mice with only silk achieved euglycaemia in ~4 days, compared to ~9 days for islets in silk with MSCs and ~15 days for pelleted islets (Hamilton et al., 2017). However, the

IPGTT at 4 weeks post-transplantation was significantly improved in recipients with islets in silk with MSCs, compared to islets in silk alone and to pelleted islets post-glucose injection (Hamilton et al., 2017). As suggested by the authors, the dual immunomodulatory and angiogenic attributes of MSCs might have prevented the islet damage through immune cell infiltration and simultaneously aiding the graft revascularization (Hamilton et al., 2017). However, after retrieval, histological analysis of the retrieved graft showed spontaneous osteogenesis and chondrogenesis in MSCs-containing silk islet grafts. In the sections, undesired bone-like structures were noticed showing the limitations in using MSCs for immunomodulation during islet transplantation. Authors suggested that the future study will evaluate MSC stability and as an improvement silk matrices would be utilized for the localized delivery of the biomolecules (Hamilton et al., 2017). Also, for the functionalization of silk hydrogels, authors utilized external ECM derived proteins, collagen IV and laminin, for enhanced islet viability and function. Non-mulberry, *A. assama* fibroin with inherent integrin-binding RGD peptide can overcome this limitation.

1.2.8.2. Scaffolds

1.2.8.2.1. Silkworm silk scaffolds

A macroporous heparin-releasing silk fibroin scaffold (H-SF) was investigated for islet transplantation in diabetic mice (Mao et al., 2017). The scaffold was found to improve the transplantation outcomes in syngeneic animal model by promoting islet revascularization and survival. Scaffold was prepared by lyophilisation to preserve the biological activity of the encapsulated heparin. In further *in vitro* studies, islet when cultured on H-SF and SF (without heparin) scaffolds in the epididymal fat pad of the STZ-induced syngeneic diabetic mice, all the animal achieved euglycaemia and maintained for one year. Interestingly, the H-SF scaffolds seeded with islets achieved rapid reversal of hyperglycaemia with normal glucose responsiveness. The superior transplantation outcomes for H-SF are attributed to heparin which promotes islet revascularization and proliferation. This result was endorsed by the histology images from retrieved implants wherein islets and endothelial cells proliferation was observed which was further attested by vascular endothelial growth factor (VEGF) upregulation and better intra-islet vascular reformation. As evident from *in vivo* diabetic mice study, heparin-dependent activation of endogenous VEGF/VEGFR2 pathway was responsible for promoting islet revascularization and proliferation. This study for diabetes reversal

was conducted in syngeneic mice model. However, for allogenic or xenogenic transplantation, immunoisolation and immunomodulation is required for long term islet viability and function.

1.2.8.2.2. Spider silk scaffolds

To re-establish the microenvironment of isolated islets and enhance the engraftment post-transplantation, the usage of recombinant spider silk-based matrices functionalized with selected cell binding motifs has been studied (Johansson et al., 2015). The spider silk protein 4RepCT was designed in three different formats; 2D-film, fiber mesh and 3D-foam to provide physical support to the isolated islets. Cell-binding motifs from laminin (an ECM protein) were incorporated into the spider silk to mimic native islet microenvironment. Cultured mouse islets were examined for survival and physiology maintenance on these material formats. Follow up *in vivo* diabetes reversal studies were conducted in a mouse eye model for the ease of *in vivo* islet imaging of engraftment. Islets cultured on these silk foams *in vitro*, helped in enhanced revascularization with neighbouring endothelial cells as attested by intact islet morphology. Screened matrices were further assessed for long term culture and maintenance of human islets wherein the matrices having RGD cell-binding motifs showed enhanced human islet maintenance; 36% to 79% compared to 28% for control islets (suspended). Also, the islet's morphology and physiology were preserved for over 3 months *in vitro* with cell-matrix connections formed with blood vessel-like structures along the silk matrices. Also, RGD motifs helped in the development of new islet-like clusters. Interestingly, in 1 month culture study, the islets from younger donors (< 35 year) had double the newly formed islet-like clusters compared to initial seeded islets (Johansson et al., 2015). In another study with spider silk, authors tried *ex vivo* expansion of endocrine islet cells for the development of transplantable pancreatic islets (Shalaly et al., 2016).

The authors developed a protocol wherein spider silk matrices were functionalized with ECM-derived motifs. These scaffolds were utilized for insulin-secreting islet-like spheroid formation from mouse (MIN6m9 cell line) and human endocrine cells. Conventional molecular cloning techniques were used to insert short peptides (RGD, RGE, FN and VN) at the N-terminus or in the repetitive part (2R and 3R) of the recombinant spider silk protein 4RepCT (herein denoted WT) (Hedhammar et al., 2008). It was seen that 3D silk matrices promoted islet-like spheroid development and maintained glucose-responsiveness *in vitro*. Further, *in vivo* imaging

of the transplanted murine clusters showed engraftment with increased vessel density overtime. Overall, the results showed that the spider silk-based 3D matrices are promising biomaterial platforms for developing islet-like clusters from insulin-secreting beta cells which are functional *in vivo*. Although, the bioactive recombinant silk shows great potential, but the production is less cost-effective than silkworm silk (Nilebäck et al., 2017). Bulk production of *Bombyx mori* silk fibroin and inherent RGD peptide rich non-mulberry *A. assama* silk fibroin may also help in this regard.

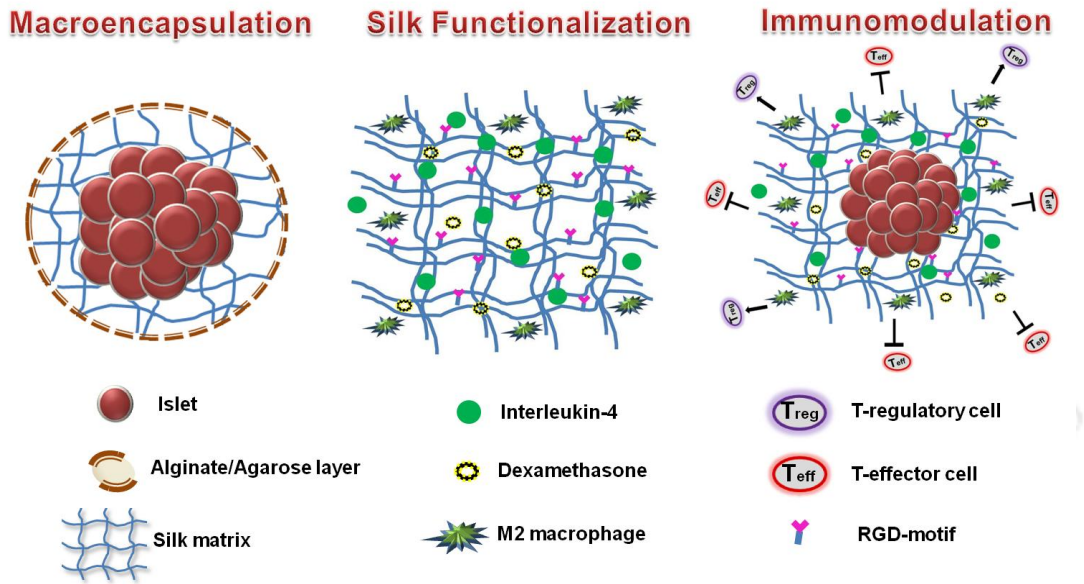

Figure 1.1. *Schematic illustration of the overall approach for islet protection using silk-based macroencapsulation which confers immunoisolation and immunomodulation. In macroencapsulation approach, silk-scaffold was utilized as islet culture platform and alginate/agarose was incorporated as barrier to provide protection i.e. immunoisolation. The barrier prevents the infiltration of host immune cells, simultaneously allowing the exchange of glucose, oxygen, and insulin. Immunomodulation approach involves localized and controlled release of dexamethasone and interleukin-4 from functionalized silk matrices creating a favourable local immunomodulatory microenvironment by promoting local anti-inflammatory macrophages (M2).*

Keeping in mind the above-mentioned challenges, we target islet encapsulation through silk by opting two strategies. Firstly, encapsulation of islets to prevent infiltration of immune cells and secondly, the local release of immunomodulatory molecules (dexamethasone and interleukin-4) from silk-based biomaterial systems that suppress local immunity (**Figure 1.1**).

MOTIVATION AND OBJECTIVES OF THE PRESENT INVESTIGATION

MOTIVATION AND OBJECTIVES OF THE PRESENT INVESTIGATION

Based on the existing literature, as highlighted in Chapter 1, it is quite evident that the silk biomaterial-based islet encapsulation approach provides an attractive proposition for islet delivery *in vivo* by providing protective three-dimensional (3D) support for islet function. It has thus come to the forefront as potential therapeutic approach for treating type 1 diabetes. Furthermore, the assistive approach of immunoisolation and immunomodulation associated with this encapsulation technique helps in enhancing the utility of the implant by overcoming immune rejection. The origin of the present investigation and the salient motivating factors stem from the following assertions:

1. Current therapeutic approaches for type 1 diabetes include exogenous insulin injection and pancreas transplantation. However, both the techniques are associated with several limitations viz., rapid blood glucose fluctuations and poor blood glucose control in insulin therapy and major surgery, shortage of donor and life-long immunosuppression in case of pancreas transplantation. Given this backdrop, there is an urgent need to create alternate therapeutic approaches which could adequately address the dual issue of blood glucose level maintenance and islet rejection. Upon encapsulation in 3D biomimetic microenvironment with suitable biochemical cues, the islet functions are preserved as the 3D matrix compensates for the native extracellular matrix (ECM) with enhanced cell viability, proliferation and desired insulin production.

2. Islet transplantation happens to be a promising treatment strategy for type 1 diabetes owing to its minimal invasiveness, and improved efficacy. However, majority of the work regarding islet encapsulation deals with microencapsulation of single or small groups of islets. However, this technique has inherent limitations like lower mechanical strength of the capsules, poor retrieval and short life span *in vivo.*

3. Silk sutures already have an existing history of safe use in surgeries. The recent exponential growth in tissue engineering and regenerative medicine has considered silk as a potential biomaterial. Silk, being a structural protein, is biocompatible, non-immunogenic, mechanically robust with tunable degradation rates. Silk protein is easy to process under a mild (aqueous) physiological-like conditions, and its degradation products are amino acids which can easily be metabolized *in vivo*. Silk bioresources are available in abundance and silk-based matrices have demonstrated exceptional advantages over conventional synthetic and other natural biomaterials in tissue engineering applications.

4. Arg-Gly-Asp (RGD) sequence has conspicuous effect on islet adherence, viability and revascularization owing to its interaction with several integrin variants. Natural and synthetic 3D matrices with externally tethered RGD peptides have shown promising outcomes for islet encapsulation and function maintenance. Recently, it has been reported that the non-mulberry silk, *Antheraea assama*, is enriched with RGD sequences which makes silk as an essential matrix for islet encapsulation.

5. Rapid to gel, injectable hydrogels are promising vehicles that can deliver encapsulated islets *in vivo* in a minimally invasive manner. The gelation property of such hydrogels under a mild (aqueous) physiological-like condition allows encapsulation of islets by preserving their functions. Moreover, accelerated gelation without any external stimulus or cross-linker provides an excellent platform for islet encapsulation and delivery. Blend of mulberry *B. mori* silk with non-mulberry *A. assama* fabricates a well integrated matrix with inherent cell binding Arg-Gly-Asp (RGD) sequence.

6. Being an autoimmune disease, pancreatic beta cells are selectively destroyed by the patient's own immune system. Furthermore, surgery-associated tissue damage evokes inflammation which alters the immune environment of the implants. Under such adverse conditions, encapsulated islets undergo tremendous stress and secrete their own pro-inflammatory molecules amplifying the local inflammation. To prevent such pitfalls, the recipients

require life-long administration of systemic immunosuppressive drugs which have detrimental side-effects. In contrast to systemic delivery, localized delivery of immunosuppressant at the implantation site is likely to ensure minimal side-effects and eliminate the need for systemic immunosuppression.

7. Recent advances in tissue engineering and regenerative medicine illustrate the significance of 'immuno-informed' biomaterials to regulate the microenvironment of biomedical implants. Macrophages, the key players in immunoregulation, are actively involved in tissue remodelling and vascularization. Macrophages are also the prevalent infiltrating immune cells attacking islets post-transplantation which play crucial role in implant rejection. Mature macrophages (M0) when exposed to appropriate stimuli (cytokines, drugs, pathogens etc.), are polarized towards pro-inflammatory (M1) or anti-inflammatory (M2) phenotype. Silk has been explored extensively for delivery of biomolecules and growth factors for different tissue-specific applications. Controlled localized release of anti-inflammatory cytokine interleukin-4 (IL-4) and dexamethasone might polarize resting M0 macrophages to M2 phenotype reducing local foreign body response and maintain immunosuppressive function.

In the light of the enormous scope of exploring silk biomaterial and its attributes for islet encapsulation, combating local inflammation, and improvement in islet engraftment, we analyzed our hypothetic approach through the pursuit of the following essential objectives:

Objectives:

1. Development of localized immunomodulatory silk-alginate/agarose-based scaffolds for islet-like spheroid formation and immunoisolation.
2. Macrophage polarization for immunomodulation and tailoring local biological response.
3. Development of minimally invasive injectable silk hydrogel as potential islet encapsulation and delivery matrix.

Chapter 2

Development of Localized Immunomodulatory Silk-Alginate/Agarose-based Scaffolds for Islet-like Spheroid Formation and Immunoisolation

This chapter enumerates the efficacy of silk-based islet-encapsulating 3D scaffolds to support islet functions and confer immunoisolation and immunomodulation. The primary islet maintenance, islet-like spheroid formation, immunomodulation and in vivo immunoisolation attributes are illustrated in detail.

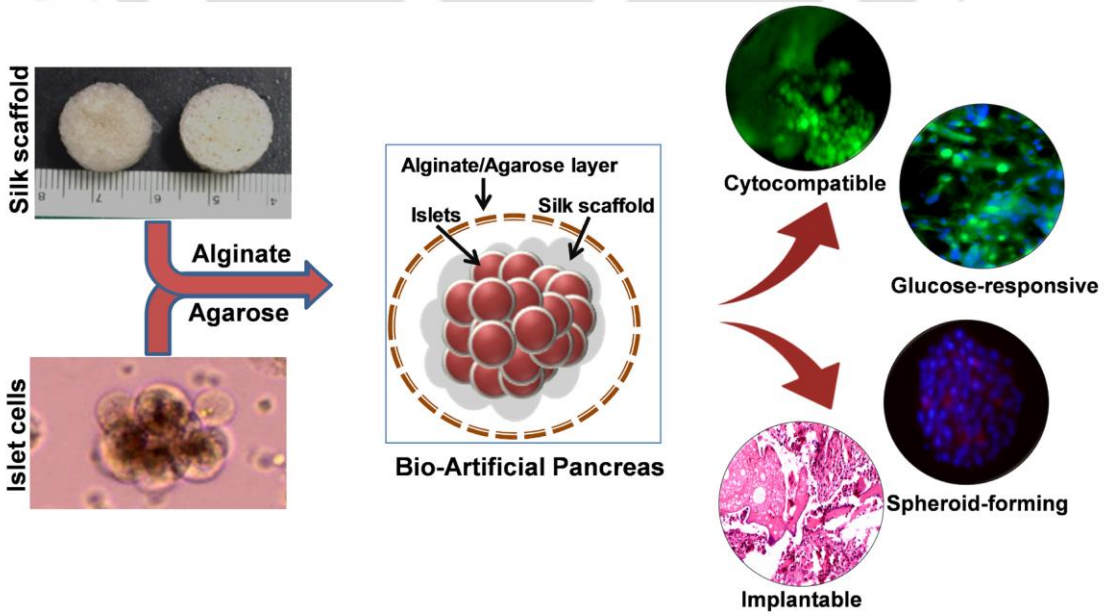

ABSTRACT

Pancreatic islet encapsulation in a 3D scaffolding matrix has achieved limited clinical success due to loss of islet function and cell death, shortly after transplantation. Also, transplant-associated inflammatory responses create an unfavorable microenvironment for islet survival. The current study delineates the development of cell-encapsulating immunomodulatory 3D silk scaffolds as bio-artificial pancreas (BAP) systems for sustained insulin release. Insulin producing cells were encapsulated inside silk scaffolds with either alginate or agarose for immunoisolation to augment islet survival and function. The scaffolds were extensively characterized for pore architecture, porosity, swelling index, water uptake and density. Further, suitability of these scaffolds was assessed through diverse in *vitro* tests, including cell adherence, viability, proliferation, 3D spheroid like pancreatic structures development, glucose stimulated insulin secretion and macrophage polarization. Rat insulinoma cells (RIN-5) cells were metabolically active within the macroencapsulates and proliferated up to 2.5-fold over 5 weeks in culture. Cultured cells formed 3D islet-like spheroids spontaneously. Primary islets maintained their function in macroencapsulates with enhanced glucose stimulation index when compared to non-encapsulated islet, 1.2 vs 1.7. RT-qPCR and immunohistochemistry results supported the results obtained from glucose challenge assay. Controlled release profiles of anti-inflammatory cytokine interleukine-4 (IL-4) and dexamethasone evinced their prospective application in reducing local foreign body response and immunosuppression. Released IL-4 was biologically active and polarized M0 macrophages to the M2 phenotype, advocating immunosuppressive function. Reduced inflammatory responses illustrated the biocompatibility of these scaffolds. In conclusion, this novel biomaterial system was successfully used to encapsulate insulin-producing cells with enhanced cell functions. Further development of the system may have potential BAP applications.

2.1. Introduction

Diabetes is a metabolic disorder affecting millions of people globally and a leading cause of morbidity and mortality (Daneman, 2006; Muthyala et al., 2011). The global incidence of diabetes is increasing exponentially as suggested by recent statistical data (National Diabetes Statistics Reports, 2014). Within the total diabetic population, type 1 diabetes represents around 10% of all diabetic patients, worldwide (Shalaly et al., 2016). Clinically, this form of diabetes is associated with hyperglycemia due to defects in insulin secretion, insulin production or both. The resultant symptomatic hyperglycemia is associated with eventual failure of several vital organs (Association, 2006). Islet transplantation is considered a promising treatment to restore normoglycemia in type 1 diabetic patients; more successful than insulin injections because the islets can function both as detectors of glucose concentration and as a source of new insulin. However, a shortage of donors, a high rate of implant rejection and the associated complicated procedures restrict widespread utility (Niknamasl et al., 2014; Shapiro et al., 2000).

To rein in the "diabetes epidemic", tissue engineering and regenerative medicine present a novel, effective solution for the replacement of diseased pancreas with engineered implants (Vacanti and Langer, 1999). Islets removed from natural extracellular matrices (ECM) and maintained in 2D culture become fragile and senescent, show decreased insulin expression (Shalaly et al., 2016) and tend to clump together leading to limited nutrient transfer (Beck et al., 2007). To address these issues, researchers have resorted to tissue engineering wherein, islets maintain structure and function when cultured in 3D porous scaffolds (Burdick and Vunjak-Novakovic, 2008). Different biopolymers have been investigated for these needs, including alginate, gelatin, collagen, chitosan, and agarose. Several devices such as hollow fibers, membrane chambers, and intervascular devices have also been designed to maintain 3D cultures (O'Sullivan et al., 2011).

The additional and vital requirement in type 1 diabetes treatment is combating the autoimmune aspect which demands immunoisolation of the islets from the host's immune system. For this, islets have been encapsulated within selectively permeable polymeric membranes that permit the diffusion of glucose, nutrients, oxygen and insulin while restricting the influx of immune cells and their molecular components (Lim and Sun, 1980; Narang and Mahato, 2006). This strategy circumvented the use of immunosuppressive drugs and their multiple side-effects that encompass systemic

immune suppression and secondary complications (O'Sullivan et al., 2011). The general immunoisolation techniques include both micro and macroencapsulation. Much of the work for bio-artificial pancreas (BAP) development has focused on microencapsulation of single or small groups of islets. This technique had inherent detrimental limitations like low mechanical strength of the capsules, poor retrieval if necessary and short lifespan *in vivo* (O'Sullivan et al., 2011). These limitations establish the portal for exploiting "macroencapsulation", endowed with multiple advantages including concepts such as reloadable scaffolds with cells (O'Sullivan et al., 2011; Qi et al., 2004). Currently, tissue engineering using silk protein as a biomaterial has been invigorated due to its biocompatibility, enhanced mechanical strength, easy sterilization, controlled rate of degradation and minimal inflammation *in vivo* (Thurber et al., 2015; Vepari and Kaplan, 2007). Silk has been processed into various formats such as gels, scaffolds or films for tissue engineering and drug delivery (Rockwood et al., 2011). These formats have been widely used for the development of range of engineered tissues with promising outcomes *in vivo* (Kasoju and Bora, 2012; Kundu et al., 2013). Pancreatic cell culture has been conducted with different materials and recent work with silk has shown promising results both *in vitro* (Davis et al., 2012) and *in vivo* (Hamilton et al., 2015) systems.

Alginate, a linear copolymer extracted from brown seaweed, has been extensively used in encapsulating proteins and cells under mild conditions of room temperature, physiological pH, isotonic solutions, and without harmful cross-linkers (de Vos et al., 2006). As an encapsulating agent, alginate has shown major advantages over other materials as it does not hinder islet cellular functions. Earlier, sodium alginate was used with calcium chloride ($CaCl_2$) (Pathak et al., 2010) for capsule formation, but these capsules had inferior mechanical strength. To improve upon this, poly-L-lysine (PLL) membranes have been used for making the capsules stronger and more selectively permeable (O'Sullivan et al., 2011); unfortunately, PLL is associated with enhanced foreign body responses (Strand et al., 2001). In the same mode, barium chloride ($BaCl_2$) was used to make efficient capsules with appropriate robustness and selectivity but without using polycationic PLL-like membranes (Zimmermann et al., 2007). Furthermore, silk-alginate blends promoted cell proliferation and functional outcomes in different tissue engineering and drug delivery applications (Mandal and Kundu, 2009; Ziv et al., 2014). Similar to alginate, agarose has also been extensively

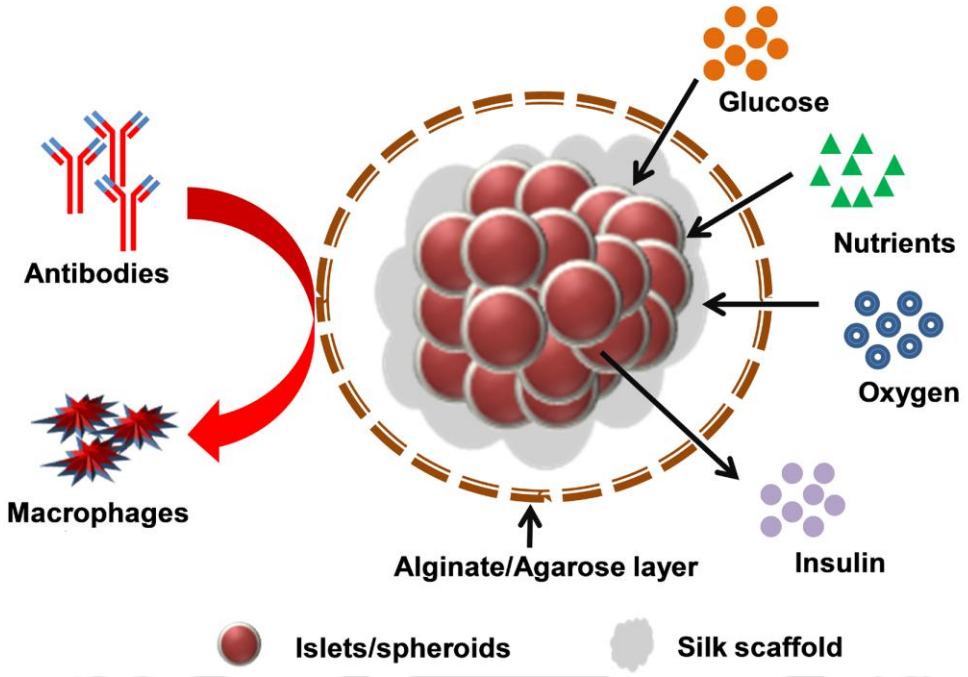

Figure 2.1. *Principle of silk-based bio-artificial pancreas (BAP) with three different attributes of spheroid formation, local immunomodulation and immunoisolation.*

used for islet encapsulation. Agarose is a linear polysaccharide and forms a thermo-reversible hydrogel. It is amenable to tissue engineering applications because of its biocompatibility, interconnected porous microstructure, tunable mechanical properties and long-term stability *in vivo* (Iwata et al., 1994; Iwata et al., 1992). In the present work, the objective was to exploit alginate and agarose as cell macroencapsulating agents along with silk as substrates for insulin-producing-cell adherence and proliferation with immunoisolatory attributes.

Despite of biological cues presented by 3D matrices, tissue damage due to surgery and implantation evoked inflammation and altered the immune environment of the implants (Liu et al., 2016). This process generated additional challenges for islet transplantation where stressed islets secrete their own pro-inflammatory factors, amplify local inflammation (Piemonti et al., 2002) and culminating in considerable islet tissue loss and dysfunction (McDaniel et al., 1996; Weaver et al., 2015; Wilson and Chaikof, 2008). Localized delivery of immunomodulatory factors with enhanced efficacy, reduced systemic side effects and toxicity has emerged as a strategy to control the immune response at implant site (Weaver et al., 2015). Thus, we hypothesized that IL-4 (anti-inflammatory cytokine) and dexamethasone (immunosuppressive drug) released from cell encapsulating scaffolds might decrease inflammation and delay immune rejection of the transplanted cells *in vivo*. This approach suggests that

macrocapsules primed with cytokines and drug could be used for local immunomodulation. Therefore, the developed macroencapsulating scaffolds were evaluated for three different attributes, (a) spheroid formation (b) local immunomodulation and (c) immunoisolation (**Figure 2.1**). Use of protein (silk) and saccharide (alginate/agarose) molecules as scaffolding matrix ensured minimal immunogenic response. Further, mild encapsulation conditions for both, alginate and agarose minimized islet loss during the process. Porous scaffold architecture was assumed to prevent islet aggregation and necrosis while facilitating good mass transport ability related to oxygen and glucose. It was also envisaged that the semi-permeable encapsulation membrane (alginate/agarose) would safeguard against direct blood contact and blood-mediated inflammation reactions (BMIR), while enhancing implant viability (Liao et al., 2013). We finally report the performance of these new silk-based macrocapsules with cultured islets/ islet-like spheroids with potential for bio-artificial pancreas.

2.2. Materials and Methods

2.2.1. Isolation of silk fibroin protein

Silk fibroin was extracted according to the procedures previously described (Mandal et al., 2009; Rockwood et al., 2011). Briefly, *B. mori* silk cocoons were cut into small pieces and degummed by boiling for 20 min in an aqueous solution of 0.02 M Na_2CO_3 (Sigma-Aldrich, USA). Degummed fibers were washed with distilled water and dried at 37 ºC. Fibers were dissolved in 9.3 M LiBr (Sigma-Aldrich, USA) solution at 60ºC for 4h. Further, the solution was dialyzed against distilled water for 3 days with frequent water changes (**Figure 2.2**). After dialysis the solution was centrifuged at 2000 rpm for 10 min to remove impurities. The final concentration was determined by gravimetric method by weighing the dry weight of protein.

2.2.2. Silk scaffold fabrication

Scaffolds were fabricated as reported previously (Rockwood et al., 2011). Briefly, 4 g of granular NaCl (particle size; 400-600 µm) was mixed in 2 mL of 8% (w/v) silk fibroin aqueous solution in a 24 well tissue culture plate (Tarsons, India). Plates were dried overnight at room temperature. After 24 h, ethanol (80% v/v) treatment was done for 1 h and porous 3D scaffolds were obtained by salt leaching (**Figure 2.2**).

2.2.3. Morphological analysis of scaffolds

Surface morphology and internal structure of scaffolds were analyzed using a field emission scanning electron microscope **(**FESEM, Zeiss, Sigma, USA**)**. Samples were frozen at ─80 ºC, followed by lyophilization and cross sections of the freeze-dried samples were prepared. FESEM images were acquired after gold sputtering at operating voltage of 20 kV.

2.2.4. Density and porosity measurements

The density and porosity of the scaffolds were measured using a liquid displacement method (Kim et al., 2005). Different scaffold variants (dry weight, W) were immersed in a known volume (V_1) of hexane in a graduated cylinder for 5 min. The total volume of hexane with the hexane-impregnated scaffold was recorded as V_2. The scaffold was then removed from the cylinder, and the residual hexane volume was recorded as V_3.

The density of the scaffolds was expressed as

$$\text{Density}=W/(V_2 - V_3) \quad \text{.....[2.1]}$$

and the porosity of the scaffolds was obtained by

$$\text{Porosity (\%)} = [(V_1 - V_3)/(V_2 - V_3)]\text{x}100. \quad \text{.....[2.2]}$$

2.2.5. Swelling

Swelling was studied using a conventional gravimetric procedure (Mandal et al., 2009). The initial dry weights of lyophilized scaffolds were recorded using an electronic balance (Sartorious, AG Germany). Scaffolds were immersed in phosphate buffered saline (PBS, pH 7.4, 37 ºC) and recovered after specific time points. Excess surface water was wiped off, and the rehydrated weight (W_r) was measured. The swelling ratio and water uptake in the scaffolds were calculated from the equations

$$\text{Swelling ratio}= (W_r - W_i)/W_i \quad \text{.....[2.3]}$$

$$\text{Water uptake (\%)} = [(W_r - W_i)/W_i]\times 100 \quad \text{.....[2.4]}$$

where W_r is the weight of the rehydrated sample and W_i is the initial dry weight (mg).

2.2.6. Maintenance of RIN-5 cell line

RIN-5 cells (rat insulinoma cell line) were procured from the National Centre for Cell Science (NCCS), Pune, India. Cells were maintained in RPMI 1640 medium supplemented with 10% fetal bovine serum (FBS), 2 mM of L-glutamine, 1 mM sodium pyruvate, 100 U/mL penicillin, and 100 µg/mL streptomycin (Gibco BRL

Rockville, USA). Cells were cultured in tissue culture flasks at 37 ºC in a humidified atmosphere of 5% CO_2. Once the cells reached 80-90% confluent state, they were split using 0.25% trypsin/EDTA (Gibco BRL Rockville, USA), and media were replenished twice a week.

2.2.7. Isolation and culture of primary rat islets

Primary rat islets were isolated per reported protocol (Li et al., 2009). Male Sprague Dawley rats (age 8─10 weeks) were used for pancreas harvesting. Animal experiments for harvesting pancreas were conducted under protocols approved by the Tufts Institutional Animal Care and Use Committee (IACUC, Tufts University, MA, USA). For islet isolation, rats were anesthetized and sacrificed with cervical dislocation. After excision, the pancreas was placed in a 50 mL tube containing 5 mL of collagenase XI (1000 U/ml, Sigma-Aldrich, USA) in 1× Hanks' balanced salt solution (HBSS, Sigma-Aldrich, USA; for one pancreas). The tube was placed in a water bath at 37 °C for 15 min and shaken two to three times manually during the incubation. Post-incubation, the tube was again shaken to disrupt the pancreas until the suspension turned homogeneous. Once the tissue suspension had dissolved into very fine particles, digestion was terminated by placing the tube on ice and adding 25 mL of 1 mM $CaCl_2$ (Sigma-Aldrich, USA) in 1× HBSS. This suspension was centrifuged at 290*g* for 30 s at 4 °C, and the supernatant was discarded. Then, the pellet was resuspended with 20 mL ice-cold 1× HBSS, centrifuged again at 290*g* for 30 s at 4 °C and the supernatant was discarded. For islet purification, the resulting pellet was resuspended with 15 mL of 1×HBSS. This resuspended solution was poured onto a pre-wetted 70 µm cell strainer. The tube was washed with 20 mL of 1× HBSS and poured again onto the strainer. Another 25 mL of 1× HBSS was poured through the filter. The strainer was turned upside down over a new Petri dish, and the captured islets were rinsed into the dish with 15 mL of RPMI 1640 with 20 mM L-glutamine. The isolated islets were counted and placed in 5% CO_2 incubator at 37 °C.

2.2.8. Preparation of cell macroencapsulating scaffolds

The scaffolds were pre-sterilized in a laminar flow hood with 70% (v/v) ethanol followed by repeated washing with sterilized PBS (pH 7.4) to remove residual alcohol. Scaffolds of desired dimensions (6 mm diameter, 2 mm height) were conditioned for 4

h in RPMI 1640 media. Further, media were completely removed from the scaffolds. Conditioned scaffolds were incubated for 30 min in 3% (w/v) $BaCl_2$ (Sigma-Aldrich, USA) solution, prepared in 0.9% (w/v) NaCl (pH 7.4). Prior to encapsulation, sodium alginate (Sigma-Aldrich, USA, from brown algae**,** Medium Viscosity) was filtered through 0.2 µm cellulose nitrate filter (Sartorius, Germany) (Zekorn et al., 1992). Islets (~800) pellets dissolved in 2% (w/v) sodium alginate solution (40 µL) were seeded into scaffolds uniformly in separate wells of 24 well plates. The scaffolds were left for 2 min for proper cross-linking of Ba^{2+} ions with sodium alginate to encapsulate the cells in the core. Further 30 µL of sodium alginate was added on the periphery of the scaffolds for complete encapsulation. Finally, scaffolds were washed three times with saline to wash out the residual $BaCl_2$. The encapsulated cells were maintained in incubators for further cell studies. For agarose-based macroencapsulation, previously reported protocols were followed with some modifications (Iwata et al., 1992; Yang et al., 1994). Low-gelling agarose type VII (Sigma-Aldrich, USA) was used. Conditioned scaffolds were seeded with ~800 islets and then left for 4 h in an incubator. A 5% (w/v) agarose solution was prepared in incomplete RPMI media by autoclaving. The solution was kept at 45 °C. Islet seeded scaffolds were individually dipped in 200 µL of agarose solution to cover the scaffold surface and left on ice for 1 min to allow agarose gelation. Cell culture was also conducted on control silk scaffolds without encapsulation. All the scaffolds were kept in incubators for further studies. A similar protocol was followed for RIN-5 with 5×10^5 cells. Also, similar number of islet cells was seeded in 24 well tissue culture plates for 2D controls.

2.2.9. Cell proliferation

Cell proliferation of RIN-5 cells on all the variants of scaffolds were monitored using AlamarBlue dye reduction assay (Life Technologies, Grand Island, NY, USA) at specified intervals following the manufacturers' protocol. Scaffolds without cells incubated with 10% AlamarBlue were used as experimental controls for all the scaffold variants. The seeded constructs were incubated for 4 h at 37 °C with 5% CO_2. Then, 100 µL of medium from each sample was taken, and absorbance was measured at 570 and 600 nm using a multiplate reader (Tecan infinite M 200 reader with i-control software).

2.2.10. Evaluation of spheroid formation and cell distribution in the scaffolds

Cell viability was assessed by Calcein AM (Sigma-Aldrich, USA) staining following the manufacturer's instructions. Briefly, cell seeded scaffolds were washed twice with PBS (pH 7.4) and incubated with 4 μM calcein AM, prepared in incomplete media (DMEM without FBS), for 20 min (at 37°C) to stain live cells. Post-staining, scaffolds were rinsed thrice with PBS, and fluorescent images were taken using an Inverted Florescence Microscope (EVOS FL, Life Technologies, USA) with a green filter (470 nm Ex, 525 nm Em). Viable cells convert calcein AM to calcein and fluoresce green. For comparison, images of RIN-5 cells in 2D culture were also captured. Cells were fixed in 10% neutral buffered formalin for 2 h. After fixation, cells were permeabilized using 0.1% (v/v) Triton X-100 in PBS for 30 min. Further, cells were stained with rhodamine-phalloidin (Life Technologies, USA), for F-actin (cytoskeleton) and counterstained with Hoechst 33342 for the nucleus. For evaluation of cell distribution, the scaffolds were incubated for 30 min in staining solution containing 1% (w/v) BSA, 0.1% (v/v) Triton X-100, 0.1% (v/v) Hoechst 33342 (Sigma-Aldrich, USA), and 0.1% (v/v) AdipoRed (AdipoRed Assay Reagent, Lonza, USA) in PBS. AdipoRed stains the silk matrix (red), and the nucleus was counterstained with Hoechst 33342 (blue). After staining, scaffolds were washed thrice, and images were captured using a KEYENCE all-in-one fluorescence microscope BZ-X700 (USA), and Z-stacking was performed using BZ-X Analyzer software.

2.2.11. *In vitro* cell function assessment in scaffolds

2.2.11.1. Insulin release study and enzyme-linked immunosorbent assay (ELISA)

Cell function was assessed *in vitro* by glucose challenge assay as previously reported (Davis et al., 2012). RIN-5 cells and primary islets were seeded in the scaffolds and cultured in a 24-well culture plates. For RIN-5 cells, assays were done after 35 days of culture and for primary islets after 14 days. Scaffolds were washed for 5 min with 3.3 mM glucose in Krebs-Ringer buffer (0.1% BSA, 25 mM HEPES, 115 mM NaCl, 5 mM KCl, 1 mM $MgCl_2$, and 24 mM $NaHCO_3$). After washing, the samples underwent a static incubation for 60 min each, with low (3.3 mM) followed by high (17 mM) glucose concentrations in a Krebs-Ringer buffer. Insulin secretion was measured using a rat insulin ELISA kit (Mercodia, Uppsala, Sweden). For islets in TCP (tissue culture plate), cells were centrifuged, pelleted and incubated similar to the scaffold groups. Values were obtained from standard curves and are reported as stimulation index (SI),

which is the ratio of insulin secreted with high glucose stimulation over insulin secreted with low glucose stimulation (Davis et al., 2012).

2.2.11.2. Immunofluorescence for insulin and glucagon

To confirm the presence of insulin and glucagon, cell-seeded scaffolds were immunostained. RIN-5 cells and primary islets were immunostained after 35 and 14 days of culture, respectively. Cell-seeded scaffolds were washed in PBS followed by fixation in 10% neutral buffered formalin for 24 h at room temperature. Further, samples were dehydrated through a series of graded ethanol and cleared in xylene. Subsequently, they were embedded in paraffin wax and sectioned at 5 μm thickness using microtome (Leica BIOSYSTEMS). For immunofluorescence, sections were deparaffinized, cleared, and rehydrated through a series of graded ethanol and permeabilized in PBS containing 0.1% Triton-X 100 for 30 min. The sections were then incubated for 1 h with 1% bovine serum albumin at 37 °C followed by incubation with primary antibody against rat insulin (diluted 1:1000; Sigma-Aldrich, USA) overnight at 4°C. The sections were washed and incubated with FITC-bound anti-mouse secondary antibody (diluted 1:1000, Sigma-Aldrich, USA) for 1 h. Similarly, primary antibody against rat glucagon was used (diluted 1:2000; Sigma-Aldrich, USA) for pancreatic alpha cells (glucagon). After washing, sections were incubated with R-phycoerythrin bound anti-mouse secondary antibody (Sigma-Aldrich, USA) for 1 h. The sections were counterstained with Hoechst 33342 (diluted 1:1000, Sigma-Aldrich, U.S.A.) for 30 min and images were captured using KEYENCE all-in-one fluorescence microscope BZ-X700.

2.2.11.3. RNA extraction and gene expression analysis by RT-qPCR

Analysis of mRNA expression of islet functional genes was performed with RT-qPCR after 14 days of islet culture. Cells were lysed, and RNA was isolated and purified using an RNeasy Plus Mini Kit (Qiagen, Valencia, CA) according to the manufacturer's instructions for on-column treatment. Total RNA was extracted from the scaffolds by treatment with Trizol (Invitrogen, USA) for 15 min. Further treated scaffolds were centrifuged (12000g, 10 min, 4°C), and the supernatant was incubated with chloroform. After centrifugation (12000g, 15 min, 4 °C), the upper aqueous layer was transferred to RNeasy Plus Mini Kits. RNA concentration and quality were measured by NanoDrop 1000 Spectrophotometer (Thermo Scientific, USA). For

reverse transcription 1 µg of RNA was used to generate cDNA, using a High Capacity cDNA Reverse Transcription Kit (Applied Biosystems, Carlsbad, CA). RT-qPCR was performed using primers with Power SYBRGreen (Thermo Fisher Scientific) using the Stratagene Mx3000P QPCR

Table 2.1. *Primers for RT-qPCR*

Gene	Forward sequence	Reverse sequence
Rat GAPDH	GCATCTTCTTGTGCAGTGCC	GAGAAGGCAGCCCTGGTAAC
Rat Insulin I	AAACAGCACCTTTGTGGTCCT	ACTTCACGACGGGACTTGGG
Rat Insulin II	GGAGCGTGGATTCTTCTACACA	AGTGCCAAGGTCTGAAGGTCAC
Rat Glucagon	CCAAAGGAGCTCCACCTGTC	TCCAGCCACGATGTAAACGG
Rat Somatostatin	CCCCAGACTCCGTCAGTTTC	GGCATCGTTCTCTGTCTGGT
Rat PDX-1	CCTTTCCCGAATGGAACCGA	TTTTCCACGCGTGAGCTTTG
Human GAPDH	ACAACTTTGGTATCGTGGAAGG	GCCATCACGCCACAGTTTC
Human CD68	CTTCTCTCATTCCCCTATGGACA	GAAGGACACATTGTACTCCACC
Human CD206	CTACAAGGGATCGGGTTTATGGA	TTGGCATTGCCTAGTAGCGTA
Human CD209	AATGGCTGGAACGACGACAAA	CAGGAGGCTGCGGACTTTTT
Human CCR7	TGAGGTCACGGACGATTACAT	GTAGGCCCACGAAACAAATGAT

system (Stratagene, CA). All assays were carried out in duplicate in 96-well format plates. Primers (**Table 2.1**) were used at 1 µM concentration and run with cycles of 15 s at 95 °C and 45 s at 60 °C for 40 cycles. Transcript expression data were normalized to the housekeeping gene, glyceraldehyde-3-phosphate-dehydrogenase (GAPDH) and the $2^{-\Delta\Delta C}{}_{T}$ method was used to calculate relative gene expression per reported protocols for islet genes (Daoud et al., 2011; Davis et al., 2012; Livak and Schmittgen, 2001). Changes in target gene expression in M0, M1, and M2 macrophages were expressed as fold change from control groups.

2.2.12. Material biocompatibility assay

2.2.12.1. Macrophage stimulation and determination of *in vitro* inflammatory response

Immunogenicity of macroencapsulating scaffolds was evaluated by the release of tumour necrosis factor alpha (TNF α) when co-incubated with RAW 264.7 cells (murine macrophage cell line). Cells were cultured in DMEM supplemented with 10% FBS and 1% antibiotic-antimycotic at 37 °C and 5% CO_2. Cells were seeded at a density of 5×10^4 cells per well in 12 well cell culture plate and left overnight. Further,

scaffolds were added to cell culture wells. Tissue culture plate wells with similar cell density (and without scaffolds) were taken as negative controls. Tissue culture wells containing 1000 ng/mL lipopolysaccharide (LPS, Sigma-Aldrich,USA) were used as positive controls per the protocols reported in the literature (Gupta et al., 2016; Kumar et al., 2016b). After 12 h and 24 h of incubation, media were collected and stored at -80 °C. The released TNF α was determined by ELISA (mouse TNF α ELISA kit, Invitrogen, USA) per the manufacturer's instructions. The TNF α release by macrophages was calculated from a standard curve and plotted accordingly.

2.2.12.2. *In vivo* immune response to scaffolds

All *in vivo* experiments were conducted per the animal care protocols approved by Institutional Animal Ethical Committee (IAEC), West Bengal University of Animal and Fishery Sciences (WBUAFS), Kolkata, India (Permit No. Pharma/IAEC/36 dated 30.6.2014) in accordance with "Principles of Laboratory Animal Care". The animals used in this study were Swiss (I.B.) mice of 30-35 g body weight of either sex. Experimental mice were subcutaneously implanted with acellular scaffolds from all three variants. Scaffolds of specific dimensions (6 mm in diameter, 2 mm in height) were used for subcutaneous implantation for 4 week studies. Wound healing at the incision site was observed for the course of the experiment, and no animal death was documented within this period. After 4 weeks of implantation, scaffolds were retrieved from the implant site with the overlying native tissues. Histological analysis was subsequently performed. Briefly, individual scaffold explants were fixed in 10% neutral buffered formalin for 24 h and then dehydrated through a series of graded ethanol, cleared with xylene, and embedded in paraffin wax. For histological studies, sections were deparaffinized, cleared, and rehydrated. Slices were stained further with hematoxylin and eosin (H&E, Sigma-Aldrich, USA) following the manufacturer's instructions, and sections were assessed for the infiltration of inflammatory cells.

For immunofluorescence, tissue sections were deparaffinized, cleared, and rehydrated through a series of graded ethanol and permeabilized. The sections were further blocked for 1 h with 1% bovine serum albumin at 37 °C followed by incubation with the primary antibody against CD68 (Anti-CD68, diluted 1:200, Abcam, U.K.**)** overnight at 4°C. The sections were washed and incubated with the FITC-tagged anti-mouse secondary antibody for 1 h (diluted 1:1000, Abcam, U.K.) and images were captured using a KEYENCE all-in-one fluorescence microscope BZ-X700.

2.2.13. Dexamethasone (Dex) and IL-4 release from scaffolds

Dexamethasone and IL-4 loading in silk-control, silk-alginate, and silk-agarose scaffolds was performed as cell encapsulation described in section 2.2.8. Scaffolds were incubated for 30 min in 3% (w/v) $BaCl_2$ (Sigma-Aldrich, USA) solution, prepared in 0.9% (w/v) NaCl (pH 7.4). A total of 3 µg of dexamethasone (Sigma-Aldrich, USA) dissolved in 2% (w/v) of sodium alginate solution (40 µL) was loaded into scaffolds in separate wells of a 24 well plate. The scaffolds were left for 2 min for proper cross-linking of Ba^{2+} ions with sodium alginate to encapsulate the Dex in the scaffolds. Further, 30 µL of sodium alginate was added on the periphery of the scaffolds for complete encapsulation. The Dex-loaded scaffolds were submerged in 1 mL of PBS (pH 7.4) in a tube and maintained in a shaker incubator (37 °C) for release studies. At pre-specified time intervals, PBS medium was replaced, and absorbance was recorded at 241 nm (Vacanti et al., 2012; Weaver et al., 2015). Similarly, recombinant human cytokine IL-4 (Peprotech, Rocky Hill, NJ, USA) was encapsulated in the scaffolds. IL-4-loaded scaffolds containing 0.5 µg of cytokines were incubated in LoBind Microcentrifuge tubes (Fisher Scientific) in 1 mL PBS (pH 7.4) and placed on a shaker. PBS was replenished at specified time points until day 21. Collected samples were stored at -80 °C for the further enzyme-linked immunosorbent assay (Human ELISA Development Kit, Peprotech, Rocky Hill, NJ, USA) of IL-4, following the manufacturer's instruction (Reeves et al., 2015).

For agarose-based macroencapsulation, previously reported protocols were followed with some modifications (Iwata et al., 1992; Yang et al., 1994). Low-gelling agarose type VII (Sigma-Aldrich, USA) was used for encapsulation. Dry scaffolds were loaded with 3 µg of dexamethasone and 0.5 µg of IL-4 cytokine and then left for 1 h in an incubator at 37 °C. A 5% (w/v) agarose solution was prepared in PBS and the solution was kept at 45 °C. Dex and IL-4 loaded scaffolds were individually coated with 200 µL of agarose solution to cover the scaffold surface and left on ice for 1 min to allow agarose gelation. For the control group, no coating was provided.

2.2.14. Islet cytotoxicity study

Cytotoxicity of IL-4 and Dex on rat islets was carried out using the MTT assay (Sigma-Aldrich, USA) following the manufacturer's instructions. Equal numbers of islets (~300) were incubated in a 24 well plates. Dex and IL-4 loaded silk-alginate scaffolds were placed in transwell for 48 h. After incubation, MTT (5 mg/mL) diluted 1:10 times

in RPMI was added to each well followed by incubation for 4 h at 37°C. By adding 200 µL of dimethyl sulfoxide (DMSO), the insoluble formazan product was dissolved, and the absorbance was measured at 595 nm. Islet function was determined through glucose challenge assay as described in section 2.2.11.1. Islets (~300) were incubated in a 24 well plate with Dex and IL-4 loaded silk-alginate scaffolds placed in transwells inserts for 48 h. Islets were washed for 5 min with 3.3 mM glucose in a Krebs-Ringer buffer. After washing, samples underwent a static incubation for 60 min each, with low (3.3 mM) followed by high (17 mM) glucose concentrations in Krebs-Ringer buffer. Insulin secretion was measured using a rat insulin ELISA kit (Mercodia, Sweden). Non-treated islets were used as a control for all these studies.

2.2.15. Immunomodulation study

For the immunomodulation study, the human acute monocytic leukemia cell line (THP-1) was purchased from ATCC (Manassas, VA). Cells were cultured in RPMI media supplemented with 10% FBS and 1% antibiotics. Further, 10^5 THP-1 cells per well were seeded in 24 well Corning transwell plates (Fisher Scientific, USA). THP-1 cells were induced to a macrophage (M0) using 100 ng/mL (162 nM) of phorbol 12-myristate 13-acetate (PMA; Sigma-Aldrich, USA) in RPMI media kept overnight. After PMA treatment, macrophage differentiation (M0) was confirmed by their adherence to well plates and CD68 gene expression. Adherent cells were washed and the medium was switched to polarization conditions through IL-4 cytokine-releasing silk-alginate scaffolds placed in the transwell inserts. Macrophage polarization potential was evaluated after 72 h of IL-4 treatment. Cells were lysed, and isolated mRNA was preserved for gene expression analysis for M2 (CD206 and CD209) and M1 (CCR7) macrophage markers.

2.2.16. Statistical analysis

All data are reported as mean ± standard deviation. For each experiment, n = 3 samples were used. Statistical analysis was performed by one-way analysis of variance (ANOVA). All statistical analyses were executed using OriginPro 8. Differences between groups of $p \leq 0.05$ and $p \leq 0.01$ were considered statistically significant.

2.3. Results

2.3.1. Scaffold morphology

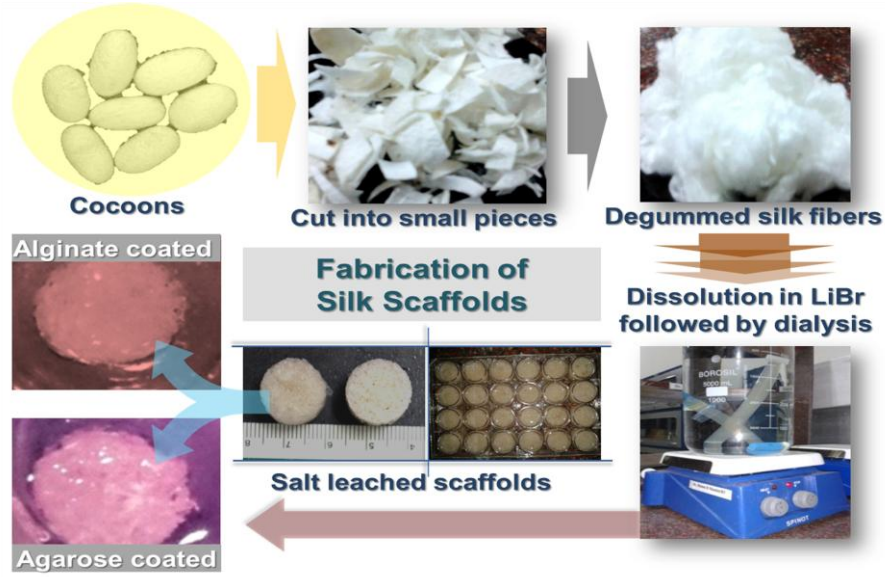

Figure 2.2. *Scheme representing fabrication of cell encapsulating silk scaffolds.*

Porous silk scaffolds were successfully fabricated using a salt-leaching technique (**Figure 2.2**). FESEM images revealed highly heterogeneous porous structures for all scaffold variants with excellent interconnectivity (**Figure 2.3A**). Pores ranged 150-500 µm, suitable to support 3D cell spheroid formation and nutrient transport (Daoud et al., 2011).

2.3.2. Porosity and density of scaffolds

The porosity and density of the scaffolds are important features to be evaluated for tissue engineering applications, as they impact cellular migration and proliferation within scaffolds. Aqueous-derived scaffolds with up to 91% porosity were formed depending on the compositions (e.g., silk-control, silk-alginate and silk-agarose; **Figure 2.3B**). The scaffolds prepared with only silk resulted in ~91% porosity. After alginate and agarose encapsulation, the porosities were ~85 and ~75%, respectively. The densities were ~82, 105, and 126 mg/mL for the silk-control, silk-alginate, and silk-agarose scaffold, respectively (**Table 2.2**).

2.3.3. Swelling ratio and water uptake

Absorption and retention of large quantities of PBS/ culture media plays a key role in scaffold functions. Swelling ratio and water uptake by the different scaffolds was

monitored until equilibrium was achieved. Swelling ratios were determined by eq (2.3) and plotted with material composition. Swelling ratio was a function of scaffold

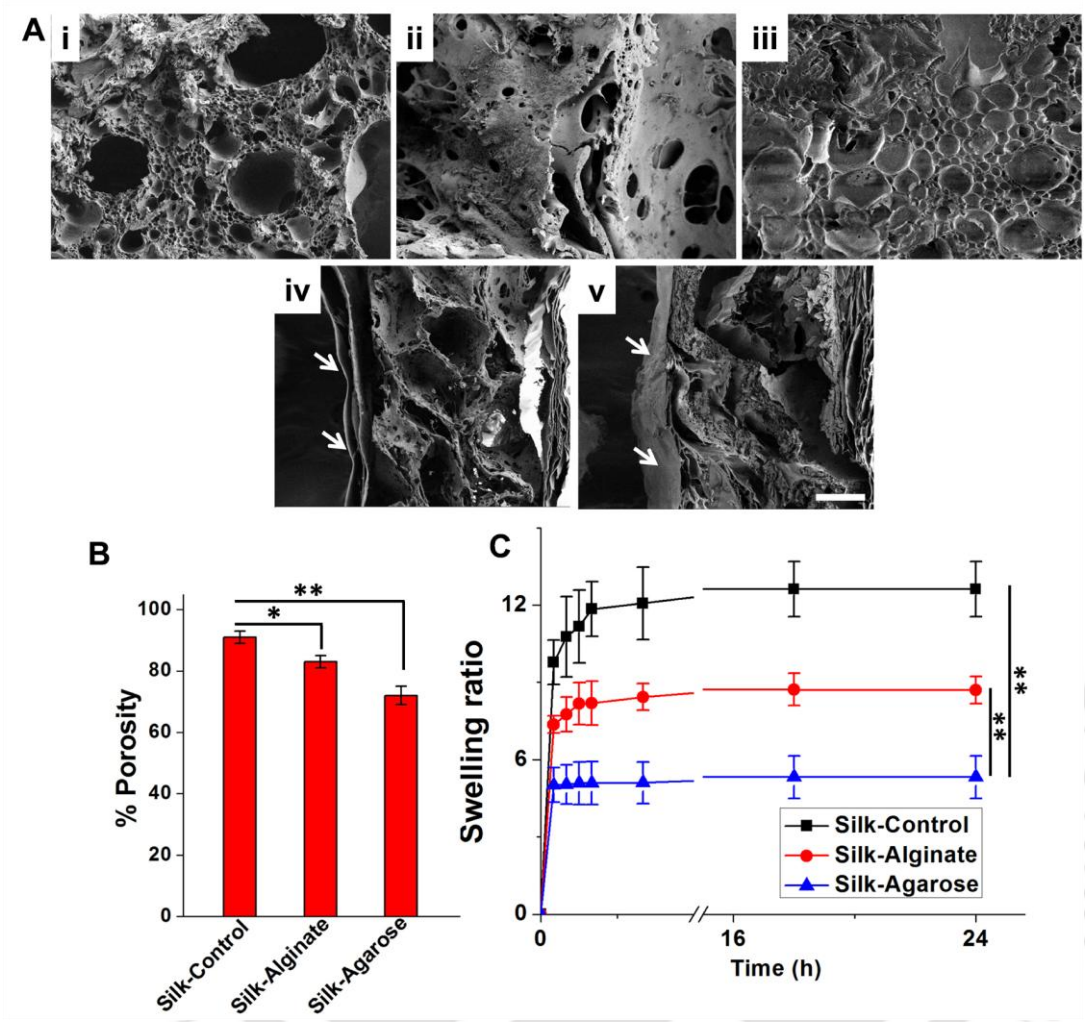

Figure 2.3. *Physical characterization. (A) FESEM images representing cross sectional morphology and interconnectivity within 3D scaffolds: (i) silk-control, (ii) silk-alginate, (iii) silk-agarose, (iv) alginate coating layer, and (v) agarose coating layer (white arrows). Scale bar 100 µm. (B) Porosity of different scaffolds. (C) Swelling ratio of scaffolds in PBS at 37ºC (pH 7.4) against time. (*p≤0.05, **p ≤ 0.01).*

composition. Scaffolds swelled abruptly and achieved equilibrium within 24 h. The swelling ratio of different scaffolds decreased with different hydrogel fillers: alginate and agarose. Silk-control scaffolds exhibited a maximum swelling ratio of 12.6 which could be attributed to inherent voids, compared to silk-alginate and silk-agarose-based hydrogels with swelling ratios of 8.7 and 5.3, respectively (**Figure 2.3C**).

The percentage of water uptake was determined by eq 2 4 and plotted with material composition (**Table 2.2**). The water uptake percentages were 94, 91, and 81% for silk-control, silk-alginate, and silk-agarose scaffolds, respectively.

Table 2.2. *Density and percentage of water uptake for the different scaffold compositions.*

Matrix	Density (mg/mL)	Water uptake (%)
Silk-control	82 ± 2	94±0.3
Silk-alginate	105 ± 4	91±0.2
Silk-agarose	126 ± 4	81±0.4

2.3.4. Cell proliferation studies in 3D scaffolds

In vitro cell proliferation studies were performed on all scaffold variants. AlamarBlue assay was performed to quantify enhancement of cell number over time. A reduction in AlamarBlue corresponds to cell metabolism, which correlates with the number of

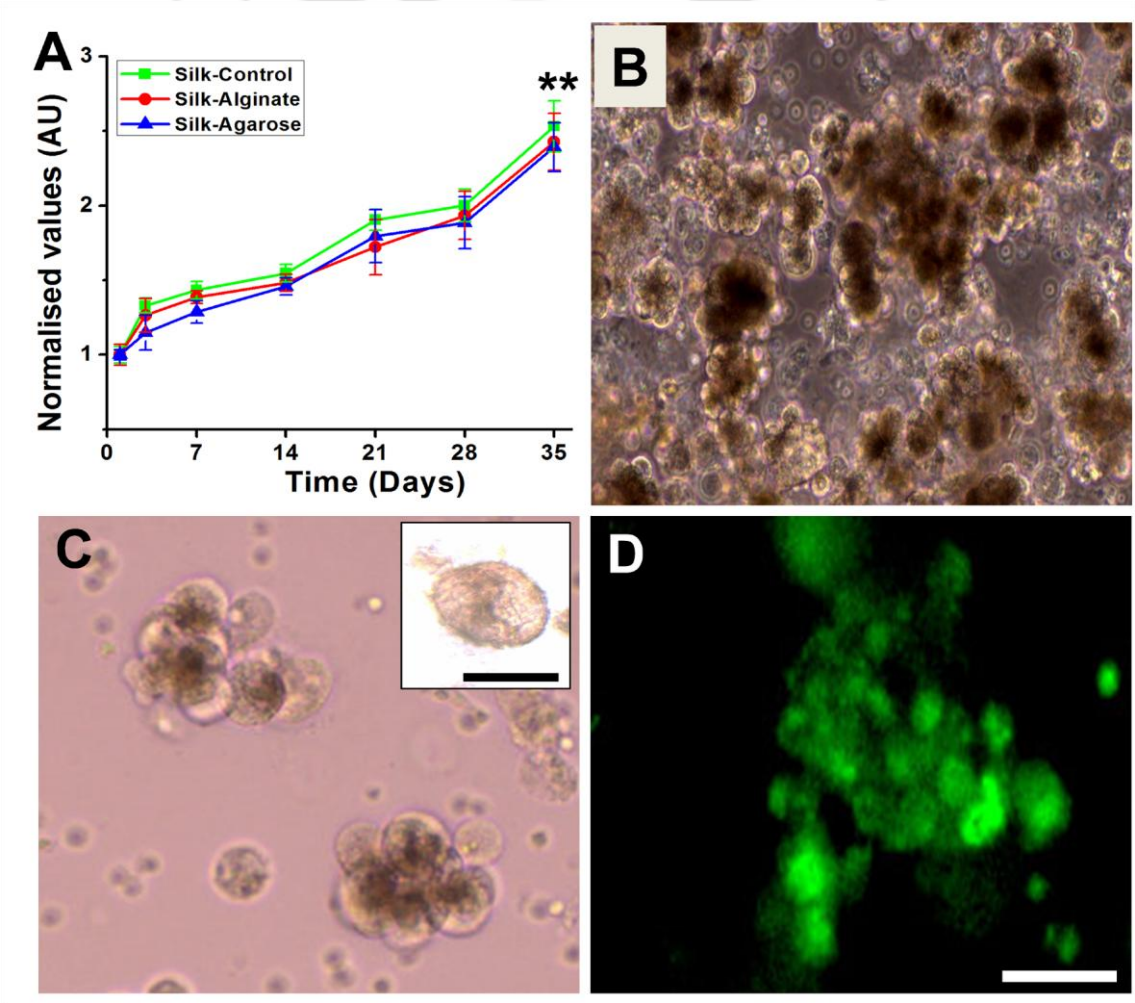

Figure 2.4. *Cell proliferation and islet culture. (A) Cell proliferation for 35 days in macroencapsulated 3D scaffolds prepared with different compositions using RIN-5 cell line spheroids (**p≤0.01). (B) Primary rat islets clusters growing in 2D culture plate after isolation. (C) Small primary islet aggregates (D) Calcein AM stained live primary islets. Scale bar: 50 μm.*

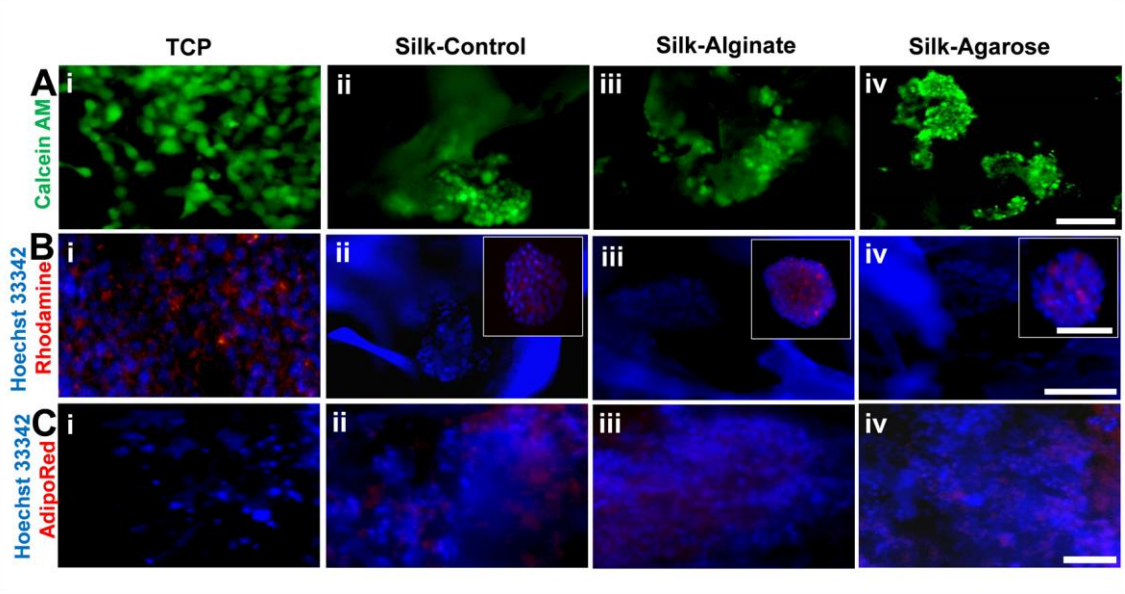

Figure 2.5. *Comparative morphology of RIN-5 cells and islets in 2D and 3D culture. (A) Fluorescent images of RIN-5 cells showing live islet-like spheroid on 3D scaffolds (35 days culture) and compared with TCP (7 days culture). Green color shows calcein-stained live cells. (B) Islet-like 3D spheroids after fixation and staining compared with TCP (7 days). Red shows cellular actin filaments, and blue shows nucleus. Scale bar: 200 µm. (C) Fluorescent microscopic images of primary islets after 14 days culture. Red shows adipo red-stained silk matrices, and blue shows nucleus. Scale bar: 100 µm.*

proliferating cells. On day 35, RIN-5 cells proliferated ~ 2.53-fold on silk-controls, ~ 2.42-fold on silk-alginate, and ~ 2.39-fold on silk-agarose scaffolds when compared to day 1 in culture (**Figure 2.4A**). All the scaffolds exhibited significant differences when compared with day 1 ($p < 0.01$).

2.3.5. Evaluation of spheroid formation and cell distribution in the scaffolds

In all the scaffolds, cells proliferated, suggesting matrix cytocompatibility. Primary rat islets were cultured in 2D cell culture plates prior to scaffold seeding (**Figure 2.4B-D**). Live cell imaging showed prolonged proliferation of RIN-5 cells in all the scaffolds. Proliferating cells formed 3D cell spheroids which are in contrast to typical 2D morphology of RIN-5 cells cultured on TCP (tissue culture plate; **Figure 2.5A**). Cell spheroids, ~200-300 µm, were stained with calcein AM (**Figure 2.5A**) and rhodamine-phalloidin (**Figure 2.5B**). In the case of primary rat islets, cells were distributed all over the three scaffolds when compared with TCP control (**Figure 2.5C**).

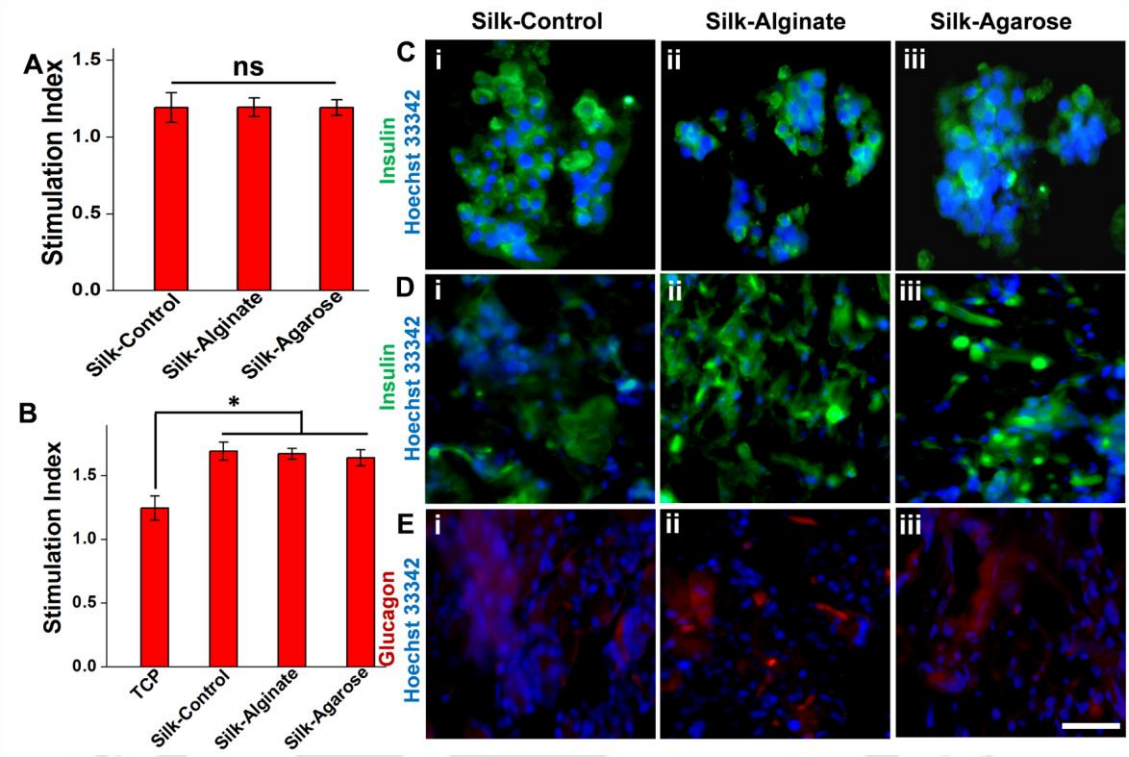

Figure 2.6. *Glucose challenge assay showing insulin secretion from (A) RIN-5 spheroids and (B) primary islets encapsulated in different scaffolds. Stimulation index (SI) was calculated as the ratio of insulin secreted in high glucose to low glucose. Immunofluorescence images showing insulin in (C) RIN-5 seeded scaffolds (35 days), (D) primary islets (14 days) and (E) glucagon in primary islets (14 days), cultured on scaffolds. Blue color shows nucleus. Scale bar: 50 µm. (*p < 0.05). "ns" indicates not significant (p > 0.05).*

2.3.6. Functional assessment of the encapsulated cells *in vitro*

2.3.6.1. Insulin release

To elucidate if the macroencapsulated RIN-5 spheroids and cultured primary islets were functional, it was important to analyze the glucose sensing and insulin releasing potential of cultured cells when subjected to glucose challenge test (**Figure 2.6A,B**). After 35 days of culture in scaffolds, RIN-5 spheroids showed an SI index of ~1.2 for all three scaffolds (**Figure 2.6A**; $p > 0.05$). Insulin released from RIN-5 cells cultured in TCP wells could not be incorporated for this assay because in a 2D culture environment, cells could not be maintained for such a long time to perform a glucose challenge assay. There were no significant differences between the groups ($p > 0.05$). In the case of primary islets, after 14 days of culture, islets showed a significant difference in SI compared to non-encapsulated islets (1.2 vs. 1.7, $p < 0.05$) (**Figure 2.6B**). No significant differences were found between the different scaffold groups ($p > 0.05$).

2.3.6.2. Insulin and glucagon immunofluorescence study

In order to complement the proliferation and insulin release findings, immunofluorescence was carried out with characteristic islet hormones: insulin and glucagon (**Figure 2.6C-E**). Immunofluorescence results revealed cytoplasmic insulin within scaffold sections. For all three types of scaffolds, insulin expression was abundant on day 35 for RIN-5 cells (**Figure 2.6C**). For islet cells also, in all variants, insulin was homogeneously distributed throughout the cross sections, which relates to the homogenous cell distribution. Insulin secretion is a characteristic signature of islet cells, which agrees with insulin release experiments where cells maintained insulin production for 14 days of cell culture (**Figure 2.6D**). For islet cultures, glucagon was also localized in scaffold sections (**Figure 2.6E**).

2.3.6.3. Gene expression analysis

For functional characterization of macroencapsulating scaffolds, real time PCR was performed with signature islet genes insulin I, insulin II, glucagon, somatostatin, and pancreatic and duodenal homeobox 1 (PDX-1; **Figure 2.7A-E**). Islets cultured on 3D scaffolds had upregulated gene expression when compared with islets cultured in 2D. Expressions of insulin I (~3-fold) and insulin II (~5-fold) showed higher insulin production in line with the glucose challenge assay results. Similarly, glucagon gene expression (~4-5-fold) also supported islet functionality. Enhanced expression of somatostatin (~4-fold) and the PDX-1 (~5-fold) gene was also found, and these are key factors with a vital role in pancreatic development and β-cell maturation. Pancreatic gene expression for all scaffold variants was significantly upregulated when compared with non-encapsulated islets in 2D ($p < 0.05$). However, no significant differences were noticed among the different scaffold groups ($p > 0.05$).

2.3.7. Macrophage stimulation and determination of *in vitro* inflammatory response

Macrophages are the primary source of inflammatory responses in the body; upon activation, they secrete cytokine mediators and regulate immune responses. A TNF α cytokine release study was conducted over a period of 24 h using the RAW 264.7 macrophage cell line with silk-control, silk-alginate, and silk-agarose acellular scaffolds. After 12 h, macrophages evoked very low levels of TNF α release as compared to LPS positive controls (~2-fold; $p < 0.05$). The values were comparable to

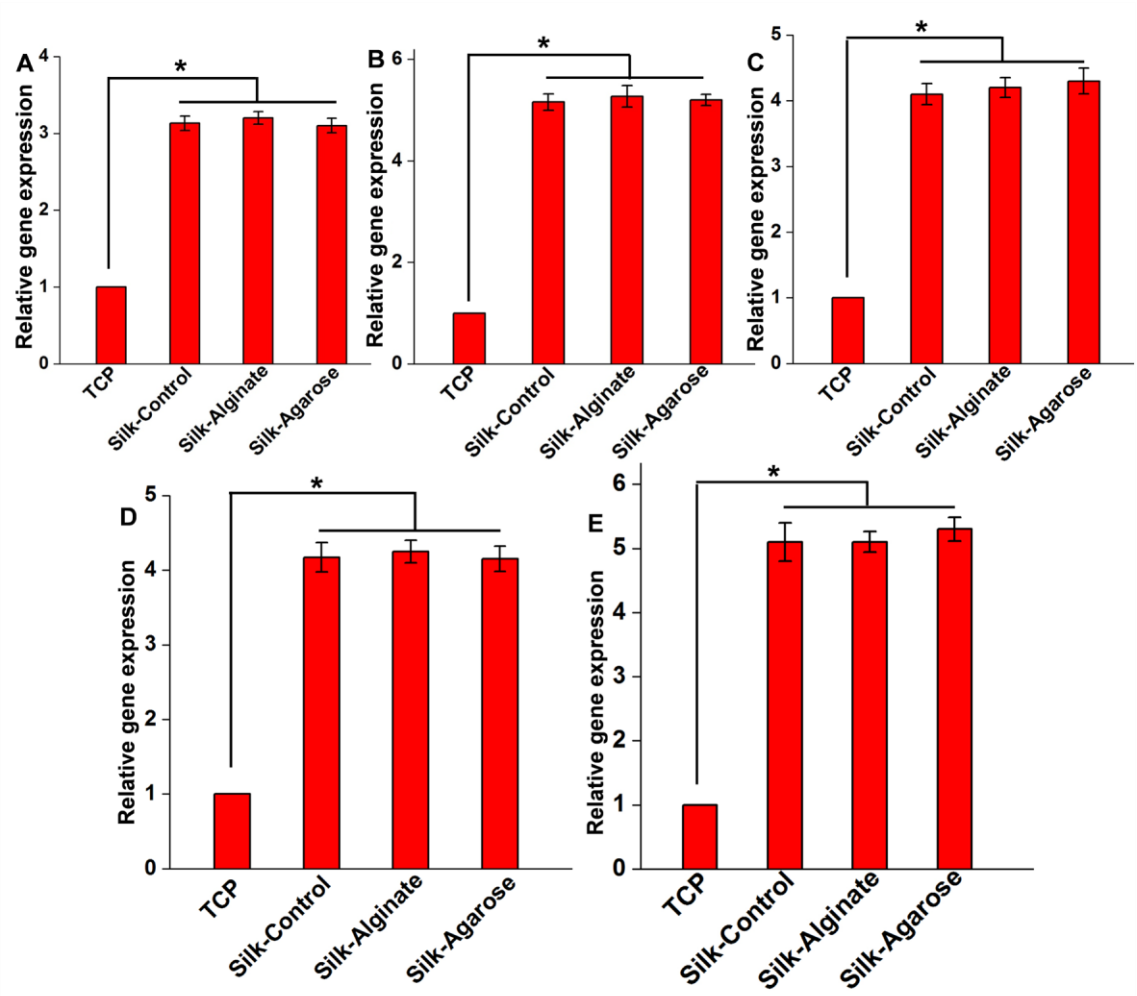

Figure 2.7. *Relative expression of functional islet genes in different scaffolds after 14 days culture of rat islets. Gene expression was relative to GAPDH gene and normalized to non-encapsulated islets in 2D. (A) insulin I, (B) insulin II, (C) glucagon, (D) somatostatin, and (E) PDX-1 (*p≤0.05).*

the negative control (**Figure 2.8A**). After 24h culture, TNF α release was very high in the positive control ($p < 0.01$). For all scaffolds, TNF α release was significantly lower than the LPS-treated group ($p < 0.01$) and comparable to negative control wells, suggesting lower levels of inflammatory responses *in vitro*.

2.3.8. *In vivo* immune response to scaffolds

In vivo studies were performed to evaluate the host immune response, implant integration, and immunoisolation behavior of the scaffolds. After 4 weeks of *in vivo* implantation, retrieved acellular scaffolds were evaluated for infiltration of inflammatory cells (**Figure 2.8B,C**). Following retrieval and H & E staining, a close integration of implants with mouse native tissue was documented (**Figure 2.8B**). An

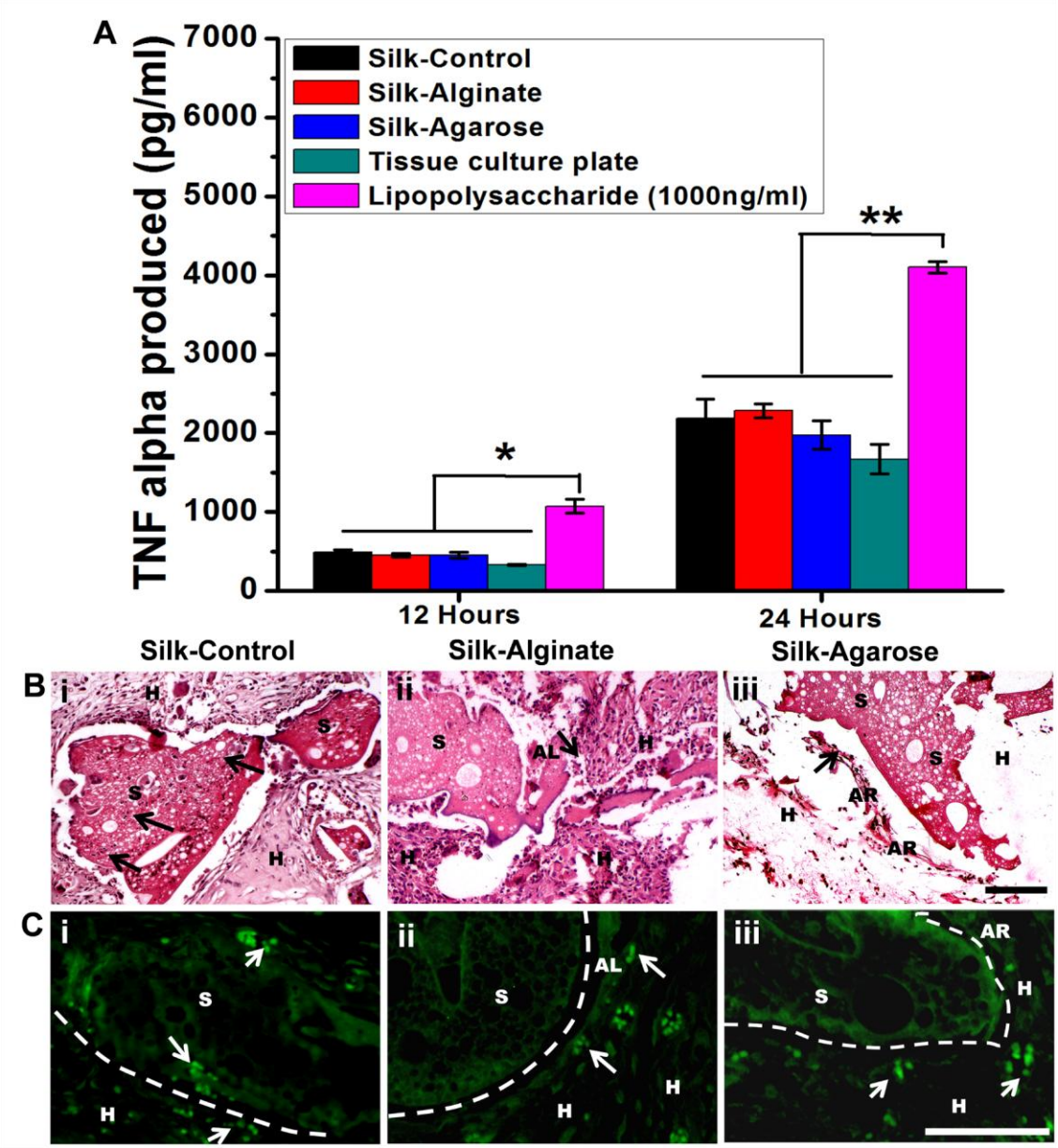

Figure 2.8. *In vitro and in vivo immune response. (A) TNF alpha production by RAW 264.7 macrophages (in vitro study; *p < 0.05,**p < 0.01). (B) H & E staining and (C) immunofluorescence of retrieved acellular scaffolds after 4 weeks of subcutaneous implantation in mice. Symbols S, AL, AR, and H stand for silk scaffold, alginate, agarose, and host tissue, respectively. Arrows indicate infiltrating monocytes/macrophage (green), and dashed lines indicate scaffold-host tissue interface. Scale bar: 400 µm.*

irregular pattern of infiltrating putative immune cells was noticed within the immediate vicinity of the host/implant interface. Further, immunostaining of sections showed CD68 positive cells, *i.e.,* host monocytes or macrophages (green), surrounding the implants (**Figure 2.8C**). CD68 was chosen as a macrophage marker for analyzing

infiltration of the macrophages in the subcutaneously implanted cell-encapsulating scaffolds (Bellas et al., 2015; Wang et al., 2016). Alginate and agarose hydrogel layers acting as barriers could also be located in H & E and immunofluorescence images. In silk-control scaffolds (without encapsulation) greater host cell infiltration was noticed. However, in the case of the silk-alginate and silk-agarose scaffolds, host cells (monocyte/macrophages) were restricted to outer encapsulating layer only (**Figure 2.8C**).

2.3.9. Dexamethasone and IL-4 release

In vitro release of dexamethasone (Dex) and IL-4 cytokine from all the scaffolds was measured by UV-spectroscopy and ELISA, respectively. Within 24 h, the cumulative release of Dex from silk-control, silk-alginate, and silk-agarose scaffolds was ~91%, 42%, and 30%, respectively. The silk-control scaffolds exhibited a burst release in the initial 24 h and plateaued in 48 h with a cumulative release of ~97%. Further, the corresponding release values for day 21 were ~97%, 77%, and 62% (**Figure 2.9A,i**). Dex release was significantly higher in silk-control when compared to silk-alginate and silk-agarose scaffold variants ($p < 0.001$). There was a significant difference in the release profile of silk-alginate and silk-agarose scaffolds as depicted in the graph ($p < 0.01$). The cumulative release of IL-4 from silk-control, silk-alginate, and silk-agarose scaffolds was ~74%, 11%, and 7%, respectively, within 24 h. Here also, silk-control scaffolds exhibited a burst release in initial 24 h with a cumulative release of ~74%. The release was significantly higher in silk-control when compared to silk-alginate and silk-agarose scaffold variants ($p < 0.001$). The corresponding IL-4 release values for day 21 were ~94%, 44%, and 33% (**Figure 2.9A,ii**). Silk-alginate and silk-agarose scaffolds could maintain sustained release of Dex and IL-4 over time.

2.3.10. Cytotoxicity study on islets

In vitro studies were conducted to evaluate the influence of local release of IL-4 and Dex on primary islets. IL-4 and Dex-loaded silk-alginate scaffolds were selected for this study and incubated with primary rat islets. IL-4 and Dex had no effect on islet metabolic activity when compared with control (without treatment; **Figure 2.9C**). Also, the stimulation index (SI) was similar to the control group ($p > 0.05$; **Figure 2.9D**).

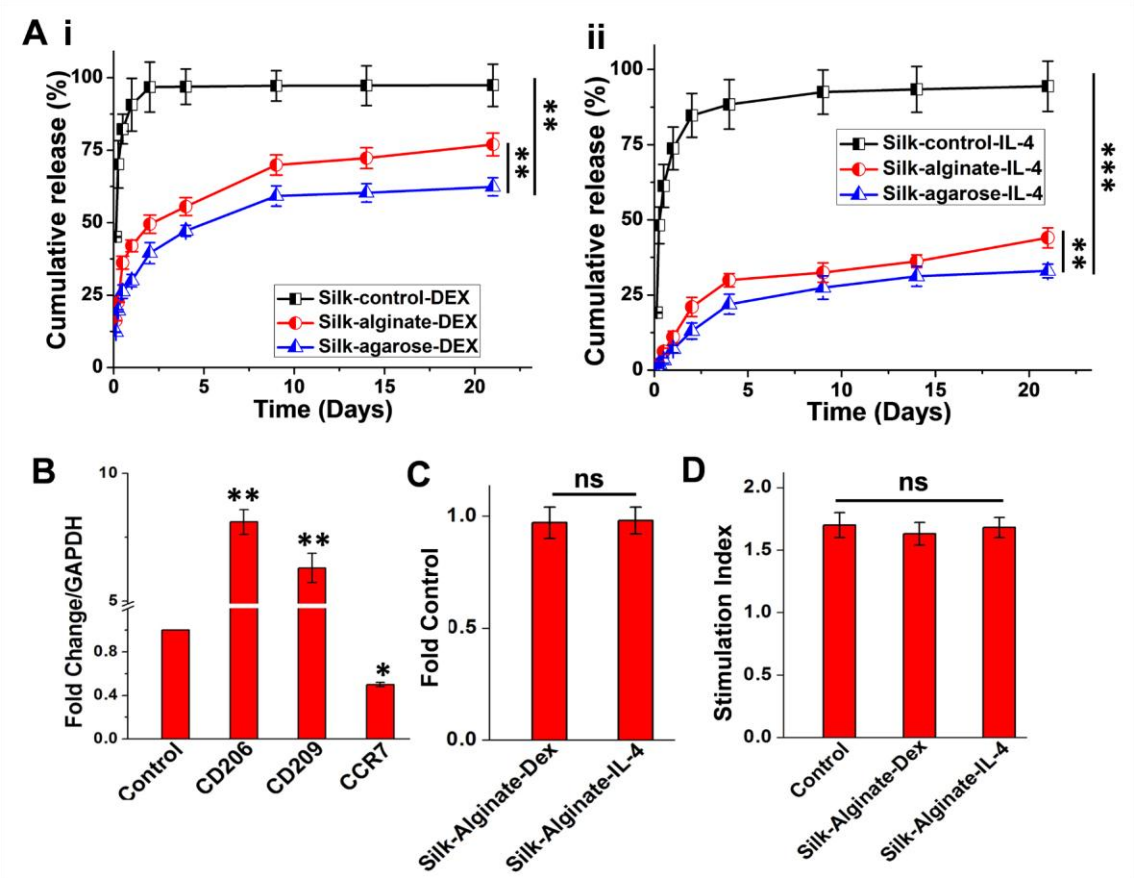

Figure 2.9. *Immunomodulation analysis. (A) Cumulative Dex (i) and IL-4 (ii) release from different scaffold compositions. (B) Gene expression analysis for M1 and M2 macrophage surface markers (relative to untreated M0 monocytes) when incubated with IL-4-loaded silk-alginate scaffolds for 72 h. (C) MTT assay showing islet viability post-incubation with Dex and IL-4 eluting silk-alginate scaffolds compared with control (islets without treatment). (D) Glucose stimulated insulin release by islet incubated with Dex and IL-4-eluting silk-alginate scaffolds. The results are representative from three independent experiments and performed as n=3 (*p < 0.05,**p < 0.01, ***p < 0.001). "ns" indicates not significant (p > 0.05).*

2.3.11. Immunomodulation analysis

To evaluate the influence of IL-4-loaded scaffolds on inflammatory cell activation, human monocyte THP-1 cells were induced to macrophages (M0) and incubated with IL-4 releasing silk-alginate scaffolds for 72 h. Monocyte (THP-1) to M0 conversion was confirmed with CD68 marker expression (**Figure A2.1**). The results showed significant upregulation of CD206 and CD209 surface markers (**Figure 2.9B**, $p < 0.01$). A significant down regulation in CCR7 expression (inflammatory marker) was also observed (**Figure 2.9B**, $p < 0.05$). There was an ~8-fold increase in CD206 compared to the control group (untreated THP-1 monocytes; $p < 0.05$). Similarly, a ~6-fold increase in CD209 expression was observed. Together these data indicate that IL-4 loaded scaffolds can effectively polarize the M0 macrophage to the M2 phenotype.

Thus, the system might reduce inflammatory responses that arise during inflammatory stages of islet implantation.

2.4. Discussion

In the native pancreas, endocrine cells remain clustered into 3D spheroid-like islet structures which are supported with peri-vascular and peri-insular basement membranes (Nikolova et al., 2006; Van Deijnen et al., 1992). During islet isolation this structure is lost, leading to islet dysfunction and death either during *in vitro* culture or after *in vivo* transplantation (Bosco et al., 2000; Rosenberg et al., 1999). *In vitro* expansion of islets in 2D culture results in cell senescence and dedifferentiation (Beattie et al., 2002; Muthyala et al., 2011). It has been previously shown that islet and cell line survival is improved when encapsulated in 3D matrices (Davis et al., 2012; Weber et al., 2008). Such results have been also validated for silk hydrogels *in vitro* (Davis et al., 2012) and *in vivo* (Hamilton et al., 2015). In this study, macroencapsulating silk scaffolds were evaluated as a potential biomaterial for spontaneous formation of islet-like spheroids with immunoisolatory and immunomodulatory attributes (**Figure 2.1**).

Different methods have already been used to develop islet-like spheroids, including a hanging drop method, HydroCell with shaker, microwells and cell droplets embedded with high cell concentrations (Shalaly et al., 2016). In the current study, we observed the spontaneous aggregation of beta cells into islet-like insulin-positive spheroid structures in a 3D silk biomaterial environment under static culture conditions. This property of silk scaffolds may be harnessed for islet-like structure development from other insulin-producing cell lines and primary human beta cells. In our study silk scaffolds supported prolonged cell proliferation, prevented necrosis and maintained islet functions.

As stated, islets *in vitro* need a 3D platform to compensate for the natural extracellular matrix (ECM) that is lost during isolation (Daoud et al., 2011; O'Sullivan et al., 2011). Thus, salt-leached silk scaffolds were considered as an alternative because of their highly porous, mechanically robust features for cell culture (**Figure 2.2**). The slow degradation of the silk scaffolds allows the structural and functional persistence of the implant in the body (Thurber et al., 2015). The silk scaffolds were fabricated using a salt-leaching process to generate highly porous matrices - a prime requisite for primary islet culture (Daoud et al., 2011; Rockwood et al., 2011). These scaffolds have been widely used for different tissue engineering applications with promising outcomes

(Kasoju and Bora, 2012; Kundu et al., 2013). Thus, when combined with alginate and agarose as macroencapsulating agents, these immunoisolating scaffolds would help in implant protection by preventing the infiltration of immune cells to the islets encapsulated in the scaffolds. The developed scaffolds were highly porous (**Figure 2.3A**), with excellent swelling and interconnected pores for nutrient transfer. These characteristics are known to aid better distribution and survival of cells during seeding and culture (Daoud et al., 2011). The porosity of the fabricated scaffolds was high (75 to 90%) and sufficient for islet culture (**Figure 2.3B**) (Daoud et al., 2011). The swelling ratio of the scaffolds decreased gradually from silk-control to silk-alginate/agarose. The decrease in porosity may be attributed to the filling of the pores in the silk matrices with alginate or agarose. This high swellability indirectly reflects that the scaffolds may absorb nutrient media to provide nourishment to the cultured/encapsulated cells (**Figure 2.3C**). The total water absorbed by the scaffolds was characterized by its equilibrium water content (EWC; **Table 2.2)**. The EWC of all the hydrogels was found to be well above 80%.

Macroencapsulating scaffolds supported prolonged viability of RIN-5 cells (35 days) (**Figure 2.4A**). Metabolically active RIN-5 clusters within the macroencapsulates, by AlamarBlue, suggested non-hypoxic conditions in scaffolds, thereby, assisting in the prolonged maintenance of cellular physiology (**Figure 2.5A, B**). The alginate and agarose concentrations used here were based on reported protocols with biocompatibility and immunoisolation properties for microcapsules. Furthermore, the pores in alginate and agarose membranes at the concentrations used were sufficient for glucose, oxygen, insulin and metabolite exchange (Iwata et al., 1992; Yang et al., 1994; Zekorn et al., 1996; Zekorn et al., 1992). For RIN-5 cells, insulin secretion was monitored for 35 days and the results suggested that the cells were glucose responsive even after encapsulation (**Figure 2.6A**). For islet cells, the stimulation index was ~1.7, indicative of healthy islets after 14 days of culture (Daoud et al., 2011; Davis et al., 2012) (**Figure 2.6B**). Islets suspended in 2D culture failed to secrete adequate insulin (Daoud et al., 2011) but on 3D supports they maintain function of pancreatic hormones; corroborated by our results. Three dimensional scaffolds showed well defined insulin and glucagon distribution **(Figure 2.6C-E)** (Daoud et al., 2011). The significantly upregulated expression of pancreatic functional genes (compared with suspended islets) is attributed to physical cues provided by the silk 3D scaffolds. This result is in agreement with earlier reports showing upregulated expression of functional pancreatic

genes (insulin, glucagon, somatostatin, and PDX-1) on 3D matrices as compared with suspended islets in 2D (**Figure 2.7A-E**) (Daoud et al., 2011; Davis et al., 2012). Enhanced expression of the PDX-1 gene, a key factor playing a vital role in pancreatic development and β-cell maturation, shows the effects of 3D silk scaffolds in islet function maintenance (Daoud et al., 2011). The RT-qPCR experiments were performed in accordance with the available literature using GAPDH, an extensively used housekeeping gene for islet genes (Daoud et al., 2011; Davis et al., 2012). However, use of 18S as a housekeeping gene would be another proposition for critically evaluating islet cells' functionality considering the role of GAPDH in glucose metabolism (Rodriguez-Mulero and Montanya, 2005).

Macrophages are immune cells which primarily identify foreign materials and regulate immune responses (Reeves et al., 2015). Very low TNF-α release from activated macrophages (RAW 264.7) when incubated with scaffolds showed that macroencapsulates might be useful to explore for *in vivo* applications. The level of TNF-α production was significantly lower than for the positive LPS control (**Figure 2.8A**). This result is in line with published silk, silk-alginate (Ziv et al., 2014) and silk-agarose (Singh et al., 2016b) studies for other tissue-specific applications. Per the literature pertaining to silk, we used a 1000 ng/mL concentration of LPS (Gupta et al., 2016; Kumar et al., 2016b). However, it would be relevant to look into the use of IFN-γ or TNF-α as a stimulant for macrophage activation (Kumar et al., 2016a). Also, the minimal level of inflammation and cell infiltration *in vivo* shows that the cell encapsulating immunoisolatory scaffolds are potential scaffold systems for islet transplantation (**Figure 2.8B-C**) (Ziv et al., 2014). For both the cell-encapsulating scaffolds, infiltrating immune cells were restricted to alginate and agarose encapsulating semi permeable layers (**Figure 2.8C**). In the case of the silk-control group (without encapsulation), infiltrated macrophages were observed in silk scaffolds. The *in vivo* subcutaneous study was conducted in mice of either sex, and there were no differences noted in the results in relation to the sexes, which was in agreement with the available literature (Gupta et al., 2016; Modulevsky et al., 2016).

Macrophages are the dominant infiltrating immune cells in adult and fetal pancreatic islets that help in implant rejection due to host inflammatory reactions (Karlsson-Parra et al., 1996; Wu et al., 2000; Zekorn et al., 1996). IL-4 is known as an immunosuppressive cytokine which helps in decreasing inflammation and immunogenicity through macrophage polarization (from M0/M1 to M2) (Reeves et al.,

2015). As reported earlier, CD206 and CCR7 markers are widely used to characterize the phenotype of macrophages in animal models (Badylak et al., 2008; Brown et al., 2012; Mantovani et al., 2004; Martinez et al., 2006). The porous scaffolds without immune isolation would allow the infiltration of immune cells, which will lead to graft failure (Brauker et al., 1992). Thus, immunoisolating scaffolds would help in implant protection by preventing the infiltration of immune cells to the islets encapsulated in the scaffolds.

With regard to using macroporous scaffolds for sustained delivery of biomolecules, there are certain inherent limitations. These scaffolds possess larger pores which may lead to undesirable burst release. Thus, a hybrid (scaffold-hydrogel) matrix loaded with biomolecules can help in this regard (Singh et al., 2016a). In our study, silk scaffolds encapsulated with alginate/agarose hydrogel layers exhibited sustained release of preloaded Dex and IL-4 as compared to silk-control scaffolds without protective encapsulation. A significant difference was noted in the cumulative release between silk-control and silk-alginate/silk-agarose groups (**Figure 2.9A,i and ii**), which may be attributed to the encapsulating layer acting as a barrier. Per the literature, restricted swelling in the case of silk-alginate and silk-agarose hydrogels may aid to slow and sustain the release of loaded biomolecules as compared to control silk scaffolds (Figure 3C) (Mandal et al., 2009; Singh et al., 2016a). Alginate and agarose hydrogel infusion into silk scaffolds made it a robust matrix system with reduced swelling and limited expandability of the scaffold-hydrogel hybrid construct. These constructs with lower swelling capability are expected to release a lower amount of loaded/encapsulated molecules (Singh et al., 2016a). Additionally, the varying cumulative release for Dex and IL-4 might be a consequence of differences in their molecular weights (IL-4 at 15.1 kDa and Dex at 392.46 Da).

For the immunomodulation study, we switched from RAW264.7 to THP-1 monocyte cells as the response of THP-1 cells to cytokines IFN-γ and IL-4 has been reported to be similar to that of primary peripheral blood monocyte derived macrophages (PBMCs) (Daigneault et al., 2010; Reeves et al., 2015). Encapsulated IL-4 maintained bioactivity and prolonged release and the released IL-4 polarized M0 macrophage to the M2 phenotype. Enhanced expression of CD206 and CD209 associated with downregulated expression of CCR7 showed the polarization of the M0 macrophage phenotype to the M2 phenotype (**Figure 2.9B**). These M2 immuno-suppressive macrophages are known to create an immunologically permissive

microenvironment *in vivo.* (Jiang et al., 2017; Liu et al., 2016). From silk-alginate and silk-agarose scaffolds sustained release was achieved with a maximum 77% Dex release and 44% IL-4 in a 21 day release study. The residual Dex and IL-4 were strongly adsorbed with the hydrogels. As reported previously, these cross-linked IL-4 may have the potential of prolonged localized immune-modulation, even after the plateau release as the macrophages gradually degrade the matrix to access trapped cytokines (Kumar et al., 2016a; Reeves et al., 2015). Also, the released Dex and IL-4 showed no adverse effects on islet viability and insulin secretion (**Figure 2.9C-D**). Thus, these scaffolds can suppress the inflammatory response locally, while simultaneously maintaining cellular physiology (Vacanti et al., 2012; Weaver et al., 2015). The overall short or long phase release of molecules from these scaffolds may be modulated by the quantity of drug loaded (Weaver et al., 2015). A better alternative would be to load islets and the drug individually on different scaffolds to avoid the exposure of islets to detrimental amounts of Dex/IL-4 (Weaver et al., 2015). Short-term release of Dex and IL-4 has shown long-term effects on immunomodulation and immune cell infiltration (Vacanti et al., 2012; Weaver et al., 2015).

As discussed, for islet culture in type 1 diabetes, cell encapsulation is a vital requirement for combating the autoimmune aspects, which demands immunoisolation of materials from the host's immune system. Therefore, we utilized porous silk scaffolds for a cell culture matrix and alginate and agarose as selectively permeable polymeric encapsulating agents that permit the diffusion of glucose, nutrients, oxygen, and insulin while restricting the influx of immune cells and their molecular components (Lim and Sun, 1980; Narang and Mahato, 2006). This strategy circumvents the systemic administration of immunosuppressive drugs and their multiple side-effects that encompass systemic immune suppression and secondary complications (O'Sullivan et al., 2011). The conventional microencapsulation technique had inherent detrimental limitations like low mechanical strength of the capsules, poor retrieval if necessary and short lifespan *in vivo* (O'Sullivan et al., 2011). These limitations establish the portal for exploiting "macroencapsulation" endowed with multiple advantages including concepts such as reloadable scaffolds with functional cells (O'Sullivan et al., 2011; Qi et al., 2004). As a cell encapsulating agent, alginate and agarose microcapsules have been extensively used for islet encapsulation (de Vos et al., 2006; Iwata et al., 1992; Yang et al., 1994; Zimmermann et al., 2007). However, both these microcapsules had inherent

limitations like inferior mechanical strength, poor retrieval and short lifespan *in vivo* (O'Sullivan et al., 2011).

The prior report on silk hydrogel for islet encapsulation involved mesenchymal stromal cells (MSCs) co-encapsulated with islets for immunomodulation and enhanced insulin secretion (Hamilton et al., 2015). However, the authors observed undesired spontaneous osteogenesis and chondrogenesis in the silk grafts containing MSCs, raising questions regarding the stability of the islet grafts. Also, bone-like structures were identified on histological sections of islets in the silk explants (Hamilton et al., 2015). Therefore, the authors reported limitations in using MSCs for immunomodulation in islet culture. Our objective was to exploit alginate and agarose as cell macroencapsulating agents along with silk as a substrate for insulin-producing-cell adherence and proliferation with immunoisolatory attributes. The localization of islets within a defined scaffold/matrix permits ease of monitoring and retrieval with the integration of anti-inflammatory biologics (Dex and IL-4), which may help in modulating the local immune environment and direct macrophage phenotype at the implantation site (Jiang et al., 2017; Liu et al., 2016). These biomolecules have shown promising outcomes when compared with cell-based immunoisolation (Jiang et al., 2017; Weaver et al., 2015). Also, we utilized localized delivery of immunomodulatory factors with enhanced efficacy, and with reduced detrimental systemic side effects and toxicity as a strategy to control the immune response at the implant site (Jiang et al., 2017; Weaver et al., 2015). Since silk-alginate and silk-agarose scaffolds have macroencapsulated islet/ islet-like cells; it therefore makes them the best option for further *in vivo* investigation. Here, we report that islet cell culture on these scaffolds with immunoisolatory and immunomodulatory attributes results in "silk-based bio-artificial pancreas-like functions". Promising results with RIN-5 spheroids and rat primary islets suggest that the developed scaffolds can be used for human primary islets, which may be useful to explore in future work for improved clinical outcomes.

2.5. Significant Findings

The salient findings of this chapter are as follows:

1. Islet encapsulation holds promise as a treatment plan for type 1 diabetes owing to its immense benefits. Majority of the work for islet encapsulation focus on microencapsulation of single or small groups of islets. This technique has

inherent limitations like lower mechanical strength of the capsules, poor retrieval and, short life span in vivo. Herein, we have successfully employed silk-based macroencapsulation for islet encapsulation.

2. Primary rat islets when cultured on silk scaffolds and macroencapsulated in semi-permeable alginate and agarose layers, maintained islet viability and glucose responsiveness. On the contrary, the control islets (in 2D) failed to survive and lost glucose responsiveness.

3. The 3D silk scaffold facilitated islet-like spheroid formation and mimicked native pancreatic-like niche; glucose challenge assay suggested desired insulin secretion in response to varied glucose concentrations.

4. Assessment of the immunoisolatory attributes showed restricted infiltrations of macrophage/inflammatory cells in the scaffolds *in vivo* projecting alginate and agarose as potential cell macroencapsulating agents.

5. Immunomodulatory effects were observed *in vitro* through release of anti-inflammatory biomolecules (Dexamethasone and IL-4) and localized polarization of macrophages (M0 to M2).

In the constant endeavor to improve islet encapsulation platform, the present study describes a macroencapsulation approach comprising of a silk-scaffold and semi-permeable encapsulating layers of alginate or agarose. The chapter presents a promising avenue for development of pancreas-like niche for encapsulated islets. In particular, it would be interesting to validate the potential of this approach in *in vivo* models for diabetes reversal. In concurrence with this rational, the next chapter describes the ability of silk-based matrices (hydrogels) for localized cytokine delivery and immunomodulation in an *in vitro* macrophage cell culture model with three approaches: cytokine encapsulation, macrophage encapsulation and co-encapsulation.

Chapter 3

Macrophage Polarization for Immunomodulation and Tailoring Local Biological Response

This chapter explores the potential of silk hydrogels to release the loaded cytokines and control macrophage polarization and plasticity. The extent of cytokine release and the polarization were explored and correlated with the physicochemical properties of the hydrogels.

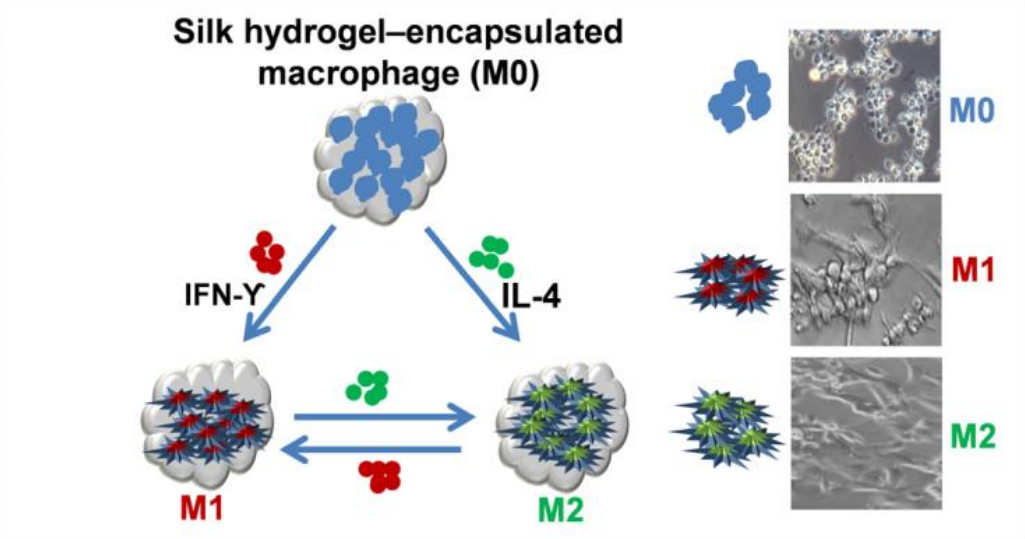

ABSTRACT

Macrophages, the key players in immunoregulation, are actively involved in tissue remodelling and vascularization. Recent advances in tissue engineering and regenerative medicine illustrate the importance of 'immuno-informed' biomaterials to regulate the microenvironment of biomedical implants. In the current study, silk-based 3D hydrogels were utilized to regulate cytokine delivery for macrophage, a type of immune cell, differentiation and polarization. Three different hydrogel variants, silk-poly (ethylene glycol) (PEG) (SP), silk-horseradish peroxidase (HRP) (SH) and silk-sonicated (SS) hydrogels were studied. Hydrogels were loaded with the M1 and M2 polarizing cytokines interferon-γ (IFN-γ) and interleukin-4 (IL-4), respectively. Functional cytokine release and macrophage polarization studies were conducted using three cytokine exposure approaches: cytokine encapsulation (macrophage in culture well), macrophage encapsulation (cytokine in culture media) and cytokine with macrophage co-encapsulation. The extent of macrophage polarization by cytokine-eluting and macrophage-encapsulating hydrogels was investigated using gene expression analysis for C-C chemokine receptor 7 (CCR7), Interleukin-1 beta (IL-1β), cluster of differentiation 206 (CD206) and cluster of differentiation 209 (CD209). The released cytokines polarized macrophages from an M0 phenotype to an M1/M2 phenotype. Also, lineage committed M1/M2 macrophages could be "switched" to their M2/M1 counterparts (M1-to-M2 or M2-to-M1 transition) exhibiting their well-established plasticity. When macrophages were encapsulated in hydrogels, polarization could be induced to the lineage committed M1 or M2 phenotypes either in polarizing media or when co-encapsulated with cytokines. Through this study, silk hydrogels demonstrated utility as a novel system for focal delivery of cytokines and macrophages as 'immuno-informed' 3D silk-biomaterials.

3.1. Introduction

Tissue engineering and regenerative medicine have emerged as interdisciplinary fields with importance in many areas of medicine (Vacanti and Langer, 1999). The success of tissue engineered implants relies on their long-term survival and function without eliciting detrimental immune responses (Franz et al., 2011). Biomaterial implants evoke host immune responses which lead to changes in the implant microenvironment. Recent studies showed that harnessing local inflammatory responses towards biomaterial implants can help modulate physiological outcomes in favour of the host/patient (Franz et al., 2011; Reeves et al., 2015; Spiller et al., 2015). These outcomes include implant integration, vascularization, wound healing, tissue remodelling and immune-suppression (Franz et al., 2011; Liu et al., 2016; Reeves et al., 2015; Roh et al., 2010; Spiller et al., 2015). Thus the development of potential "immunomodulating" or "immuno-informed" biomaterials is desirable (Franz et al., 2011).

As the most plastic cell of the hematopoietic system, macrophages are a suitable target for immunological studies (George et al., 2014). These cells play a pivotal role in normal physiology and disease states (Davies et al., 2013). There is a spectrum of tissue-resident macrophages in the body, including microglia (central nervous system), Langerhans cells (skin), alveolar (lung), osteoclast (bone), histiocytes (connective tissues), Kupffer cells (hepatic), intraocular (eyes), splenic, intestinal, synovial type A cells (synovial joints), peritoneum and bone marrow (Brown et al., 2012; George et al., 2014; Sanberg et al., 2010). During homeostatic conditions, native tissue-resident macrophages maintain their quiescent state as monocytes and are subsequently recruited to the site of inflammation and differentiated into macrophages. Mature macrophages are polarized to M1 (classical activation) or M2 (alternative activation) macrophages (George et al., 2014). Further, they are characterized on the basis of surface markers or secreted cytokines (George et al., 2014). Classically activated M1 macrophages, induced by IFN-γ, show microbicidal properties and promote a strong Type 1 T helper (Th1) response. Macrophages induced by IL-4 or IL-13 are known as alternatively activated/tissue regeneration macrophages because of their involvement in extracellular matrix (ECM) production (George et al., 2014; Reeves et al., 2015). Biomaterials that locally release cytokines without systemically activating the immune system may be beneficial for the regulation and treatment of macrophage-associated diseases such as atherosclerosis (Hansson and Libby, 2006; Khallou-Laschet et al.,

2010), insulin resistance (Odegaard and Chawla, 2013) cancer (Noy and Pollard, 2014) and metabolic syndrome (Chawla et al., 2011).

Silk is a biocompatible biomaterial with tunable biodegradation, and can be morphed into a range of biomaterial formats using aqueous-based processing techniques. All aqueous processing makes silk matrices amenable to protein and drugs incorporation while maintaining functionality (Partlow et al., 2014). Silk elicits a low immunogenicity/inflammatory response at the site of implantation that decreases gradually within a few weeks of implantation (Thurber et al., 2015). The diverse array of silk-based matrices exhibit the ability to be remodelled *in vivo* via degradation and vascularization, ultimately leading to complete replacement by native tissue (Thurber et al., 2015). The degree of remodelling, vascularization and tissue ingrowth can be modulated with the addition of bioactive signalling molecules involved in recruitment and activation of macrophages (Sridharan et al., 2015). Silk hydrogels are promising ferries for sustained and tuneable release (antibody, drug, antibiotic and growth factors) and may be used for loading of cytokines for immunomodulation (Reeves et al., 2015). Additionally, the degraded/leached products from the hydrogels can be detected by immune cells to initiate signalling cascades leading to release of inflammatory cytokines, recruitment of additional immune cells and phagocytosis (Thurber et al., 2015). Macrophages anchoring to the surface of the cytokine-loaded silk hydrogels may be activated/polarized at the location nearer to the implant (silk hydrogel in this case). The recruited monocyte/macrophages may be polarized by the release of specific cytokine encapsulated in the hydrogel (Reeves et al., 2015). Thus, the control of macrophage phenotype ratio (M1:M2) through modulation of silk biomaterial microenvironment would be useful for the development of silk-based next generation immuno-informed biomaterials (Reeves et al., 2015; Spiller et al., 2015), in this case with injectable formats as hydrogels.

Studies have shown the positive immune-modulatory effects of anti-inflammatory cytokines (IL-4 and IL-10) on the reversal of auto-immune disease. IL-4 and IL-10 plasmid suppresses the progression of autoimmune insulitis in a non-obese diabetic (NOD) mice model when injected with chimeric plasmids utilizing a gene therapy approach (Koh et al., 2000; Lee et al., 2002; Nitta et al., 1998). Also, the sequential delivery of immunomodulatory cytokines (IFN-γ and IL-4) from decellularized bone scaffolds facilitated the M1 to M2 transition of macrophages (*in vitro*) and exhibited enhanced vascularization (*in vivo*) (Spiller et al., 2015). Similarly,

in vivo early response to biomaterials was tuned with the release of anti-inflammatory cytokine (IL-4) contributing to accelerated resolution of the inflammatory phase (Minardi et al., 2016). In a recent study, scaffolds containing transforming growth factor beta-1 (TGF-β1) showed a decrease in inflammation post-implantation in mice (Liu et al., 2016). This approach also enhanced the function of the transplanted islets and reversal of diabetes (Liu et al., 2016).

In the current study, silk hydrogels (**Figure 3.1**) were utilized for cytokine release and macrophage polarization for prospective immuno-modulatory applications. Molecule release from silk biomaterial matrices depends on many factors, including silk concentration (% w/v), degree of physical cross-linking (crystallization) and the physicochemical properties of the loaded molecules (molecular weight, solubility, charge, etc.) (Guziewicz et al., 2011; Reeves et al., 2015; Uebersax et al., 2007; Wang et al., 2015a; Zhang et al., 2011). These features of silk 3D hydrogels were harnessed for slow, moderate and rapid release of the cytokines and subsequently hydrogel-encapsulated macrophage polarization. Such approaches have been utilized for antibiotic and drug release from silk hydrogels maintaining high local concentration and minimizing systemic exposure (Pritchard et al., 2013). We anticipate that the types of hydrogels, cytokines and release profiles described will have broad applicability for local cytokine/macrophage delivery for the treatment of pathological conditions currently complicated by systemic delivery approaches (Khademhosseini et al., 2009).

3.2. Materials and Methods

3.2.1. Silk processing and fibroin isolation

Silkworm cocoons from *Bombyx mori* were purchased from Tajima Shoji Co., LTD (Yokohama, Japan) (Rockwood et al., 2011). Cocoons were cut into small pieces and boiled in 0.02 M Na_2CO_3 (Sigma-Aldrich, St. Louis, MO) for 30 min. After boiling, fibers were washed using ultrapure water. Degummed fibers were dried in a fume hood overnight. The dried fibers were dissolved in 9.3 M LiBr (Sigma-Aldrich, St. Louis, MO) solution at 60 ºC for 4 h (20% w/v) and dialyzed against deionized water for 3 days to remove the LiBr. Post-dialysis, solution was centrifuged (4000g, 20 min, 4 ºC) to remove insoluble particulates. To determine the concentration of regenerated silk fibroin solution, a gravimetric method was adopted and silk solution was stored at 4 ºC for further use.

3.2.2. Silk hydrogel preparations

3.2.2.1. Silk-PEG (SP) hydrogel preparation

PEG MW 400 g mol^{-1} (Sigma-Aldrich, Kollisolv PEG E 400) liquid was used for SP hydrogel preparation with the technique previously described (Wang et al., 2015a). PEG-400 was dissolved in ultrapure distilled water (Invitrogen, USA), mixed homogenously to prepare 80% (v/v) PEG solution, filtered through 0.22 µm filter and stored at room temperature (~25 ºC).

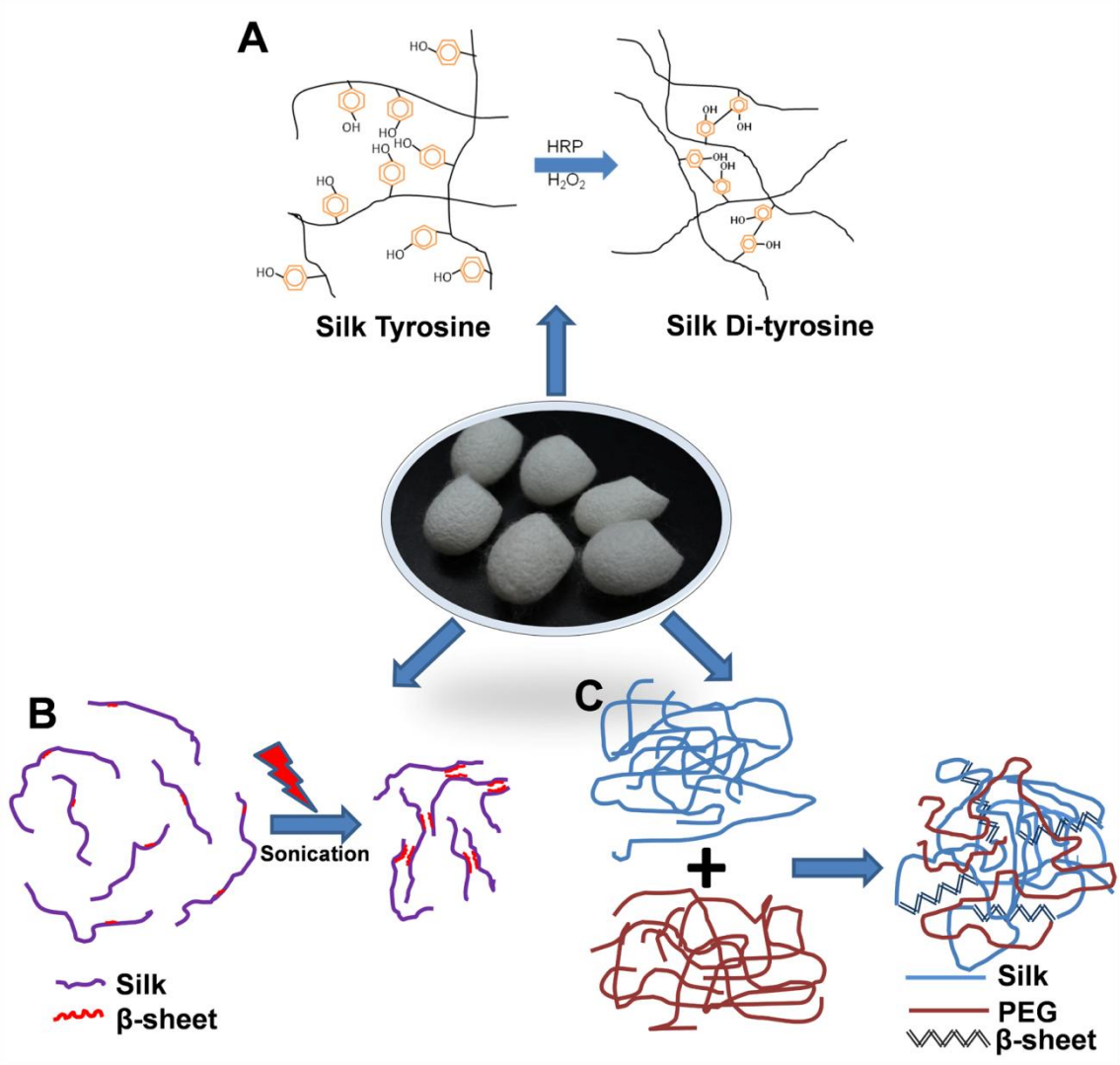

Figure 3.1. *Schematic representation of silk hydrogel preparation. Covalent cross-linking of tyrosine residues on silk protein chains in enzymatically formed SH hydrogels (A). Sonication-induced assembly of silk solution into hydrogels (B). Silk-PEG gel formation with β-sheet structure (C).*

To prepare 8% and 1% SP (w/v) hydrogels, 16% and 2% (w/v) of silk was gently mixed to equal volume of 80% (v/v) PEG-400 solution (1:1) in Lobind Microcentrifuge

tubes (Fisher Scientific, USA), separately. The mixture was incubated at 37 ºC until gelation. For cell culture studies, sterile silk and PEG solutions were used.

3.2.2.2. Silk-HRP (SH) hydrogel preparation

Silk-HRP hydrogel was fabricated as previously described, with some modifications (Partlow et al., 2014). Lyophilized HRP type VI (Sigma-Aldrich, St. Louis, MO) powder was mixed with ultrapure distilled water to prepare a stock of 1 mg/mL. Similarly, 1% (v/v) hydrogen peroxide (H_2O_2, Sigma-Aldrich, St. Louis, MO) stock solution was prepared in ultrapure distilled water. Enzyme stock solution of 20 µL was mixed with 1 mL of silk solution followed by addition of 20 µL H_2O_2 stock solution to initiate gelation. A similar protocol was followed for 8% and 1% SH hydrogel preparation. The solutions were mixed by gentle pipetting until gelation.

3.2.2.3. Silk-sonicated (SS) hydrogel preparation

SS hydrogels were prepared by sonicating 2 mL of silk solution (8% and 1%) in a 15 mL tube (Fisher Scientific) using a Branson 450 Sonifier (Branson Digital Sonifier, Model 450 power supply). The solution was sonicated at 10% amplitude for 20 s and left at 37 ºC for gelation which could be monitored visually (Soffer et al., 2008).

3.2.3. Cytokine loading on hydrogels and *in vitro* release

Recombinant human cytokines (IFN-γ and IL-4, Peprotech, Rocky Hill, NJ, USA) were encapsulated in all hydrogel variants during gelation. For release studies, 20 µL hydrogels containing 1 µg of cytokine (IFN-γ or IL-4) was incubated in Lobind Microcentrifuge tubes in 1 mL phosphate buffered saline (PBS) (Gibco, ThermoFisher Scientific, pH 7.4) and placed on a shaker (Reeves et al., 2015). PBS was replenished at specified time points (day 1, 3, 5, 7, 14, 21). Collected samples were stored at -80 ºC for further enzyme-linked immunosorbent assay (Human ELISA Development Kit, Peprotech, Rocky Hill, NJ, USA) for IFN-γ and IL-4, following manufacturer's instruction.

3.2.4. *In vitro* cytotoxicity of hydrogels with human mesenchymal stem cell (hMSCs)

Human mesenchymal stem cells (hMSCs, P0) were isolated from fresh bone marrow aspirate (Lonza, Basel, Switzerland) as described previously (Altman et al., 2002).

Cells were cultured in high glucose Dulbecco's Modified Eagle Medium (DMEM) supplemented with 10% fetal bovine serum (FBS), 1% antibiotic (100 U/mL penicillin and 100 mg/mL streptomycin, Gibco, Thermo Fisher Scientific), L-glutamine and non-essential amino acids (Life Technologies, Grand Island, NY). Cells were maintained in T175 flasks at optimal density and expanded in an incubator at 37 ºC and 5% CO_2. Cell culture medium was replenished two times per week. Cells were cultured to 90% confluence and trypsin passaged. For surface seeding, the three hydrogels types (100 µL) with a final silk concentration of 5% (w/v) were prepared in a 48 well plate and allowed to solidify in an incubator at 37 ºC for 1 h. Cells at passage 2 were used for seeding at a density of 5×10^4 cells (in 100 µL) per well and placed in an incubator for 1 h prior to flooding the wells with 1 mL media.

For cell encapsulation in SH hydrogels, the following steps were utilized (Partlow et al., 2014; Zhao et al., 2016). Silk, HRP and H_2O_2 were mixed and allowed to pre-gel for approximately 20 min, at which time 4×10^6 per mL cell suspension was mixed with silk in 1:1 volume ratio. Then 100 µL of the cell suspension in the pre-gelled silk solution was added to 48 well and allowed to gel for an additional 20 min and 1 mL media added to the wells. For cell encapsulation in 5% SP hydrogels, 500 µL of 10% silk was mixed with 500 µL of 80% (v/v) PEG. Cells were mixed to achieve a final cell concentration of 2×10^6 cells per mL and 100 µL of hydrogel was added to 48 well plates. For SS gel, 2 mL of silk solution (5% w/v) was sonicated at 10% amplitude for 20 s in a laminar flow hood and final cell concentration was maintained. Cell pellets, containing 2×10^6 cells, were dissolved in 100 µL of silk and further mixed with 900 µL of silk 8% (w/v). Then 100 µL of solution was added to 48 well plates. All cell culture studies were performed in an incubator (37 ºC, 5% CO_2).

Cytotoxicity and metabolic activity of the hydrogel encapsulated cells was determined after 1, 4 and 7 days of culture via AlamarBlue assay (Life Technologies, Grand Island, NY) following to the manufacturer's instructions. AlamarBlue, a non-toxic dye, measures the viability of the same batch of seeded cells at different time points. Briefly, cells were incubated in medium supplemented with 10% (v/v) AlamarBlue dye for 5 h at 37 ºC with 5% CO_2. After incubation, the absorbance of 100 µL of medium from each sample was read at 570/600 nm in a multiplate reader. Non-seeded wells supplemented with 10% AlamarBlue dye were used as negative control.

Imaging of the surface seeded cells was performed with Calcein AM (Sigma-Aldrich, USA) staining following the manufacturer's instructions. Live cells convert calcein AM

to calcein and fluoresce green showing viability (Wang et al., 2015a). Briefly, hydrogels were washed twice with PBS and incubated with 4 μM of Calcein AM, prepared in incomplete media (DMEM without FBS), for 20 min to stain live cells. After staining, hydrogels were washed thrice and images were taken using Zeiss fluorescence microscope (Carl Zeiss, Jena, Germany).

3.2.5. THP-1 cell culture and polarization in 2D

Human acute monocytic leukemia cell line (THP-1) was purchased through ATCC (Manassas, VA). Cells were cultured in RPMI media supplemented with 10% FBS and 1% antibiotics. Cells were cultured in T175 flasks at optimal density and expanded in a humidified incubator (37 ºC, 5% CO_2). For macrophage polarization study, 5×10^4 cells per well were seeded in Corning transwells plates (Fisher Scientific, USA). THP-1 cells were induced to macrophage (M0) using 100 ng/mL (162 nM) of phorbol 12-myristate 13-acetate (PMA) (Sigma-Aldrich, USA) in basal RPMI media for 16 h. After PMA treatment, macrophage differentiation (M0) was confirmed by their adherence to well plates.

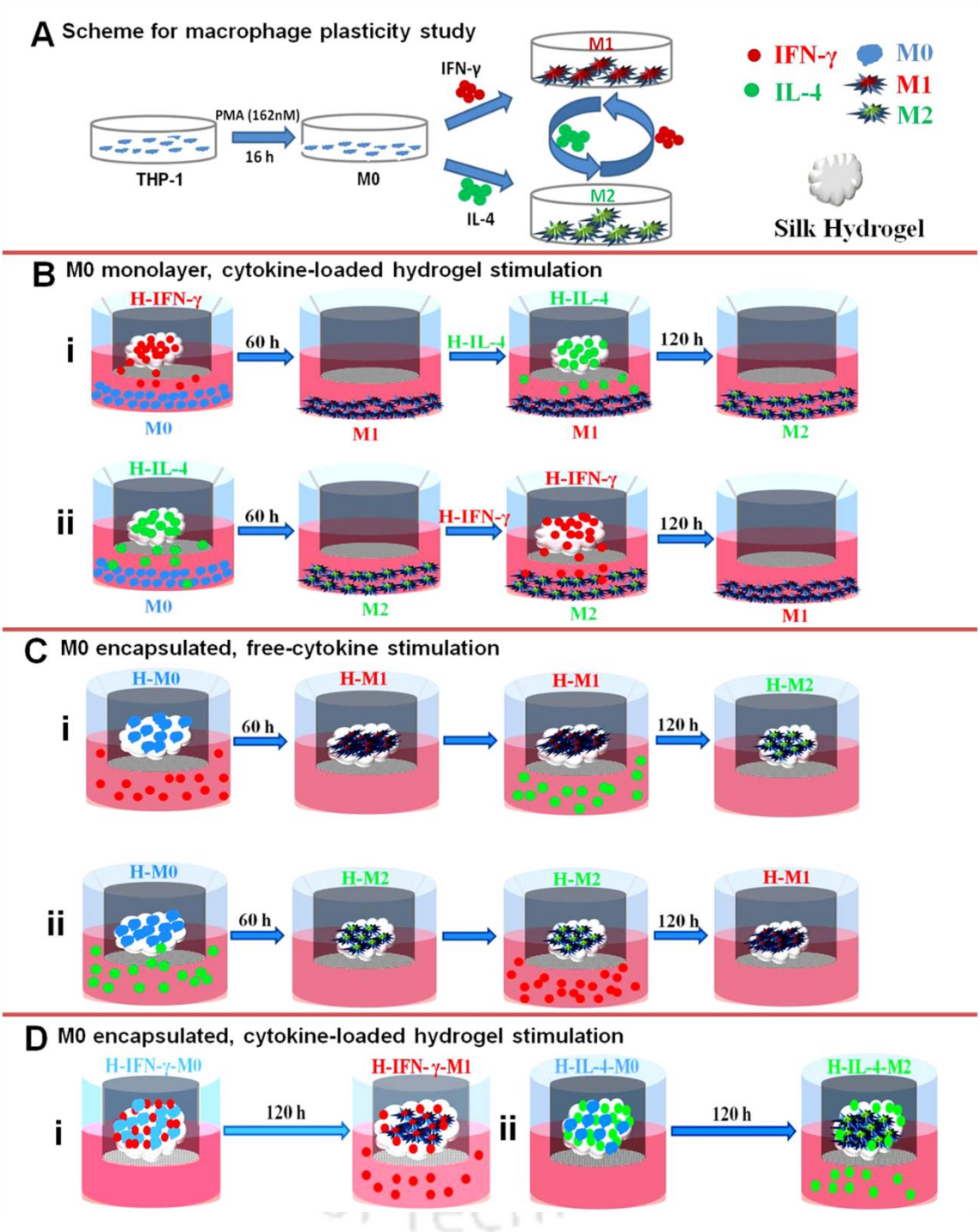

Figure 3.2. *Study design for in vitro macrophage polarization and plasticity using three different approaches. General scheme showing monocyte (THP-1) to macrophage (M0) conversion using PMA. Further, macrophage polarization and plasticity studies were conducted using pro-inflammatory IFN-γ and anti-inflammatory IL-4 cytokines (A). In the first approach, M0 cells were cultured in TCP wells and cytokine-loaded hydrogels were placed in transwell inserts. H-IFN-γ and H-IL-4 represent IFN-γ and IL-4 encapsulated in hydrogels, respectively (B). In the second approach, M0 cells were encapsulated in hydrogels (placed in transwell inserts); polarizing cytokines were provided through cell culture media. H-M0, H-M1 and H-M2 represent hydrogel-encapsulated M0, polarized M1 and polarized M2, respectively at different stages of polarization (C). In the third approach, M0 cells and individual cytokines were co-*

encapsulated in silk hydrogels. H-IFN-γ-M0, H-IFN-γ-M1, H-IL-4-M0 and H-IL-4-M2 represent M0 encapsulated with IFN-γ, polarized M1 encapsulated with IFN-γ, M0 encapsulated with IL-4, and polarized M2 encapsulated with IL-4, respectively (D).

After PMA treatment, the medium was switched to polarization conditions through cytokine-releasing hydrogels (8% SP, 8% SH and 8% SS) placed in the transwell inserts (**Figure 3.2B**). Macrophages (M0) were incubated with different silk hydrogels loaded with M1 (IFN-γ) and M2 (IL-4) polarizing cytokines to evaluate macrophage polarization potential of hydrogels on a time-dependent basis for 60 h and 120 h. Cell morphology was analyzed to assess macrophage polarization. At pre-specified time points (60 h and 120 h), cells were lysed and preserved for gene expression analysis for M1 and M2 markers.

3.2.6. Polarization in hydrogel-encapsulated M0 macrophages

Cell-encapsulating hydrogels were prepared as described in section 3.2.4. Briefly, THP-1 cells were induced to M0 using 100 ng/mL (162 nM) PMA in basal RPMI media for 16 h and cells were collected from tissue culture flasks using cell scrapper (Corning, USA). Macrophage polarization was conducted with M0 cells encapsulated within the hydrogels. The hydrogel volume (100 μL), final silk concentration (5% w/v) and THP-1 cell density (2×10^6/mL) were held constant for 3D polarization studies similar to hMSCs encapsulation. Cell-encapsulated hydrogels were added to transwell inserts and wells were flooded with media after gelation (**Figure 3.2C**). All cell culture studies were performed in an incubator (37 ºC, 5% CO_2). Polarization media was used as RPMI supplemented with 10% FBS and 20 ng/mL IFN-γ (for M1) and 20 ng/mL IL-4 (for M2) (**Figure 3.2C**). Imaging of hydrogel-encapsulated M0 cells was performed with 4 μM calcein AM (prepared in incomplete media) after 5 days of culture. Hydrogels were washed twice with PBS and incubated in staining solution for 20 min. Post incubation, hydrogels were washed thrice with PBS and images were taken under fluorescence microscope.

3.2.7. Polarization in hydrogel co-encapsulated macrophages and cytokines

Cell-encapsulated hydrogels were prepared as described in section 3.2.4. Macrophage polarization was done with M0 cells encapsulated in hydrogels with cytokines (IFN-γ/ IL-4). Cytokines were added during the cell encapsulation step. After gelation, cytokine-loaded hydrogels were incubated for 1 h in cell culture media to remove any

surface bound cytokine. These polarization studies were performed for five days with RPMI basal media changed every other day (**Figure 3.2D**). Hydrogel volume (100 µL), final silk concentration (5% w/v), cell concentration (2×10^6 per mL) and cytokine loading (200 ng/gel, IFN-γ /IL-4) were kept constant for 3D polarization studies. M0 cells entrapped in respective hydrogels were used as control for each time point. For cell imaging, M0 and IL-4 encapsulating hydrogels were incubated for 30 min in staining solution (1% (w/v) BSA, 0.5% (v/v) Triton X-100 in PBS) containing 0.1% (v/v) Hoechst 33342 (Sigma-Aldrich, USA) and AdipoRed (AdipoRed Assay Reagent, Lonza, USA). Cytoskeleton was stained using Fluorescein Phalloidin (ThermoFisher scientific) for F-actin and counterstained with Hoechst 33342 for nucleus. After staining, hydrogels were washed thrice and images were taken using KEYENCE all-in-one fluorescence microscope BZ-X700 (USA) and Z-stacking was performed using BZ-X Analyzer software.

3.2.8. RNA extraction and gene expression by real-time RT-qPCR

Analysis of gene expression specific to M1 and M2 was performed by quantifying the mRNA levels of respective genes. Cells were lysed and RNA was isolated and purified using RNeasy Plus Mini Kit (Qiagen, CA) according to manufacturer's protocol for on-column treatment. From hydrogels, total RNA was extracted by thoroughly pipetting the hydrogel to disrupt the gel network. Hydrogels were treated with Trizol (Invitrogen, USA) for 15 min. The treated hydrogels were centrifuged (12000g, 10 min, 4 ºC) and the supernatant was incubated in a new tube with chloroform. After centrifugation (12000g, 15 min, 4 ºC), the upper aqueous layer was transferred to RNeasy Plus Mini Kit and extracted as above. The RNA concentration and quality was measured by NanoDrop 1000 Spectrophotometer (Thermo Scientific). For reverse transcription, 1 µg of RNA was converted to cDNA using High Capacity cDNA Reverse Transcription Kit (Applied Biosystems, Carlsbad, CA). RT-qPCR was performed using Power SybrGreen (Thermo Fisher Scientific) using the Stratagene Mx3000P QPCR system (Stratagene, CA). All assays were carried out in duplicate in 96-well format plates. Primers (**Table 3.1**) were used at 1 µM concentration and run with cycles of 15 s at 95 ºC and 45 s at 60 ºC for 40 cycles. To quantify relative gene expression changes, the $\Delta\Delta C_T$ method was used with Glyceraldehyde-3-phosphate-dehydrogenase (GAPDH) as a housekeeping gene (Livak and Schmittgen, 2001). Changes in target gene expression in M1 and M2 macrophages were expressed as fold change from control groups.

Table 3.1. *Primers for RT-qPCR*

Gene	Forward sequence	Reverse sequence	Phenotype
GAPDH	ACAACTTTGGTATCGTGGAAGG	GCCATCACGCCACAGTTTC	N/A
CD68	CTTCTCTCATTCCCCTATGGACA	GAAGGACACATTGTACTCCACC	M0
CCR7	TGAGGTCACGGACGATTACAT	GTAGGCCCACGAAACAAATGAT	M1
CD206	CTACAAGGGATCGGGTTTATGGA	TTGGCATTGCCTAGTAGCGTA	M2
IL1B	ATGATGGCTTATTACAGTGGCAA	GTCGGAGATTCGTAGCTGGA	M1
CD209	AATGGCTGGAACGACGACAAA	CAGGAGGCTGCGGACTTTTT	M2

3.2.9. Statistical analysis

All experiments were performed in triplicate and results represented as mean ± standard deviation (S.D.). One-way analysis of variance (ANOVA) was performed to calculate statistical significance between different groups followed by Tukey's test. All statistical analysis was performed using OriginPro 8 (Originlab Corporation, USA). Differences between groups were considered statistically significant when $p \leq 0.05$.

3.3. Results

3.3.1. *In vitro* cytokine release profile

In vitro release of IFN-γ and IL-4 cytokines from silk hydrogels (SP, SH and SS) in PBS was measured by ELISA over 21 days. The cumulative and percentage of cytokine released are shown in **Figure 3.3**. An average of 212 ng (21%) and 282 ng (28%) of IFN-γ and IL-4, respectively, were rapidly released from the 1% SH hydrogels within 24 h. The corresponding values for these cytokines were 18 ng (1.8%) and 20 ng (2%) respectively for the 1% SS hydrogels. As revealed from **Figure 3.3**, 1% SH hydrogel showed the highest release. An inverse relationship was observed between the release for both the cytokines ($p \leq 0.01$) and the increased silk concentration in the hydrogels (from 1-8%w/v)

.

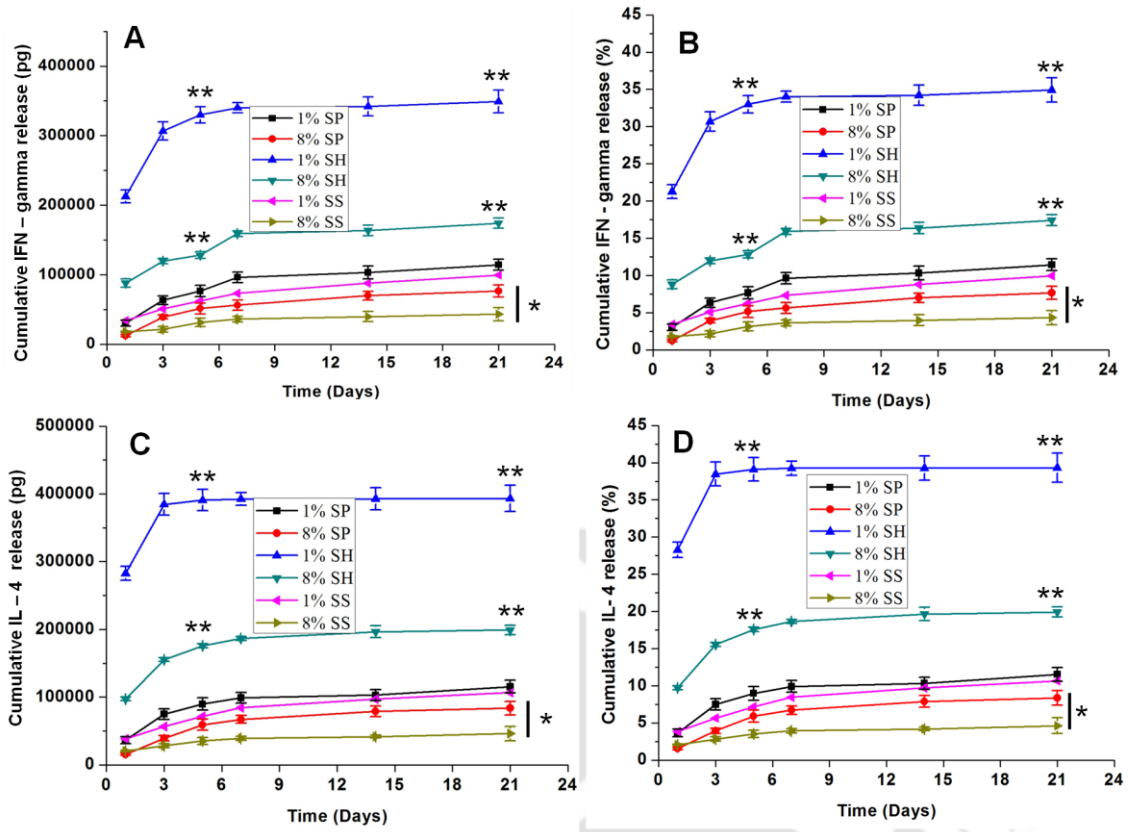

Figure 3.3. *Cumulative IFN-γ and IL-4 release (Picogram (pg)) from the silk-based hydrogels. Each hydrogel (20 µL) was loaded with 1 µg cytokine (A and C). Cumulative IFN-γ and IL-4 release (%) from all the six hydrogels (B and D) was monitored via ELISAs. Data represents mean ± standard deviation (n=3). Statistical differences were determined with one-way ANOVA. (* $p \leq 0.05$,** $p \leq 0.01$).*

There was a significant difference in the amount of released cytokine from 8% SP and 8% SS ($p \leq 0.05$). Based on the release data for both the cytokines, differences among the silk hydogels may be predicted. SP hydrogels showed a reduced burst release initially and relatively sustained release in following days when compared to SS hydrogel. Statistically higher cumulative release was observed in case of SH hydrogels on day 21 when compared to other groups (SP and SS) ($p \leq 0.01$). The plateaued region suggested that the residual cytokines were entrapped in the hydrogels, hindering their further release (Wang et al., 2015a; Zhang et al., 2011).

3.3.2. *In vitro* cytocompatibility of hydrogels with human mesenchymal stem cells (hMSCs)

The *in vitro* assay showed attachment and viability of hMSCs when cultured on hydrogel surfaces (**Figure 3.4A**). hMSCs exhibited fibroblast-like spindle morphology on hydrogel surfaces. Cells were evenly distributed on hydrogel surfaces similar to

TCP (control) suggesting suitability of these hydrogels for cell studies. Viable cells stained using Calcein (green) were visible all over the gel surface. The hydrogels supported cell survival and proliferation over the 7 days of testing (**Figure 3.4B**). The SH hydrogel group exhibited a significant increase in cell viability (day 7 versus day 1, $p \leq 0.01$). SS and SP hydrogels showed ~1.45 and 1.23 fold increase in cell viability, respectively (day 7 versus day 1, $p \leq 0.05$). The SH hydrogels exhibited the highest increase in cell viability, ~1.7 fold.

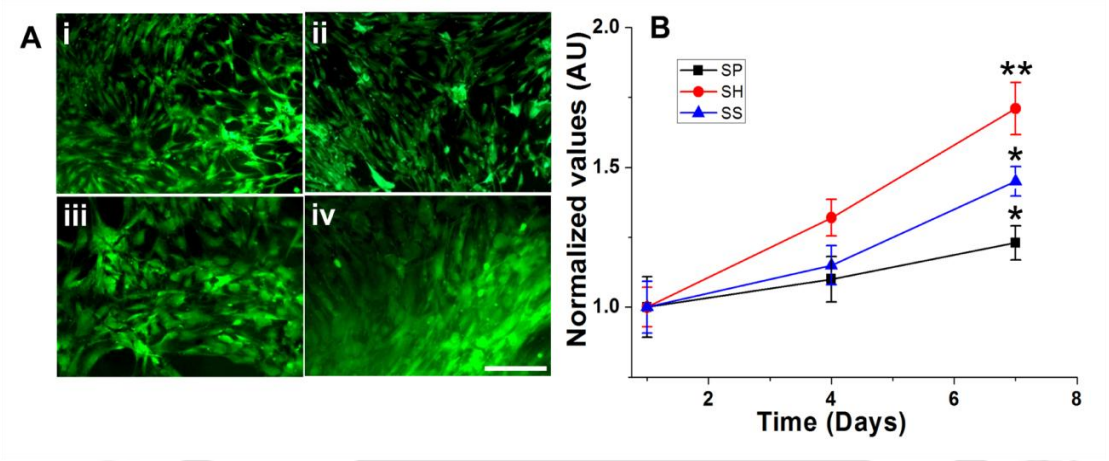

Figure 3.4. *Human mesenchymal stem cell interaction with hydrogel surfaces. Viable cells were stained in green using Calcein AM (A). Cell attachment on TCP (i), 5% SP (ii), 5% SH (iii), and 5% SS gels (iv). Scale bar represents 200 µm. Cell proliferation after hMSCs encapsulation in silk hydrogels (5% w/v) over 7 days period as determined by AlamarBlue assay and presented as fold change compared to day 1 (B). (*$p \leq 0.05$, **$p \leq 0.01$)*

3.3.3. THP-1 cell culture and polarization in 2D

Macrophages are well-known for their plasticity (Kumar et al., 2015; Reeves et al., 2015). This fact was evident in our two stage macrophage polarization study. Macrophages treated with control hydrogels (without loaded cytokines) adhered to the plate as round cell/clusters without spread (**Figure 3.5A**).

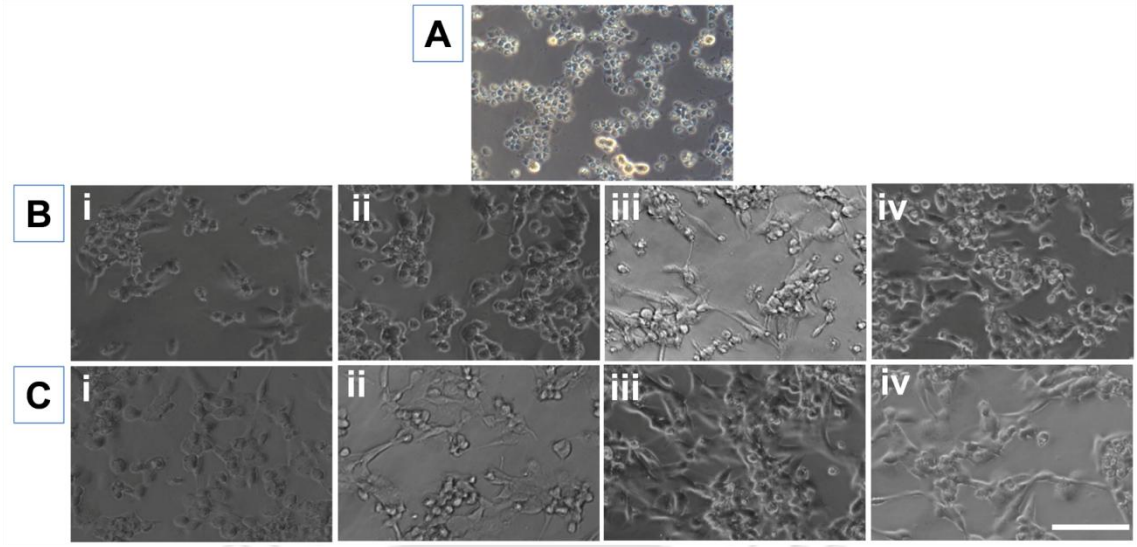

Figure 3.5. *Morphology of macrophage when polarized with cytokine-releasing silk hydrogels. Morphology of THP-1 cells (M0) after overnight PMA (162 nM) treatment and incubation with control SH hydrogel (A). Morphology of M0 cells after treatment for 60 h with 20 ng/mL IFN-γ directly added to culture media (i), with SP (ii), SH (iii) and SS hydrogel (iv) loaded with 1µg IFN-γ (B). Morphology of M0 cells after treatment for 60 h with 20 ng/mL IL-4 directly added to culture media (i), with SP (ii), SH (iii) and SS hydrogel (iv) loaded with 1µg IL-4 (C). Scale bar represents 100 µm.*

THP-1 cells were treated with PMA (Kumar et al., 2015; Li et al., 2016; Reeves et al., 2015) to differentiate into macrophage (M0), followed by treatment with hydrogels loaded with IFN-γ (H-IFN-γ) or IL-4 (H-IL-4) (8% SP, 8% SH and 8% SS) for 60 h. To validate the macrophage plasticity, cells were treated with hydrogels, containing the opposing cytokine, for an additional 60 h (**Figure 3.2B**).

For example, cells treated with H-IFN-γ were switched to transwell inserts with H-IL-4 for additional 60 h (**Figure 3.2B,i**) and vice versa (**Figure 3.2B,ii**). QPCR was used to quantify the M1 and M2 cell-specific markers expressions. As shown in **Figure 3.6A,i**, cells treated with H-IFN-γ for 60 h showed strong upregulation of CCR7 (M1 macrophage marker) and downregulated CD206 expression (M2 macrophage marker) (**Figure 3.6A,ii**). When switch to the well with H-IL-4, CD206 expression was significantly upregulated (**Figure 3.6A,iii**) with a reduction in CCR7 expression (**Figure 3.6A,iv**). H-IFN-γ caused the macrophages to adopt a dendritic phenotype with multiple protrusions (**Figure 3.5B**). On the other hand, H-IL-4-treatment induced the cells to spread over a wider area than the control (without the numerous projections) (**Figure 3.5C**) (Reeves et al., 2015). Together these data indicate that IFN-γ and IL-4 loaded hydrogels induced the M1 and M2 phenotype (Chan et al., 2008; Kuss et al., 2014), respectively.

In line with the release study, all of the hydrogels induced a M1 and M2 polarization of M0 macrophage and the M1-to-M2 or M2-to-M1 "switch" ($p \leq 0.01$) in a cytokine release concentration dependent manner. SH hydrogels polarized macrophages to a greater extent compared to the SS hydrogels ($p \leq 0.01$). SP hydrogels exerted moderate polarization, in line with the cytokine release profile from 8% SP hydrogel.

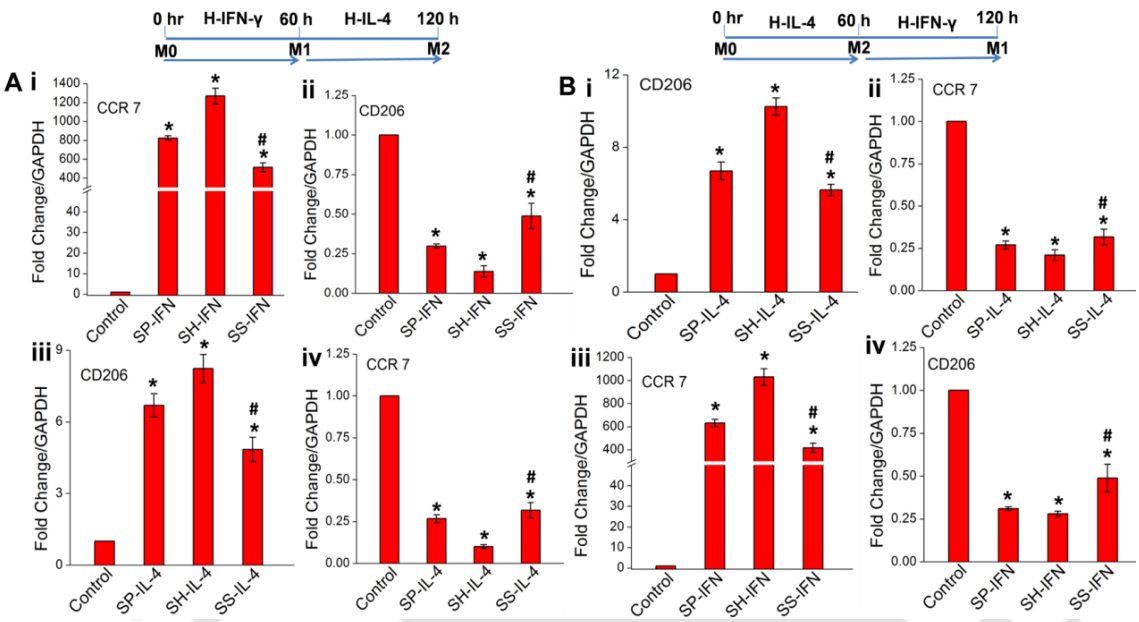

Figure 3.6. *Monolayer macrophage plasticity upon cytokine release from silk hydrogels. Macrophages were initially differentiated with H-IFN-γ for 60 h then media was switched to H-IL-4 for the following 60 h (A). Macrophages were initially differentiated with H-IL-4 for 60 h then media was switched to H-IFN-γ for the following 60 h (B). Expression of CCR7 and CD206 was quantified by qPCR at 60 h after initial polarization and 120 h after hydrogel switching. *$p \leq 0.01$ vs. control, $^{\#}p \leq 0.05$ vs. SH. H-IFN-γ represents. IFN-γ encapsulated in hydrogels and H-IL-4 represents IL-4 encapsulated in hydrogels.*

3.3.4. Polarization of hydrogel-encapsulated M0 macrophages

Efficacy of macrophage polarization was determined when M0 cells were encapsulated in 3D silk hydrogel. M0 macrophage remained viable after encapsulation in all three silk hydrogel formats (**Figure 3.7**). To validate the macrophage differentiation and plasticity, macrophage-encapsulating hydrogels (H-M0 in 5% SP, 5% SH and 5% SS) were loaded on transwell inserts and treated with polarizing media for 60 h. The cells were then incubated with media containing the opposing cytokine (IL-4 → IFN-γ or IFN-γ → IL-4), for an additional 60 h (**Figure 3.2C**).

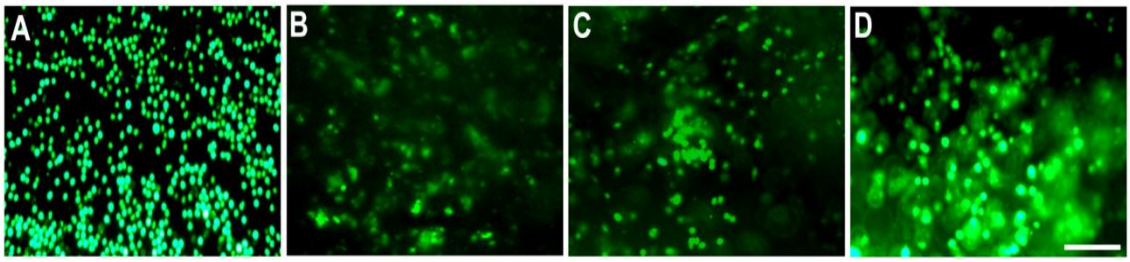

Figure 3.7. *Images of monolayer and silk hydrogel-encapsulated M0 macrophage. Cultured on TCP (A), encapsulated in 5% SP (B), 5% SH (C), and 5% SS hydrogels (D). Viable cells were stained in green using Calcein AM on culture day 5. Scale bar represents 50 μm.*

M1 and M2 cell-polarization was quantified via qPCR. H-M0 treated with IFN-γ for 60 h showed significant upregulation of CCR7 (**Figure 3.8A,i**) and downregulation of CD206 expression (**Figure 3.8A,ii**). When the medium was switched to IL-4 supplementation for the following 60 h, CD206 expression significantly increased (**Figure 3.8A,iii**) and CCR7 expression reduced (**Figure 3.8A,iv**). Similar polarization results were obtained when H-M0 cells were first polarized to an M2 phenotype and then repolarized to an M1 phenotype (**Figure 3.8B**). H-M0 treated with IL-4 for 60 h showed significant upregulation of CD206 expression and strong downregulation of CCR7 expression (**Figure 3.8B,i and ii**). After 60 h, switching to M1 polarizing media showed upregulated CCR7 and downregulated CD206 expression (**Figure 3.8B,iii and iv**). In all the cases SP hydrogels showed the maximum extent of polarization as compared to SH and SS. SH hydrogels showed a moderate extent of polarization. The results indicated that hydrogel-encapsulated M0 macrophages polarized to lineage committed M1/M2 macrophages when cultured in polarizing culture conditions.

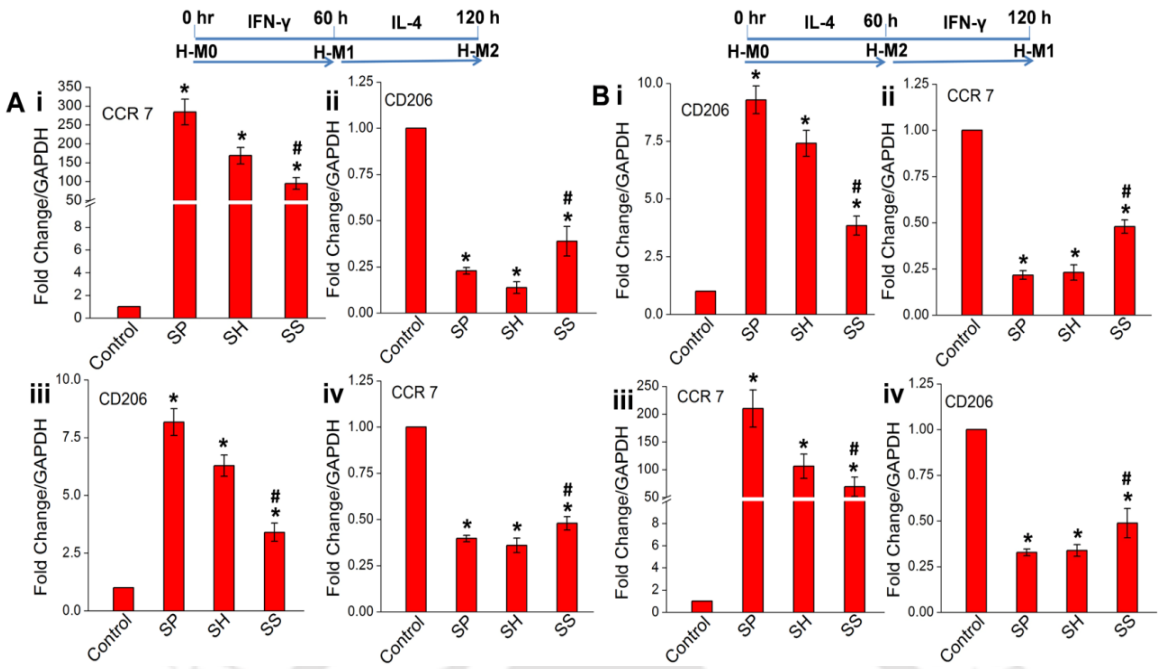

Figure 3.8. *Encapsulated macrophage plasticity upon exposure to free-cytokines in the media. H-M0 were initially differentiated with IFN-γ in media for 60 h then hydrogels were switched to IL-4 containing media for the following 60 h (A). H-M0 was initially differentiated with IL-4 in media for 60 h then hydrogels were switched to IFN-γ containing media for the following 60 h (B). Expression of CCR7 and CD206 was quantified by qPCR at 60 h after initial polarization and 120 h after media switching. *$p \leq 0.01$ vs. control and $^{\#}p \leq 0.05$ vs. SP. H-M0, H-M1 and H-M2 represent hydrogel-encapsulated M0, polarized M1 and polarized M2, respectively.*

3.3.5. Macrophage plasticity in hydrogel co-encapsulated macrophages and cytokines

M0 cell-loaded hydrogels containing cytokines were evaluated for macrophage polarization (**Figure 3.2D**). M0 cells encapsulated in different hydrogels with cytokine (IL-4) showed homogenous cell distributions (**Figure 3.9**). Silk matrices, cell nucleus (DAPI) and cytoskeleton (phalloidin) were stained in red, blue and green, respectively.

For polarization studies, hydrogels containing cells and cytokines were incubated for 1 h in cell culture media to remove any surface bound cytokines. Cells co-encapsulated with IFN-γ and IL-4 (H-IFN-γ-M0 and H-IL-4-M0), were evaluated for macrophage polarization study after 120 h of exposure. After polarization, four macrophage markers, CCR7, IL1β, CD206 and CD209 were quantified.

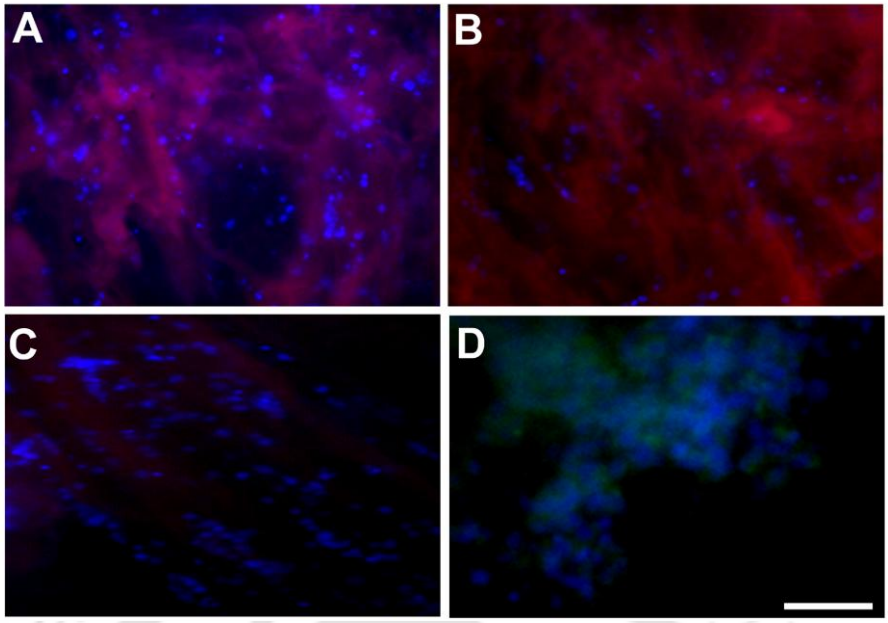

Figure 3.9. *Representative images of M0 macrophages encapsulated in hydrogels with IL-4 cytokine after 120 h. Encapsulated in 5% SP (A), 5% SH (B), 5% SS (C), and 5% SH hydrogels (D). Red shows silk matrices stained with Adipo red, blue shows nucleus and green for cytoskeleton. Scale bars represent 50 μm.*

Macrophages co-encapsulated with IFN-γ, (H-IFN-γ-M0) for 120 h showed significant upregulation of CCR7 (**Figure 3.10A,i**) and downregulated CD206 expression (**Figure 3.10A,ii**). Similarly, H-IFN-γ-M0 showed a significant upregulation of IL1β (**Figure 3.10A,iii**) and downregulated CD209 expression (**Figure 3.10A,iv**). When co-encapsulated with IL-4 (H-IL-4-M0), cells exhibited strong upregulation of CD206 (**Figure 3.10B,i**) and CD209 (**Figure 3.10B,iii**). Conversely, expression of IFN-γ (**Figure 3.10B,ii**) and IL1β (**Figure 3.10B,iv**) was downregulated. Using this approach, SP hydrogels showed maximum polarization followed by SH and SS hydrogels. The results indicated that M0 macrophage, when co-encapsulated with cytokines, can effectively be polarized to lineage committed M1/M2 macrophages.

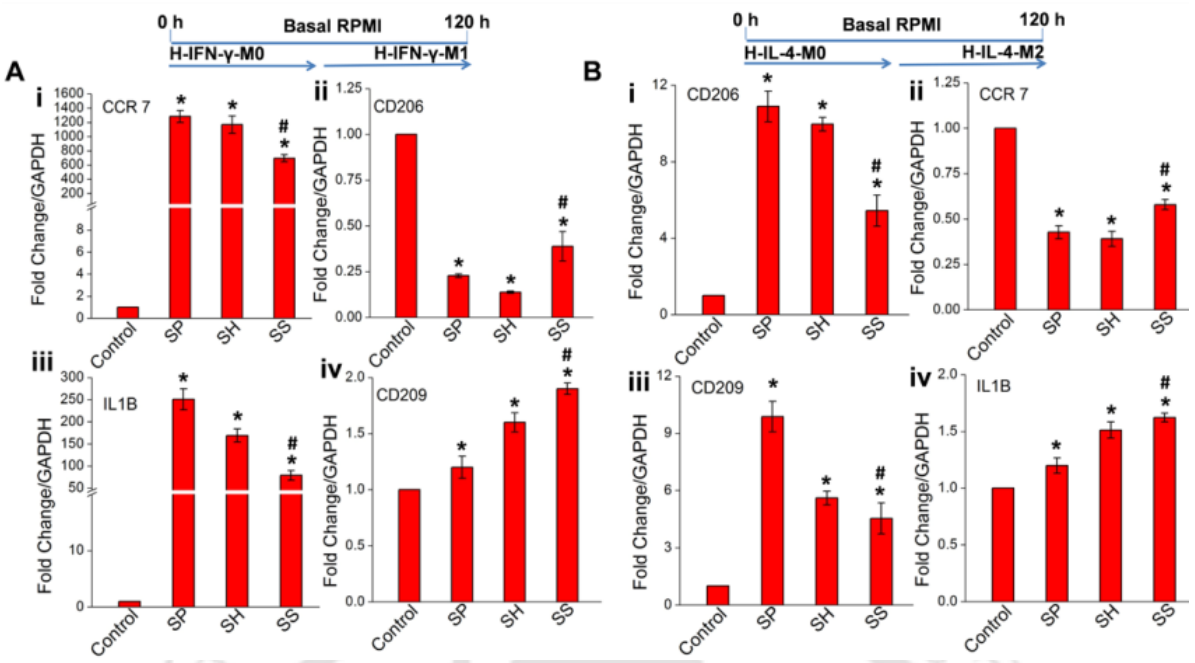

Figure 3.10. *M0 macrophage polarization when encapsulated in silk hydrogels containing cytokines. M0 macrophages encapsulated in 5% SP, 5% SH, and 5% SS hydrogels with IFN-γ (A) and IL-4 (B) cytokine for five day (120 h). Expression of CCR7, IL1B, CD206 and CD209 was quantified by qPCR at 60 h after initial polarization and 120 h after media switching. *p ≤ 0.01 vs. control, #p ≤ 0.05 vs. SP. H-IFN-γ-M0, H-IFN-γ-M1, H-IL-4-M0 and H-IL-4-M2 H-M2 means M0 encapsulated with IFN-γ, polarized M1 encapsulated with IFN-γ, M0 encapsulated with IL-4, and polarized M2 encapsulated with IL-4, respectively.*

3.4. Discussion

Cytokine mediated macrophage phenotypic 'biasing' as pro-inflammatory (M1) or pro-healing (M2) was investigated via three different silk-based approaches: a) delivery of human IFN-γ or IL-4 through silk hydrogels and encapsulation of the macrophages b) with and c) without the cytokines within the hydrogels. IFN-γ and IL-4 were chosen because of their robust M1 and M2 stimulating activities (Spiller et al., 2015). Cytokine-macrophage interaction is often species specific (Gordon and Taylor, 2005; Kumar et al., 2015) and as such we used human THP-1 monocytic leukemia cell line, a well reported homogeneous model for macrophage polarization studies (Daigneault et al., 2010; Maeß et al., 2010; Tjiu et al., 2009).

The current study was performed with three different hydrogel types, namely, silk-poly (ethylene glycol) (SP), silk-horse radish peroxidase (SH) and silk-sonicated (SS) (**Figure 3.1**). Each of these three hydrogels had two variants, fabricated using either 1% or 8% (w/v) *Bombyx mori* silk (purified fibroin). Previously reported

protocols were used to fabricate the hydrogels with proven biocompatibility and biodegradability based on as attested by *in vitro* and *in vivo* studies (Partlow et al., 2014; Wang et al., 2008; Wang et al., 2015a; Wang et al., 2015b; Zhang et al., 2011; Zhao et al., 2016). In SP hydrogels, PEG, a highly hydrophilic molecule, induces silk secondary structure transitions from random coils to β-sheets and hydrogel network formation (Wang et al., 2015a; Wang et al., 2015b). PEG forces the silk hydrophobic domains to assemble, due to excluded volume effect, resulting into crystalline β-sheets (Wang et al., 2015a; Wang et al., 2015b). HRP enzyme, when added to silk solution in the presence of H_2O_2, results in the formation of a highly elastic and stable hydrogel. In this reaction, HRP facilitates covalent cross-linking of tyrosine residues in silk using H_2O_2 as a substrate. For SS hydrogel, gelation was accompanied by β-sheet structure formation, due to changes in hydrophobic hydration (Wang et al., 2008).

Silk biomaterials used here and their modifications have been extensively used for tissue engineering applications. SH offers utility in diverse applications (Partlow et al., 2014) and smart biomaterial uses (Zhao et al., 2016). SP hydrogel has shown potential for bone (Acharya et al., 2009), cervical tissue (Heard et al., 2013), ear (Yu et al., 2016) and cornea (Suzuki et al., 2015) among other tissue-specific outcomes. It has been widely used for tissue adhesives (Burke et al., 2015; Serban et al., 2011), adhesion prevention (Vepari et al., 2010; Wang et al., 2015b) and antithrombotic (Vepari et al., 2010; Wang et al., 2015a; Wang et al., 2015b) applications both *in vitro* and *in vivo*. SS hydrogels have been utilized for islet encapsulation (Davis et al., 2012), cartilage (Yodmuang et al., 2015), growth factor delivery for elevation of the maxillary sinus floor (Zhang et al., 2011), and drug delivery for cancer treatment and many other biomaterial applications (Lovett et al., 2015; Wang et al., 2008).

The ratio of pro-healing to pro-inflammatory population of macrophages (CD206+/CCR7+), defined as 'regenerative bias', shows that, rather than the extent of macrophage presence, the specific phenotype (M2/M1) at the site of injury regulates regenerative outcomes (Mokarram et al., 2012). Considering the dual importance of M1 and M2 macrophages, we focused our studies on three different approaches. The first was encapsulation of cytokines in different silk hydrogels to regulate their release profile (**Figure 3.3**) and macrophage polarization (**Figure 3.6**). These cytokine loaded hydrogels successfully polarized macrophages *in vitro* (**Figure 3.5**). In the second approach, M0 macrophages were encapsulated in 3D silk hydrogels mimicking the *in vivo* situation where tissue-resident macrophages are polarized to lineage-committed

macrophages by cytokines in microenvironments (**Figure 3.7**). In the third approach, co-encapsulated macrophages (M0 and cytokine together) polarized macrophages to M1/M2 to a greater extent (**Figure 3.10**).

Cytokines for M1 polarization (IFN-γ, TNF-α) are known to enhance angiogenesis leading to matrix vascularization in its microenvironment. Similarly, cytokines for M2 polarization (IL-4, IL-10) lead to tissue regeneration and proliferation (Reeves et al., 2015), with suppressive effects on innate immune cell population growth, thus a delay in fully activated T cell responses (Liu et al., 2016). Thus, the cytokines locally regulate biomaterial implantation outcomes to enable the long term functioning of allogenic grafts. Cytokine release studies, from silk-based hydrogels were conducted to optimize the release profile from the different hydrogels (**Figure 3.3**). The hydrogels could maintain a sustained release of cytokines in 21 days of study. The degree of cross-linking/entanglement in the hydrogel matrix regulated the cytokine release kinetics. As per the result, the bulk matrix provides a diffusion barrier to cytokine release, along with the interactions between the cytokines and the silk protein matrices. β-sheet content aids cytokine entrapment and sustained release (Wang et al., 2015a).

Difference in molecular weight IFN-γ (16.8 kDa) and IL-4 (15.1 kDa) might be one reason for relatively more IL-4 release (28%) when compared with IFN-γ (21%) in initial 24 h. The rapid release exhibited by SH hydrogels may be due to the absence of β-sheets (Partlow et al., 2014). Similarly, SS and SP hydrogels exhibited altered release profiles based on the silk concentration (1 or 8 % w/v) (Katayama et al., 2000; Wenk et al., 2008) and amount of β-sheet (Wang et al., 2015a). As reported previously, 7.5% SP gels have more than 50% β-sheet of the total secondary structures. On the other hand, SS gels of the same concentration have less than 40% β-sheet content (Wang et al., 2015a). The presence of PEG in SP hydrogels inhibited the burst release; longer-term release was achieved with SP hydrogels as compared to SS hydrogel of same concentration (8% w/v). This difference in release may be attributed to competitive diffusion with PEG (Wang et al., 2015a). However, strong silk-cytokine interactions were observed and major fractions of the cytokines were entrapped in the silk hydrogels. This has previously been reported for silk biomaterials when biomolecules (growth factors and drugs) were encapsulated in hydrogels (Guziewicz et al., 2011; Uebersax et al., 2007).

When implanted *in vivo*, proteolytic enzymes degrade silk matrices and

destabilize silk-protein interactions. These factors may lead to faster release and greater total released amount (Coburn et al., 2015). Previous studies with silk films showed that the macrophages gradually degraded the silk matrix to access trapped cytokines (Reeves et al., 2015). This accessibility shows that cytokine-loaded hydrogels may have potential of prolonged localized immune-modulation even after the plateau release of cytokines. The entrapped cytokines may play other significant roles in immune-modulation when macrophages grow directly on these matrices either on surface or encapsulated (Reeves et al., 2015). The 8% SH, SP, SS hydrogels for fast, moderate and slow release, respectively, were used in the macrophage polarization studies. The released cytokines from all the hydrogels were at physiologically viable levels for macrophage polarization (M1→M2) and repolarization (M2→M1) (**Figure 3.6**). With adequate cytokine loading, inflammatory responses, variation in degradation profile and remodelling rate of hydrogels might be examined.

To verify that the hydrogels were viable substrate for cell studies, hMSCs were (a) cultured on surface of preformed hydrogels and (b) encapsulated during gelation. Cell seeded on hydrogel surfaces showed good adhesion and confluence similar to TCP. Cells were in well spread morphology exhibiting good interaction with hydrogel matrices for cytocompatibility (**Figure 3.4A**). This result is in accordance with previous studies (Partlow et al., 2014; Wang et al., 2008; Wang et al., 2015b). Live cell fluorescence imaging confirmed homogeneous distribution of viable M0 macrophages when encapsulated in the different hydrogels (**Figure 3.7**). Similarly, M0 macrophages when encapsulated with IL-4 cytokines in different hydrogels were well dispersed. Staining of cytoskeleton and nucleus on SH hydrogels confirmed the even cell distribution (**Figure 3.9**).

As reported previously (Wang et al., 2008), in cell-encapsulating 4% (w/v) SS hydrogels, cells were in a non-aggregated form throughout, and maintained viability and metabolic activity until 21 days in contrast to 8 and 12% (w/v) hydrogels. The loss of cell viability and proliferation in hydrogels with higher protein concentrations (8 and 12% w/v) was likely due to reduced nutrient diffusion and mechanical restrictions at higher gel concentrations (Wang et al., 2008). However, poor physical stability of the < 4% (w/v) hydrogel restricted usability.

In our experiments, 5% (w/v) SH, SS and SP hydrogels were shown to support mesenchymal stem cell proliferation. Thus, macrophage encapsulation studies were carried out with 5% (w/v) silk as reported earlier for static culture (Partlow et al., 2014;

Wang et al., 2008; Zhao et al., 2016). All three hydrogels maintained their integrity and mechanical robustness throughout the polarization and plasticity studies. Hydrogel-encapsulated M0 macrophages with cytokine stimulation via media supplementation could be polarized to lineage dependent macrophages (M1/M2) (**Figure 3.8**). Additionally, the encapsulated and differentiated macrophage maintained their plasticity as evidenced by the ability to transition from an M1 to an M2 phenotype and an M2 phenotype to an M1 phenotype. Furthermore, the extent of polarization depends on the access of cytokines to the encapsulated cells. SP hydrogels supported enhanced polarization possibly due to increased diffusivity of cytokines. PEG components in SP hydrogels have been previously shown to slowly leach out resulting in highly porous structure (Wang et al., 2015a). Similarly, SH hydrogels are having relatively elastic networks which help high diffusion of cytokine-supplemented media (Partlow et al., 2014). SS hydrogels are known to be stiffer with highly intricate hydrogel networks posing a diffusion barrier to cytokine perfusion to hydrogels (**Figure 3.8**) (Wang et al., 2008).

M0 cells co-encapsulated with cytokines could also be polarized in a 5 day macrophage polarization studies when examined for CCR7 and CD206 expression (**Figure 3.10**). In yet another validation experiment, IL1β and CD209 expressions were quantified. The enhanced expression of IL1β and decreased expression of CD209 was observed in hydrogels with IFN-γ. Conversely, IL-4 treatment increased CD209 expression and decreased IL1β expression (**Figure 3.10**). This enhanced gene expression might be attributed to cumulative effects of direct contact of cytokines with macrophages as reported in case of silk films (Reeves et al., 2015) and release of cytokines through hydrogels (5% w/v). Taken together, these studies showed the potential of silk hydrogels to modulate macrophage polarization through localized release and direct contact of cytokines in the matrix (**Figure 3.2**). These immuno-informed silk biomaterials may be used for tissue regeneration in different pathological conditions. Circulating monocytes may be recruited to implant site and further polarized to desired phenotypes. Hydrogel-encapsulated macrophages may help in simulating tissue-resident macrophages for *in vitro* studies. Understanding polarization of macrophages is indispensable for improving the therapeutic strategies for different chronic diseases (George et al., 2014). As reported earlier, local injection of peritoneal macrophages, through cell implantation therapy, induces neovascularization in rat ischemic hind limb muscles (Hirose et al., 2008). Thus, the macrophage-encapsulating

injectable silk hydrogels might be a viable option for localized delivery of cytokines and macrophages for cell therapy. Such hydrogels may retain the localized distribution of macrophages preventing their systemic invasion.

Macrophages are also the key players in giant cell formation which subsequently encapsulate biomedical implants and devices (glucose sensor, insulin pump, and stents) through inflammation, granulation and fibrosis leading to occluded cannula (Heinemann and Krinelke, 2012; Patte et al., 2013; Yutani et al., 2000). Cytokine/macrophage-loaded hydrogels may be used to improve the performance of such implanted devices by preventing initial giant cell formation and biofouling (Butruk et al., 2012; Yu et al., 2008). Such hydrogels may modulate macrophage phenotype (M1/M2) through direct cytokine release and polarized macrophages. As reported earlier, atherosclerotic lesions have high levels of IFN-γ and M1 functional phenotype of macrophage in lesion microenvironment. Subsequently, infiltrating monocytes are polarized to M1 by IFN-γ and enhances plaque formation (Panousis and Zuckerman, 2000). In an early atherosclerosis mice model fed with high-cholesterol diet, injections of IL-4 showed a 90% reduction in lesion size (Huber et al., 2001). It indicates that exogenous IL-4 may act to limit Th1-cell response, further suppressing the formation of plaque. The *in vitro* release of encapsulated IL-4 from silk hydrogels could repolarize M1 macrophages to M2 phenotype which may further be used to locally inhibit Th1-cell response.

M1 macrophages are well known for tumour growth inhibition, M2 macrophages are known for tumour growth promotion. Thus, the implantation of IFN-γ loaded silk hydrogels at the site of solid tumour may be a novel immunotherapy strategy for polarization of tumour-associated macrophages (TAMs), M2-like macrophages known to accelerate tumour growth, to M1 (Liu et al., 2013). Also, polarization of TAMs to M1 phenotypes will help in reduced tumour growth and metastasis (invasiveness) leading to clearance of tumour by M1 macrophages (Liu et al., 2013). In a previous study, silk films were studied for controlled release of cytokines for macrophage polarization (Reeves et al., 2015). Films could be modified for long-term release (10 days) of cytokines for macrophage polarization. In the present study, 3D hydrogels are projected as potent injectable vehicle for encapsulating and ferrying cytokine and macrophage cargoes: an unmet challenge for 2D silk films. Furthermore, the hydrogels are expected to have better loading efficiency than that of films (Bellas et al., 2015; Seib et al., 2013). Sequential delivery of immunomodulatory

cytokines (IFN-γ and IL-4) from silk hydrogels may help in robust M1 to M2 transition leading to enhanced vascularization and integration of biomaterials *in vivo*. This sequential delivery approach may be applied without exogenous cell seeding on the implants (Spiller et al., 2015).

This work was on *in vitro* evaluation of the cytokine-loaded hydrogel formats. The *in vitro* environment may be different from the complex *in vivo* environment in release and polarization profiles. However, the response of THP-1 cells to IFN-γ and IL-4 has been shown to be similar as primary peripheral blood monocyte derived macrophages (PBMCs) (Chanput et al., 2013; Daigneault et al., 2010; Reeves et al., 2015). Evaluation of cytokine secretion profiles shall validate phenotypic outcomes of macrophage polarization/plasticity in addition to gene expression and cell morphology analyses. Despite these limitations, these studies clearly prove that the cytokine-loaded silk hydrogels have the potential to polarize encapsulated macrophages. These may serve as *in vitro* model for biomaterial-cytokine interactions and minimally invasive injectable immunomodulatory hydrogels.

3.5. Significant Findings

The salient findings of the present study are enlisted as follows:

1. The chapter investigates the potential of different silk hydrogels (silk-PEG, silk-HRP and silk-sonicated) to release cytokines (IFN-γ and IL-4) and control macrophage polarization/plasticity (M1 or M2).

2. Cytokine-loaded and macrophage-encapsulating hydrogels were able to polarize monocytes/macrophages to desired phenotypes (M1/M2). The release of cytokines and extent of polarization were found to be correlated with the physicochemical properties of the hydrogels.

3. Macrophage polarization study was conducted with three approaches: cytokine encapsulation, macrophage encapsulation and co-encapsulation approach with efficient and desired macrophage polarization and plasticity.

Based on the findings of the present study, analysis of the *in vivo* immunomodulatory potential of these immuno-informed hydrogels will be an interesting proposition. On the basis of these outcomes, the next chapter highlights the detailed study on the injectable silk-hydrogel-based *in vivo* immunomodulation, illustrating their ability to

promote anti-inflammatory macrophages in subcutaneous mice model and further exploration for islet encapsulation.

Chapter 4

Development of Minimally Invasive Injectable Silk Hydrogel as Potential Islet Encapsulation and Delivery Matrix

This chapter illustrates the improved efficacy of the inherent cell-binding motif containing injectable silk hydrogel in islet encapsulation. The multidimensional approaches towards cross-linker-free gelation, minimal invasiveness and in vivo immunomodulation have also been explored.

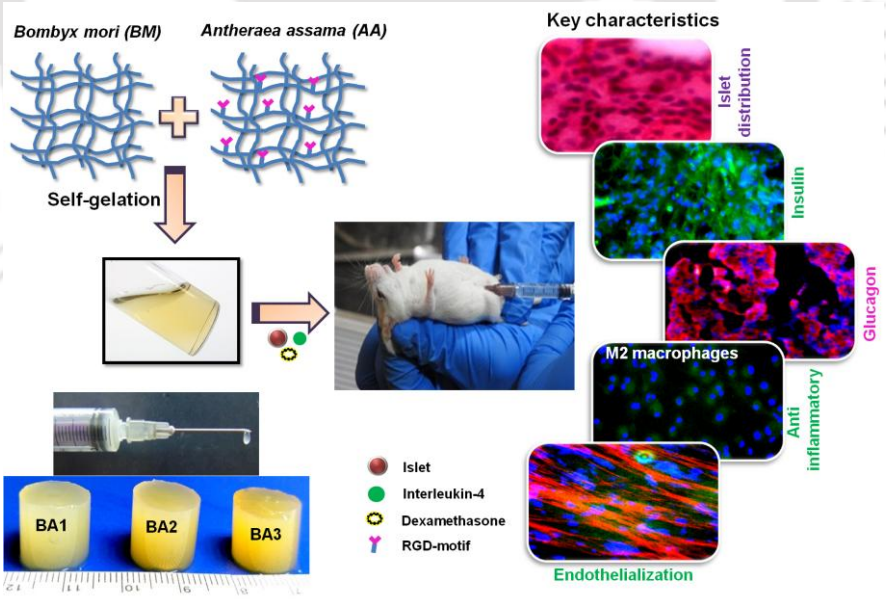

ABSTRACT

Islet transplantation is considered the most promising treatment for type 1 diabetes. However, the clinical success is limited by islet dysfunction in long-term culture. In this study, we have utilized the rapid self-gelation and injectability offered by blending of mulberry silk (*Bombyx mori*) with non-mulberry (*Antheraea assama*) silk, resulting in a biomimetic hydrogel. Unlike the previously reported silk gelation techniques, herein differences in amino acid sequences of the two silk varieties result in accelerated gelation without requiring any external stimulus/cross-linker. Gelation study and rheological assessment depicts a tuneable gelation as a function of protein concentration and blending ratio with minimum gelation time of ~13 minutes. *In vitro* biological results reveal that the blend hydrogels provide an ideal 3D matrix for primary rat islets. Also, *A. assama* fibroin, with inherent Arg-Gly-Asp (RGD), shows a marked positive influence on islet viability, insulin secretion and endothelial cell maintenance. Further utility of these hydrogels has demonstrated the sustained release of Interleukin-4 (IL-4) and Dexamethasone, with effective M2 macrophage polarization while preserving islet physiology. The immuno-informed hydrogel demonstrates local modulation of inflammatory responses at the implant site *in vivo*. Altogether, the results exhibit the promising attributes of injectable silk hydrogel and the utility of non-mulberry silk fibroin as an alternative biomaterial for islet encapsulation.

4.1. Introduction

Islet transplantation, following the Edmonton Protocol, has emerged as a promising therapeutic approach for insulin-dependent type 1 diabetes reversal (Daoud et al., 2011; Vlahos et al., 2017). However, the considerable loss of islets (~60%) during islet infusion through portal vein necessitates multiple donors (2-4) for one diabetic patient (Del Toro-Arreola et al., 2016; Vlahos et al., 2017). Biomaterial-based islet encapsulation provides an attractive alternative proposition for islet delivery *in vivo* by providing protective three-dimensional (3D) support for islet function (Daoud et al., 2011; Hamilton et al., 2017; Stendahl et al., 2009). In the native pancreas, islets are surrounded by a capsule of extracellular matrix (ECM) comprising of different matrix components (Davis et al., 2012; Stendahl et al., 2009). These ECM components bind to integrins on the islet surface mediating cell adhesion, proliferation, and insulin secretion (Stendahl et al., 2009; Wang and Rosenberg, 1999). During islet isolation, due to enzymatic digestion, majority of islet microvasculature and islet-matrix connections are disrupted resulting in islet fragmentation, and glucose irresponsiveness (Brendel et al., 1994; Ilieva et al., 1999). Upon encapsulation in 3D biomimetic microenvironment with ECM-like biochemical cues, the islet functions are preserved as the 3D matrix compensates for the native ECM (Daoud et al., 2011; Davis et al., 2012; Kumar et al., 2017).

In this direction, several biomaterials have been utilized for islet encapsulation to provide native-like micromilieu (Borg and Bonifacio, 2011). Natural biopolymers like collagen, alginate, heparin and fibronectin often suffer from drawbacks like batch-to-batch variation, pathogen/endotoxin contamination, lack of tunability, and immunogenicity (Liao et al., 2013). Similarly, a plethora of synthetic polymers have been utilized for islet encapsulation (Hamilton et al., 2017; Liao et al., 2013) wherein poly (lactic acid) (PLA), and poly (lactic-co-glycolic acid) (PLGA) demand pre-fabricated scaffolds with additional ECM components (Blomeier et al., 2006; Liao et al., 2013; Salvay et al., 2008). Also, degradation of these synthetic polymers releases acidic by-products leading to pro-inflammatory responses *in vivo* (Liao et al., 2013). Furthermore, the application of poly (vinyl alcohol) (PVA) for islet encapsulation necessitates sub-zero temperature to form hydrogels resulting in islet dysfunction and glucose irresponsiveness (Liao et al., 2013; Saudek et al., 1999).

In comparison to other material formats, hydrogels are specifically attractive for islet culture as they closely mimic the natural ECM and deliver islets in minimally

invasive manner (Cushing and Anseth, 2007; Seliktar, 2012). This is due to their high water content; ~30% to over 90%, mimicking the hydrophilic content of ECM (Cushing and Anseth, 2007; Liao et al., 2013; Park and Lakes, 2007; Seliktar, 2012; Wang et al., 2008a). Further, the hydrogels can be injected with islets co-encapsulated with therapeutic molecules for local release without systemic side-effects (Drury and Mooney, 2003). For an ideal injectable hydrogel, gelation must be induced under physiological-like environment, within a short time, without damaging islets and encapsulated therapeutic molecules (Drury and Mooney, 2003; Wu et al., 2012b). Use of harsh chemicals and conditions during gelation limits the incorporation of cells or bioactive molecules (Daoud et al., 2011; Yang et al., 2001). Among the reported hydrogels, polyethylene glycol (PEG) has been explored extensively for islet encapsulation (Liao et al., 2013; Su et al., 2010). Despite numerous favorable features, it has many restrictions including poor islet viability, non-degradable backbone and lack of functionality (Liao et al., 2013; Lin and Anseth, 2009) and PEG hydrogels alone are not ideal for maintaining prolonged islet function *in vivo* (Liao et al., 2013; Lin and Anseth, 2009). Therefore, the development of an ideal alternative hydrogel system for clinically applicable islet encapsulation is of the utmost need (Liao et al., 2013).

Silk, a structural protein, is biocompatible, biodegradable, mechanically robust biomaterial with tuneable degradation rates (Davis et al., 2012; Hamilton et al., 2017; Kumar et al., 2016a; Kumar et al., 2017; Wang et al., 2008a). Silk based matrices are easy to handle; cross-linkable at mild (aqueous) physiological conditions, inexpensive to produce and as a biomaterial, have demonstrated exceptional advantages over conventional synthetic and natural biomaterials (Chouhan et al., 2017; Gupta et al., 2016a; Gupta et al., 2016b; Reardon et al., 2017; Singh et al., 2016b; Wang et al., 2008a). Silk-based hydrogels have also found increasing applications in tissue engineering (Davis et al., 2012; Kapoor and Kundu, 2016). Aqueous solution of silk under the influence of external stimuli undergoes self-assembly giving rise to β-sheet formation resulting in hydrogelation (Wang et al., 2008a). Despite the fact that the applied external stimulus reduces the time of gelation, it increases the chances of contamination (Wang et al., 2008a; Wu et al., 2012b). Earlier reports have shown silk hydrogelation via different external stimuli like alcohol, (Numata et al., 2011) acid (low pH), (Wu et al., 2012a) carbon dioxide (Floren et al., 2012) or with the help of non-physiological stimuli like temperature, (Matsumoto et al., 2006) sonication, (Wang et al., 2008b) vortexing (Yucel et al., 2009) etc (Kapoor and Kundu, 2016). However,

without the use of any external stimulus, the gelation time of silk solution is very high (in days) (Kapoor and Kundu, 2016; Wang et al., 2008a). There are few reports which attest the applicability of mulberry *B. mori* silk hydrogel for islet encapsulation *in vitro* (Davis et al., 2012) and *in vivo* (Hamilton et al., 2017). In these reports, ECM proteins (collagen and laminin) were externally incorporated to mulberry *B. mori* fibroin (devoid of RGD) to enhance the function of the encapsulated islets (Davis et al., 2012). In the subsequent *in vivo* transplantation study, islets were co-encapsulated with mesenchymal stromal cells (MSCs) for immunomodulation (Hamilton et al., 2017). However, the co-encapsulated immunomodulatory MSCs were observed to differentiate spontaneously and undesired bone-like structures were identified on the explants showing the limitations in using MSCs for immunomodulation during islet transplantation (Hamilton et al., 2017). In other studies with modified recombinant spider silk scaffolds/foams, RGD-containing matrices assisted in insulin-secreting islet-like clusters formation (Shalaly et al., 2016) and showed enhanced islet maintenance (Johansson et al., 2015).

RGD, the most widely characterized cell binding motif, is found in several ECM proteins (Johansson et al., 2015). It has pronounced effects on islet adherence, viability and revascularization owing to its interactions with several integrin variants (Johansson et al., 2015). Recently, RGD motif has been reported in *A. assama* non-mulberry silk variety (Gupta et al., 2015). This variety of silk, with intrinsic RGD motif is unexplored for islet encapsulation. However, it supports better adhesion and proliferation of a range of cell types by virtue of intrinsic RGD peptide which has been witnessed in many recent reports (Chouhan et al., 2017; Gupta et al., 2016a; Gupta et al., 2016b; Janani et al., 2017; Reardon et al., 2017; Singh et al., 2016b). Although, the biological cues are provided by 3D matrices, however, the autoimmunity in case of type 1 diabetes and tissue damage due to surgery evokes inflammation and alters the immune environment of the implants (Kumar et al., 2017; Liu et al., 2016). This process poses additional hurdles as the transplanted islets under such stress secrete pro-inflammatory factors thus amplifying local inflammation (Kumar et al., 2017; Piemonti et al., 2002; Weaver et al., 2015). In order to improve the long-term function of transplanted islets, a biodegradable encapsulating matrix primed with anti-inflammatory and immunomodulatory factors is a better option as it facilitates implant vascularization and islet engraftment simultaneously preventing islet destruction by immune cells (Davis et al., 2012; Foster and García, 2017; Hamilton et al., 2017; Jiang

et al., 2017; Kumar et al., 2017; Liu et al., 2016). Localized delivery of such factors at implantation site has shown promising outcomes as an effective therapy to prevent immune targeting of islets and eliminate the need for lifelong systemic immunosuppression (Foster and García, 2017).

To overcome the aforementioned limitations associated with currently available hydrogels and islet delivery vehicles, the present study illustrates a rapid self-gelling silk based injectable hydrogel. This hydrogel has been developed by blending two different varieties of silk i.e., mulberry *B. mori* and non-mulberry *A. assama*, without any external stimulus or cross-linker. This silk gelation behaviour, in mild encapsulation conditions, facilitates incorporation of islets and biomolecules (drug/growth factor) without compromising their biological activities. Herein, we have prepared Interleukin-4 (anti-inflammatory cytokine) and Dexamethasone (immunosuppressive drug) -loaded silk-blended hydrogels to investigate the versatility of these hydrogels for islet encapsulation and biological functionalization (immunomodulation and endothelialisation). As developed injectable blended hydrogels were investigated for three attributes namely, (a) the biocompatibility for islet viability and physiology maintenance, (b) local macrophage polarization and immunomodulation with encapsulated-IL-4/Dex *in vivo* and (iii) the potential for endothelialisation. We report the performance of this novel silk blended hydrogel as a potential matrix for islet encapsulation.

4.2. Materials and Methods

4.2.1. Silk fibroin isolation from *B. mori* cocoon

B. mori silk fibroin solution was prepared as per the protocol previously reported by our group (Kumar et al., 2016a; Kumar et al., 2017). Briefly, cocoons were cut and degummed in 0.02 M sodium carbonate (Sigma-Aldrich, USA). Post-degumming, silk fibers were dried overnight. Further, fibers were dissolved in 9.3 M LiBr solution (Sigma-Aldrich, USA) at 60 °C for 4 h. The solution was then subjected to dialysis against deionized water using 12 kDa dialysis membrane (Sigma-Aldrich, USA) for 3 days with frequent water changes to remove the LiBr. After dialysis, regenerated silk solution was centrifuged (4000g, 20 min, 4 ºC) to remove insoluble particulates. The final acquired concentration of regenerated protein was 10% (w/v) and the solution was diluted to 8, 6, 4 and 2% (w/v) for further studies.

4.2.2. Silk fibroin isolation from *A. Assama* silkworm glands

Non-mulberry *A. assama* silk protein was isolated from posterior silk glands of 5th instar larvae of *A. assama* as reported previously (Gupta et al., 2016a; Gupta et al., 2016b; Singh et al., 2016b). Briefly, the glands were washed in distilled water to remove traces of water soluble sericin. The obtained fibroin protein was then dissolved in 1% (w/v) aqueous sodium dodecyl sulfate (SDS, Himedia, India) at room temperature. Further, SDS was removed by dialysis against milli-Q water for 6 h at 4 ºC using a cellulose dialysis membrane (Sigma-Aldrich, USA). The final concentration of the silk solution obtained was determined by gravimetric method.

4.2.3. Silk blended hydrogel fabrication

B. mori (BM) silk protein of 8, 6, 4 and 2% (w/v) and *A. assama* (AA) protein of 2% (w/v) were mixed to prepare four different types of hydrogel blend (8:2, 6:2, 4:2 and 2:2). These four groups of hydrogels were used only for gelation study to validate the effect of silk concentration on gelation time. For further experimentation, blend hydrogels of final 2% (w/v) were prepared and designated as BA0, BA1, BA2, BA3 and BA4. For the preparation of 2:0 (BA0), 2:1 (BA1), 1:1 (BA2), 1:2 (BA3) and 0:2 (BA4) ratio of *B. mori* and *A. assama* blend hydrogels, specific ratios of both the proteins (*B. mori* and *A. assama*, 2% w/v) were respectively mixed to reach the final desired volume.

4.2.4. Gelation pattern and time analysis

Blended solutions of 200 µL volume were investigated for gelation pattern analysis. After mixing at specific ratios, 200 µL of mixed solution was pipetted in 96 well plate. To monitor the turbidity change along the gelation process, absorbance was observed at 550 nm and 37 ºC at predefined time intervals. Gelation times, which refer to the time required for sol-gel transformation for the hydrogels, were estimated by tube inversion method with 2 mL of mixed solution (n = 4) (Singh et al., 2016a).

4.2.5. Rheological characterization (gelation time and complex viscosity study)

Rheological measurements were carried out using a strain controlled Rheometer Physica MCR 302 (Anton-Paar, USA) to study the gelation profiles and complex viscosity (η). *B. mori* and *A. assama* silk blend solution (500 µL) in the ratio 2:0 (BA0), 2:1 (BA1), 1:1 (BA2), 1:2 (BA3) and 0:2 (BA4) was placed over the

rheological platform under the stainless steel parallel plate of 50 mm diameter with 1 mm gap. At constant shear strain (1%) and angular frequency (3 rad/s), the measurements were performed for 20 min at 37 ºC. As obtained storage (G') and loss modulus (G") were plotted against time to calculate the gelation point.

4.2.6. Morphological analysis of hydrogels

Hydrogel surface morphology; pore interconnectivity and internal architecture were analyzed using a field emission scanning electron microscopy (FESEM, Zeiss, Sigma, USA). Representative samples from each group (BA1, BA2 and BA3) were selected for imaging. Samples were prepared by sequential dehydration by treatment with graded ethanol (50, 70, 80, 90, 95 and 100%), frozen at -80 ºC and lyophilized. Subsequently, images were acquired after gold sputtering at an operating voltage of 20 kV. The pore size was estimated using ImageJ software with a minimum of 25 pores examined per hydrogel.

4.2.7. *In vitro* enzymatic degradation

Silk blend hydrogels (diameter = 13 mm; height = 13 mm) were prepared for degradation study following the protocol described above. *In vitro* degradation analysis was carried out in PBS (control, pH 7.4) and freshly prepared protease XIV (Sigma-Aldrich, USA) at 37 ºC in a 24 well plate with 0.05% sodium azide (Wang et al., 2008a). The initial weight of hydrogels was measured using an electronic balance (Sartorious, AG Germany). Samples were replenished with fresh protease solution after every 72 h. The control samples were kept in 1X PBS (control) with 0.05% sodium azide. At day 4, 7, 14 and 21, hydrogels were washed with MilliQ water, wiped with tissue paper to remove excess water and weighed.

Percent mass remaining = $(M_t / M_i) \times 100$ [4.1]

Where, M_t is weight at specified day and M_i is initial weight.

4.2.8. Fourier Transform Infrared spectroscopy (FTIR)

FTIR spectroscopic analysis was performed using FTIR Spectrophotometer (Nicolet iS 10) to analyse the structural transition of hydrogel blend due to mixing of two different silk fibroin proteins (Gupta et al., 2016b; Janani et al., 2017). Infrared spectra of the pure *B. mori* and *A. assama* were also recorded as a control in the range of 1000-2000 cm^{-1}. A total of 32 scans with a resolution of 4 cm^{-1} were collected (Gupta et al.,

2016b). Pure silk solutions (*B. mori* and *A. assama*) and pre-fabricated hydrogel blend (BA3, 1:2) were frozen at -80 ºC overnight and further lyophilized. Dry pellets were prepared using potassium bromide (KBr). The variation in the FTIR spectra was analyzed using Origin Pro 8 (Microcal version, USA) (Gupta et al., 2016b; Janani et al., 2017).

4.2.9. Isolation of primary rat islets and maintenance of islets and RIN-5 cell line

Primary rat islets were isolated per the reported protocol (Kumar et al., 2017; Li et al., 2009). Wistar rats (age 8-10 weeks) of either sex were used for pancreas harvesting (Kumar et al., 2017). Animal experiments were conducted per the animal care protocols approved by Institutional Animal Ethical Committee (IAEC), West Bengal University of Animal and Fishery Sciences (WBUAFS), Kolkata, India in accordance with "Principles of Laboratory Animal Care." Briefly, after excision, pancreas was digested in collagenase XI and the isolated islets were counted and placed in 5% CO_2 incubator at 37 °C for further experiments. RIN-5 cells (rat insulinoma cell line) procured from National Centre for Cell Science (NCCS), Pune, India, were maintained in RPMI 1640 medium supplemented with 10% fetal bovine serum (FBS), 100 U/mL penicillin, 100 µg/mL streptomycin, 1 mM sodium pyruvate and 2 mM L-Glutamine (Kumar et al., 2017).

4.2.10. Cell viability and proliferation studies with hydrogels

4.2.10.1. RIN-5 cell proliferation on hydrogel surface

RIN-5 cells were maintained in T75 flasks and cell culture medium was replenished twice a week. For surface seeding, the three hydrogels types (600 µL) of 2% (w/v) silk were coated in a 6 well plate and allowed to solidify. Further, RIN-5 cells were seeded at a density of 10^4 cells per well (in 500 µL culture media) and placed in a humidified incubator. Cytotoxicity of the hydrogels and metabolic activity of the seeded cells was monitored after specified intervals of culture (day 1, 3, 5, 7 and 9 days) via AlamarBlue dye reduction assay (Life Technologies, Grand Island, NY) following the manufacturer's protocol and as reported previously (Gupta et al., 2016b; Kumar et al., 2016a; Kumar et al., 2017).

4.2.10.2. RIN-5 and islet cell viability in 3D encapsulated hydrogels

Total fifty (50) freshly isolated islets were encapsulated in 50 µL of hydrogels, (BA1, BA2 and BA3) and islets seeded in tissue culture plate (TCP) wells were taken as control (Davis et al., 2012). Similarly, a total of 10^6 RIN-5 cells were encapsulated in 50 µL of all the three hydrogels (Kumar et al., 2016a; Wang et al., 2008a). Post-encapsulation, proliferation of hydrogel encapsulated RIN-5 cells and primary islets was monitored using PicoGreen assay kit (Molecular Probes, Life Technologies, USA) following the manufacturers' protocol (Gupta et al., 2016a; Wang et al., 2008a). The total DNA content in the sample was calculated using standard curve obtained in the same assay. Cell viability was assessed by Calcein AM (Sigma-Aldrich, USA) staining following the manufacturer's instructions and previous reports (Kumar et al., 2016a; Wang et al., 2008a). Briefly, cell seeded hydrogels were washed twice with PBS and incubated with 4 µM Calcein AM for 20 min at 37 °C. Post-staining, hydrogels were rinsed twice with PBS and fluorescent images were captured using fluorescent microscope (EVOS FL, Life Technologies, USA).

4.2.11. Functional assessment of islet cells encapsulated in hydrogels

4.2.11.1. RNA extraction and gene expression analysis

Analysis of islet gene expression was performed with RT-qPCR after 14 days of islet encapsulation in hydrogels (Kumar et al., 2017). Islets were lysed and RNA was isolated and purified using an RNeasy Plus Mini Kit (Qiagen, CA, USA) (Gupta et al., 2016b; Kumar et al., 2016a; Kumar et al., 2017). From hydrogels, total RNA was extracted by disrupting the gel network and further treatment with Trizol (Invitrogen, USA) (Davis et al., 2012; Kumar et al., 2016a). Subsequently, for reverse transcription, 1 µg of RNA was converted to cDNA and RT-qPCR was performed using primers with Power SYBRGreen (Thermo Fisher Scientific). All assays were performed in duplicate in 96-well format plates as reported previously (Kumar et al., 2017). Primers (**Table 4.1**) were used at 1 µM concentration and run for 40 cycles (Kumar et al., 2017). To quantify relative gene expression, data were normalized to the housekeeping gene, glyceraldehyde-3-phosphate-dehydrogenase (GAPDH), and the $2^{-\Delta\Delta C}{}_T$ method was used per reported protocols for islet genes (Daoud et al., 2011; Davis et al., 2012; Kumar et al., 2017) Changes in target gene expression in encapsulated islets were expressed as fold-change of islets cultured in 2D (Davis et al., 2012; Kumar et al., 2017). Changes in target gene expressions in further macrophage polarization study

were expressed as fold change from control groups (Kumar et al., 2016a; Reeves et al., 2015).

Table 4.1. *Primers for RT-qPCR*

Gene	Forward sequence	Reverse sequence
Rat GAPDH	GCATCTTCTTGTGCAGTGCC	GAGAAGGCAGCCCTGGTAAC
Rat Insulin I	AAACAGCACCTTTGTGGTCCT	ACTTCACGACGGGACTTGGG
Rat Insulin II	GGAGCGTGGATTCTTCTACACA	AGTGCCAAGGTCTGAAGGTCAC
Rat Glucagon	CCAAAGGAGCTCCACCTGTC	TCCAGCCACGATGTAAACGG
Rat Somatostatin	CCCCAGACTCCGTCAGTTTC	GGCATCGTTCTCTGTCTGGT
Human GAPDH	ACAACTTTGGTATCGTGGAAGG	GCCATCACGCCACAGTTTC
Human CD68	CTTCTCTCATTCCCCTATGGACA	GAAGGACACATTGTACTCCACC
Human CD206	CTACAAGGGATCGGGTTTATGGA	TTGGCATTGCCTAGTAGCGTA
Human CD209	AATGGCTGGAACGACGACAAA	CAGGAGGCTGCGGACTTTTT
Human CCR7	TGAGGTCACGGACGATTACAT	GTAGGCCCACGAAACAAATGAT

4.2.11.2. Glucose challenge assay

Islet function was assessed *in vitro* by glucose challenge assay using a rat insulin ELISA kit (Mercodia, Uppsala, Sweden) (Davis et al., 2012; Kumar et al., 2017). Glucose challenge assay was performed after 7 and 14 days of islet encapsulation. Islet-seeded hydrogels (50 freshly isolated islets encapsulated in 50 µL of hydrogels) were washed for 5 min with 3.3 mM glucose in Krebs-Ringer buffer. After washing, the samples were incubated for 1 h each, with low (3.3 mM) followed by high (17 mM) glucose in a Krebs-Ringer buffer (Davis et al., 2012; Kumar et al., 2017). For islets in suspension, islets were centrifuged, pelleted and incubated similar to the islet-encapsulating hydrogel groups. Values are reported as stimulation index (SI), which is the ratio of insulin secreted with high glucose stimulation over insulin secreted with low glucose stimulation (Davis et al., 2012; Kumar et al., 2017).

4.2.11.3. Immunohistochemistry and Hematoxylin and Eosin (H & E) staining

To confirm the expression of islet hormones (insulin and glucagon), RIN-5 and islet-seeded BA3 hydrogels were harvested for immunostaining. Samples were harvested on day 3, 7 and 14 and processed for sectioning as per the reported protocols (Kumar et al., 2017; Wang et al., 2008a) Immunostaining was performed with primary rat anti-insulin antibody (Sigma-Aldrich, USA) and primary rat anti-glucagon antibody (Sigma-Aldrich, USA). Secondary antibodies used were; FITC-conjugated anti-mouse

secondary antibody (Sigma-Aldrich, USA) and R-phycoerythrin-conjugated anti-mouse secondary antibody (Sigma-Aldrich, USA) (Kumar et al., 2017). The sections were counterstained with Hoechst 33342 (Sigma-Aldrich, U.S.A.). For general morphology and cell distribution analysis, sections were stained with hematoxylin and eosin **(**H & E, Sigma-Aldrich, USA) stains and histological analysis was performed as per the reported protocol (Kumar et al., 2017; Wang et al., 2008a). Briefly, cell-seeded hydrogels were fixed in 10% neutral buffered formalin for 24 h and processed sections were stained for further assessment of cell distribution in hydrogels (Kumar et al., 2017; Wang et al., 2008a).

4.2.12. Interleukin-4 (IL-4) and Dexamethasone (Dex) release from hydrogels

Recombinant human cytokine IL-4 (Peprotech, Rocky Hill, NJ, USA) was encapsulated in all hydrogels during gelation (Kumar et al., 2016a). For release studies, 50 µL hydrogels (BA1, BA2 and BA3) containing 0.5 µg of IL-4 cytokine was incubated in Lobind Microcentrifuge tubes (Fisher Scientific) in 1 mL PBS (pH 7.4). PBS was replenished at specified time points (day 0.25, 0.5, 1, 3, 5, 7, 14). Collected samples were stored at -80 °C for ELISA (Human ELISA Development Kit, Peprotech, Rocky Hill, NJ) for IL-4 (Kumar et al., 2017). Similarly, 1 µg of Dexamethasone (Sigma-Aldrich, USA) was encapsulated in 50 µL hydrogels (BA1, BA2 and BA3). Dex-loaded hydrogels were incubated in 1 mL of PBS (pH 7.4) and maintained for release study. At pre-specified time intervals, PBS medium was changed and absorbance was recorded at 241 nm (Kumar et al., 2017; Vacanti et al., 2012; Weaver et al., 2015).

4.2.13. Immunomodulation study

For immunomodulation study, human acute monocytic leukemia cells (THP-1) were cultured in RPMI media and maintained in T75 flasks at optimal density. THP-1 cells, 10^5 cells were seeded per well in 24-well transwell plates and induced to macrophage (M0) using 100 ng/mL (162 nM) of phorbol 12-myristate 13-acetate (PMA) (Sigma-Aldrich, USA). After overnight PMA treatment, medium was switched to macrophage polarization conditions through IL-4-releasing BA3 hydrogels (50 µL of hydrogels with 0.5 µg of IL-4) placed in the transwell inserts for 72 h. Further, cells were lysed, and isolated mRNA was analysed for gene expression of M1 (CCR7) and M2 (CD206 and CD209) macrophage markers (Kumar et al., 2016a; Kumar et al., 2017; Reeves et al., 2015). M2 polarization was also confirmed by immunofluorescence study.

Immunostaining protocol was similar to insulin and glucagon staining using primary antibody against CD206 (Abcam-ab64693, U.K.). FITC-tagged anti-mouse secondary antibody (diluted 1:1000, Abcam, U.K.) was used as secondary antibody.

4.2.14. Cytotoxicity study with islets

Cytotoxicity of IL-4 and Dex on islets was assessed by PicoGreen assay kit (Molecular Probes, Life Technologies, USA) following the manufacturer's protocol. Briefly, 50 islets were encapsulated in 50 µL of BA3 hydrogels with 0.5 µg of IL-4 and 1 µg of Dex, separately. Islet encapsulated without IL-4 and Dex were kept as control. Further, the hydrogels were placed in transwell inserts for 72 h. Post-incubation, the total DNA content in the sample was calculated using standard curve obtained in the same assay. Similarly, islet function was determined through glucose challenge assay for the islets co-encapsulated with IL-4 and Dex (Davis et al., 2012; Kumar et al., 2017; Weaver et al., 2015).

4.2.15. Endothelial cell culture and functional studies

4.2.15.1. Isolation, culture and maintenance of primary endothelial cells

A part of descending porcine aorta was collected in sterile ice-cold phosphate buffered saline (PBS, pH 7.4) from the local slaughterhouse immediately after animal sacrifice. Endothelial cells were isolated per our previously reported protocol (Gupta et al., 2016b). After extensive wash with sterile PBS, aortic tube was further cut open to expose the luminal surface (lined with endothelial cells monolayer) and treated with 0.01% Collagenase Type IA from *Clostridium histolyticum* (Sigma-Aldrich, USA) for 1 h in a humidified incubator with 5% CO_2 level. Post collagenase treatment, luminal surface was scraped off gently to detach the endothelial cells and washed with sterile culture media. Cells were further cultured and maintained in Dulbecco's Modified Eagle Medium (DMEM; Gibco, USA) supplemented with 10% Fetal Bovine Serum (FBS, Gibco, USA), 2% ECGS (Endothelial cell growth supplement, Sigma Aldrich, USA) and 1% antibiotic-antimycotic solution (Himedia, India). Cells of passages P3 to P5 were used for further experimentation.

4.2.15.2. Endothelial cell viability and proliferation on silk hydrogel

Silk hydrogel (100 µL of BA3) was coated onto 48 well tissue culture plate and conditioned in complete media (high glucose DMEM supplemented with 10% FBS)

overnight. A total of ~5 × 10^4 porcine endothelial cells were cultured on hydrogel-coated wells with TCP as control and cellular viability was analyzed with Calcein AM fluorescent dye after 7 days of culture. Endothelial cells were incubated with working Calcein AM dye solution for 15 min in a humidified incubator with 5% CO_2. Post incubation, excess dye was washed off with sterile PBS and cells were further visualized under florescent microscope (EVOS FL, Life Technologies, USA). For assessing the cell proliferation, ~5 × 10^4 endothelial cells were seeded on silk hydrogels and control TCP wells. Cell proliferation was analyzed using AlamarBlue dye reduction assay at predetermined time points (day 1, 3 and 7) following manufacturer's protocol (Gupta et al., 2016b; Kumar et al., 2016a; Kumar et al., 2017).

4.2.15.3. Functional assessment of endothelial cells

Functionality of endothelial cells cultured on silk hydrogel was assessed by immunostaining with primary antibody against von Willebrand factor (vWF) (Anti-vWF, diluted 1:250, Abcam, U.K.) followed by FITC-tagged anti-rabbit secondary antibody (1:500, Abcam U.K.). Further, Hoechst 33342 (1:1000, Sigma-Aldrich, USA) for nucleus and rhodamine-phalloidin (1:40, Invitrogen USA) for cytoskeleton was performed (Gupta et al., 2016b). Production of nitric oxide (NO) is another vital characteristic of endothelial cell physiology (Yang et al., 2012). For assessing the NO activity, relatively high (~5 × 10^5) number of cells were seeded on silk hydrogel and uncoated TCP wells to assure the formation of complete monolayer of cells. After 24 h of culture, fresh cell culture media was added to the wells. After 12 h incubation, media was collected for assessment of NO activity using Griess reagent (Sigma-Aldrich, USA) following manufacturer's protocol (Yang et al., 2012). Amount of NO produced was quantified by standard curve prepared using sodium nitrite (Yang et al., 2012).

4.2.16. *In vitro* inflammatory response towards hydrogels

Immunogenicity of the hydrogels was evaluated by the release of tumor necrosis factor alpha (TNF α) when incubated with murine macrophage cells RAW 264.7. Cells were cultured at a density of 5 × 10^4 cells per well in a 12-well tissue culture plate for overnight. Further, hydrogels were added to the wells. TCP wells without hydrogels and with 500 ng/mL lipopolysaccharide (LPS, Sigma-Aldrich, USA) were kept as negative and positive controls, respectively (Kumar et al., 2016b; Reardon et al., 2017; Singh et al., 2016b). The released TNF α was estimated by ELISA (mouse TNF α

ELISA kit, Invitrogen, USA) using standard curve (Kumar et al., 2016b; Reardon et al., 2017; Singh et al., 2016b).

4.2.17. *In vivo* immunomodulation study

All *in vivo* experiments were conducted per the animal care protocols approved by IAEC, WBUAFS, Kolkata, India. The animals used in this study were female Swiss (I.B.) mice of 30−35 g body weight. Hydrogels were loaded in syringes and 200 µL subcutaneous injections of each BA3-control (no IL-4/Dex), BA3-IL-4 (2 µg) and BA3-Dex (4 µg) were made, n = 4 for each hydrogels, for each time point (Kumar et al., 2015). Inflammatory responses (redness/swelling) at the injection site were monitored and no animal death was recorded during the entire experimental duration.

At predefined time points, day 3 and 10, the dorsal skin was removed around the entire implant and histological analysis was performed. Briefly, explants were washed in PBS and fixed in neutral buffered formalin for 24 h and dehydrated, cleared, and embedded in paraffin wax. Further, sections (5-7 µm thickness) were deparaffinized, cleared, and rehydrated. For immunomodulation study, immunostaining was performed for pan-macrophage Anti-CD68 antibody (diluted 1:200, Abcam, U.K.) and M2 macrophage Anti-Mannose receptor (CD206) antibody (Abcam-ab64693, U.K.). Secondary, 1) FITC-conjugated anti-mouse secondary antibody (diluted 1:1000, Abcam, U.K.) and 2) DyLight®594 conjugated secondary goat anti-rabbit (Abcam, UK, 1:500 dilutions) were used. The sections were counterstained with Hoechst 33342 and images were captured.

For semi-automated digital analysis of IHC stained slides, IHC profiler and colour de-convolution technique were utilized (Bhardwaj et al., 2014). Five different IHC images per sample were analysed and one representative image has been shown in this study. Using the threshold feature of the ImageJ program, the zones were identified and after thresholding, the colour deconvolution technique was adopted to un-mix the blue (nucleus) and red (CD206) areas leaving a complimentary image. The pixel intensities of separated blue or red images range from 0 (darkest shades) to 255 (lightest shade) (Bhardwaj et al., 2014).

4.2.18. Statistical analysis

All quantitative experimental data are reported as mean ± standard deviation (SD). For each experiment, n = 3 samples were used if unless noted otherwise. All statistical

analysis was performed by a one-way analysis of variance (ANOVA) using Microcal OriginPro 8. Tukey's test was carried out to assess variance across groups. The differences between groups of * $p \leq 0.05$, ** $p \leq 0.01$ and *** $p \leq 0.001$ were considered statistically significant.

4.3. Results

4.3.1. Hydrogel fabrication and gelation time estimation

The tunable gelation rate of the hydrogel is a pre-requisite for its biomedical applications and delivery of cells, growth factors, and bioactive molecules *in vivo*. *B. mori* and *A. assama* silk solutions were mixed in the ratio as discussed in methods section and observed for gelation (**Figure 4.1A**). Comparative analysis revealed that higher amount of total silk fibroin in the hydrogels resulted in higher optical density (absorbance) equilibrium value for absorbance leading to faster gelation and lesser gelation time (**Figure 4.1B,i and iii**). Also, with a constant concentration of protein, solution with more percent of *B. mori* gelled slower (**Figure 4.1B,ii and iii**). The gelation process depicted three different stages, pre gelation, gelation and hardening stage. During pre gelation phase, there was a slight increase in the optical density of silk solution. Further in the gelation phase there was an exponential increase in the optical density followed by a constant value which could be attributed to hardening of the hydrogel.

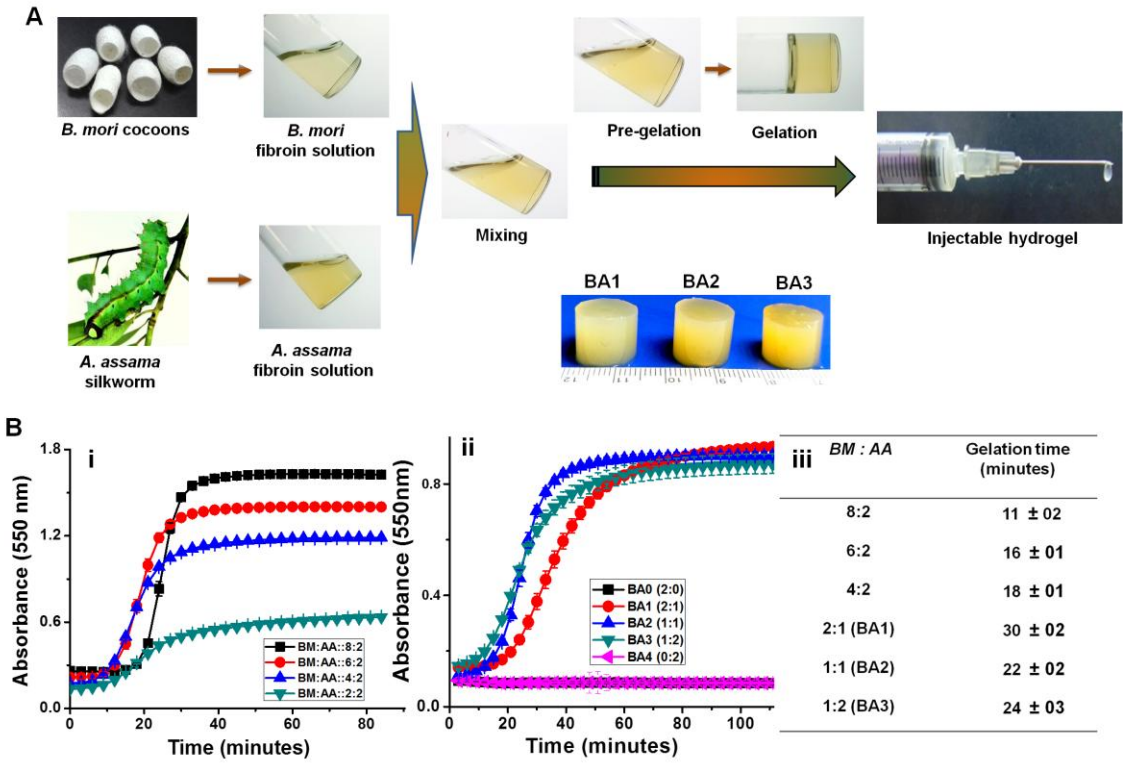

Figure 4.1. *Silk blend hydrogel fabrication and hydrogelation study. (A) Scheme representing fabrication of silk hydrogel blend (BA1, BA2 and BA3). (B) Change in absorbance observed after mixing B. mori (8, 6, 4 and 2% w/v) with A. assama (2% w/v) silk solutions in equal volume (i). Change in absorbance observed after mixing B. mori (2% w/v) with A. assama (2% w/v) in different ratio (2:1, 1:1 and 1:2) (ii). Absorbance was recorded at 550 nm. Table showing gelation time for different hydrogel blend ratio (iii).*

4.3.2. Rheology (Gelation kinetics and complex viscosity)

The rheological experiments were performed to analyze the physical nature of the hydrogel. As depicted on the graphs, storage modulus (G') and loss modulus (G") represent elastic and viscous behavior of the hydrogels, respectively.(Singh et al., 2016b) With the increase in strain at a fixed angular frequency (ω), the storage modulus decreased and the loss modulus increased and at a distinct strain, G' and G" intersected each other. A similar gelation pattern was observed through rheological assessment as in optical density measurement and tube inversion methods (**Figure A4.1**).

4.3.3. Morphological analysis of hydrogels (FESEM)

Surface morphology, pore distribution and pore interconnectivity of freeze-dried hydrogels were observed with FESEM. The captured images revealed uniformly distributed pores with round and interconnected structures. Gross microstructure of the

hydrogels is depicted in **Figure 4.2A,i and iii**. The pore sizes for BA1, BA2 and BA3 were 45 ± 08, 36 ± 08, and 29 ± 06 µm, respectively.

4.3.4. Enzymatic degradation

Degradation properties of a biomaterial plays a decisive role in its performance *in vivo* (Horan et al., 2005). Protease XIV is known to degrade the fibroin crystalline structure (Gupta et al., 2016a). Hydrogel degradation was determined in presence of both; protease XIV and PBS (control) and the results showed that the hydrogels incubated in PBS (control) exhibited minimal degradation (~10%) over 28 days study. In contrast, protease-treated hydrogels degraded to ~40-70% of its initial weight. The maximum degradation was recorded in BA3 (~72%) followed by BA2 (64%) and BA1 (~40%), respectively (**Figure 4.2B**).

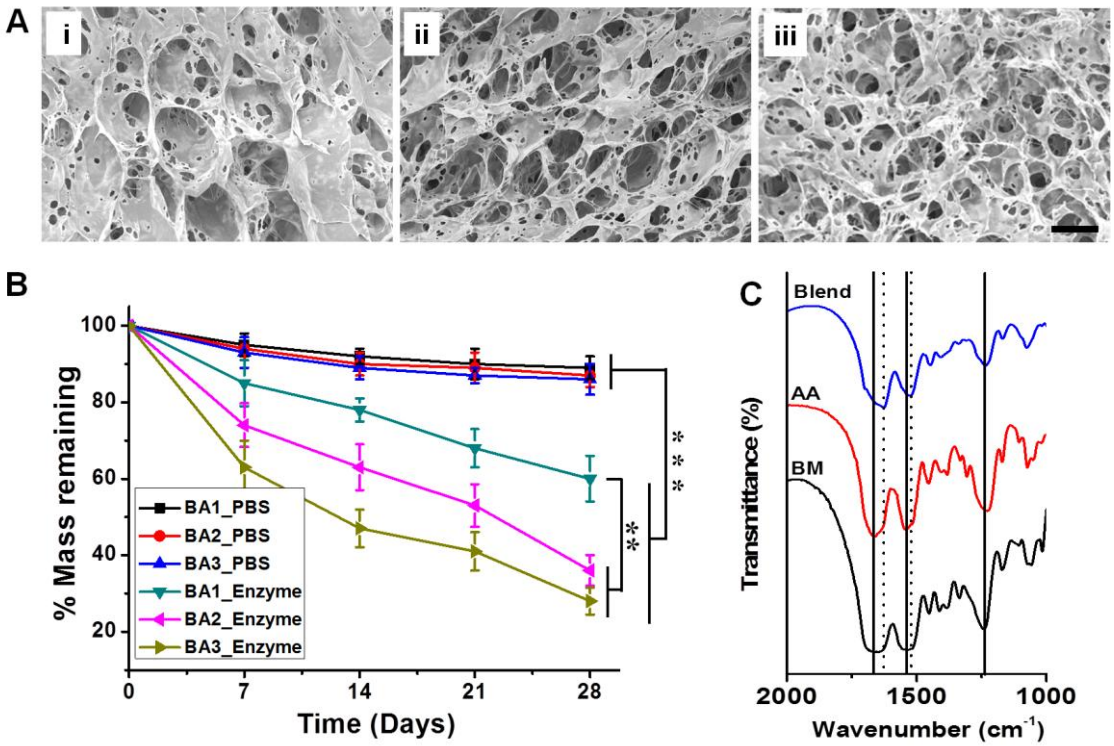

Figure 4.2. *Physico-chemical characterization. (A) FESEM images showing hydrogel morphology and interconnectivity; BA1 (i), BA2 (ii) and BA3 (iii). (B) Enzymatic degradation profile of hydrogels in protease XIV and PBS control (pH 7.4). Mass remaining was determined by comparing the wet weight at each time point with original wet weight. (C) FTIR spectra of BA3 blend hydrogel and individual silk proteins. Scale bar 20 µm. (n = 3,***p ≤ 0.001, **p ≤ 0.01).*

4.3.5. FTIR

Peptide bonds (-CONH-) have characteristic amide signature peaks ranging 1610-1660 cm^{-1} (amide I), 1510-1560 cm^{-1} (amide II), and 1210-1260 cm^{-1} (amide III) that is related to C=O stretching, N-H bending and C-N stretching, respectively (Janani et al., 2017). FTIR measurements were performed with the blend hydrogel (BA3, 1:2) and individual fibroin proteins (*B. mori* & *A. assama*) to study the secondary structures (**Figure 4.2C**). Secondary structure transition in blend hydrogel as compared to individual protein was detected in the range of 2000 cm^{-1} to 1000 cm^{-1}. Blend hydrogels demonstrated shifts in vibration bands from 1622 cm^{-1} and 1521 cm^{-1} to 1660 cm^{-1} and 1540 cm^{-1}, respectively. The shift in spectral band for blend hydrogel were observed due to the rearrangement of hydrogen bonding to make it more stable (Gupta et al., 2016b; Janani et al., 2017). The IR spectrum shows the transition from native predominant structure (random coil) in the silk solution to β-sheet structures in hydrogel which confirms the gelation (Gupta et al., 2016b).

4.3.6. Cell proliferation studies with hydrogels

Cell encapsulation and its metabolic activity in the hydrogels were evaluated for their potential applicability in tissue engineering (Kumar et al., 2016a; Kumar et al., 2017; Wang et al., 2008a). Cell proliferation assays were carried out with all the hydrogel variants namely; BA1, BA2 and BA3. AlamarBlue cell proliferation assay was conducted to quantify RIN-5 cell proliferation over time when cultured on hydrogel surface (Gupta et al., 2016b; Kumar et al., 2017). On day 9, RIN-5 cells proliferated ~2.4-fold on BA3, ~1.9-fold on BA2 and ~1.8-fold on BA1 hydrogels; compared to day 1 of culture. All the hydrogels exhibited significant increase in cell viability and proliferation (day 9 vs day 1, $p < 0.01$) suggesting that the hydrogels supported cell survival and proliferation over time (**Figure 4.3A,i**). There was a significant difference noted between BA1 and BA2 groups compared with BA3 ($p < 0.01$). However, no such difference could be noted between BA1 and BA2 ($p > 0.05$).

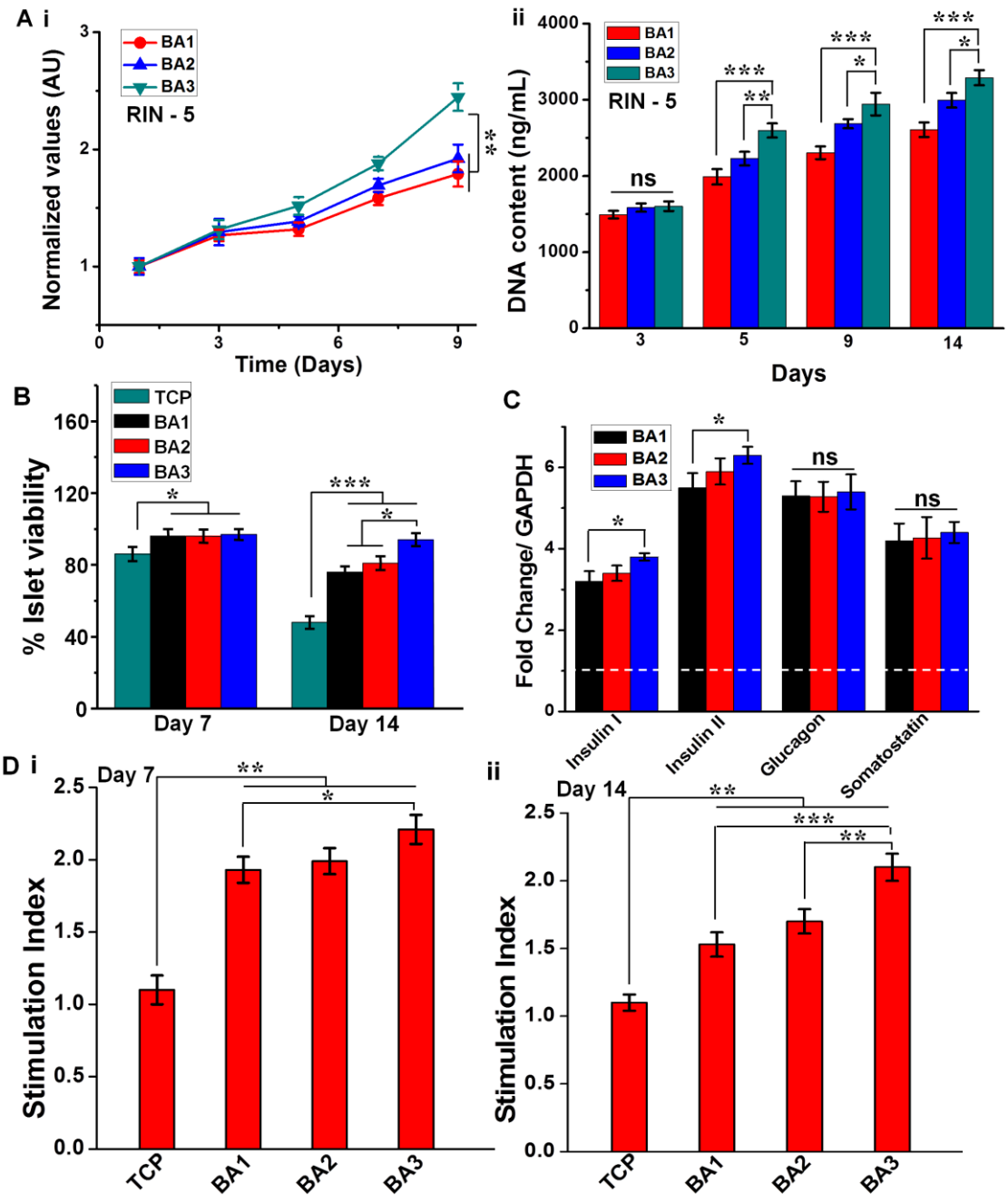

Figure 4.3. *RIN-5 cell and primary islets viability, proliferation and functional tests. (A) Alamar blue cell proliferation assay with RIN-5 cells seeded on silk hydrogel blend (BA1, BA2 and BA3) film (2D) (i). RIN-5 cell proliferation study by DNA quantification (PicoGreen assay) with encapsulation in 3D hydrogel (ii). (B) Primary rat islets viability quantified by PicoGreen assay. (C) Expression of functional islet genes after 14 days of encapsulation (normalized to 2D islet culture). (D) Glucose challenge assay showing insulin secretion from primary rat islets encapsulated in silk hydrogels (BA1, BA2 and BA3) and TCP (control) on day 7 (i) and day 14 (ii). (n = 3, ***p ≤ 0.001, **p ≤ 0.01, *p ≤ 0.05).*

RIN-5 cells exhibited increasing cell proliferation when visualized after Calcein AM staining (green) on day 3, 7 and 9 (**Figure 4.4A,i and iii**). Live cells were evenly

distributed all over the hydrogel surface suggesting suitability of these hydrogels for further encapsulation studies. Successive experiment for RIN-5 cell encapsulation was carried out in the hydrogel variants (BA1, BA2 and BA3) and viability and proliferation was evaluated. In a 14 days study, RIN-5 cells proliferated in all the hydrogels as evident from PicoGreen DNA quantification assay (**Figure 4.3A,ii**). On day 3, there was no significant difference between the groups ($p > 0.05$). On day 5, 9 and 14, there was a highly significant difference between BA1 and BA3 ($p < 0.001$). Similarly, a significant difference could be noted between BA2 and BA3 on subsequent days of study ($p < 0.05$). The representative live cell images from BA3 hydrogel-encapsulated RIN-5 cells supported the proliferation results with increasing number of cells with time (**Figure 4.4C,i-iii**). This result was also corroborated by H & E results (**Figure 4.4E,i-iii**). Similarly, live encapsulated islets could be located in the hydrogels (**Figure 4.5A,i-iii**) which is corroborated by H & E results (**Figure 4.5D,i-iii**).

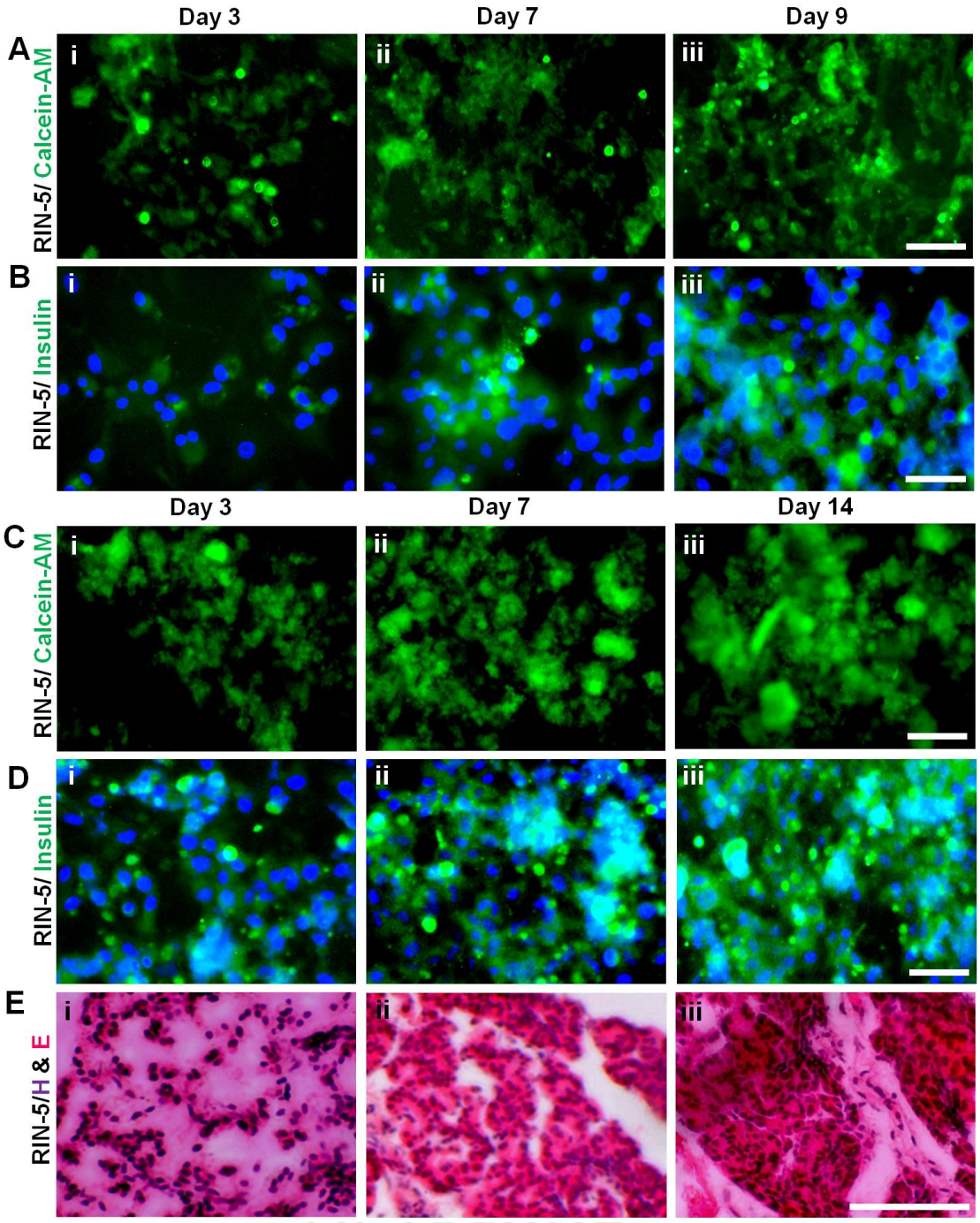

Figure 4.4. *Representative images for RIN-5 cell viability, distribution and insulin expression in 2D and 3D silk hydrogel (BA3). (A) Calcein AM stained live RIN-5 cells (green) on silk blend hydrogel 2D coating. (B) Immunofluorescence images showing insulin (green) and nucleus (blue) in 2D. (C) Calcein AM stained live RIN-5 cells (green) encapsulated in silk blend hydrogel. (D) Immunofluorescence images showing insulin (green) and nucleus (blue) in 3D. (E) Distribution of encapsulated RIN-5 in 3D silk hydrogel. Cells are stained with hematoxylin (nucleus) and eosin (cytoplasm). Scale bar 50 μm.*

The viability of the encapsulated islets were also quantified using PicoGreen assay (**Figure 4.3B**). After 7 days of encapsulation, islets maintained > 95% viability which is significantly different from TCP control, ~85% ($p < 0.05$, **Figure 4.3B**). No significant differences could be observed among the hydrogel groups on day 7. On day 14, the hydrogels BA1, BA2, and BA3 showed ~76, 81, and 94% islet viability which is significantly different from TCP control, ~48% ($p < 0.001$). A significant difference was noted among the hydrogels groups and the viability in BA1 and BA2 was significantly lower than BA3 ($p < 0.05$).

4.3.7. Functional assessment of islets encapsulated in hydrogels

4.3.7.1. RNA extraction and gene expression analysis

On day 14 of encapsulation, encapsulated islets exhibited significantly upregulated gene expression for all the signature islet genes as compared to non-encapsulated islets in 2D (TCP) ($p < 0.01$). The maximum gene expression was observed in BA3 with significantly upregulated insulin I (~3.8-fold), insulin II (~6.3-fold), glucagon (~5.4-fold) and somatostatin (~4.4-fold) genes compared to non-encapsulated islets in 2D **(Figure 4.3C)**. There was a significant difference in expression levels of insulin genes (I and II) of BA3 and BA1 ($p < 0.05$) which is supported by glucose challenge assay **(Figure 4.3D)**. Similarly, glucagon gene expression levels (~5.4-fold) suggested islet functionality. There were no significant differences in glucagon and somatostatin level among the different hydrogel groups; however the differences were highly significant when compared with suspended islets in 2D ($p > 0.05$**).**

4.3.7.2. Glucose challenge assay

Glucose challenge assay was performed to evaluate insulin releasing capability of encapsulated islets (Davis et al., 2012; Kumar et al., 2017; Liao et al., 2013). After 14 days of hydrogel encapsulation, the stimulation indices (SI) were 1.1, 1.5, 1.7 and 2.1 for TCP, BA1, BA2 and BA3, respectively. Hydrogel-encapsulated islets exhibited a significant difference in SI compared to non-encapsulated islets ($p < 0.01$; **Figure 4.3D,ii**). Also, a significant difference was noted between the groups BA1 and BA3 (1.5 vs 2.1, $p < 0.001$). Similarly, BA2 and BA3 also exhibited significant differences (1.7 vs 2.1, $p < 0.01$). As depicted on the graph, the glucose responsiveness was not

preserved in suspended islets. On day 7, the corresponding stimulation indices (SI) were 1.1, 1.9, 2.0 and 2.2 for TCP, BA1, BA2 and BA3, respectively (**Figure 4.3D,i**).

4.3.7.3. Immunohistochemistry for insulin and glucagon

In order to complement the findings from ELISA and RT-qPCR, immunofluorescence microscopy was conducted for insulin and glucagon; the chief islet hormones. The immunofluorescence study was conducted on BA3 hydrogels as they exhibited the highest proliferation and viability of RIN-5 cells and islets. The maximum stimulation index and highest level of gene upregulation (insulin I and insulin II) was also documented for this group (**Figure 4.3C-D**). The representative immunofluorescence images revealed insulin within hydrogel sections. In case of 2D culture, RIN-5 cells were distributed all over the hydrogels and showed insulin expression abundantly (**Figure 4.4B,i-iii**). On day 3, 7 and 14, the relative abundance and distribution of insulin was different as per the proliferation of RIN-5 cells in 3D (**Figure 4.4D,i-iii**). For encapsulated islets, insulin and glucagon were homogeneously distributed throughout the cross-sections (**Figure 4.5B** and **4.5C,i-iii**).

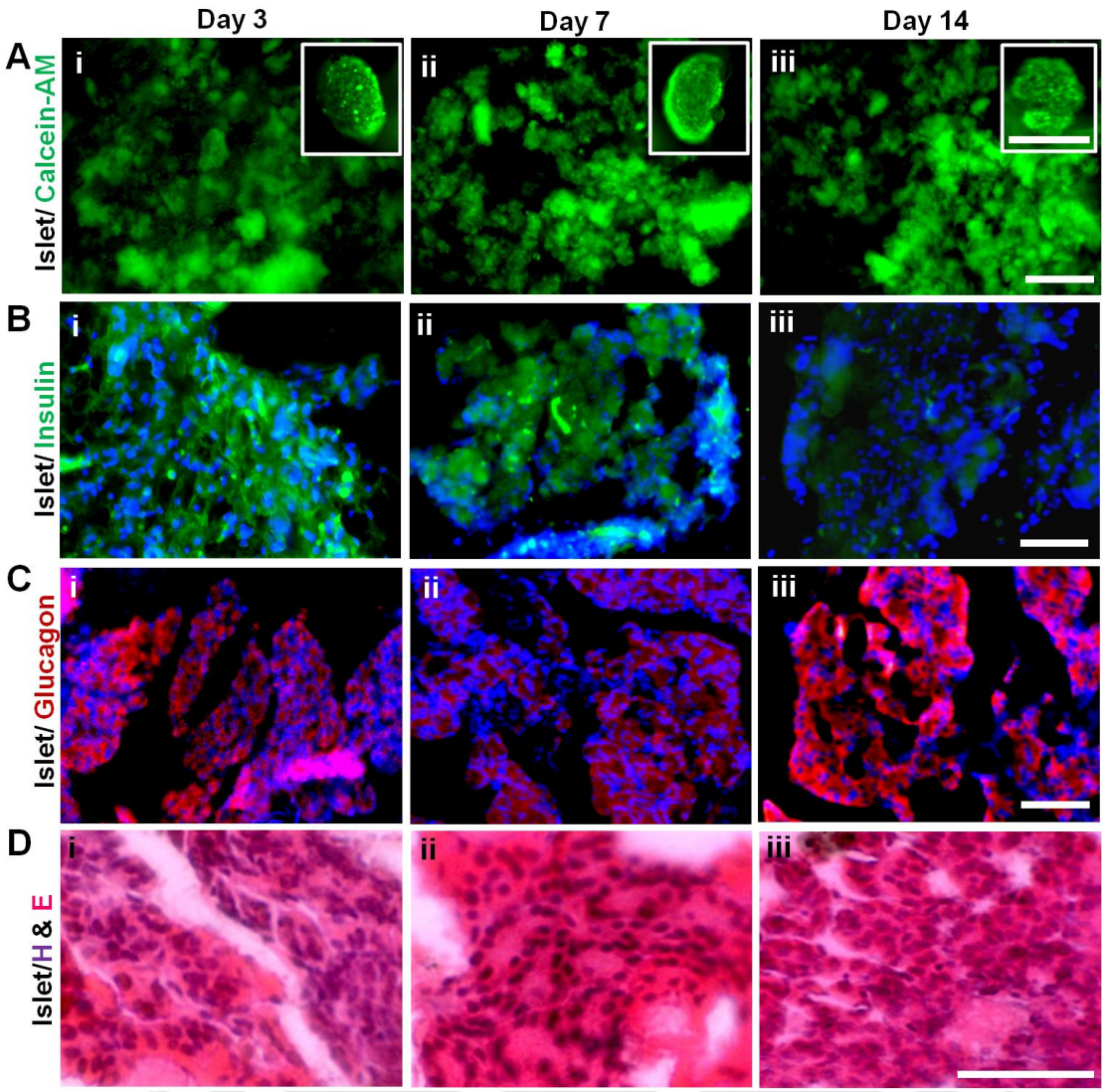

Figure 4.5. *Representative images for primary rat islet viability, insulin/glucagon expression and islet distribution post-encapsulation in 3D silk hydrogel (BA3) on day 3, 7 and 14. (A) Viable islets encapsulated in silk blend hydrogel (green) inset images show individual islet. (B) Immunofluorescence images showing the expression of insulin (green) and nucleus (blue). (C) Images showing the expression of glucagon (red). (D) Distribution of encapsulated islets in 3D silk hydrogel. Islets are stained with hematoxylin (nucleus) and eosin (cytoplasm). Scale bar 50 µm.*

4.3.8. IL-4 and Dexamethasone release profile

In vitro release of IL-4 and Dexamethasone (Dex) from all the hydrogels (BA1, BA2 and BA3) in PBS was measured over 14 days by ELISA and UV spectroscopy, respectively. The hydrogels exhibited a burst release in the initial 3 days and relatively plateaued in following days. The cumulative percent release of IL-4 from BA1, BA2 and BA3 hydrogels was ~5, 7, and 9%, respectively, within 24 h (**Figure 4.6A,i**). The corresponding release values for day 14 were ~10, 11 and 12%, respectively. Within 24

h, the cumulative percent release of Dex from BA1, BA2 and BA3 was ~9, 12, and 14%, respectively (**Figure 4.6A,ii**). Further, the corresponding release percent values for day 14 were ~22, 24, and 25%. There was no significant difference between the hydrogel groups ($p > 0.05$) and the hydrogels could maintain a slow and sustained release.

4.3.9. Immunomodulation study

Immunomodulation efficiency of released IL-4 from hydrogels was evaluated on cultured human THP-1 monocytes. The polarization results showed significantly upregulated expression of M2 surface markers, CD206 (~9-fold) and CD209 (~6-fold), which mediate anti-inflammation and immunosuppression (**Figure 4.6B**, $p < 0.01$). A significantly downregulated expression of pro-inflammatory marker CCR7 (M1 surface marker) was also recorded (**Figure 4.6B**). The expression of CD206 cell surface marker in polarized macrophages (M2) was also witnessed from immunofluorescence images (**Figure 4.6D,iii**). Also, under the bright field microscope, a clear difference could be noted between the control M0 macrophage and the polarized M2 macrophages (**Figure 4.6D,i-ii**) (Reeves et al., 2015).

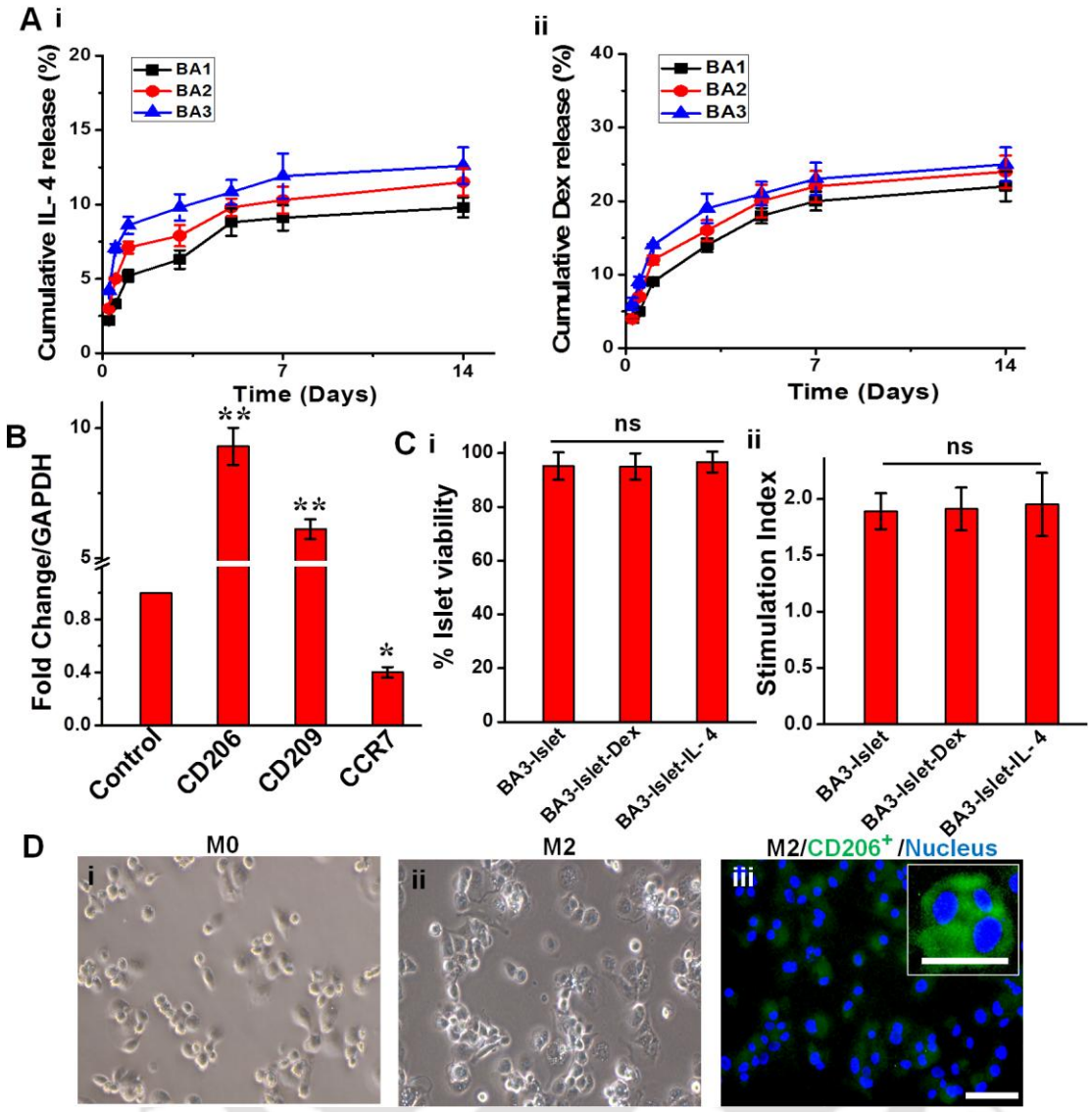

Figure 4.6. *Interleukin-4 (IL-4)/ Dexamethasone (Dex) release and immunomodulation study with silk hydrogels. (A) Cumulative IL-4 (i) and Dex (ii) release from different hydrogel compositions (BA1, BA2 and BA3). (B) Gene expression analysis for M1 (CCR7) and M2 (CD206 & CD209) macrophage surface markers when incubated with IL-4-loaded silk hydrogel blend (BA3) for 72 h. (C) Islet physiology assessment after incubation with Dex and IL-4-silk hydrogels for 72 h. PicoGreen assay showing islet viability post-incubation with islet co-encapsulated Dex and IL-4 in silk hydrogel blend (BA3) compared with control (islets without IL-4/Dex) (i). Glucose stimulated insulin release by the encapsulated islets (ii). "ns" indicates not significant ($p > 0.05$). (D) Representative images for macrophage polarization. Induced M0 macrophages from THP-1 monocytes after overnight PMA (162 nM) treatment (i) M0 to M2 polarized macrophage when incubated with IL-4-eluting silk hydrogel blend (BA3) (ii) and M2 surface marker CD206 (green) expression counterstained with Hoechst33342 (nucleus, blue) (iii). Scale bar 200 µm. ($n = 3$, $*p \leq 0.05$, $**p \leq 0.01$).*

4.3.10. Cytotoxicity and immunomodulation study on islets

In vitro cytotoxicity/proliferation studies were carried out to assess the effects of released and co-encapsulated Dex and IL-4 on islets physiology. As depicted on the graph, the released and co-encapsulated Dex and IL-4 didn't exert any detrimental effect on islet viability (**Figure 4.6C,i**) and insulin secretion (**Figure 4.6C,ii**) as compared with islets without Dex/IL-4 ($p > 0.05$).

4.3.11. Endothelial cell culture and functional studies

4.3.11.1. Viability and proliferation of endothelial cells

Islet revascularization is a vital process which determines post-transplantation islet survival and function (Mao et al., 2017). Porcine aortic endothelial cells cultured on silk hydrogel (BA3) adhered well and spread in their native-like morphology (**Figure 4.7A**). Moreover, Calcein AM staining exhibited presence of viable cells on silk hydrogel and TCP (**Figure 4.7B**). To further characterize the proliferation of endothelial cells on silk hydrogel surface, AlamarBlue dye reduction assay was performed. Over a 7 days study, there was a significant difference in cell proliferation when compared with day 1 and 3, which suggested that the hydrogel (BA3) supported endothelial cell survival and proliferation (**Figure 4.7D**).

4.3.11.2. Functionality of endothelial cells

Endothelial cells cultured on TCP and silk hydrogel (BA3) were analyzed for their functional testing by quantifying the NO release. As determined from the result, no significant difference was observed for hydrogel-seeded endothelial cells when compared with TCP (control) (**Figure 4.7E**). Furthermore, cells were immunostained for vWF, an essential marker for endothelial cell functionality. Comparable results were observed for TCP and silk hydrogel seeded endothelial cells with abundant expression of the marker in both the cases (**Figure 4.7C**).

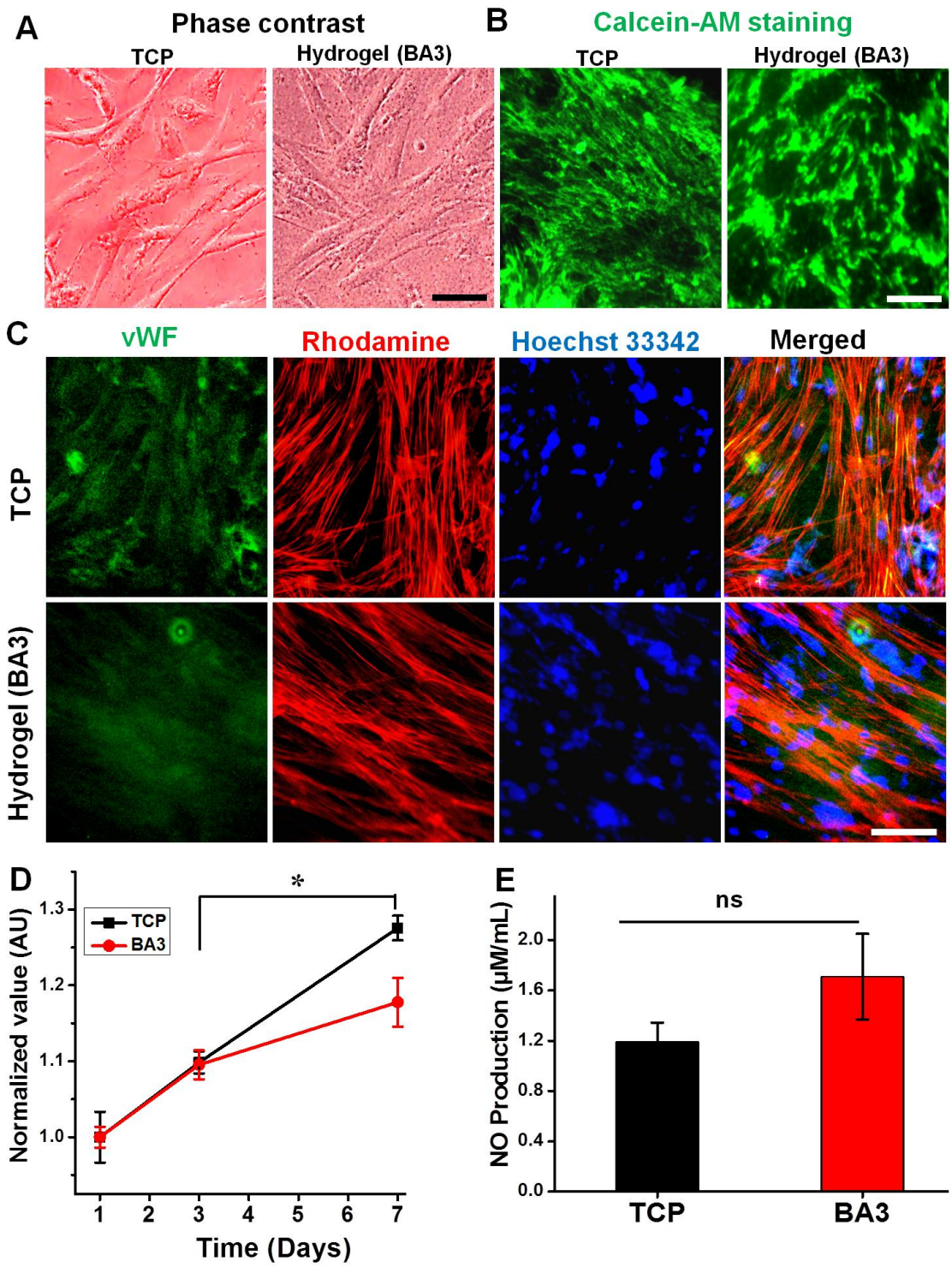

Figure 4.7. *Cytocompatibility, cell adhesion, proliferation and functional study with porcine aortic endothelial cells after 7 days of culture. (A) Phase contrast and (B) fluorescence images of the cells cultured on TCP and silk hydrogel blend (BA3). Green colour shows live cells. Scale bar: 500 µm. (C) Immunostaining for endothelial cell marker, Von Willebrand factor (vWF) on TCP and silk hydrogel (BA3). Green, red and blue colours represent positive staining for vWF, cellular cytoskeleton and the nucleus, respectively. Scale bar: 100 µm.* (D) *Alamar blue dye reduction assay and (E) production of NO from the cultured endothelial cells. n = 3, *p ≤ 0.05, "ns" indicates not significant (p > 0.05).*

4.3.12. *In vitro* inflammatory response towards hydrogels

Macrophages are the central player of immunoregulation which regulate inflammatory responses in the body (Kumar et al., 2016a; Kumar et al., 2017; Reeves et al., 2015). To evaluate possible cytokine activation caused by the acellular hydrogels (BA1, BA2, and BA3); TNF α cytokine release study was conducted using RAW 264.7 macrophage cell line. Post 12 h of incubation, significantly low level of TNF α release was recorded in hydrogel-containing wells as compared to LPS; positive control (~2-fold; $p < 0.01$) and the values were comparable to TCP wells; negative control ($p > 0.05$) (**Figure A4.2**). Post 24 h of culture, TNF α secretion was significantly more in positive wells with LPS ($p < 0.01$). Overall, for all the hydrogels, the released TNF α was significantly lower than the LPS-treated group and comparable to TCP control wells.

4.3.13. *In vivo* immunomodulation study

Cellular infiltration and immunomodulation was determined by immunostaining of the retrieved hydrogel implants. The retrieved hydrogels demonstrated greater infiltration of the host cells at the early time point; day 3 (**Figure 4.8**). At the day 10 time point, cell infiltration was comparatively lesser in all the hydrogels (**Figure 4.9**). As per the result (immunofluorescence images), loaded IL-4 and Dex appeared to release into the implant surroundings and polarizing them towards M2 phenotype as attested by CD206 expression. The results showed that within 3 days of implantation, cytokine IL-4 and Dex-loaded injectable hydrogels promoted a strong macrophage polarization towards M2 phenotype which might provide an immunopermissive environment for the implants. At both the time points, 3D representation of M2 macrophage marker (CD206) expression showed a higher expression in case of IL-4 and Dex-loaded hydrogels.

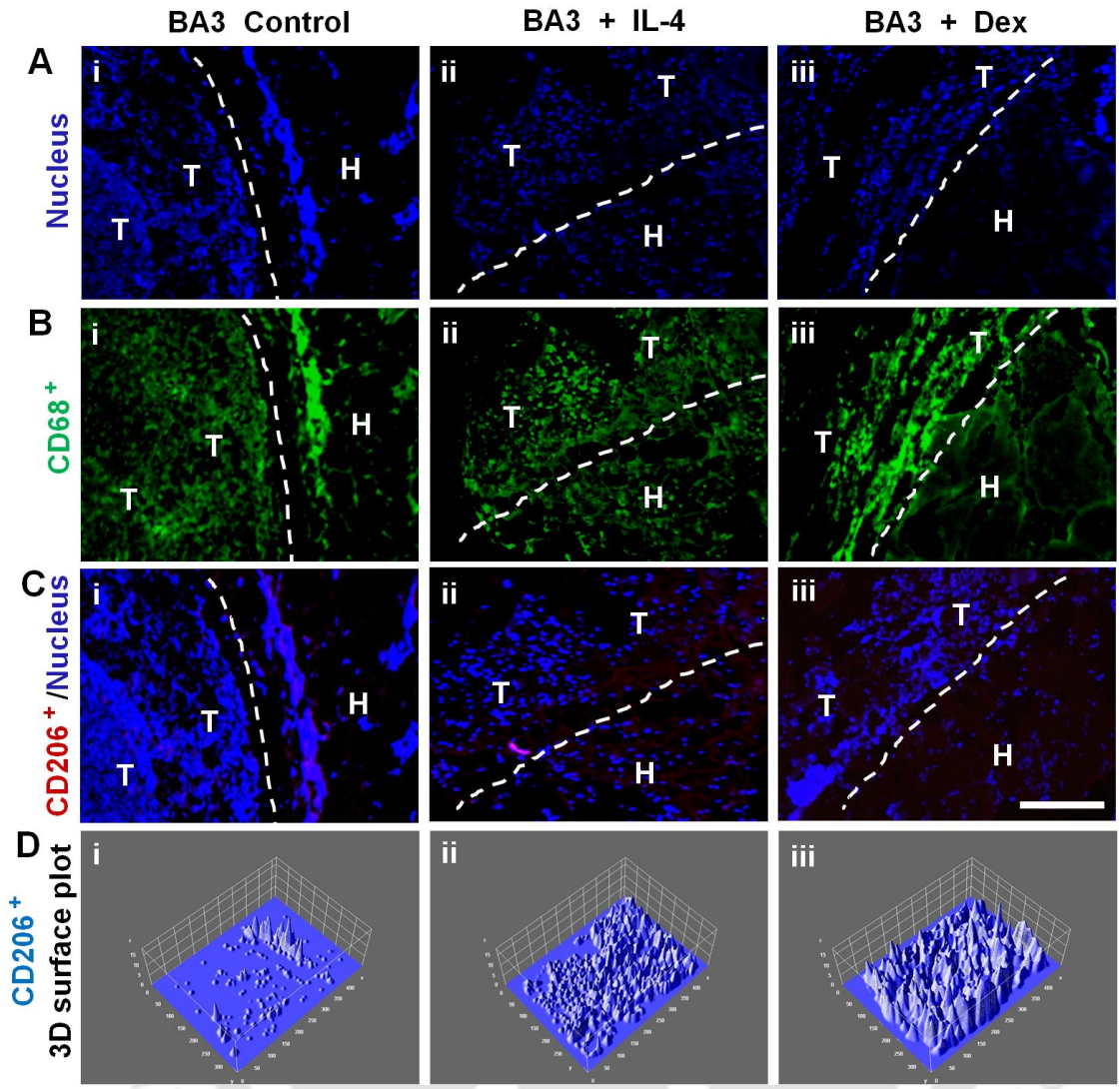

Figure 4.8. *Representative images showing immunohistochemistry of retrieved BA3 control, BA3 + IL-4 and BA3 + Dex hydrogels after 3 days of implantation. Blue, green and red colours represent nucleus, CD68 expression and CD206 expression, respectively. Scale bar represents 100 µm. 3D surface plot of IHC stained images showing distribution of CD206 positive cells using the ImageJ (NIH, USA) software. Symbols H and T stand for silk hydrogel and host tissue, respectively.*

Very less or minimal expression was recorded in control hydrogel. Analysis of infiltrating macrophage population revealed higher presence of $CD68^+$ cells as a percentage of the total cell population in mice implanted with the hydrogels. There were no redness or swelling at the implantation site over the course of the experiment. Also, no altered gait behaviour of mice was recorded.

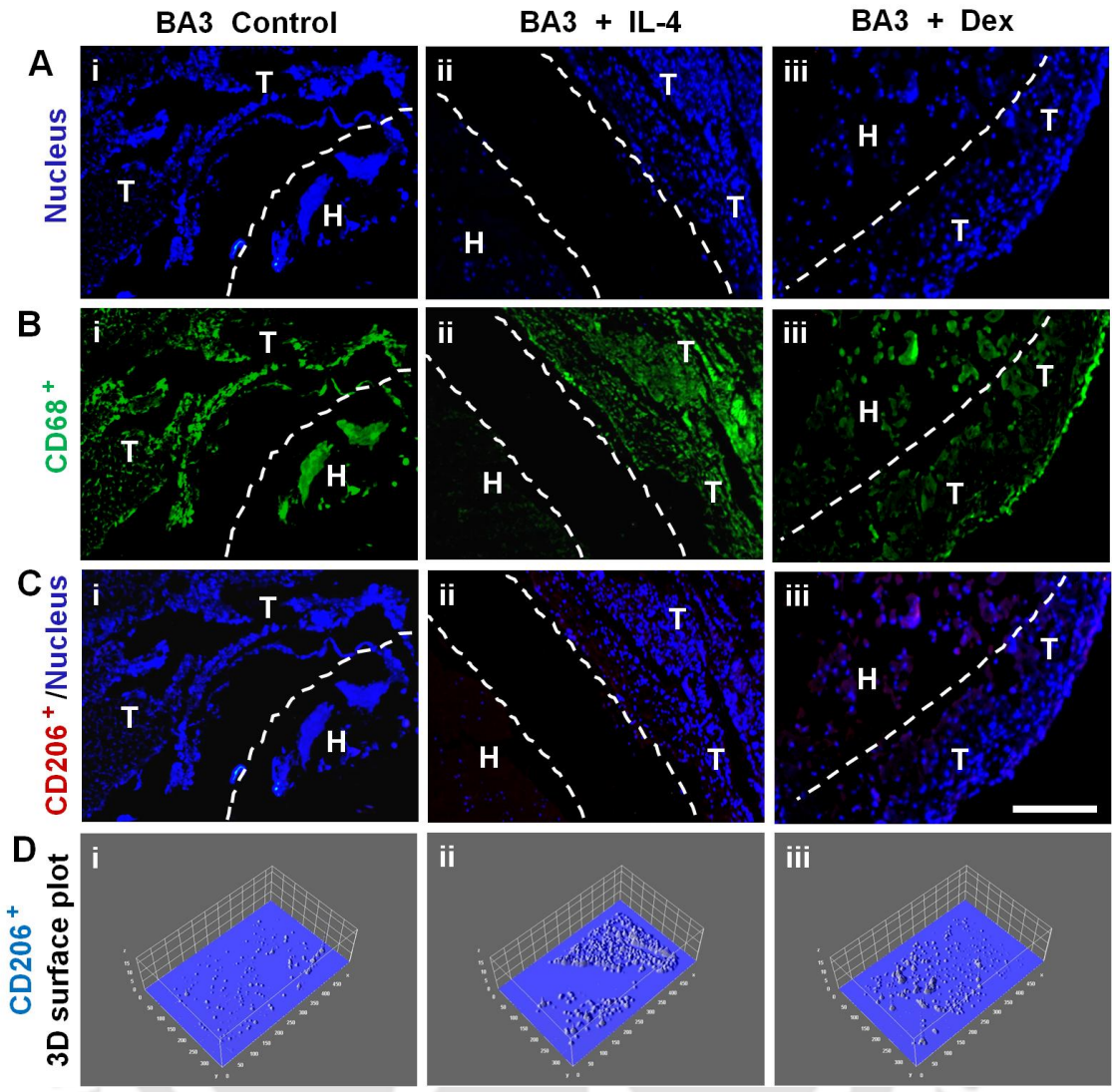

Figure 4.9. *Representative images showing immunohistochemistry of retrieved BA3 control, BA3 + IL-4 and BA3 + Dex hydrogels after 10 days of implantation. Blue, green and red colours represent nucleus, CD68 expression and CD206 expression, respectively. Scale bar represents 100 μm. 3D surface plot of IHC stained images showing distribution of CD206 positive cells using the ImageJ (NIH, USA) software. Symbols H and T stand for silk hydrogel and host tissue, respectively.*

4.4. Discussion

Injectable biodegradable hydrogels have emerged as promising matrix for islet encapsulation due to their minimally invasive mode of administration resulting in reduced pain and complexity (Miles et al., 2004). The developed silk-blend hydrogels are potential injectable islet encapsulation matrix by virtue of rapid gelation and ease of injectability (**Figure 4.1**). The hydrogels were prepared by mixing two silk fibroin solutions: mulberry *B. mori* fibroin and cell-binding RGD motif-containing non-

mulberry *A. assama* fibroin. Due to the mild gelation and encapsulation conditions, islets maintained viability and function throughout the study (Liao et al., 2013). Additionally, intrinsic RGD motifs present in *A. assama* fibroin helped in enhanced cell viability/proliferation and glucose responsiveness (Davis et al., 2012; Johansson et al., 2015; Salvay et al., 2008).

A. assama-based 3D matrices have been widely explored for the regeneration of different tissues like bone, (Gupta et al., 2016a) cartilage, (Singh et al., 2016b) blood vessels, (Gupta et al., 2016b) skin, (Chouhan et al., 2017) liver (Janani et al., 2017) and cardiac (Mehrotra et al., 2017) tissues with promising outcomes compared to its mulberry counterpart *B. mori*. In the same line, this is the first attempt to recreate the microenvironment for islets employing *A. assama* fibroin. In the present work, injectable silk-blend hydrogels were developed utilizing the differences in the properties of silk varieties that lead to hydrogelation upon mixing without requiring any external agent or cross-linker. The gelation time could be manipulated by varying protein concentration (8, 6, 4, 2% w/v) and protein blend ratio (2:1, 1:1 and 1:2) (**Figure 4.1B**). The hydrogelation observed is attributed to the hydrophobicity difference between silk fibroin proteins wherein mixing results in β sheet formation and cross-linking among the silk solutions (Li et al., 2018). In previous studies, the gelation time reported for vortex-induced silk hydrogel (2-5% w/v silk) was 2 h to 1 day (Rockwood et al., 2011; Yucel et al., 2009). Similarly, for sonication-induced hydrogels (4, 8 and 12% w/v silk) the gelation time varied from 0.5-2 h (Rockwood et al., 2011; Wang et al., 2008a). Interestingly, here, the average gelation time observed for *B. mori: A. assama* blended hydrogels (8:2, 6:2 and 4:2) is 13-16 min which is much more rapid than the previously reported methods (**Figure 4.1B**) (Rockwood et al., 2011; Wang et al., 2008a; Yucel et al., 2009). This gelation time may be further reduced by increasing the silk concentrations (Wang et al., 2008a). It is pertinent to note that no gelation could be observed in case of *B. mori* and *A. assama* alone (**Figure 4.1B,ii**). As per the previous report, *B. mori* fibroin solution of 2% w/v concentration gelled in 30 days at 37 ^{o}C (Kapoor and Kundu, 2016). On the other hand, in our case, blending *B. mori* (2% w/v) with *A. assama* (2% w/v) with a final concentration of 2% w/v gelled in 20 minutes which can always be reduced by using higher silk concentrations depending on the applications. The rheology and viscosity results also supported the gelation pattern (**Figure A4.1**). Degradation results showed that the rate of degradation can readily be tuned by manipulating the ratio of the two proteins

(**Figure 4.2B**). Results demonstrated that the hydrogels with more amount of *A. assama*, degraded comparatively faster than those with decreasing amount of *A. assama* (Li et al., 2018). However, it would be pertinent to mention here that the degradation times reported are for *in vitro* conditions which is much faster than the time taken for *in vivo* biodegradation (Wang et al., 2008a).

When encapsulated in these hydrogels, RIN-5 cells and primary islets maintained prolonged viability, proliferation, and glucose stimulated insulin secretions. As stated earlier, *in vitro* islet culture requires a 3D niche as a substitute for the natural ECM lost during enzymatic digestion (Daoud et al., 2010; Davis et al., 2012; Hamilton et al., 2017). Therefore, the silk blended hydrogels were successfully utilized as an ideal alternative islet encapsulation platform. Further, the islet integrin signalling could be upregulated for enhanced islet survival and insulin secretion. Being of hydrogel consistency these matrices absorb and retain a bulk of cell culture media to provide nourishment to the encapsulated islets (Kapoor and Kundu, 2016; Wang et al., 2008a). The metabolically active cells, as suggested by AlamarBlue assay (Kumar et al., 2016a; Kumar et al., 2017) (**Figure 4.3A,i**) and non-hypoxic environment as suggested by PicoGreen assay (Wang et al., 2008a) (**Figure 4.3A,ii**) with encapsulated RIN-5 cells attested the biocompatibility of the hydrogels. The maintenance of cellular physiology in hydrogels reflects optimum mass (oxygen, glucose, nutrient, metabolite) transport without mechanical restrictions imposed by the hydrogels (Kumar et al., 2017; Wang et al., 2008a) The detrimental effects of higher silk concentrations (*B. mori* 8 and 12 %) have been previously reported in restricting nutrient transfers (Wang et al., 2008a). Therefore, authors suggested lower gel concentrations (1 and 2%) to be explored for efficient delivery with minimal cell death (Wang et al., 2008a) which was later utilized successfully (Davis et al., 2012; Hamilton et al., 2017).

In a two week culture study, the islet viability in the hydrogels was ~90% (**Figure 4.3B**). However, in a previous report, RIN-m5F and MIN-6 cells encapsulated in unmodified PEG hydrogels demonstrated only 20% viability post 10 days of culture (Liao et al., 2013; Lin and Anseth, 2009). Similarly, islets encapsulated in alginate (without sertoli cells) maintained 41% viability by day 12 of culture (Liao et al., 2013). Islets in suspension (2D) culture fail to respond to glucose and can't secrete adequate amount of insulin; however on 3D platform they maintain adequate insulin level as supported by our results and also attested by previous reports (Daoud et al., 2011; Davis et al., 2012; Kumar et al., 2017). The incorporation of RGD-containing *A.*

assama protein improved the islet viability and insulin secretion. This pronounced effect of RGD on islets has been previously reported (Johansson et al., 2015; Salvay et al., 2008). Glucose stimulated insulin secretion (GSIS) was evaluated at physiological concentrations of basal and hyperglycaemic levels and the results are in agreement with earlier reports (Daoud et al., 2010; Davis et al., 2012). After two week culture, islets encapsulated in BA3 exhibited a stimulation index of ~2.1 which is significantly higher than the other groups (BA1, BA2 and 2D control) (**Figure 4.3D**). The enhanced islet functions in BA3 when compared to BA1 and BA2 might be due to upregulated integrin signalling mediated through RGD (Davis et al., 2012; Johansson et al., 2015; Salvay et al., 2008). Similarly, the encapsulated islets exhibited upregulated gene expression (insulin, glucagon and somatostatin) compared to control (non-encapsulated) islets which is attributed to the physicochemical cues provided by silk hydrogels further assisted by integrin receptor activation (**Figure 4.3C**) (Daoud et al., 2010; Daoud et al., 2011; Davis et al., 2012; Kumar et al., 2017). The results were corroborated by immunohistochemistry for major islet hormones, insulin and glucagon (**Figure 4.5**) (Daoud et al., 2011; Kumar et al., 2017). As reported previously, silk hydrogels maintain the differentiated state of encapsulated islets with adequate expressions of E-cadherin, vimentin and cytokeratin 19 and prevent the de-differentiation of islets to fibroblast-like cells (Davis et al., 2012). Also, the islet co-encapsulated with MSCs in silk hydrogels showed improved islet graft function post-transplantation in mice model (Hamilton et al., 2017). In addition, silk fibroin protein has intrinsic potential that enhances islet response to high glucose as in the diabetic mice when administered with silk fibroin hydrolysate orally, led to increment in islet β cell mass and function (Do et al., 2012).

Macrophages are the key immune cells which regulate immune responses against foreign materials (Kumar et al., 2016a; Reeves et al., 2015). Significantly very low TNF-α release from murine macrophage RAW 264.7 when incubated with these hydrogels demonstrated that the cell-encapsulating hydrogels might be a potential matrix for *in vivo* implementation (**Figure A4.2**). The TNF-α release result is in accordance with the published reports for mulberry and non-mulberry fibroin matrices (Gupta et al., 2016b; Reardon et al., 2017; Singh et al., 2016b). Macrophages are also the prevalent infiltrating immune cells attacking islets post-transplantation which play crucial role in implant rejection (Kumar et al., 2017; Wu et al., 2000). In this regard, hydrogel loaded with bioactive molecules is an ideal ferry for sustained release at

transplantation site (Jiang et al., 2017; Kumar et al., 2016a; Kumar et al., 2017; Zhang et al., 2011). When primed with cytokine (IL-4) or drug (Dex), these hydrogels would help in islet protection by inhibiting the immune cell infiltration and polarizing them to anti-inflammatory and immunosuppressive phenotypes (Kumar et al., 2016a; Kumar et al., 2017; Reeves et al., 2015; Weaver et al., 2015). The initial release of these molecules post-transplantation prevents the production of pro-inflammatory cytokines within/near implant thus avoiding rejection (Liu et al., 2016).

In our *in vitro* (**Figure 4.6B**) and *in vivo* (**Figure 4.8** and **Figure 4.9**) results, hydrogel-encapsulated IL-4 maintained bioactivity and polarized the M0 macrophages to M2 phenotype (Kumar et al., 2016a; Kumar et al., 2017; Reeves et al., 2015). Out of several cytokines (IL-4, IL-10 and IL-13) known to influence an anti-inflammatory phenotype, IL-4 is known as immunosuppressive (Kumar et al., 2015). It encourages pro-inflammatory M1 macrophages to re-enter the cell cycle towards M2 by decreasing M1 activation and inducing M2 cell proliferation (Kumar et al., 2015). Furthermore, IL-4-induced secretion of IL-4, IL-10, transforming growth factor-β (TGF-β) and platelete-derived growth factor (PDGF) results in an amplification of M2 response (Kumar et al., 2015). These M2 macrophages help in decreasing inflammation through macrophage polarization or immunomodulation (from M0/M1 to M2) (Kumar et al., 2016a; Kumar et al., 2017; Kumar et al., 2015; Reeves et al., 2015). The secreted TGF-β promotes the differentiation of naïve $CD4^+$ T cells into regulatory T cells (T_{regs}) and deletion of effector T cells (T_{effs}) (Liu et al., 2016). Also, IL-4 prevents insulin dependent type 1 diabetes mellitus in nonobese diabetic mice by potentiating regulatory T helper-2 cells (Cameron et al., 1997). Similarly, M1 to M2 polarization has been reported by localized delivery of glucocorticoids, like Dexamethasone (Jiang et al., 2017). The reported CD206, CD209 and CCR7 markers are highly explored to characterize the phenotype of naïve/polarized macrophages (Reeves et al., 2015). Upregulated CD206 and CD209 expression with the downregulated CCR7 expression indicated the effective macrophage polarization towards immunosuppressive M2 phenotype (Kumar et al., 2016a; Reeves et al., 2015). All the *in vitro* immunomodulation studies were conducted with THP-1 human monocyte cells as these cells respond to human cytokines (Interferon-γ and IL-4) in a similar manner as the primary peripheral blood monocyte-derived macrophages (PBMCs) do (Kumar et al., 2017; Reeves et al., 2015).

As per the available reports, restricted hydrogel swelling or limited expandability aid to slow and sustained release of encapsulated drug/molecules (Kumar et al., 2017; Singh et al., 2016a). Also, the differences in hydrodynamic volume and molecular weight of the molecules play a critical role in diffusivity through hydrogels (Kumar et al., 2015). The difference in cumulative release of IL-4/Dex from the hydrogels might be attributed to the smaller mass of dexamethasone with molecular weight (392.46 Da) compared to IL-4 which is heavier (14 kDa) and larger (hydrodynamic volume 16.9 nm^3) (**Figure 4.6A**) (Kumar et al., 2015). A significant amount of loaded biomolecules got adsorbed to the hydrogels hindering further release (Kumar et al., 2016a; Kumar et al., 2017; Reeves et al., 2015). The adsorbed IL-4 might prolong the localized immunomodulation as the local macrophages gradually degrade the silk hydrogel to access trapped cytokines (Kumar et al., 2016a; Reeves et al., 2015). Interestingly, the hydrogels showed the potential of suppressing inflammation locally while maintaining islet's functions (**Figure 4.6B,C**). Also, the released Dex and IL-4 at these concentrations didn't exert negative effects on islet function (Vacanti et al., 2012; Weaver et al., 2015). This approach circumvents the administration of immunosuppressive drugs by systemic mean preventing many associated side-effects (Jiang et al., 2017; Weaver et al., 2015).

Recent reports advocate prospective positive role of M2 macrophages to assist in desired healthy remodelling and vascularization (Weaver et al., 2015). As depicted from porcine endothelial cells culture study, silk hydrogel is biocompatible with endothelial cells and supports the maintenance of endothelial physiology (**Figure 4.7**). These results are in line with the report wherein RGD-containing non-mulberry silk films showed a better effect on endothelial cell proliferation when compared with mulberry *B. mori* silk (Gupta et al., 2016b). Since, the native ECM in the surrounding of pancreatic islet is provided by the local endothelial cells therefore, the revascularization of the implant is a pre-requisite for graft viability (Nikolova et al., 2006). Thus, the critical step of islet revascularization can also be assisted by endothelialisation of the islet-encapsulating matrix till the revascularization is complete (Vlahos et al., 2017).

In summary, with a multidimensional approach, utilizing RGD motif-containing silk with immunomodulatory molecules may have potential of improving islet transplantation outcomes with reduced inflammation. Immunomodulatory properties of Dex and IL-4, with angiogenic attributes of endothelial cells may ameliorate islet

damage by infiltrating undesired immune cells in parallel improving graft revascularization. Future work will characterize this injectable platform for its impact in islet transplantation in pre-clinical models. Such local delivery platforms or immunomodulatory biomaterials could significantly enhance clinical approaches to islet graft protection and minimize the burden of systemic immunotherapy.

4.5. Significant Findings

The salient findings of this chapter are as follows:

1. Silk protein blend of *B. mori* and *A. assama* resulted in rapid gel formation without any cross-linker or external stimulus as compared to individual protein (mori/muga) which failed to form gel. The faster gelation under physiological-like conditions allowed the encapsulation of islets, IL-4 and Dex with restored bioactivity.

2. The increasing concentrations of *A. assama* protein led to a significant increase in islet viability, islet-specific gene expression and glucose responsive insulin secretion. This enhancement could be ascribed to the 3D support provided by the hydrogel and the presence of RGD motif. In contrast, the control suspended islets failed to survive and lost glucose responsiveness.

3. The hydrogel supported the proliferation and function maintenance of primary porcine endothelial cells.

4. *In vitro* immunocompatibility assay with murine macrophages revealed that the developed hydrogels were minimally immunogenic and comparable to the standard tissue culture plate.

5. Assessment of immunomodulation using injectable hydrogel *in vitro* and *in vivo* demonstrated localized polarization of the macrophages towards anti-inflammatory phenotype (M2), thereby complimenting immunomodulatory and immunosuppressive effects.

Altogether, the results exhibit the promising attributes of injectable silk hydrogel and the utility of non-mulberry silk fibroin as an alternative biomaterial towards the development of injectable bio-artificial pancreas. It would be interesting to validate the potential of this multidimensional approach in *in vivo* diabetic models.

SUMMARY AND FUTURE PERSPECTIVE

SUMMARY AND FUTURE PERSPECTIVE

Pancreatic islet encapsulation in a 3D scaffolding matrix has achieved limited clinical success due to loss of islet function and cell death, shortly after transplantation. Also, autoimmunity and transplant-associated inflammatory responses create an unfavorable microenvironment for islet survival. The problem is further compounded as the transplanted islets under such stress secrete pro-inflammatory factors amplifying local inflammation. In this context, the present investigation which reports the potential of silk-based matrices in conferring immunoisolation and immunomodulation thereby presenting a novel therapeutic approach in treating type 1 diabetes, a global healthcare issue. The relevant advancement of the study and the future prospects associated with it are briefly enumerated in the following section:

(1) Silk scaffolds with alginate and agarose were probed for their islet-supporting attributes using array of qualitative and quantitative assays. The revelation of the *in vitro* studies was fascinating since the scaffolds supported prolonged viability of primary rat islets with sustained metabolic activity and insulin release. However, islets cultured in 2D suspension lost their functions. The scaffolds supported spontaneous formation of islet-like 3D cellular spheroids from RIN-5 cells, leading to enhanced cell viability and proliferation. Restricted infiltrations of macrophage/inflammatory cells in the scaffolds *in vivo* projects alginate and agarose as potential cell macro-encapsulating agents. It is foreseen that islet-encapsulated silk-based scaffolds, when subjected to *in vivo* functional test, might find applications in type 1 diabetes reversal.

(2) Macrophages are the prevalent infiltrating immune cells that attack islets post-transplantation and play a crucial role in islet implant rejection. In the present study, silk-based matrices were utilized to regulate cytokine delivery for macrophage differentiation, polarization and plasticity. Hydrogels were loaded with the M1 (pro-inflammatory) and M2 (anti-inflammatory/immunosuppressive) polarizing cytokines interferon-γ (IFN-γ) and interleukin-4 (IL-4), respectively. Cytokine-loaded and macrophage-encapsulated hydrogels were able to polarize monocytes/macrophages to desired phenotypes (M1/M2). The release of cytokines and extent of polarization correlated with the physicochemical properties of the hydrogels. Macrophage

polarization study was conducted with three different approaches; cytokine encapsulation, macrophage encapsulation and co-encapsulation with efficient and desired macrophage polarization and plasticity.

(3) The prospect of a multidimensional approach of islet encapsulation and delivery has been explored utilizing RGD motif-containing injectable silk hydrogel with immunomodulatory molecules (interleukine-4 and dexamethasone). This approach may have potential in improving islet transplantation outcomes with reduced inflammation. Angiogenic attribute of primary endothelial cells was also evaluated. The ability of the minimally invasive injectable silk hydrogel to significantly enhance islet functions *in vivo* projects it as a prospective islet delivery matrix. *In vivo* local delivery of IL-4 and dexamethasone molecules demonstrated localized polarization of the macrophages towards anti-inflammatory macrophages (M2), demonstrating immunomodulatory and immunosuppressive effects.

(4) In the near future, these silk-based platforms may be assessed for the application of culturing human stem cells and their differentiation toward insulin producing cells for bio-artificial pancreas development.

(5) 3D pancreatic organ models developed herein may be utilized as drug screening platform using islet-like spheroids and primary cells or stem cell-derived insulin-producing cells.

(6) Silk-based 3D printed constructs may also be developed for further validation of studies.

In summary, silk-based islet encapsulation approach has been successfully explored towards bio-artificial pancreas development. The silk platforms were investigated for immunoisolation and immunomodulation via macrophage polarization to overcome immune-associated challenges. The promising outcome of the *in vitro* experiments along with preliminary *in vivo* results highlights the potential of islet encapsulation with multifaceted approaches like injectability, localized immunomodulation and endothelialization. Moreover, this work may bring forward immense prospects of exploring non-mulberry silk fibroin as a biomaterial for islet

encapsulation and silk-based bio-artificial pancreas development that holds considerable promise in the therapeutic intervention of type 1 diabetes.

BIBLIOGRAPHY

1. Acharya, C., Kumary, T., Ghosh, S.K., and Kundu, S. (2009). Characterization of fibroin and PEG-blended fibroin matrices for *in vitro* adhesion and proliferation of osteoblasts. Journal of Biomaterials Science, Polymer Edition *20*, 543-565.
2. Altman, G., Horan, R., Martin, I., Farhadi, J., Stark, P., Volloch, V., Vunjak-Novakovic, G., Richmond, J., and Kaplan, D.L. (2002). Cell differentiation by mechanical stress. Faseb Journal *16*, 270-272.
3. Altman, G.H., Diaz, F., Jakuba, C., Calabro, T., Horan, R.L., Chen, J., Lu, H., Richmond, J., and Kaplan, D.L. (2003). Silk-based biomaterials. Biomaterials *24*, 401-416.
4. Arai, T., Freddi, G., Innocenti, R., and Tsukada, M. (2004). Biodegradation of *Bombyx mori* silk fibroin fibers and films. Journal of Applied Polymer Science *91*, 2383-2390.
5. Arango Duque, G., and Descoteaux, A. (2014). Macrophage cytokines: Involvement in immunity and infectious diseases. Frontiers in Immunology *5*, 491.
6. Association, A.D. (2006). Diagnosis and classification of diabetes mellitus. Diabetes care *29*, S43.
7. Badylak, S.F., Valentin, J.E., Ravindra, A.K., McCabe, G.P., and Stewart-Akers, A.M. (2008). Macrophage phenotype as a determinant of biologic scaffold remodeling. Tissue Engineering Part A *14*, 1835-1842.
8. Beattie, G.M., Montgomery, A.M., Lopez, A.D., Hao, E., Perez, B., Just, M.L., Lakey, J.R., Hart, M.E., and Hayek, A. (2002). A novel approach to increase human islet cell mass while preserving β-cell function. Diabetes *51*, 3435-3439.
9. Beck, J., Angus, R., Madsen, B., Britt, D., Vernon, B., and Nguyen, K.T. (2007). Islet encapsulation: Strategies to enhance islet cell functions. Tissue Engineering *13*, 589-599.
10. Bellas, E., Lo, T.J., Fournier, E.P., Brown, J.E., Abbott, R.D., Gil, E.S., Marra, K.G., Rubin, J.P., Leisk, G.G., and Kaplan, D.L. (2015). Injectable silk foams for soft tissue regeneration. Advanced Healthcare Materials *4*, 452-459.
11. Bhardwaj, N., Sow, W.T., Devi, D., Ng, K.W., Mandal, B.B., and Cho, N.J. (2014). Silk fibroin–keratin based 3D scaffolds as a dermal substitute for skin tissue engineering. Integrative Biology *7*, 53-63.
12. Blomeier, H., Zhang, X., Rives, C., Brissova, M., Hughes, E., Baker, M., Powers, A.C., Kaufman, D.B., Shea, L.D., and Lowe Jr, W.L. (2006). Polymer scaffolds as

synthetic microenvironments for extrahepatic islet transplantation. Transplantation *82*, 452.

13. Blondet, J.J., Carlson, A.M., Kobayashi, T., Jie, T., Bellin, M., Hering, B.J., Freeman, M.L., Beilman, G.J., and Sutherland, D.E. (2007). The role of total pancreatectomy and islet autotransplantation for chronic pancreatitis. Surgical Clinics *87*, 1477-1501.
14. Boninsegna, S., Bosetti, P., Carturan, G., Dellagiacoma, G., Dal Monte, R., and Rossi, M. (2003). Encapsulation of individual pancreatic islets by sol–gel SiO2: A novel procedure for perspective cellular grafts. Journal of Biotechnology *100*, 277-286.
15. Borg, D.J., and Bonifacio, E. (2011). The use of biomaterials in islet transplantation. Current Diabetes Reports *11*, 434-444.
16. Bosco, D., Meda, P., Halban, P.A., and Rouiller, D.G. (2000). Importance of cell-matrix interactions in rat islet beta-cell secretion *in vitro*: Role of alpha6beta1 integrin. Diabetes *49*, 233-243.
17. Brauker, J., Martinson, L., Loudovaris, T., Hill, R., Carr-Brendel, V., Hodgson, R., Young, S., Mandel, T., Charlton, B., and Johnson, R. (1992). Immuno-isolation with large pore membranes: Allografts are protected under conditions that result in destruction of xenografts. Cell Transplantation *1*, 164.
18. Brendel, M.D., Kong, S.S., Alejandro, R., and Mintz, D.H. (1994). Improved functional survival of human islets of Langerhans in three-dimensional matrix culture. Cell Transplantation *3*, 427-435.
19. Brown, B.N., Londono, R., Tottey, S., Zhang, L., Kukla, K.A., Wolf, M.T., Daly, K.A., Reing, J.E., and Badylak, S.F. (2012). Macrophage phenotype as a predictor of constructive remodeling following the implantation of biologically derived surgical mesh materials. Acta Biomaterialia *8*, 978-987.
20. Brown, B.N., Ratner, B.D., Goodman, S.B., Amar, S., and Badylak, S.F. (2012). Macrophage polarization: An opportunity for improved outcomes in biomaterials and regenerative medicine. Biomaterials *33*, 3792-3802.
21. Burdick, J.A., and Vunjak-Novakovic, G. (2008). Engineered microenvironments for controlled stem cell differentiation. Tissue Engineering Part A *15*, 205-219.
22. Burke, K.A., Roberts, D.C., and Kaplan, D.L. (2015). Silk fibroin aqueous-based adhesives inspired by mussel adhesive proteins. Biomacromolecules *17*, 237-245.
23. Butruk, B., Trzaskowski, M., and Ciach, T. (2012). Fabrication of biocompatible hydrogel coatings for implantable medical devices using Fenton-type reaction. Materials Science and Engineering: C *32*, 1601-1609.

24. Calafiore, R., Basta, G., Luca, G., Lemmi, A., Montanucci, M.P., Calabrese, G., Racanicchi, L., Mancuso, F., and Brunetti, P. (2006a). Microencapsulated pancreatic islet allografts into nonimmunosuppressed patients with type 1 diabetes: First two cases. Diabetes Care *29*, 137-138.
25. Calafiore, R., Basta, G., Luca, G., Lemmi, A., Racanicchi, L., Mancuso, F., Montanucci, M., and Brunetti, P. (2006b). Standard technical procedures for microencapsulation of human islets for graft into nonimmunosuppressed patients with type 1 diabetes mellitus. Paper presented at: Transplantation Proceedings (Elsevier).
26. Cameron, M.J., Arreaza, G.A., Zucker, P., Chensue, S.W., Strieter, R.M., Chakrabarti, S., and Delovitch, T.L. (1997). IL-4 prevents insulitis and insulin-dependent diabetes mellitus in nonobese diabetic mice by potentiation of regulatory T helper-2 cell function. The Journal of Immunology *159*, 4686-4692.
27. Chan, W.K., Cheung, C., Law, H., Lau, Y.L., and Chan, G. (2008). Ganoderma lucidum polysaccharides can induce human monocytic leukemia cells into dendritic cells with immuno-stimulatory function. Journal of Hematology & Oncology *1*.
28. Chang, T.M. (1964). Semipermeable microcapsules. Science *146*, 524-525.
29. Chanput, W., Mes, J.J., Savelkoul, H.F., and Wichers, H.J. (2013). Characterization of polarized THP-1 macrophages and polarizing ability of LPS and food compounds. Food & Function *4*, 266-276.
30. Chawla, A., Nguyen, K.D., and Goh, Y.S. (2011). Macrophage-mediated inflammation in metabolic disease. Nature Reviews Immunology *11*, 738-749.
31. Chick, W.L., Perna, J.J., Lauris, V., Low, D., Galletti, P.M., Panol, G., Whittemore, A.D., Like, A.A., Colton, C.K., and Lysaght, M.J. (1977). Artificial pancreas using living beta cells:. effects on glucose homeostasis in diabetic rats. Science *197*, 780-782.
32. Chouhan, D., Chakraborty, B., Nandi, S.K., and Mandal, B.B. (2017). Role of non-mulberry silk fibroin in deposition and regulation of extracellular matrix towards accelerated wound healing. Acta Biomaterialia *48*, 157-174.
33. Coburn, J.M., Na, E., and Kaplan, D.L. (2015). Modulation of vincristine and doxorubicin binding and release from silk films. Journal of Controlled Release *220*, 229-238.
34. Colton, C.K. (1995). Implantable biohybrid artificial organs. Cell Transplantation *4*, 415-436.

35. Control, D., and Group, C.T.R. (1993). The effect of intensive treatment of diabetes on the development and progression of long-term complications in insulin-dependent diabetes mellitus. New England Journal of Medicine *329*, 977-986.
36. Cushing, M.C., and Anseth, K.S. (2007). Hydrogel cell cultures. Science *316*, 1133-1134.
37. Daigneault, M., Preston, J.A., Marriott, H.M., Whyte, M.K., and Dockrell, D.H. (2010). The identification of markers of macrophage differentiation in PMA-stimulated THP-1 cells and monocyte-derived macrophages. PloS One *5*, e8668.
38. Dal Pra, I., Freddi, G., Minic, J., Chiarini, A., and Armato, U. (2005). De novo engineering of reticular connective tissue *in vivo* by silk fibroin nonwoven materials. Biomaterials *26*, 1987-1999.
39. Daneman, D. (2006). Type 1 diabetes. The Lancet *367*, 847-858.
40. Daoud, J., Petropavlovskaia, M., Rosenberg, L., and Tabrizian, M. (2010). The effect of extracellular matrix components on the preservation of human islet function *in vitro*. Biomaterials *31*, 1676-1682.
41. Daoud, J.T., Petropavlovskaia, M.S., Patapas, J.M., Degrandpré, C.E., DiRaddo, R.W., Rosenberg, L., and Tabrizian, M. (2011). Long-term *in vitro* human pancreatic islet culture using three-dimensional microfabricated scaffolds. Biomaterials *32*, 1536-1542.
42. Davies, L.C., Jenkins, S.J., Allen, J.E., and Taylor, P.R. (2013). Tissue-resident macrophages. Nature Immunology *14*, 986-995.
43. Davis, N.E., Beenken-Rothkopf, L.N., Mirsoian, A., Kojic, N., Kaplan, D.L., Barron, A.E., and Fontaine, M.J. (2012). Enhanced function of pancreatic islets co-encapsulated with ECM proteins and mesenchymal stromal cells in a silk hydrogel. Biomaterials *33*, 6691-6697.
44. De Vos, P., De Haan, B., Wolters, G., Strubbe, J., and Van Schilfgaarde, R. (1997). Improved biocompatibility but limited graft survival after purification of alginate for microencapsulation of pancreatic islets. Diabetologia *40*, 262-270.
45. de Vos, P., de Haan, B.J., Kamps, J.A., Faas, M.M., and Kitano, T. (2007). Zeta-potentials of alginate-PLL capsules: A predictive measure for biocompatibility ? Journal of Biomedical Materials Research Part A *80*, 813-819.
46. de Vos, P., Faas, M.M., Strand, B., and Calafiore, R. (2006). Alginate-based microcapsules for immunoisolation of pancreatic islets. Biomaterials *27*, 5603-5617.

47. Del Toro-Arreola, A., Robles-Murillo, A.K., Daneri-Navarro, A., and Rivas-Carrillo, J.D. (2016). The role of endothelial cells on islet function and revascularization after islet transplantation. Organogenesis *12*, 28-32.
48. Do, S.G., Park, J.H., Nam, H., Kim, J.B., Lee, J.Y., Oh, Y.S., and Suh, J.G. (2012). Silk fibroin hydrolysate exerts an anti-diabetic effect by increasing pancreatic β cell mass in C57BL/KsJ-db/db mice. Journal of Veterinary Science *13*, 339-344.
49. Drury, J.L., and Mooney, D.J. (2003). Hydrogels for tissue engineering: scaffold design variables and applications. Biomaterials *24*, 4337-4351.
50. Dufour, J.M., Rajotte, R.V., Zimmerman, M., Rezania, A., Kin, T., Dixon, D.E., and Korbutt, G.S. (2005). Development of an ectopic site for islet transplantation, using biodegradable scaffolds. Tissue Engineering *11*, 1323-1331.
51. Duvivier-Kali, V.F., Omer, A., Parent, R.J., O'Neil, J.J., and Weir, G.C. (2001). Complete protection of islets against allorejection and autoimmunity by a simple barium-alginate membrane. Diabetes *50*, 1698-1705.
52. Elliott, R.B., Escobar, L., Tan, P.L., Muzina, M., Zwain, S., and Buchanan, C. (2007). Live encapsulated porcine islets from a type 1 diabetic patient 9.5 yr after xenotransplantation. Xenotransplantation *14*, 157-161.
53. Faradji, R.N., Tharavanij, T., Messinger, S., Froud, T., Pileggi, A., Monroy, K., Mineo, D., Baidal, D.A., Cure, P., and Ponte, G. (2008). Long term insulin independence and improvement in insulin secretion after supplemental islet infusion under exenatide and étanercept. Transplantation *86*, 1658.
54. Floren, M.L., Spilimbergo, S., Motta, A., and Migliaresi, C. (2012). Carbon dioxide induced silk protein gelation for biomedical applications. Biomacromolecules *13*, 2060-2072.
55. Foster, G.A., and García, A.J. (2017). Bio-synthetic materials for immunomodulation of islet transplants. Advanced Drug Delivery Reviews *114*, 266-271.
56. Fotino, N., Fotino, C., and Pileggi, A. (2015). Re-engineering islet cell transplantation. Pharmacological Research *98*, 76-85.
57. Frank, A., Deng, S., Huang, X., Velidedeoglu, E., Bae, Y.-S., Liu, C., Abt, P., Stephenson, R., Mohiuddin, M., and Thambipillai, T. (2004). Transplantation for type I diabetes: comparison of vascularized whole-organ pancreas with isolated pancreatic islets. Annals of Surgery *240*, 631-640.

58. Franz, S., Rammelt, S., Scharnweber, D., and Simon, J.C. (2011). Immune responses to implants – A review of the implications for the design of immunomodulatory biomaterials. Biomaterials *32*, 6692-6709.
59. Gazda, L.S., Vinerean, H.V., Laramore, M.A., Diehl, C.H., Hall, R.D., Rubin, A.L., and Smith, B.H. (2007). Encapsulation of porcine islets permits extended culture time and insulin independence in spontaneously diabetic BB rats. Cell Transplantation *16*, 609-620.
60. George, L., Upadhyay, S., Ganguly, K., and Stoeger, T. (2014). Macrophage polarization in lung biology and diseases. In Lung Inflammation (InTech).
61. Giesa, T., Arslan, M., Pugno, N.M., and Buehler, M.J. (2011). Nanoconfinement of spider silk fibrils begets superior strength, extensibility, and toughness. Nano Letters *11*, 5038-5046.
62. Go, A.S., Mozaffarian, D., Roger, V.L., Benjamin, E.J., Berry, J.D., Blaha, M.J., Dai, S., Ford, E.S., Fox, C.S., and Franco, S. (2014). Heart disease and stroke statistics—2014 update: a report from the American Heart Association. Circulation *129*, e28-e292.
63. Gordon, S., and Taylor, P.R. (2005). Monocyte and macrophage heterogeneity. Nature Reviews Immunology *5*, 953-964.
64. Gupta, A., Mita, K., Arunkumar, K.P., and Nagaraju, J. (2015). Molecular architecture of silk fibroin of Indian golden silkmoth, Antheraea assama. Scientific Reports *5*.
65. Gupta, P., Adhikary, M., Kumar, M., Bhardwaj, N., and Mandal, B.B. (2016a). Biomimetic, osteoconductive non-mulberry silk fiber reinforced tricomposite scaffolds for bone tissue engineering. ACS Applied Materials & Interfaces *8*, 30797-30810.
66. Gupta, P., Kumar, M., Bhardwaj, N., Kumar, J.P., Krishnamurthy, C., Nandi, S.K., and Mandal, B.B. (2016b). Mimicking form and function of native small diameter vascular conduits using mulberry and non-mulberry patterned silk films. ACS Applied Materials & Interfaces *8*, 15874-15888.
67. Gupta, V., Mun, G.H., Choi, B., Aseh, A., Mildred, L., Patel, A., Zhang, Q., Price, J.E., Chang, D., and Robb, G. (2011). Repair and reconstruction of a resected tumor defect using a composite of tissue flap–nanotherapeutic–silk fibroin and chitosan scaffold. Annals of Biomedical Engineering *39*, 2374-2387.

68. Guziewicz, N., Best, A., Perez-Ramirez, B., and Kaplan, D.L. (2011). Lyophilized silk fibroin hydrogels for the sustained local delivery of therapeutic monoclonal antibodies. Biomaterials *32*, 2642-2650.
69. Hamilton, D.C., Shih, H.H., Schubert, R.A., Michie, S.A., Staats, P.N., Kaplan, D.L., and Fontaine, M.J. (2017). A silk-based encapsulation platform for pancreatic islet transplantation improves islet function *in vivo*. Journal of Tissue Engineering and Regenerative Medicine *11*, 887-895.
70. Hansson, G.K., and Libby, P. (2006). The immune response in atherosclerosis: A double-edged sword. Nature Reviews Immunology *6*, 508-519.
71. Hatziavramidis, D.T., Karatzas, T.M., and Chrousos, G.P. (2013). Pancreatic islet cell transplantation: an update. Annals of Biomedical Engineering *41*, 469-476.
72. Heard, A.J., Socrate, S., Burke, K.A., Norwitz, E.R., Kaplan, D.L., and House, M.D. (2013). Silk-based injectable biomaterial as an alternative to cervical cerclage an *in vitro* study. Reproductive Sciences *20*, 929-936.
73. Hedhammar, M., Rising, A., Grip, S., Martinez, A.S., Nordling, K., Casals, C., Stark, M., and Johansson, J. (2008). Structural properties of recombinant nonrepetitive and repetitive parts of major ampullate spidroin 1 from Euprosthenops australis: Implications for fiber formation. Biochemistry *47*, 3407-3417.
74. Heinemann, L., and Krinelke, L. (2012). Insulin infusion set: The Achilles heel of continuous subcutaneous insulin infusion. Journal of Diabetes Science and Technology *6*, 954-964.
75. Hill, R.S., Cruise, G.M., Hager, S.R., Lamberti, F.V., Yu, X., Garufis, C.L., Yu, Y., Mundwiler, K.E., Cole, J.F., and Hubbell, J.A. (1997). Immunoisolation of adult porcine islets for the treatment of diabetes mellitus. Annals of the New York Academy of Sciences *831*, 332-343.
76. Hirose, N., Maeda, H., Yamamoto, M., Hayashi, Y., Lee, G.-H., Chen, L., Radhakrishnan, G., Rao, P., and Sasaguri, S. (2008). The local injection of peritoneal macrophages induces neovascularization in rat ischemic hind limb muscles. Cell Transplantation *17*, 211-222.
77. Hirshberg, B., Rother, K.I., Digon, B.J., Lee, J., Gaglia, J.L., Hines, K., Read, E.J., Chang, R., Wood, B.J., and Harlan, D.M. (2003). Benefits and risks of solitary islet transplantation for type 1 diabetes using steroid-sparing immunosuppression: The National Institutes of Health experience. Diabetes Care *26*, 3288-3295.

78. Hiscox, A.M., Stone, A.L., Limesand, S., Hoying, J.B., and Williams, S.K. (2008). An islet-stabilizing implant constructed using a preformed vasculature. Tissue Engineering Part A *14*, 433-440.
79. Horan, R., Bramono, D., Stanley, J., Simmons, Q., Chen, J., Boepple, H., and Altman, G. (2009). Biological and biomechanical assessment of a long-term bioresorbable silk-derived surgical mesh in an abdominal body wall defect model. Hernia *13*, 189-199.
80. Horan, R.L., Antle, K., Collette, A.L., Wang, Y., Huang, J., Moreau, J.E., Volloch, V., Kaplan, D.L., and Altman, G.H. (2005). *In vitro* degradation of silk fibroin. Biomaterials *26*, 3385-3393.
81. Huber, S., Sakkinen, P., David, C., Newell, M., and Tracy, R. (2001). T helper–cell phenotype regulates atherosclerosis in mice under conditions of mild hypercholesterolemia. Circulation *103*, 2610-2616.
82. Ilieva, A., Yuan, S., Wang, R., Agapitos, D., Hill, D., and Rosenberg, L. (1999). Pancreatic islet cell survival following islet isolation: The role of cellular interactions in the pancreas. Journal of Endocrinology *161*, 357-364.
83. Inoo, K., Bando, H., and Tabata, Y. (2018). Insulin secretion of mixed insulinoma aggregates-gelatin hydrogel microspheres after subcutaneous transplantation. Regenerative Therapy *8*, 38-45.
84. Italiani, P., and Boraschi, D. (2014). From monocytes to M1/M2 macrophages: Phenotypical vs. functional differentiation. Frontiers in Immunology *5*, 514.
85. Iwata, H., Kobayashi, K., Takagi, T., Oka, T., Yang, H., Amemiya, H., Tsuji, T., and Ito, F. (1994). Feasibility of agarose microbeads with xenogeneic islets as a bioartificial pancreas. Journal of Biomedical Materials Research Part A *28*, 1003-1011.
86. Iwata, H., Takagi, T., Amemiya, H., Shimizu, H., Yamashita, K., Kobayashi, K., and Akutsu, T. (1992). Agarose for a bioartificial pancreas. Journal of Biomedical Materials Research *26*, 967-977.
87. Janani, G., Nandi, S.K., and Mandal, B.B. (2017). Functional hepatocyte clusters on bioactive blend silk matrices towards generating bioartificial liver constructs. Acta Biomaterialia *67*, 167-182.
88. Jiang, K., Weaver, J.D., Li, Y., Chen, X., Liang, J., and Stabler, C.L. (2017). Local release of dexamethasone from macroporous scaffolds accelerates islet transplant

engraftment by promotion of anti-inflammatory M2 macrophages. Biomaterials *114*, 71-81.

89. Johansson, U., Ria, M., Åvall, K., Shalaly, N.D., Zaitsev, S.V., and Berggren, P.O. (2015). Pancreatic islet survival and engraftment is promoted by culture on functionalized spider silk matrices. PLoS One *10*, e0130169.
90. Kapoor, S., and Kundu, S.C. (2016). Silk protein-based hydrogels: Promising advanced materials for biomedical applications. Acta Biomaterialia *31*, 17-32.
91. Karlsson-Parra, A., Ridderstad, A., Wallgren, A., Möller, E., Ljunggren, H., and Korsgren, O. (1996). Xenograft rejection of porcine islet-like cell clusters in normal and natural killer cell-depleted mice1. Transplantation *61*, 1313-1320.
92. Kasoju, N., and Bora, U. (2012). Silk fibroin in tissue engineering. Advanced Healthcare Materials *1*, 393-412.
93. Katayama, H., Issiki, M., and Yoshitomi, H. (2000). Application of fibroin in controlled release tablets containing theophylline. Biological and Pharmaceutical Bulletin *23*, 1229-1234.
94. Kelly, W., Lillehei, R., Merkel, F., Idezuki, Y., and Goetz, F. (1967). Allotransplantation of the pancreas and duodenum along with the kidney in diabetic nephropathy. Surgery *61*, 827-837.
95. Khademhosseini, A., Vacanti, J.P., and Langer, R. (2009). Progress in tissue engineering. Scientific American *300*, 64-71.
96. Khallou-Laschet, J., Varthaman, A., Fornasa, G., Compain, C., Gaston, A.T., Clement, M., Dussiot, M., Levillain, O., Graff-Dubois, S., and Nicoletti, A. (2010). Macrophage plasticity in experimental atherosclerosis. PloS One *5*, e8852.
97. Kheradmand, T., Wang, S., Gibly, R.F., Zhang, X., Holland, S., Tasch, J., Graham, J.G., Kaufman, D.B., Miller, S.D., and Shea, L.D. (2011). Permanent protection of PLG scaffold transplanted allogeneic islet grafts in diabetic mice treated with ECDI-fixed donor splenocyte infusions. Biomaterials *32*, 4517-4524.
98. Khor, E., and Lim, L.Y. (2003). Implantable applications of chitin and chitosan. Biomaterials *24*, 2339-2349.
99. Kim, U.J., Park, J., Kim, H.J., Wada, M., and Kaplan, D.L. (2005). Three-dimensional aqueous-derived biomaterial scaffolds from silk fibroin. Biomaterials *26*, 2775-2785.
100. Kin, T., Iwata, H., Aomatsu, Y., Ohyama, T., Kanehiro, H., Hisanaga, M., and Nakajima, Y. (2002). Xenotransplantation of pig islets in diabetic dogs with use of a

microcapsule composed of agarose and polystyrene sulfonic acid mixed gel. Pancreas *25*, 94-100.

101. Koh, J., Ko, K., Lee, M., Han, S., Park, J., and Kim, S. (2000). Degradable polymeric carrier for the delivery of IL-10 plasmid DNA to prevent autoimmune insulitis of NOD mice. Gene Therapy *7*, 2099-2104.
102. Konwarh, R., Bhunia, B.K., and Mandal, B.B. (2017). Opportunities and challenges in exploring indian non-mulberry silk for biomedical applications. Paper presented at: Proceedings of the Indian National Science Acadamy *83*, 85-101
103. Kort, H.D., Koning, E.J.D., Rabelink, T.J., Bruijn, J.A., and Bajema, I.M. (2011). Islet transplantation in type 1 diabetes. BMJ *342*.
104. Kumar, M., Coburn, J., Kaplan, D.L., and Mandal, B.B. (2016a). Immuno-informed 3D silk biomaterials for tailoring biological responses. ACS Applied Materials & Interfaces *8*, 29310-29322.
105. Kumar, M., Jain, D., Bhardwaj, N., Gupta, P., Nandi, S.K., and Mandal, B.B. (2016b). Native honeybee silk membrane: A potential matrix for tissue engineering and regenerative medicine. RSC Advances *6*, 54394-54403.
106. Kumar, M., Nandi, S.K., Kaplan, D.L., and Mandal, B.B. (2017). Localized immunomodulatory silk macrocapsules for islet-like spheroid formation and sustained insulin production. ACS Biomaterials Science & Engineering *3*, 2443-2456.
107. Kumar, V.A., Taylor, N.L., Shi, S., Wickremasinghe, N.C., D'Souza, R.N., and Hartgerink, J.D. (2015). Self-assembling multidomain peptides tailor biological responses through biphasic release. Biomaterials *52*, 71-78.
108. Kundu, B., Rajkhowa, R., Kundu, S.C., and Wang, X. (2013). Silk fibroin biomaterials for tissue regenerations. Advanced Drug Delivery Reviews *65*, 457-470.
109. Kundu, S., Kundu, B., Talukdar, S., Bano, S., Nayak, S., Kundu, J., Mandal, B.B., Bhardwaj, N., Botlagunta, M., and Dash, B.C. (2012). Nonmulberry silk biopolymers. Biopolymers *97*, 455-467.
110. Kurosaki, S., Otsuka, H., Kunitomo, M., Koyama, M., Pawankar, R., and Matumoto, K. (1999). Fibroin allergy IgE mediated hypersensitivity to silk suture materials. Journal of Nippon Medical School *66*, 41-44.
111. Kuss, M., Adamopoulou, E., and Kahle, P.J. (2014). Interferon-γ induces leucine-rich repeat kinase LRRK2 via extracellular signal-regulated kinase ERK5 in macrophages. Journal of Neurochemistry *129*, 980-987.

112. Lacy, P.E., Hegre, O.D., Gerasimidi-Vazeou, A., Gentile, F.T., and Dionne, K.E. (1991). Maintenance of normoglycemia in diabetic mice by subcutaneous xenografts of encapsulated islets. Science *254*, 1782-1784.
113. Lee, B.R., Hwang, J.W., Choi, Y.Y., Wong, S.F., Hwang, Y.H., Lee, D.Y., and Lee, S.H. (2012). In situ formation and collagen-alginate composite encapsulation of pancreatic islet spheroids. Biomaterials *33*, 837-845.
114. Lee, D.Y., Nam, J.H., and Byun, Y. (2004). Effect of polyethylene glycol grafted onto islet capsules on prevention of splenocyte and cytokine attacks. Journal of Biomaterials Science, Polymer Edition *15*, 753-766.
115. Lee, M., Koh, J.J., Han, S.O., Ko, K.S., and Kim, S.W. (2002). Prevention of autoimmune insulitis by delivery of interleukin-4 plasmid using a soluble and biodegradable polymeric carrier. Pharmaceutical Research *19*, 246-249.
116. Lee, S. H., Hao, E., Savinov, A.Y., Geron, I., Strongin, A.Y., and Itkin-Ansari, P. (2009). Human β-cell precursors mature into functional insulin-producing cells in an immunoisolation device: Implications for diabetes cell therapies. Transplantation *87*, 983-991.
117. Li, C., Levin, M., and Kaplan, D.L. (2016). Bioelectric modulation of macrophage polarization. Scientific Reports *6*.
118. Li, D. S., Yuan, Y. H., Tu, H. J., Liang, Q. L., and Dai, L. J. (2009). A protocol for islet isolation from mouse pancreas. Nature Protocols *4*, 1649-1652.
119. Li, X., Zhang, J., Feng, Y., Yan, S., Zhang, Q., and You, R. (2018). Tuning the structure and performance of silk biomaterials by combining mulberry and non-mulberry silk fibroin. Polymer Degradation and Stability *147*, 57-63.
120. Liao, S.W., Rawson, J., Omori, K., Ishiyama, K., Mozhdehi, D., Oancea, A.R., Ito, T., Guan, Z., and Mullen, Y. (2013). Maintaining functional islets through encapsulation in an injectable saccharide–peptide hydrogel. Biomaterials *34*, 3984-3991.
121. Lim, F., and Sun, A.M. (1980). Microencapsulated islets as bioartificial endocrine pancreas. Science *210*, 908-910.
122. Lin, C. C., and Anseth, K.S. (2009). Glucagon-like peptide-1 functionalized PEG hydrogels promote survival and function of encapsulated pancreatic β-cells. Biomacromolecules *10*, 2460-2467.
123. Lin, C. C., Metters, A.T., and Anseth, K.S. (2009). Functional PEG–peptide hydrogels to modulate local inflammation inducedby the pro-inflammatory cytokine TNFα. Biomaterials *30*, 4907-4914.

124. Liu, H., Wu, X., Wang, S., Deng, W., Zan, L., and Yu, S. (2013). *In vitro* repolarized tumor macrophages inhibit gastric tumor growth. Oncology Research Featuring Preclinical and Clinical Cancer Therapeutics *20*, 275-280.
125. Liu, J.M., Zhang, J., Zhang, X., Hlavaty, K.A., Ricci, C.F., Leonard, J.N., Shea, L.D., and Gower, R.M. (2016). Transforming growth factor-beta 1 delivery from microporous scaffolds decreases inflammation post-implant and enhances function of transplanted islets. Biomaterials *80*, 11-19.
126. Livak, K.J., and Schmittgen, T.D. (2001). Analysis of relative gene expression data using real-time quantitative PCR and the $2^{-\Delta\Delta C}{}_T$ method. Methods *25*, 402-408.
127. Lovett, M.L., Wang, X., Yucel, T., York, L., Keirstead, M., Haggerty, L., and Kaplan, D.L. (2015). Silk hydrogels for sustained ocular delivery of anti-vascular endothelial growth factor (anti-VEGF) therapeutics. European Journal of Pharmaceutics and Biopharmaceutics *95*, 271-278.
128. Luan, N.M., Teramura, Y., and Iwata, H. (2010). Immobilization of the soluble domain of human complement receptor 1 on agarose-encapsulated islets for the prevention of complement activation. Biomaterials *31*, 8847-8853.
129. Maess, M.B., Sendelbach, S., and Lorkowski, S. (2010). Selection of reliable reference genes during THP-1 monocyte differentiation into macrophages. BMC Molecular Biology *11*, 1.
130. Mandal, B.B., and Kundu, S. (2008). A novel method for dissolution and stabilization of non-mulberry silk gland protein fibroin using anionic surfactant sodium dodecyl sulfate. Biotechnology and Bioengineering *99*, 1482-1489.
131. Mandal, B.B., and Kundu, S.C. (2009). Calcium alginate beads embedded in silk fibroin as 3D dual drug releasing scaffolds. Biomaterials *30*, 5170-5177.
132. Mandal, B.B., and Kundu, S.C. (2009). Osteogenic and adipogenic differentiation of rat bone marrow cells on non-mulberry and mulberry silk gland fibroin 3D scaffolds. Biomaterials *30*, 5019-5030.
133. Mandal, B.B., Das, S., Choudhury, K., and Kundu, S.C. (2010). Implication of silk film RGD availability and surface roughness on cytoskeletal organization and proliferation of primary rat bone marrow cells. Tissue Engineering Part A *16*, 2391-2403.
134. Mandal, B.B., Kapoor, S., and Kundu, S.C. (2009). Silk fibroin/polyacrylamide semi-interpenetrating network hydrogels for controlled drug release. Biomaterials *30*, 2826-2836.

135. Mantovani, A., Sica, A., Sozzani, S., Allavena, P., Vecchi, A., and Locati, M. (2004). The chemokine system in diverse forms of macrophage activation and polarization. Trends in Immunology *25*, 677-686.
136. Mao, D., Zhu, M., Zhang, X., Ma, R., Yang, X., Ke, T., Wang, L., Li, Z., Kong, D., and Li, C. (2017). A macroporous heparin-releasing silk fibroin scaffold improves islet transplantation outcome by promoting islet revascularisation and survival. Acta Biomaterialia *59*, 210-220.
137. Martinez, F.O., Gordon, S., Locati, M., and Mantovani, A. (2006). Transcriptional profiling of the human monocyte-to-macrophage differentiation and polarization: New molecules and patterns of gene expression. The Journal of Immunology *177*, 7303-7311.
138. Martinsen, A., Skjåk-Bræk, G., and Smidsrød, O. (1989). Alginate as immobilization material: I. Correlation between chemical and physical properties of alginate gel beads. Biotechnology and Bioengineering *33*, 79-89.
139. Mathis, D., Vence, L., and Benoist, C. (2001). β-Cell death during progression to diabetes. Nature *414*, 792-798.
140. Matsumoto, A., Chen, J., Collette, A.L., Kim, U.J., Altman, G.H., Cebe, P., and Kaplan, D.L. (2006). Mechanisms of silk fibroin sol− gel transitions. The Journal of Physical Chemistry B *110*, 21630-21638.
141. McDaniel, M.L., Kwon, G., Hill, J.R., Marshall, C.A., and Corbett, J.A. (1996). Cytokines and nitric oxide in islet inflammation and diabetes. Experimental Biology and Medicine *211*, 24-32.
142. McDaniel, M.L., Kwon, G., Hill, J.R., Marshall, C.A., and Corbett, J.A. (1996). Cytokines and nitric oxide in islet inflammation and diabetes. Experimental Biology and Medicine *211*, 24-32.
143. Mehrotra, S., Nandi, S.K., and Mandal, B.B. (2017). Stacked silk-cell monolayers as a biomimetic three dimensional construct for cardiac tissue reconstruction. Journal of Materials Chemistry B *5*, 6325-6338.
144. Meinel, L., Hofmann, S., Karageorgiou, V., Kirker-Head, C., McCool, J., Gronowicz, G., Zichner, L., Langer, R., Vunjak-Novakovic, G., and Kaplan, D.L. (2005). The inflammatory responses to silk films *in vitro* and *in vivo*. Biomaterials *26*, 147-155.
145. Miles, E.J., Dunn, E., Howard, D., and Mangram, A. (2004). The role of laparoscopy in penetrating abdominal trauma. JSLS: Journal of the Society of Laparoendoscopic Surgeons *8*, 304-309.

146. Miller, R.G., Mahajan, H.D., Costacou, T., Sekikawa, A., Anderson, S.J., and Orchard, T.J. (2016). A contemporary estimate of total mortality and cardiovascular disease risk in young adults with type 1 diabetes: the Pittsburgh Epidemiology of Diabetes Complications Study. Diabetes Care *39*, 2296-2303.
147. Minardi, S., Corradetti, B., Taraballi, F., Byun, J.H., Cabrera, F., Liu, X., Ferrari, M., Weiner, B.K., and Tasciotti, E. (2016). IL-4 release from a biomimetic scaffold for the temporally controlled modulation of macrophage response. Annals of Biomedical Engineering, *44*, 2008-2019.
148. Modulevsky, D.J., Cuerrier, C.M., and Pelling, A.E. (2016). Biocompatibility of subcutaneously implanted plant-derived cellulose biomaterials. PloS One *11*, e0157894.
149. Mokarram, N., Merchant, A., Mukhatyar, V., Patel, G., and Bellamkonda, R.V. (2012). Effect of modulating macrophage phenotype on peripheral nerve repair. Biomaterials *33*, 8793-8801.
150. Muthyala, S., Raj, V.R., Mohanty, M., Mohanan, P., and Nair, P.D. (2011). The reversal of diabetes in rat model using mouse insulin producing cells – A combination approach of tissue engineering and macroencapsulation. Acta Biomaterialia *7*, 2153-2162.
151. Nafea, E., Marson, A., Poole-Warren, L., and Martens, P. (2011). Immunoisolating semi-permeable membranes for cell encapsulation: focus on hydrogels. Journal of Controlled Release *154*, 110-122.
152. Nair, L.S., and Laurencin, C.T. (2007). Biodegradable polymers as biomaterials. Progress in Polymer Ccience *32*, 762-798.
153. Narang, A.S., and Mahato, R.I. (2006). Biological and biomaterial approaches for improved islet transplantation. Pharmacological Reviews *58*, 194-243.
154. Niknamasl, A., Ostad, S.N., Soleimani, M., Azami, M., Salmani, M.K., Lotfibakhshaiesh, N., Ebrahimi-Barough, S., Karimi, R., Roozafzoon, R., and Ai, J. (2014). A new approach for pancreatic tissue engineering: human endometrial stem cells encapsulated in fibrin gel can differentiate to pancreatic islet beta-cell. Cell Biology International *38*, 1174-1182.
155. Nikolova, G., Jabs, N., Konstantinova, I., Domogatskaya, A., Tryggvason, K., Sorokin, L., Fässler, R., Gu, G., Gerber, H.-P., and Ferrara, N. (2006). The vascular basement membrane: A niche for insulin gene expression and β cell proliferation. Developmental Cell *10*, 397-405.

156. Nilebäck, L., Chouhan, D., Jansson, R., Widhe, M., Mandal, B.B., and Hedhammar, M. (2017). Silk–silk interactions between silkworm fibroin and recombinant spider silk fusion proteins enable the construction of bioactive materials. ACS Applied Materials & Interfaces *9*, 31634-31644.
157. Nitta, Y., Tashiro, F., Tokui, M., Shimada, A., Takei, I., Tabayashi, K., and Miyazaki, J.I. (1998). Systemic delivery of interleukin 10 by intramuscular injection of expression plasmid DNA prevents autoimmune diabetes in nonobese diabetic mice. Human Gene Therapy *9*, 1701-1707.
158. Noy, R., and Pollard, J.W. (2014). Tumor-associated macrophages: From mechanisms to therapy. Immunity *41*, 49-61.
159. Numata, K., Katashima, T., and Sakai, T. (2011). State of water, molecular structure, and cytotoxicity of silk hydrogels. Biomacromolecules *12*, 2137-2144.
160. Odegaard, J.I., and Chawla, A. (2013). Pleiotropic actions of insulin resistance and inflammation in metabolic homeostasis. Science *339*, 172-177.
161. Opara, E.C., Mirmalek-Sani, S. H., Khanna, O., Moya, M.L., and Brey, E.M. (2010). Design of a bioartificial pancreas. Journal of Investigative Medicine *58*, 831-837.
162. O'sullivan, E.S., Vegas, A., Anderson, D.G., and Weir, G.C. (2011). Islets transplanted in immunoisolation devices: a review of the progress and the challenges that remain. Endocrine Reviews *32*, 827-844.
163. Panousis, C.G., and Zuckerman, S.H. (2000). Regulation of cholesterol distribution in macrophage-derived foam cells by interferon-γ. Journal of Lipid Research *41*, 75-83.
164. Pareta, R., McQuilling, J.P., Farney, A.C., and Opara, E.C. (2012). Bioartificial pancreas: Evaluation of crucial barriers to clinical application. In Organ Donation and Transplantation-Public Policy and Clinical Perspectives (InTech).
165. Pareta, R.A., Farney, A.C., and Opara, E.C. (2013). Design of a bioartificial pancreas. Pathobiology *80*, 194-202.
166. Park, J., and Lakes, R.S. (2007). Biomaterials: An introduction (Springer Science & Business Media).
167. Partlow, B.P., Hanna, C.W., Rnjak-Kovacina, J., Moreau, J.E., Applegate, M.B., Burke, K.A., Marelli, B., Mitropoulos, A.N., Omenetto, F.G., and Kaplan, D.L. (2014). Highly tunable elastomeric silk biomaterials. Advanced Functional Materials *24*, 4615-4624.
168. Pathak, T.S., Yun, J. H., Lee, J., and Paeng, K. J. (2010). Effect of calcium ion (cross-linker) concentration on porosity, surface morphology and thermal behavior of

calcium alginates prepared from algae (Undaria pinnatifida). Carbohydrate Polymers *81*, 633-639.

169. Patte, C., Pleus, S., Wiegel, C., Schiltges, G., Jendrike, N., Haug, C., and Freckmann, G. (2013). Effect of infusion rate and indwelling time on tissue resistance pressure in small-volume subcutaneous infusion like in continuous subcutaneous insulin infusion. Diabetes Technology & Therapeutics *15*, 289-294.
170. Piemonti, L., Leone, B.E., Nano, R., Saccani, A., Monti, P., Maffi, P., Bianchi, G., Sica, A., Peri, G., and Melzi, R. (2002). Human pancreatic islets produce and secrete MCP-1/CCL2: Relevance in human islet transplantation. Diabetes *51*, 55-65.
171. Pritchard, E.M., Valentin, T., Panilaitis, B., Omenetto, F., and Kaplan, D.L. (2013). Antibiotic-releasing silk biomaterials for infection prevention and treatment. Advanced Functional Materials *23*, 854-861.
172. Qi, M., Gu, Y., Sakata, N., Kim, D., Shirouzu, Y., Yamamoto, C., Hiura, A., Sumi, S., and Inoue, K. (2004). PVA hydrogel sheet macroencapsulation for the bioartificial pancreas. Biomaterials *25*, 5885-5892.
173. Qi, Z., Shen, Y., Yanai, G., Yang, K., Shirouzu, Y., Hiura, A., and Sumi, S. (2010). The *in vivo* performance of polyvinyl alcohol macro-encapsulated islets. Biomaterials *31*, 4026-4031.
174. Rabanel, J.M., Banquy, X., Zouaoui, H., Mokhtar, M., and Hildgen, P. (2009). Progress technology in microencapsulation methods for cell therapy. Biotechnology Progress *25*, 946-963.
175. Reardon, P.J., Konwarh, R., Knowles, J.C., and Mandal, B.B. (2017). Mimicking hierarchical complexity of the osteochondral interface using electrospun silk–bioactive glass composites. ACS Applied Materials & Interfaces *9*, 8000-8013.
176. Reeves, A.R., Spiller, K.L., Freytes, D.O., Vunjak-Novakovic, G., and Kaplan, D.L. (2015). Controlled release of cytokines using silk-biomaterials for macrophage polarization. Biomaterials *73*, 272-283.
177. Riopel, M., and Wang, R. (2014). Collagen matrix support of pancreatic islet survival and function. Frontiers in Biosciences *19*, 77-90.
178. Robertson, R.P. (2000). Successful islet transplantation for patients with diabetes - Fact or fantasy? New England Journal of Medicine *343*, 289-290.
179. Rockwood, D.N., Preda, R.C., Yücel, T., Wang, X., Lovett, M.L., and Kaplan, D.L. (2011). Materials fabrication from *Bombyx mori* silk fibroin. Nature Protocols *6*, 1612-1631.

180. Rodriguez-Mulero, S., and Montanya, E. (2005). Selection of a suitable internal control gene for expression studies in pancreatic islet grafts. Transplantation *80*, 650-652.
181. Roh, J.D., Sawh-Martinez, R., Brennan, M.P., Jay, S.M., Devine, L., Rao, D.A., Yi, T., Mirensky, T.L., Nalbandian, A., and Udelsman, B. (2010). Tissue-engineered vascular grafts transform into mature blood vessels via an inflammation-mediated process of vascular remodeling. Proceedings of the National Academy of Sciences *107*, 4669-4674.
182. Rosenberg, L., Wang, R., Paraskevas, S., and Maysinger, D. (1999). Structural and functional changes resulting from islet isolation lead to islet cell death. Surgery *126*, 393-398.
183. Rothman, S., Tseng, H., and Goldfine, I. (2005). Oral gene therapy: A novel method for the manufacture and delivery of protein drugs. Diabetes Technology & Therapeutics *7*, 549-557.
184. Safley, S.A., Cui, H., Cauffiel, S., Tucker-Burden, C., and Weber, C.J. (2008). Biocompatibility and immune acceptance of adult porcine islets transplanted intraperitoneally in diabetic NOD mice in calcium alginate poly-L-lysine microcapsules versus barium alginate microcapsules without poly-L-lysine. Journal of Diabetes Science & Technology *2*, 760-767.
185. Salvay, D.M., Rives, C.B., Zhang, X., Chen, F., Kaufman, D.B., Lowe Jr, W.L., and Shea, L.D. (2008). Extracellular matrix protein-coated scaffolds promote the reversal of diabetes after extrahepatic islet transplantation. Transplantation *85*, 1456-1464.
186. Salvay, D.M., Rives, C.B., Zhang, X., Chen, F., Kaufman, D.B., Lowe Jr, W.L., Shea, Sanberg, P.R., Park, D.H., Kuzmin-Nichols, N., Cruz, E., Hossne Jr, N.A., Buffolo, E., and Willing, A.E. (2010). Monocyte transplantation for neural and cardiovascular ischemia repair. Journal of Cellular and Molecular Medicine *14*, 553-563.
187. Saudek, F., Karasová, L., Kobylka, P., and Lomsků, R. (1999). Increased glucagon-stimulated insulin secretion of cryopreserved rat islets transplanted into nude mice. Journal of Molecular Medicine *77*, 107-110.
188. Seib, F.P., Pritchard, E.M., and Kaplan, D.L. (2013). Self-assembling doxorubicin silk hydrogels for the focal treatment of primary breast cancer. Advanced Functional Materials *23*, 58-65.
189. Seliktar, D. (2012). Designing cell-compatible hydrogels for biomedical applications. Science *336*, 1124-1128.

190. Serban, M.A., Panilaitis, B., and Kaplan, D.L. (2011). Silk fibroin and polyethylene glycol-based biocompatible tissue adhesives. Journal of Biomedical Materials Research Part A *98*, 567-575.
191. Shalaly, N.D., Ria, M., Johansson, U., Åvall, K., and Berggren, P.O. (2016). Silk matrices promote formation of insulin-secreting islet-like clusters. Biomaterials *90*, 50-61.
192. Shao, Z., and Vollrath, F. (2002). Materials: Surprising strength of silkworm silk. Nature *418*, 741-741.
193. Shapiro, A.J., Lakey, J.R., Ryan, E.A., Korbutt, G.S., Toth, E., Warnock, G.L., Kneteman, N.M., and Rajotte, R.V. (2000). Islet transplantation in seven patients with type 1 diabetes mellitus using a glucocorticoid-free immunosuppressive regimen. New England Journal of Medicine *343*, 230-238.
194. Singh, S.K., Bhunia, B.K., Bhardwaj, N., Gilotra, S., and Mandal, B.B. (2016a). Reloadable silk-hydrogel hybrid scaffolds for sustained and targeted delivery of molecules. Molecular Pharmaceutics *13*, 4066-4081.
195. Singh, Y.P., Bhardwaj, N., and Mandal, B.B. (2016b). Potential of agarose/silk fibroin blended hydrogel for *in vitro* cartilage tissue engineering. ACS Applied Materials & Interfaces *8*, 21236-21249.
196. Soffer, L., Wang, X., Zhang, X., Kluge, J., Dorfmann, L., Kaplan, D.L., and Leisk, G. (2008). Silk-based electrospun tubular scaffolds for tissue-engineered vascular grafts. Journal of Biomaterials Science, Polymer Edition *19*, 653-664.
197. Soon-Shiong, P., Feldman, E., Nelson, R., Heintz, R., Yao, Q., Yao, Z., Zheng, T., Merideth, N., Skjak-Braek, G., and Espevik, T. (1993). Long-term reversal of diabetes by the injection of immunoprotected islets. Proceedings of the National Academy of Sciences *90*, 5843-5847.
198. Soon-Shiong, P., Heintz, R.E., Merideth, N., Yao, Q.X., Yao, Z., Zheng, T., Murphy, M., Moloney, M.K., Schmehl, M., and Harris, M. (1994). Insulin independence in a type 1 diabetic patient after encapsulated islet transplantation. The Lancet *343*, 950-951.
199. Spiller, K.L., Nassiri, S., Witherel, C.E., Anfang, R.R., Ng, J., Nakazawa, K.R., Yu, T., and Vunjak-Novakovic, G. (2015). Sequential delivery of immunomodulatory cytokines to facilitate the M1-to-M2 transition of macrophages and enhance vascularization of bone scaffolds. Biomaterials *37*, 194-207.

200. Sridharan, R., Cameron, A.R., Kelly, D.J., Kearney, C.J., and O'Brien, F.J. (2015). Biomaterial based modulation of macrophage polarization: A review and suggested design principles. Materials Today *18*, 313-325.
201. Stendahl, J.C., Kaufman, D.B., and Stupp, S.I. (2009). Extracellular matrix in pancreatic islets: relevance to scaffold design and transplantation. Cell Transplantation *18*, 1-12.
202. Strand, B.L., Ryan, L., Veld, P.I.t., Kulseng, B., Rokstad, A.M., Skjak-Brek, G., and Espevik, T. (2001). Poly-L-lysine induces fibrosis on alginate microcapsules via the induction of cytokines. Cell Transplantation *10*, 263-275.
203. Su, J., Hu, B.H., Lowe Jr, W.L., Kaufman, D.B., and Messersmith, P.B. (2010). Anti-inflammatory peptide-functionalized hydrogels for insulin-secreting cell encapsulation. Biomaterials *31*, 308-314.
204. Sutherland, D.E., Gruessner, R.W., and Gruessner, A.C. (2001). Pancreas transplantation for treatment of diabetes mellitus. World Journal of Surgery *25*, 487-496.
205. Sutherland, D.E., Radosevich, D., Gruessner, R., Gruessner, A., and Kandaswamy, R. (2012). Pushing the envelope: living donor pancreas transplantation. Current Opinion in Organ Transplantation *17*, 106-115.
206. Suzuki, K., Bonner-Weir, S., Hollister-Lock, J., Colton, C.K., and Weir, G.C. (1998). Number and volume of islets transplanted in immunobarrier devices. Cell Transplantation *7*, 47-52.
207. Suzuki, S., Dawson, R.A., Chirila, T.V., Shadforth, A., Hogerheyde, T.A., Edwards, G.A., and Harkin, D.G. (2015). Treatment of silk fibroin with poly (ethylene glycol) for the enhancement of corneal epithelial cell growth. Journal of Functional Biomaterials *6*, 345-366.
208. Teramura, Y., Kaneda, Y., and Iwata, H. (2007). Islet-encapsulation in ultra-thin layer-by-layer membranes of poly (vinyl alcohol) anchored to poly (ethylene glycol)–lipids in the cell membrane. Biomaterials *28*, 4818-4825.
209. Thurber, A.E., Omenetto, F.G., and Kaplan, D.L. (2015). *In vivo* bioresponses to silk proteins. Biomaterials *71*, 145-157.
210. Tjiu, J.W., Chen, J.S., Shun, C.T., Lin, S.J., Liao, Y.H., Chu, C.Y., Tsai, T.F., Chiu, H.C., Dai, Y.S., and Inoue, H. (2009). Tumor-associated macrophage-induced invasion and angiogenesis of human basal cell carcinoma cells by cyclooxygenase-2 induction. Journal of Investigative Dermatology *129*, 1016-1025.

211. Trivedi, N., Steil, G., Colton, C., Bonner-Weir, S., and Weir, G. (2000). Improved vascularization of planar membrane diffusion devices following continuous infusion of vascular endothelial growth factor. Cell Transplantation *9*, 115-124.
212. Uebersax, L., Mattotti, M., Papaloïzos, M., Merkle, H.P., Gander, B., and Meinel, L. (2007). Silk fibroin matrices for the controlled release of nerve growth factor (NGF). Biomaterials *28*, 4449-4460.
213. Vacanti, J.P., and Langer, R. (1999). Tissue engineering: The design and fabrication of living replacement devices for surgical reconstruction and transplantation. The Lancet *354*, S32-S34.
214. Vacanti, N.M., Cheng, H., Hill, P.S., Guerreiro, J.o.D., Dang, T.T., Ma, M., Watson, S.e., Hwang, N.S., Langer, R., and Anderson, D.G. (2012). Localized delivery of dexamethasone from electrospun fibers reduces the foreign body response. Biomacromolecules *13*, 3031-3038.
215. Vaithilingam, V., Evans, M.D., Lewy, D.M., Bean, P.A., Bal, S., and Tuch, B.E. (2017). Co-encapsulation and co-transplantation of mesenchymal stem cells reduces pericapsular fibrosis and improves encapsulated islet survival and function when allografted. Scientific Reports *7*, 10059.
216. Van Deijnen, J., Hulstaert, C., Wolters, G., and Van Schilfgaarde, R. (1992). Significance of the peri-insular extracellular matrix for islet isolation from the pancreas of rat, dog, pig, and man. Cell and Tissue Research *267*, 139-146.
217. Vegas, A.J., Veiseh, O., Gürtler, M., Millman, J.R., Pagliuca, F.W., Bader, A.R., Doloff, J.C., Li, J., Chen, M., and Olejnik, K. (2016). Long-term glycemic control using polymer-encapsulated human stem cell–derived beta cells in immune-competent mice. Nature Medicine *22*, 306-311.
218. Vepari, C., and Kaplan, D.L. (2007). Silk as a biomaterial. Progress in Polymer Science *32*, 991-1007.
219. Vepari, C., Matheson, D., Drummy, L., Naik, R., and Kaplan, D.L. (2010). Surface modification of silk fibroin with poly (ethylene glycol) for antiadhesion and antithrombotic applications. Journal of Biomedical Materials Research Part A *93*, 595-606.
220. Vlahos, A.E., Cober, N., and Sefton, M.V. (2017). Modular tissue engineering for the vascularization of subcutaneously transplanted pancreatic islets. Proceedings of the National Academy of Sciences *114*, 9337-9342.

221. Vollrath, F., and Knight, D.P. (2001). Liquid crystalline spinning of spider silk. Nature *410*, 541-548.
222. Wang, R., and Rosenberg, L. (1999). Maintenance of beta-cell function and survival following islet isolation requires re-establishment of the islet-matrix relationship. Journal of Endocrinology *163*, 181-190.
223. Wang, X., Kluge, J.A., Leisk, G.G., and Kaplan, D.L. (2008). Sonication-induced gelation of silk fibroin for cell encapsulation. Biomaterials *29*, 1054-1064.
224. Wang, X., Partlow, B., Liu, J., Zheng, Z., Su, B., Wang, Y., and Kaplan, D.L. (2015a). Injectable silk-polyethylene glycol hydrogels. Acta Biomaterialia *12*, 51-61.
225. Wang, Y., Bao, J., Wu, X., Wu, Q., Li, Y., Zhou, Y., Li, L., and Bu, H. (2016). Genipin crosslinking reduced the immunogenicity of xenogeneic decellularized porcine whole-liver matrices through regulation of immune cell proliferation and polarization. Scientific Reports *6*, 24779.
226. Wang, Y., Kim, H.J., Vunjak-Novakovic, G., and Kaplan, D.L. (2006). Stem cell-based tissue engineering with silk biomaterials. Biomaterials *27*, 6064-6082.
227. Wang, Y., Liang, M., Zheng, Z., Shi, L., Su, B., Liu, J., Kaplan, D.L., Zhang, B., and Wang, X. (2015b). Adhesion prevention after laminectomy using silk-polyethylene glycol hydrogels. Advanced Healthcare Materials *4*, 2120-2127.
228. Wang, Y., Rudym, D.D., Walsh, A., Abrahamsen, L., Kim, H.J., Kim, H.S., Kirker-Head, C., and Kaplan, D.L. (2008). *In vivo* degradation of three-dimensional silk fibroin scaffolds. Biomaterials *29*, 3415-3428.
229. Weaver, J.D., Song, Y., Yang, E.Y., Ricordi, C., Pileggi, A., Buchwald, P., and Stabler, C.L. (2015). Controlled release of dexamethasone from organosilicone constructs for local modulation of inflammation in islet transplantation. Tissue Engineering Part A *21*, 2250-2261.
230. Weber, L.M., Hayda, K.N., and Anseth, K.S. (2008). Cell–matrix interactions improve β-cell survival and insulin secretion in three-dimensional culture. Tissue Engineering Part A *14*, 1959-1968.
231. Wenk, E., Wandrey, A.J., Merkle, H.P., and Meinel, L. (2008). Silk fibroin spheres as a platform for controlled drug delivery. Journal of Controlled Release *132*, 26-34.
232. Wiegand, F., Kröncke, K., and Kolb-Bachofen, V. (1993). Macrophage-generated nitric oxide as cytotoxic factor in destruction of alginate-encapsulated islets. Protection by arginine analogs and/or coencapsulated erythrocytes. Transplantation *56*, 1206-1212.

233. Wilson, J.T., and Chaikof, E.L. (2008). Thrombosis and inflammation in intraportal islet transplantation: a review of pathophysiology and emerging therapeutics. Journal of Diabetes Science and Technology *2*, 746-759.
234. Wilson, J.T., Cui, W., and Chaikof, E.L. (2008). Layer-by-layer assembly of a conformal nanothin PEG coating for intraportal islet transplantation. Nano Letters *8*, 1940-1948.
235. Wong, H., and Chang, T. (1991). A novel two step procedure for immobilizing living cells in microcapsules for improving xenograft survival. Biomaterials, Artificial Cells and Immobilization Biotechnology *19*, 687-697.
236. Wu, G., Korsgren, O., Zhang, J., Song, Z., Van Rooijen, N., and Tibell, A. (2000). Role of macrophages and natural killer cells in the rejection of pig islet xenografts in mice. Transplantation Proceedings *32*, 1069.
237. Wu, H., Ni, B.B., Wang, C., Zhai, F., and Ma, Y. (2012a). Acid-responsive organogel mediated by arene–perfluoroarene and hydrogen bonding interactions. Soft Matter *8*, 5486-5492.
238. Wu, X., Hou, J., Li, M., Wang, J., Kaplan, D.L., and Lu, S. (2012b). Sodium dodecyl sulfate-induced rapid gelation of silk fibroin. Acta Biomaterialia *8*, 2185-2192.
239. Yang, H., and Wright Jr, J.R. (1999). Co-encapsulation of sertoli enriched testicular cell fractions further prolongs fish-to-mouse islet xenograft survival1. Transplantation *67*, 815-820.
240. Yang, H., Iwata, H., Shimizu, H., Takagi, T., Tsuji, T., and Ito, F. (1994). Comparative studies of *in vitro* and *in vivo* function of three different shaped bioartificial pancreases made of agarose hydrogel. Biomaterials *15*, 113-120.
241. Yang, H.K., Ham, D.S., Park, H.S., Rhee, M., You, Y.H., Kim, M.J., Shin, J., Kim, O.Y., Khang, G., and Hong, T.H. (2016). Long-term efficacy and biocompatibility of encapsulated islet transplantation with chitosan-coated alginate capsules in mice and canine models of diabetes. Transplantation *100*, 334-343.
242. Yang, K.C., Qi, Z., Wu, C.C., Shirouza, Y., Lin, F.H., Yanai, G., and Sumi, S. (2010). The cytoprotection of chitosan based hydrogels in xenogeneic islet transplantation: An *in vivo* study in streptozotocin-induced diabetic mouse. Biochemical and Biophysical Research Communications *393*, 818-823.
243. Yang, S., Leong, K.-F., Du, Z., and Chua, C.K. (2001). The design of scaffolds for use in tissue engineering. Part I. Traditional factors. Tissue Engineering *7*, 679-689.

244. Yang, Z., Tu, Q., Maitz, M.F., Zhou, S., Wang, J., and Huang, N. (2012). Direct thrombin inhibitor-bivalirudin functionalized plasma polymerized allylamine coating for improved biocompatibility of vascular devices. Biomaterials *33*, 7959-7971.
245. Yodmuang, S., McNamara, S.L., Nover, A.B., Mandal, B.B., Agarwal, M., Kelly, T.A.N., Chao, P.H.G., Hung, C., Kaplan, D.L., and Vunjak-Novakovic, G. (2015). Silk microfiber-reinforced silk hydrogel composites for functional cartilage tissue repair. Acta Biomaterialia *11*, 27-36.
246. Yu, B., Wang, C., Ju, Y.M., West, L., Harmon, J., Moussy, Y., and Moussy, F. (2008). Use of hydrogel coating to improve the performance of implanted glucose sensors. Biosensors and Bioelectronics *23*, 1278-1284.
247. Yu, D., Sun, C., Zheng, Z., Wang, X., Chen, D., Wu, H., Wang, X., and Shi, F. (2016). Inner ear delivery of dexamethasone using injectable silk-polyethylene glycol (PEG) hydrogel. International Journal of Pharmaceutics *503*, 229-237.
248. Yucel, T., Cebe, P., and Kaplan, D.L. (2009). Vortex-induced injectable silk fibroin hydrogels. Biophysical Journal *97*, 2044-2050.
249. Yutani, C., Ishibashi-Ueda, H., Suzuki, T., and Kojima, A. (2000). Histologic evidence of foreign body granulation tissue and de novo lesions in patients with coronary stent restenosis. Cardiology *92*, 171-177.
250. Zekorn, T., Horcher, A., Mellert, J., Siebers, U., Altug, T., Emre, A., Hahn, H., and Federlin, K. (1996). Biocompatibility and immunology in the encapsulation of islets of Langerhans (bioartificial pancreas). The International Journal of Artificial Organs *19*, 251-257.
251. Zekorn, T., Horcher, A., Siebers, U., Schnettler, R., Klöck, G., Hering, B., Zimmermann, U., Bretzel, R., and Federlin, K. (1992). Barium-cross-linked alginate beads: A simple, one-step method for successful immunoisolated transplantation of islets of Langerhans. Acta Diabetologica *29*, 99-106.
252. Zhang, W., Wang, X., Wang, S., Zhao, J., Xu, L., Zhu, C., Zeng, D., Chen, J., Zhang, Z., and Kaplan, D.L. (2011). The use of injectable sonication-induced silk hydrogel for VEGF 165 and BMP-2 delivery for elevation of the maxillary sinus floor. Biomaterials *32*, 9415-9424.
253. Zhao, S., Chen, Y., Partlow, B.P., Golding, A.S., Tseng, P., Coburn, J., Applegate, M.B., Moreau, J.E., Omenetto, F.G., and Kaplan, D.L. (2016). Bio-functionalized silk hydrogel microfluidic systems. Biomaterials *93*, 60-70.

254. Zhi, Z.-l., Liu, B., Jones, P.M., and Pickup, J.C. (2010). Polysaccharide multilayer nanoencapsulation of insulin-producing β-cells grown as pseudoislets for potential cellular delivery of insulin. Biomacromolecules *11*, 610-616.

255. Zimmermann, H., Wählisch, F., Baier, C., Westhoff, M., Reuss, R., Zimmermann, D., Behringer, M., Ehrhart, F., Katsen-Globa, A., and Giese, C. (2007). Physical and biological properties of barium cross-linked alginate membranes. Biomaterials *28*, 1327-1345.

256. Ziv, K., Nuhn, H., Ben-Haim, Y., Sasportas, L.S., Kempen, P.J., Niedringhaus, T.P., Hrynyk, M., Sinclair, R., Barron, A.E., and Gambhir, S.S. (2014). A tunable silk–alginate hydrogel scaffold for stem cell culture and transplantation. Biomaterials *35*, 3736-3743.

APPENDIX

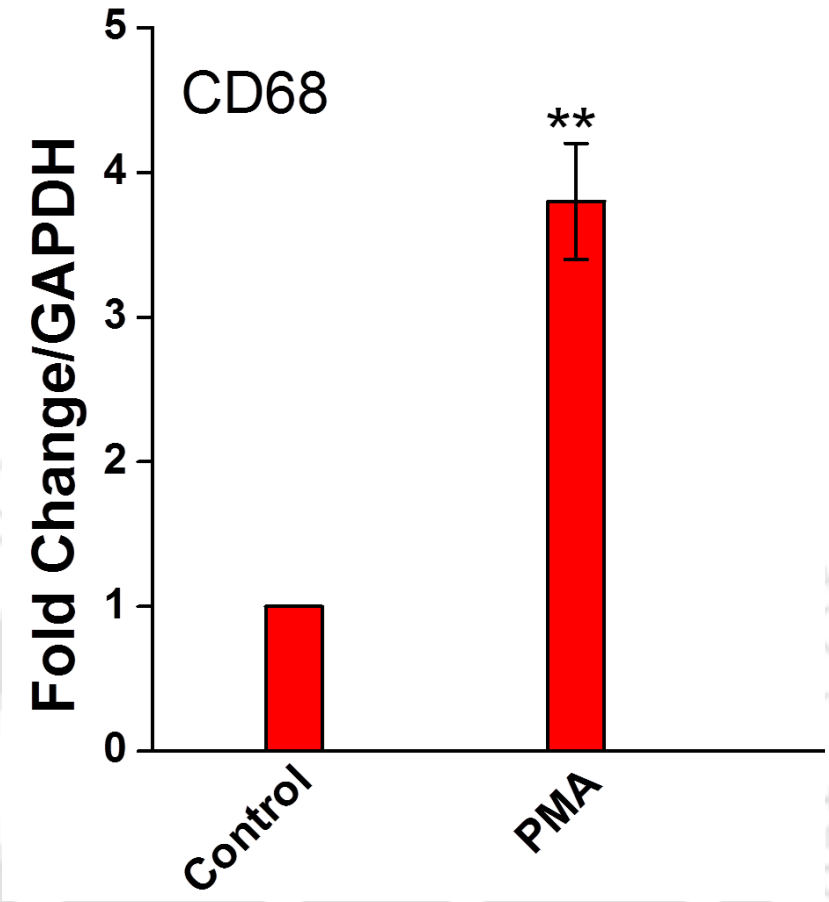

Figure A2.1. *Expression of CD68 after PMA treatment compared to THP-1 (control). (**$p < 0.01$).*

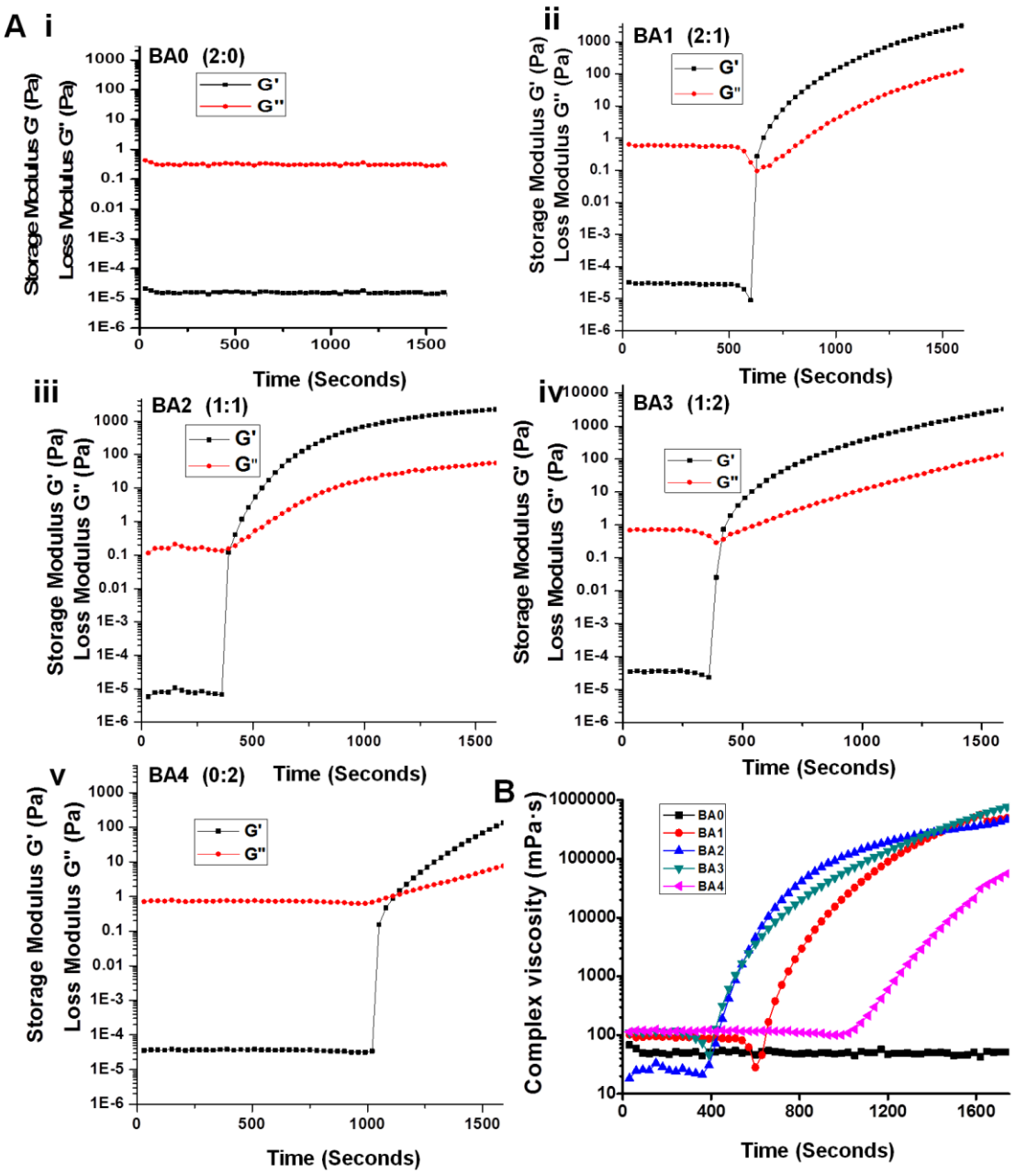

Figure A4.1. *Rheology study. (A) Gelation characterization of silk blend solutions. BA0 (2:0) (i), BA1 (2:1) (ii), BA2 (1:1) (iii), BA3 (1:2) (iv) and BA4 (0:2) (v). (B) Complex viscosities of silk blend solutions as a function of time.*

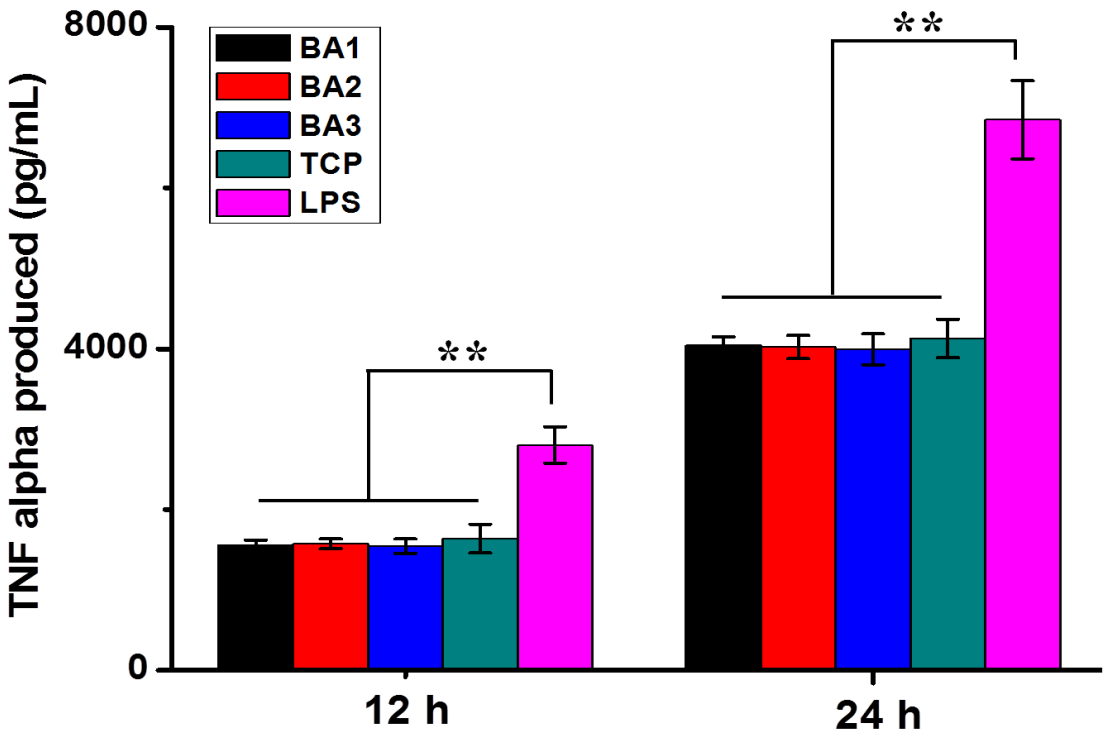

Figure A4.2. *TNF alpha production by RAW 264.7 mouse macrophages in response to silk hydrogels (in vitro study). Lipopolysaccharide (LPS) and standard tissue culture plate (TCP) were considered as positive and negative controls, respectively. (n = 3, **p < 0.01).*

LIST OF PUBLICATIONS

List of Publications

Publications from Ph.D. Thesis:

(A) Journal Publications:

1. **Manishekhar Kumar**, Jeannine Coburn, David L. Kaplan, and Biman B. Mandal. "Immuno-Informed 3D Silk Biomaterials for Tailoring Biological Responses." *ACS Applied Materials & Interfaces* 8, no. 43 (2016): 29310-22.

2. **Manishekhar Kumar**, Samit K. Nandi, David L. Kaplan and Biman B. Mandal. "Localized Immunomodulatory Silk Macrocapsules for Islet-like Spheroid Formation and Sustained Insulin Production." *ACS Biomaterials Science & Engineering* 3, 10 (2017): 2443-56.

3. **Manishekhar Kumar**, Rocktotpal Konwarh, Joseph Christakiran M, David L. Kaplan and Biman B. Mandal. "Silk Based 3D Tissues". *Progress in Polymer Science.* (Under Review)

4. **Manishekhar Kumar**, Prerak Gupta, Sohenii Bhattacharjee, Samit K. Nandi, Biman. B. Mandal. "Immunomodulatory Injectable Silk Hydrogels Maintaining Functional Islets and Promoting Anti-inflammatory M2 Macrophage Polarization." *Biomaterials.* (Under Review)

(B) Book Chapters:

1. **Manishekhar Kumar**, Janani G, David L. Kaplan and Biman B. Mandal**.** Silk-based Encapsulation Platforms to Enhance Pancreatic Cells' Function **(**Invited book chapter, Book title: Transplantation, Bioengineering and Regeneration of the Endocrine Pancreas, Editor - Prof. Giuseppe Orlando, Wake Forest School of Medicine, USA)

(C) Conference Proceedings:

1. **Manishekhar Kumar**, Samit K. Nandi, David L. Kaplan and Biman B. Mandal. "Immunomodulatory Bio Artificial Pancreas for Sustained Insulin Production in Diabetic Patients". *European cells & materials***,** 2017; 33.

2. **Manishekhar Kumar**, Biman B. Mandal. "Silk-based Macro Encapsulates for Sustained Insulin Release". *Tissue Engineering Part A*, 21 (2015):S65-S66.

Publications from Other Collaborative Research Projects:

(A) Journal Publications:

1. **Manishekhar Kumar**, Deepak Jain, Nandana Bhardwaj, Prerak Gupta, Samit K. Nandi, and Biman B. Mandal. "Native Honeybee Silk Membrane: A Potential Matrix for Tissue Engineering and Regenerative Medicine." *RSC Advances* 6, no. 59 (2016): 54394-403.

2. Prerak Gupta, **Manishekhar Kumar**, Nandana Bhardwaj, Jadi Praveen Kumar, CS Krishnamurthy, Samit Kumar Nandi, and Biman B. Mandal. "Mimicking Form and Function of Native Small Diameter Vascular Conduits Using Mulberry and Non-Mulberry Patterned Silk Films." *ACS Applied Materials & Interfaces* 8, no. 25 (2016): 15874-88.

3. Prerak Gupta, Mimi Adhikary, **Manishekhar Kumar**, Nandana Bhardwaj, and Biman B. Mandal. "Biomimetic, Osteoconductive Non-Mulberry Silk Fiber Reinforced Tricomposite Scaffolds for Bone Tissue Engineering." *ACS Applied Materials & Interfaces* 8, no. 45 (2016): 30797-810.

4. Jadi Praveen Kumar, Rocktotpal Konwarh, **Manishekhar Kuma**r, Ankit Gangrade, and Biman B. Mandal. "Potential Nanomedicine Applications of Multifunctional Carbon Nanoparticles Developed using Green Technology." *ACS Sustainable Chemistry & Engineering* (2017).

5. Bibekananda De, **Manishekhar Kumar**, Biman B. Mandal, and Niranjan Karak. "An in Situ Prepared Photo-Luminescent Transparent Biocompatible Hyperbranched Epoxy/Carbon Dot Nanocomposite." *RSC Advances* 5, no. 91 (2015): 74692-704.

6. Satyabrat Gogoi, **Manishekhar Kumar**, Biman B. Mandal, and Niranjan Karak. "High Performance Luminescent Thermosetting Waterborne Hyperbranched Polyurethane/Carbon Quantum Dot Nanocomposite with in Vitro Cytocompatibility." *Composites Science and Technology* 118 (2015): 39-46.

7. Satyabrat Gogoi, **Manishekhar Kumar**, Biman B. Mandal, and Niranjan Karak. "A Renewable Resource Based Carbon Dot Decorated Hydroxyapatite Nanohybrid and Its Fabrication with Waterborne Hyperbranched Polyurethane for Bone Tissue Engineering." *RSC Advances* 6, no. 31 (2016): 26066-76.

8. Nisha Shankhwar, **Manishekhar Kumar**, Biman B. Mandal, PS Robi, and A Srinivasan. "Electrospun Polyvinyl Alcohol-Polyvinyl Pyrrolidone Nanofibrous Membranes for Interactive Wound Dressing Application." *Journal of Biomaterials Science, Polymer Edition* 27, no. 3 (2016): 247-62.

9. Nisha Shankhawar, **Manishekhar Kumar**, Biman B. Mandal, and A Srinivasan. "Novel Polyvinyl Alcohol-Bioglass 45s5 Based Composite Nanofibrous Membranes as Bone Scaffolds." *Materials Science and Engineering: C* 69 (2016): 1167-74.

10. Santosh Kumar Behera, Anwesha Murkherjee, G. Sadhuragiri, Palani Elumalai, M. Sathiyendiran, **Manishekhar Kumar**, Biman B. Mandal, and G. Krishnamoorthy. "Aggregation Induced Enhanced and Exclusively Highly Stokes Shifted Emission from an Excited State Intramolecular Proton Transfer Exhibiting Molecule." *Faraday Discussions* (2017).

11. Nihar Dash, Ashim Malakar, **Manishekhar Kumar**, Biman B. Mandal, and G Krishnamoorthy. "Metal Ion Dependent “on” Intramolecular Charge Transfer

(Ict) and "Off" Normal Switching of the Fluorescence: Sensing of Zn 2+ by Ict Emission in Living Cells." *Sensors and Actuators B: Chemical* 202 (2014): 1154-63.

12. Ashim Malakar, **Manishekhar Kumar**, Anki Reddy, Himadree T Biswal, Biman B. Mandal, and G Krishnamoorthy. "Aggregation Induced Enhanced Emission of 2-(2′-Hydroxyphenyl) Benzimidazole." *Photochemical & Photobiological Sciences* 15, no. 7 (2016): 937-48.

13. Shreya Mehrotra, Rocktotpal Konwarh, **Manishekhar Kumar**, Dimple Chouhan and Biman. B. Mandal. Silk Based Nanomaterials for Biomedical Applications. (Under preparation)

(B) Book Chapters:

1. Janani G, **Manishekhar Kumar**, Dimple Chouhan, Joseph Christakiran M., Ankit Gangrade, Sohenii Bhattacharjee, Biman B. Mandal. Silk Fibroin Biomaterials for Medical Applications. **(**Invited book chapter, Book title: Composites in Biomedical Engineering: Matrices, Volume 3: Resorbable polymer Matrices, Editor – Alexandru Mihai Grumezescu, University Politehnica of Bucharest, Romania)

(C) Conference Proceedings:

1. Bibhas K Bhunia, **Manishekhar Kumar** and Biman B Mandal. "Development of Silk-based Angle-ply Construct for Annulus Fibrosus Tissue Engineering". *European cells & materials***,** 2017; 33.

2. Prerak Gupta, **Manishekhar Kumar**, Nandana Bhardwaj, Jadi Praveen Kumar, C. S. Krishnamurthy, Samit K. Nandi and Biman B. Mandal. Bioengineered Silk Vascular Grafts for Coronary Artery Bypass Surgery. *European cells & materials*, 2016; 31:231.

3. Mimi Adhikary, Prerak Gupta, **Manishekhar Kumar**, Salma Jasmine, Nandana Bhardwaj, Dimple Chouhan and Biman B. Mandal. Hydroxyapatite-silk fiber-silk fibroin Tri-composite Scaffolds for Bone Tissue Engineering. *European cells & materials*, 2016; 31:18.